UNIVERSITAT POLITÈCNICA DE CATALUNYA

Programa de Doctorat:

AUTOMÀTICA, ROBÒTICA I VISIÓ

Tesi Doctoral

Control and management of energy storage systems in microgrids

Unnikrishnan Raveendran Nair

Director: Dr. Ramon Costa-Castelló

May 2020

Universitat Politècnica de Catalunya- Campus Barcelona

Automatic Control Department

Title:
Control and management of energy storage systems in microgrids

This PhD thesis was completed at
Institut de Robòtica i Informàtica Industrial, CSIC-UPC
C/ Llorens i Artigas 4-6. 08028 Barcelona, Spain

Advisors:
Dr. Ramon Costa-Castelló

To my parents ...

To my wife ....,

To my family.

Acknowledgement

This Ph.D work was carried out in Institut de Robòtica i Informàtica Industrial at the Universitat Politècnica de Catalunya. The work was done as part of the INCITE project funded though Marie Skłodowska-Curie grant agreement No 675318 from the European Union. The author would like to acknowledge the support from the above institutions.

This period I spent pursuing my Ph.D represents an important chapter in my life and looking back at this journey I started more than three years ago it has been an eventful, happy and gratifying experience. The journey had its fair share of ups and downs but at the end I will fondly remember it as a period where I enjoyed in a new country, new culture, met new people, made new friends and further learned about me. There are a lot of people I would like to thank at this stage for having made this time great.

First and foremost I would like to thank my supervisor Associate Professor Ramon Costa-Castelló. He presented me with this opportunity to do the Ph.D and has always supported me throughout this period. His guidance, feedback during this period had been invaluable and the freedom he had offered me in defining my research path was immense. I whole heartedly thank him for being available and approachable every time, to discuss and solve research problems during my Ph.D. I would also like to extend my sincerest thanks to Vicente Roda Serrat, from UPC, who had helped a lot during this period in my experimental works. His help and suggestions had been instrumental in allowing me to perform experimental verifications.

I would like to thank Prof. Alfonso Baños from University of Murcia, with whom I had collaborated on multiple occasions during this period and for providing me with valuable ideas for research in the domain of reset control. During this research I had the opportunity to do two external stays. I would like to thank Prof. Frede Blaabjerg for receiving me at Aalborg University in Denmark to work with his group and for the

opportunity to broaden my understanding on battery management and degradation. I am also grateful to my colleagues, Monika Sandelic, Dr. Ariya Sangwongwanich and Associate Professor Tomislav Dragičević in Aalborg University for the intense discussions, support and collaboration during this period. I would also like to thank Dr. Nuno Silva of EFACEC, Portugal who gave me the opportunity to do an industrial stay during my Ph.D and work with his ream in Portugal. Finally, I would like to thank Dr. German A Ramos Fuentes for his collaboration in developing observer based control systems.

I want to thank my colleagues and friends from UPC Wicak Anaduta, Pau Segovia, José Luis Sampietro, Ye Wang, Masoud Pourasghar, Fatemeh Karimi Pour, Jenny Lorena Dıaz for their technical discussions, support and for all the good times spend in the last few years. I also want to thank all my colleagues from the INCITE project for their discussion and feedback at workshops organised every year. A big thanks to Dr. Marta Fonrodona, the project manager from INCITE for her coordination during the project and for her support extended to me.

I would like to thank my family who has always provided me with their unerring support throughout my life. My father Raveendran Nair, my mother Jayalekshmi and my brother Gopikrishnan have always backed my decisions, motivated me and without their support I would never have reached where I am now. Last, but not the least I would like to thank the special person in my life, my wife Sneha. Getting married to her was the biggest and most memorable moment from this Ph.D period. I am grateful to her for always being there for me during my highs and lows. If there is one thing I have learned without uncertainty, it is that she will be there for me always.

Unnikrishnan Raveendran Nair
Barcelona, Spain, 2020

Abstract

The rate of integration of the renewable energy sources in modern grids have significantly increased in the last decade. These intermittent, non-dispatchable renewable sources, though environment friendly tend to be grid unfriendly. This is precisely due to the issues pertaining to grid congestion, voltage regulation and stability of grids being reported as a result of the incorporation of renewable sources. In this scenario, the use of energy storage systems (ESS) in electric grids is being widely proposed to overcome these issues. However, integrating energy storage systems alone will not compensate for the issue created by renewable generation. The control and management of the ESS should be done optimally so that their full capabilities are exploited to overcome the issues in the power grids and to ensure their lower cost of investment by prolonging ESS lifetime through minimising degradation.

Motivated by this aspect this Ph.D work focusses on developing an efficient, optimal control and management strategy for ESS in a microgrid, especially hybrid ESS. The Ph.D work addresses this issue by proposing a hierarchical control scheme comprising of a lower power management and higher energy management stage with contributions in each stage.

In the power management stage this work focusses on improving aspects of real time control of power converters interfacing ESS to grid and the microgrid system as whole. The work proposes control systems with improved dynamic behaviour for power converters based on the reset control framework. In the microgrid control the work presents a primary+secondary control scheme with improved voltage regulation performance under disturbances, using an observer. The real time power splitting strategies among hybrid ESS accounting for the ESS operating efficiencies and degradation mechanisms will also be addressed in the primary+secondary control of power management stage. The design criteria, stability and robustness analysis will be carried out, along with simulation or experimental verifications.

In the higher level energy management stage, the contribution of this work involves application of an economic MPC framework for the management of ESS in microgrids. The work specifically addresses the problems of mitigating grid congestion from renewable power feed-in, minimising ESS degradation and maximising self consumption of generated renewable energy using the MPC based energy management system. A survey of the forecasting methods that can be used for MPC will be carried out and a neural network based forecasting unit for time series prediction will be developed. The practical issue of accounting for forecasting error in the decision making of MPC will be addressed and impact of the resulting conservative decision making on the system performance will be analysed. The improvement in performance with the proposed energy management scheme will be demonstrated and quantified.

Keywords: Energy storage system, renewable generation, power management, energy management, reset control, disturbance observer, power splitting, stability, MPC, ESS degradation, grid congestion, self consumption.

Resumen

La integración de las fuentes de energía renovables en las redes modernas ha aumentado significativamente en la última década. Estas fuentes renovables, aunque muy convenientes para el medio ambiente son de naturaleza intermitente, y son no planificables, cosa que genera problemas en la red de distribución. Esto se debe precisamente a los problemas relacionados con la congestión de la red y la regulación del voltaje. En este escenario, el uso de sistemas de almacenamiento de energía (ESS) en redes eléctricas está siendo ampliamente propuesto para superar estos problemas. Sin embargo, la integración de sistemas de almacenamiento de energía por sí solos no compensará el problema creado por la generación renovable. El control y la gestión del ESS deben realizarse de manera óptima, de modo que se aprovechen al máximo sus capacidades para superar los problemas en las redes eléctricas, garantizar un coste de inversión razonable y prolongar la vida útil del ESS minimizando su degradación.

Motivado por esta problemática, esta tesis doctoral se centra en desarrollar una estrategia de control y gestión eficiente para los ESS integrados en una microrred, especialmente cuando se trata de ESS de naturaleza hibride. El trabajo de doctorado propone un esquema de control jerárquico compuesto por un control de bajo nivel y una parte de gestión de energía operando a más alto nivel. El trabajo realiza aportaciones en los dos campos.

En el control de bajo nivel, este trabajo se centra en mejorar aspectos del control en tiempo real de los convertidores que interconectan el ESS con la red y el sistema de micro red en su conjunto. El trabajo propone sistemas de control con comportamiento dinámico mejorado para convertidores de potencia desarrollados en el marco del control de tipo reset. En el control de microrred, el trabajo presenta un esquema de control primario y uno secundario de regulación de voltaje mejorado bajo perturbaciones, utilizando un observador. Además, el trabajo plantea estrategias de reparto del flujo de potencia entre los diferentes ESS. Durante el diseño de estos algoritmos de control se

tienen en cuenta los mecanismos de degradación de los diferentes ESS. Los algoritmos diseados se validarán mediante simulaciones y trabajos experimentales.

En el apartado de gestión de energía, la contribución de este trabajo se centra en la aplicación del un control predictivo económico basado en modelo (EMPC) para la gestión de ESS en microrredes. El trabajo aborda específicamente los problemas de mitigar la congestión de la red a partir de la alimentación de energía renovable, minimizando la degradación de ESS y maximizando el autoconsumo de energía renovable generada. Se ha realizado una revisión de los métodos de predicción del consumo/generación que pueden usarse en el marco del EMPC y se ha desarrollado un mecanismo de predicción basado en el uso de las redes neuronales. Se ha abordado el análisis del efecto del error de predicción sobre el EMPC y el impacto que la toma de decisiones conservadoras produce en el rendimiento del sistema. La mejora en el rendimiento del esquema de gestión energética propuesto se ha cuantificado.

Palabras clave: Sistema de almacenamiento de energía, generación renovable, administración de energía, administración de energía, control de reinicio, observador de perturbaciones, división de energía, estabilidad, MPC, degradación de ESS, congestión de red, autoconsumo.

Resum

La integració de les fonts d'energia renovables a les xarxes modernes ha augmentat significativament en l'última dècada. Aquestes fonts renovables, encara que molt convenients per al medi ambient són de naturalesa intermitent, i són no panificables, cosa que genera problemes a la xarxa de distribució. Això es deu precisament als problemes relacionats amb la congestió de la xarxa i la regulació de la tensió. En aquest escenari, l'ús de sistemes d'emmagatzematge d'energia (ESS) en xarxes elèctriques està sent àmpliament proposat per superar aquests problemes. No obstant això, la integració de sistemes d'emmagatzematge d'energia per si sols no compensarà el problema creat per la generació renovable. El control i la gestió de l'ESS s'han de fer de manera òptima, de manera que s'aprofitin al màxim les seves capacitats per superar els problemes en les xarxes elèctriques, garantir un cost d'inversió raonable i allargar la vida útil de l'ESS minimitzant la seva degradació.

Motivat per aquesta problemàtica, aquesta tesi doctoral es centra a desenvolupar una estratègia de control i gestió eficient per als ESS integrats en una microxarxa, especialment quan es tracta d'ESS de natura híbrida. El treball de doctorat proposa un esquema de control jeràrquic compost per un control de baix nivell i una part de gestió d'energia operant a més alt nivell. El treball realitza aportacions en els dos camps.

En el control de baix nivell, aquest treball es centra a millorar aspectes del control en temps real dels convertidors que interconnecten el ESS amb la xarxa i el sistema de micro xarxa en el seu conjunt. El treball proposa sistemes de control amb comportament dinàmic millorat per a convertidors de potència desenvolupats en el marc del control de tipus reset. En el control de micro-xarxa, el treball presenta un esquema de control primari i un de secundari de regulació de voltatge millorat sota pertorbacions, utilitzant un observador. A més, el treball planteja estratègies de repartiment de el flux de potència entre els diferents ESS. Durant el disseny d'aquests algoritmes de control es tenen en compte els mecanismes de degradació dels diferents ESS. Els algoritmes dissenyats es

validaran mitjanant simulacions i treballs experimentals.

En l'apartat de gestió d'energia, la contribució d'aquest treball se centra en l'aplicació de l'un control predictiu econòmic basat en model (EMPC) per a la gestió d'ESS en microxarxes. El treball aborda especficament els problemes de mitigar la congestió de la xarxa a partir de l'alimentació d'energia renovable, minimitzant la degradació d'ESS i maximitzant l'autoconsum d'energia renovable generada. S'ha realitzat una revisió dels mètodes de predicció del consum/generació que poden usar-se en el marc de l'EMPC i s'ha desenvolupat un mecanisme de predicció basat en l'ús de les xarxes neuronals. S'ha abordat l'anàlisi de l'efecte de l'error de predicció sobre el EMPC i l'impacte que la presa de decisions conservadores produeix en el rendiment de el sistema. La millora en el rendiment de l'esquema de gestió energètica proposat s'ha quantificat.

Paraules clau: Sistema d'emmagatzematge d'energia, generació de renovables, gestió d'energia, gestió d'energia, control de restabliment, observador de pertorbacions, desdoblament d'energia, estabilitat, MPC, degradació ESS, congestió de xarxa, autoconsum.

Acronyms

RES	Renewable Energy Source
PV	Photovoltaic
LV	Low voltage
DR	Demand response
ESS	Energy Storage Systems
BESS	Battery Energy Storage System
PHS	Pumped Hydro Storage
CAES	Compressed Air Energy Storage
SC	Supercapacitor
SMES	Superconducting magnetic energy storage
DG	Distributed generation
DER	Distributed energy resource
SOC	State of Charge
SOH	State of Hydrogen
MPC	Model Predictive Control
FC	Fuel cell
PEM	Proton exchange membrane
EOL	End of life
PI	Proportional integral
CI	Clegg integrator
FORE	First Order Reset Elements
DF	Describing function
ISS	Input to state stability
EMI	Electromagnetic interference
EMC	Electromagnetic compatibility
DO	Disturbance observers

ESO	Extended state observer
ADRC	Adaptive disturbance rejection control
LMI	Linear matrix inequality
MA	Moving average
ES	Exponential smoothing
ARIMA	Auto regressive integrated moving average
ARMA	Auto regressive moving average
AIC	Akaike's Information Criterion
SVR	Support vector regressor
ANN	Artificial neural networks
DNN	Deep neural network
RNN	Recurrent neural network
LSTM	Long short-term memory
RR	Ridge regressor
LR	Lasso regressor
SARIMA	Seasonal ARIMA
NN	Neural Network
ReLU	Rectified linear unit
RMSE	Root mean squared error
GA	Genetic algorithm
SA	Simulated Annealing
LQR	Linear quadratic regulator
MSC	Maximising self consumption
ASCR	Annual self-consumption ratio
APPR	Annual average peak power reduction
MPPT	Maximum Power Point Tracking
QP	Quadratic programming
MIQP	Mixed Integer Quadratic programming
CPG	Constant Power Generation
LOH	Level of hydrogen
MLD	Mixed Logical Dynamics

Notation

Throughout the thesis...

$\mathcal{R}$	Reset controller
$\mathbb{R}$	set of real numbers
$\mathbf{x}_r$	Reset controller states
$\mathbf{x}_r^+$	Reset controller state after reset instance
$\mathbf{A}_r$	Reset controller state matrix
$\mathbf{b}_r$	Reset controller input matrix
$\mathbf{c}_r$	Reset controller output matrix
$\mathbf{A}_\rho$	Reset matrix for reset controller
$u_\mathcal{R}$	Reset controller output
e	Reset controller input
u_{ci}	Clegg integrator output
u_{pi}	PI output
$\mathcal{F}$	Flow set of reset controller
$\mathcal{J}$	Jump set of reset controller
n	Measurement noise
$\mathbf{w}_1$	States for exogenous signal
$\mathbf{A}_1$	Exogenous signal state matrix
$\mathbf{c}_1$	Exogenous signal output matrix
r	reference signal
$\mathbf{x}_p$	Generic plant states
$\mathbf{A}_p$	Generic plant state matrix
$\mathbf{b}_p$	Generic plant input matrix
$\mathbf{c}_p$	Generic plant output matrix
y	Generic plant output
$\mathbf{x}$	Reset control system states

$\mathbf{x}^+$	Reset control system state after reset instance
$\mathbf{A}(\rho_r)$	Reset control system state matrix
$\mathbf{c}$	Reset control system output matrix
$\mathbf{A}_{\mathcal{R}}$	Reset matrix for rest control system
$\mathcal{F}_{\mathcal{C}}$	Flow set of reset control system
$\mathcal{J}_{\mathcal{C}}$	Jump set of reset control system
e	System reference tracking error
$\mathcal{G}_{eu}(s)$	Transfer function from e to u_{ci}
$G(s)$	DC-DC converter transfer function
$P_{red}(s)$	DC-DC converter transfer function reduced order
$F_c(s)$	Compensating filter
k_p	Constant gain in PI controller for DC-DC converter
k_i	Integral gain in PI controller for DC-DC converter
$T(s)$	Complementary sensitivity transfer function
$S(s)$	Sensitivity transfer function
$CS(s)$	Noise sensitivity transfer function
$PS(s)$	Load sensitivity transfer function
ω_b	cut-off frequency
v_{nom}	Nominal microgrid voltage
v_{grid}	Measured voltage at microgrid
i_{gridr}	Reference value of total current injected to grid
i_{grid}	Total current injected into grid
$C_v(s)$	Voltage loop controller model
$G_i(s)$	Equivalent inner loop transfer function
$G_g(s)$	Grid model
ξ	Disturbance input to microgrid
$\hat{\xi}$	Disturbance estimation
$G_{cd}(s)$	Feed-forward controller
C_{grid}	Equivalent capacitance of the microgrid
$\mathbf{x}_o$	Augmented system state
n_o	order of the ESO
$\mathbf{A}_o$	Augmented system state matrix
$\mathbf{b}_o$	Augmented system input matrix
$\mathbf{c}_y$	ESO output matrix pertaining to grid voltage
$\mathbf{c}_o$	ESO output matrix pertaining to disturbance extimation

l_o	ESO gain
$\hat{\mathbf{x}}_\mathbf{o}$	ESO states
e_b	Tracking error of grid voltage
k_{pv}, k_{iv}	Gain constants of voltage loop PI controller
$F(s)$	Filter for power splitting between high power and energy density ESS
τ_f	Time constant for $F(s)$
$i_{scr}^{'}$	High frequency part of control action from $C_v(s)$
$i_{hess}^{'}$	Low frequency part of control action from $C_v(s)$
i_{res}	Control action from SC charge restoration control.
$\mathcal{S}$	Sigmoid Function
a_s, c_s	Sigmoid function constant
i_{batr}	Set point for battery current loop
i_{fcr}	Set point for FC current loop
i_{sc}, i_{bat}, i_{fc}	Aggregated output from SC, battery and FC storage system
$G_1(s)$	Transfer function of SC current loop
$G_2(s)$	Transfer function of battery current loop
$G_3(s)$	Transfer function of FC current loop
$Q(s)$	Low pass behaviour representation from equivalent model of ESO
$G_{y\xi}(s)$	Approximated disturbance rejection transfer for ADRC scheme
$W_\xi(s)$	Weighting function for ESO design
$P_e(s)$	Extended plant model used in L_o determination
n_e	Order of extended plant
$v_1, v_2, ...v_{k-1}$	previous values of the time series used in forecasting unit
$\hat{V}_t$	Forecast output of the time series for instant t
p, d, q	Parameters of ARIMA model
$f(l)$	Function defining behaviour of ReLU
N	Prediction horizon length
$u_{k\|i}$	Output sequence from MPC for sampling instant i $(u(0+1), u(i+i)..u(k+i))$
c_b	Battery capacity
c_{sc}	SC capacity
c_{fc}	Hydrogen storage capacity of FC
E_{load}	Total annual energy demanded by load
E_{pv}	Total annual energy generated by PV
T_s	Sampling time for MPC
η	Converter efficiency

x	ESS state
x_{α}^{lo}	Value of lower limit of ESS state
x_{α}^{up}	Value of upper limit of ESS state
p_{b}	Battery power
p_g	Power exchanged to main grid from microgrid
$d_{k\|i}$	Sequence of bounds on forecast error at sampling instant i
p_{pv}	Generated PV power
p_l	Load power
λ	Penalising weights in MPC cost function
ϵ	Slack variable for soft constraints
J	MPC cost function term
pv_{cons}	Amount of annual PV energy generated utilised by the consumer
pv_{gen}	Total annual PV energy generated
C_f	Capacity fade of battery
p_{curr}	Curtailed power in PV generation
p_{pvm}	Maximum output from a PV array for an irradiation level
p_{sc}	SC power
p_{fc}	FC system power
p_{gen}	Dispatchable generator power
z	Auxiliary variable in MLD formulation
δ	Boolean variable in MLD formulation
$\mathcal{O}$	Computational time complexity.

Contents

List of Tables

List of Figures

Part I

Introduction

Chapter 1

Introduction

1.1 Why energy storage systems in grids??

The need for contribution from renewable energy sources (RES) towards the global energy consumption is increasingly evident [3, 9]. In light of this, at least in the electric power sector, the least decade has seen more than doubling of the renewable energy generation capacity being integrated. This has coincided with renewable power being more cost-competitive compared to conventional fossil fuel power plants [3]. Currently there is a global installed capacity of more than 33% from renewable sources which had produced 26.2% of the global electrical energy production in 2018 [3, 10]. The share of various renewable sources in the total electrical energy production is shown in Figure1.1. This share is only projected to increase and by 2023 it is expected that renewable sources produce 30% electric power demand [10].

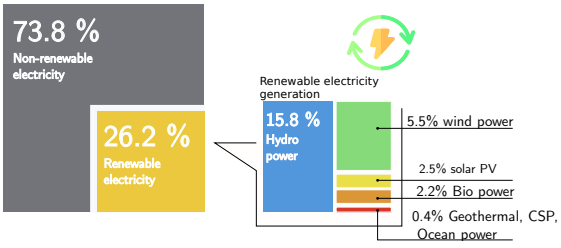

Figure 1.1: The share of renewable sources in the global electrical energy production (Source: [3])

The renewable generation, from an environmental standpoint, is highly beneficial but from perspective of electric power networks they do not tend to be grid friendly. This is due to the inherent nature of renewable sources that can be characterised as decentralised, non-dispatchable and intermittent [11]. As a result, the increased integration of renewable sources has led to many issues reported in power networks related to grid congestion and stability [12–16].

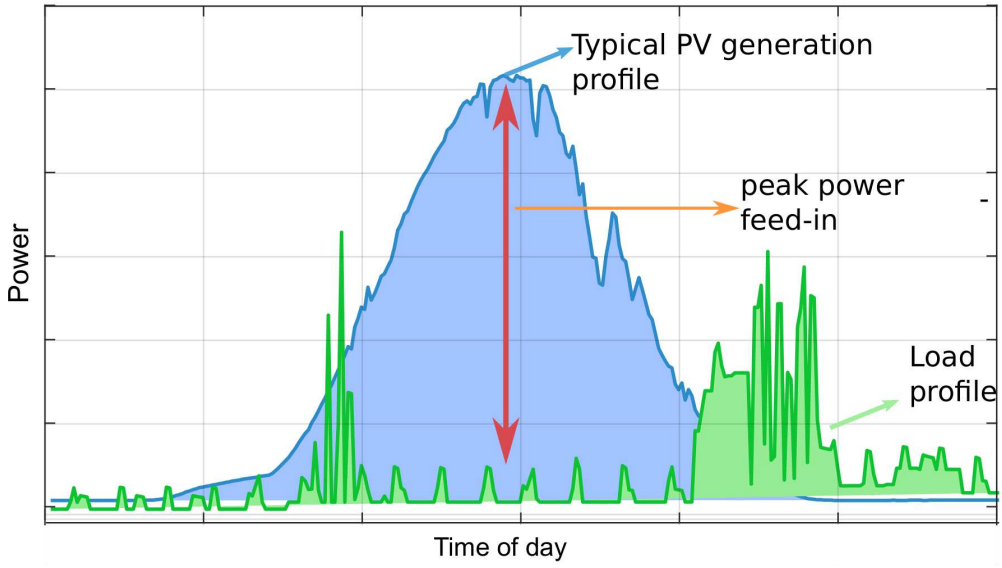

Figure 1.2: The supply/demand imbalance arising from mismatch between typical PV generation and load demand. Data from Lindenberg, Germany [7].

Grid congestion is any situation in power networks which can drive the voltage and frequency (in AC grids) beyond their permissible limits. It arises when there is too much electricity demand or generation in grid. In electric networks with conventional generation this was mostly isolated to periods of peak demand. The non dispatchable, intermittent nature of renewable generation increases the likelihood of this scenario as the generation is not coupled to load demand. This results in generation not occurring during peak load period, resulting in grid imbalance. A classical case is shown in Figure 1.2, where PV generation in a power network and the associated load profile is shown. The high PV generation in the afternoon is not countered by the load demand, resulting in peak PV power feed-in to the grid. Considering increasing penetration of renewable sources such feed-ins from multiple sources can severely congest the grid. This is capable of affecting the voltage quality in the grid. [12, 17–19]. There has been many reported incidents in European countries like Germany, Spain , Ireland and Belgium among others. pertaining to voltage quality in the grids, especially on the low voltage (LV) side, resulting from the increased penetration of renewable energy sources [13, 15, 20]

The issue with stability stems from the reduced inertia associated with the grid under increased renewable energy penetration. In the conventional generation there is energy buffer (inertia) available through the kinetic energy of large rotational masses formed by the synchronously connected generators and turbines. This inertia caters to sudden power imbalances in grids, thereby arresting the frequency drop in the network,

while the control system increases the set points for the generators. In case of renewable sources this is not the case. Source like PV system have very little stored power in them leading to low energy buffer. In cases like wind turbines the power converter interface connecting them to grid electrically decouples them, thereby limiting their contribution to the total system inertia. [21,22]. A recent blackout event in Australia [23] highlighted the limited contribution from wind generation in preventing the same.

These issues calls for supplementary measures to be put in place to facilitate a better transition to a renewable source based generation in electric grids. Currently a widely employed practise by the grid operators is curtailing the renewable generation by putting limits on the maximum feed-in power from these sources to the grid. An example of this is the German Renewable Sources Act of 2012, where PV systems with capacity less than 30 kW are to limit their grid feed-in to 70% of their nominal power rating. This brings about 30% curtailment of PV power during peak generation period [24] and thereby limiting their contribution to the total electricity demand.

Alternate enabling techniques, for integrating RES, that are now being considered involve Demand response (DR) and Energy storage systems (ESS). DR encompasses "different strategies by which commercial, residential, and industrial electricity customers are incentivized to adjust, in the short-term, when they use electricity" [25]. This will ultimately result in peak shaving and valley filling from the load perspective promoting more supply-demand balance in the grid. The pre-requisite, though, for DR is that there are willing consumers having flexible loads whose operation can be shifted in time to coincide with the peak generation period of renewable sources. The major drawback of DR is that they are constrained by the spatial and temporal patterns of load consumption [25,26].

ESS includes various technologies like battery storage system (BESS) [27, 28], pumped hydro storage (PHS) [29], compressed air energy storage (CAES) [30], hydrogen storage [31], supercapacitors (SC) [32]. These ESS can store energy during periods of high generation to be used at later time, thereby providing valley filling and peak shaving capabilities. The advantage with ESS is that they don't have the spatial and temporal constraints. The major drawback is the technological readiness in some case and the storage capacity of these systems [1]. It should be noted that not one technique alone, DR or ESS, can effectively solve all the issues that can rise in electric networks due to renewable generation. In fact both these (DR and ESS) have been earmarked as strategic techniques to facilitate the integration of renewable sources [25]. This Ph.D

work focusses on the role of ESS in facilitating the growing integration of renewable sources. The specific focus area will be discussed in the upcoming sections.

1.2 An overview of ESS in electric grids

The use of ESS in stationary applications like grid connected system can be traced back to early days of power generation where lead acid accumulators were used to provide residual DC load when power generating units where shut down at night. In the era of AC generation and transmission, when utility companies identified the flexibility offered by the ESS the first energy storage system, PHS, was put to use in 1929. Nevertheless, they were all limited to very specific application [33]. During the oil crisis of 1970s the idea of ESS as an alternative for intermediate and peak loading units gained prominence. Nevertheless, a large scale implementation of this never materialised due the price reduction in fossil fuels once the oil crisis was over [34]. Nonetheless, large scale storage system like PHS and CAES continued to be used sparsely in the grid to achieve load levelling, valley filling functionalities [35]. Currently integration of ESS in electric grids is undergoing a renaissance, mainly driven by the following factors [36–38]

- Increased penetration of intermittent renewable sources
- Need for alleviating transmission network congestion due to capacity constraints
- Obtaining maximum benefit from price arbitrage, through load shifting in a deregulated electricity market.
- Increasing interest in electric vehicles
- Growing emphasis to smart grids, distributed generation and load aggregation
- Advancements in various ESS technologies.

The ESS provide different roles and services across the network for various stakeholders namely, power system operators, utilities and customers. In the case of utility operators, the benefits that can be drawn from ESS vary depending on the nature of the storage systems, whether they are long or short terms storages. The long term storage systems provide functionalities like energy arbitrage, load levelling, peak shaving, non-spinning/spinning reserve and black start capabilities which improve the flexibility

Power system operator	**Utilities**	**Consumer**
Load levelling	Transmission deferral	Improved power quality
Peak Shaving	Distribution deferral	Increased self sufficiency
Spinning reserve	Resource adequacy	Back-up power
Energy arbitrage	Congestion relief	Bill management exploiting variable pricing
Black start capabilities		
Frequency, voltage control		
Improving grid resiliency		

Table 1.1: Functionalities of ESS in the electric grids.

of grid operation. The short term storages enable improving power quality through ancillary services like frequency, voltage control. They can also improve the grid resiliency during increased and prolonged outages caused by extreme weather scenarios [1, 4, 38].

Utility services including the transmission and distribution networks are mainly benefited by the ESS through upgrade deferral of these networks, by providing resource adequacy and congestion relief. Through proper deployment of ESS, infrastructure upgrade can be delayed or entirely avoided providing economic benefits. They can also provide cheaper alternatives to generation upgrade and alleviate congestion in the networks. In the customer level, deployment of ESS as a behind the meter system can provide bill management capabilities by enabling selective drawing of power during periods of low power pricing. In the customer premises ESS can ensure more self-sufficiency for prosumer (producer/consumer) effectively managing the power within them through minimum interaction with main grids. They can also provide ride through capabilities during minor grid anomalies and improvement of power quality. The different functions provided by the ESS across the grid is summed up in Table 1.1 [1, 4, 38].

1.2.1 Classification of ESS

As mentioned above there are different types of ESS, being considered and currently employed in the electric grids. Nevertheless, not all ESS are of the same type, nor can

Electrical energy storage	**Mechanical energy storage**	**Chemical energy storage**	**Thermal energy storage**
Supercapacitors	PHS	Battery (Lead acid, Li-ion, NiCd, NiMH, NaS, Redox flow Batteries)	Aquiferous cold energy storage, cryogenic energy storage
Superconducting magnetic energy storage (SMES)	CAES	Fuel cells (Hydrogen based or Methanol)	Steam or hot water accumulators
	Flywheel	Solar hydrogen, Solar Metal	

Table 1.2: ESS classification based on the form of energy storage.

they do all the above mentioned functions and they differ in the way energy is stored. An understanding of the different ESS is essential in identifying which ESS is to be considered for a specific application.

The different ESS store electrical energy in different forms. This can be as electrical, mechanical, chemical or thermal energy. The classification of ESS based on the nature of their energy storage is provided in Table 1.2 [1, 2, 39].

The ESS can also be classified based on the applications they are subjected to in the grid. This is shown in Figure 1.3, where the ESS are classified based on the two generic functionalities they are subjected to in the grid namely, power quality-reliability management and energy management. This categorization is done based on the physical capabilities of the ESS, whether they have high power or energy density. High energy density storage systems are those characterised by their ability to store large amount of energy. These include the storage systems that are used for energy management due to their ability to take in and supply energy for longer durations. Nonetheless, these storage systems are usually characterised by their slow response sometimes mostly due to

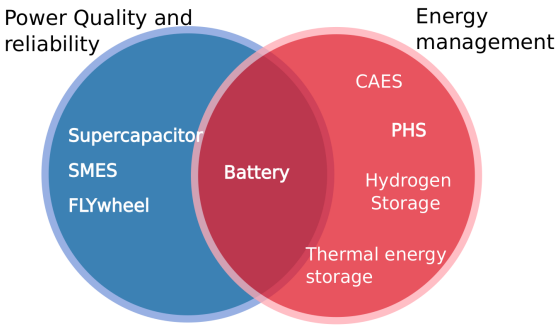

Figure 1.3: Classification of ESS based on their functionality [1, 2].

their physical constraints [1, 37, 39, 40]. The high energy density ESS contribute mainly towards alleviating congestion issues in the power grids and energy arbitrage.

The ESS used in the power quality and reliability (stability) management usually exhibit high power density. The power quality and reliability issues in electric grids are caused by sudden power variations. In this scenario, to ensure the power quality, the ESS used should be capable of very fast power response to counteract sudden changes. High power density ESS can provide or absorb large amount of power, albeit for a short duration as they have low energy capacity. Battery storage can fall under both categories depending on their sizing. The high power density ESS contributes to tackling the stability issues through emulation of virtual inertia in the grid [1, 37, 39].

The ESS should also be identified based on their ability to store energy without undergoing self discharge. ESS like Flywheels are characterised by their very high self discharge rates, which limits their energy retention capabilities. This requires that the energy stored in them be utilised quickly and cannot be used in scenarios where high storage duration is needed [1]. Lithium ion (Li-ion), Nickel Cadmium (NiCD) and lead acid based battery technologies can store energy in them for several days due to very less self discharge (2%-5% per month). On the other hand Nickel metal Hydriode (NiMH) and Sodium Sulphur (NaS) based battery technology shows higher self discharge rate of 5%-30% per month [1,4,27]. Electrical energy based storage systems like supercapacitors, SMES have discharge rate in the range of 5%-40% and 10%-30% per day receptively [4, 41, 42]. Finally hydrogen based storage technologies, Redox flow Batteries, PHS, CAES and thermal energy based storage systems exhibit negligible if not no self discharge [1].

ESS are also characterised based on the round cycle efficiency. The round cycle efficiency is indicative of the energy lost in a charge discharge cycle of the ESS. This measure can provide a good indication in the selection process of the ESS technology for a particular application. The comparison of round cycle efficiency of the different ESS technology is provided in Table 1.3. It should be noted that the conclusion depicted here does not consider the self discharge of the ESS [1, 37].

Efficiency range	**Energy Storage System**
$< 60\%$	Hydrogen Storage (with Fuel cell), Solar Hydrogen, Solar Metal, Thermal energy storage
60%-90%	PHS, CAES, Batteries (Lead acid, NiCd, NaS, Redox flow batteries)
$> 90\%$	Batteries- Li-ion, SMES, flywheel, supercapacitors

Table 1.3: Round cycle efficiency comparison of different ESS technology [1, 2].

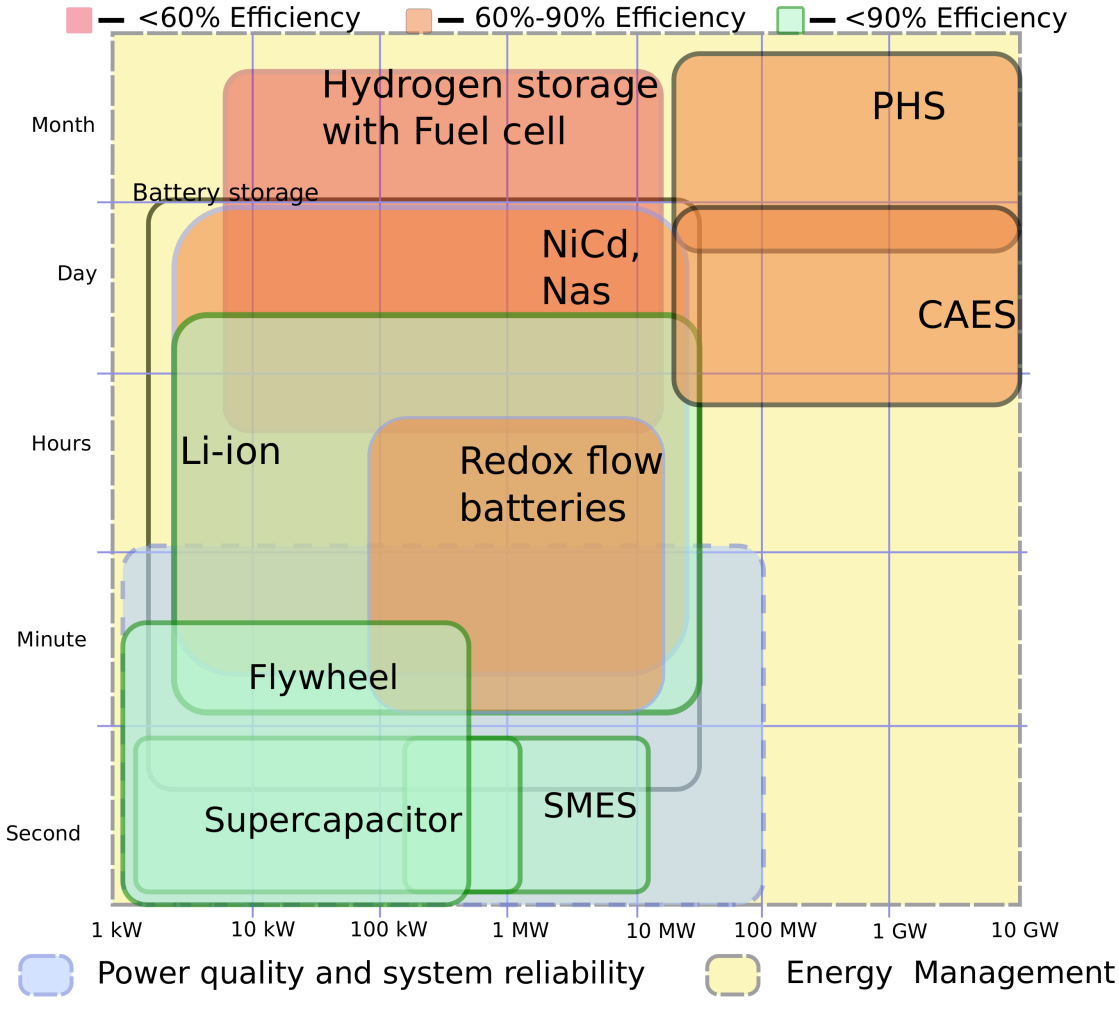

Figure 1.4: Comprehensive representation of ESS classification based on their capacity, functionality and efficiency [1, 4, 5].

1.2.2 Need for hybrid storage solutions

As evident from the previous section a single ESS technology cannot solve the multitude of problems arising in electric networks. Therefore, it is essential that hybrid storage solutions comprising of ESS belonging to different groups as shown in Figure1.3, 1.4 be considered in electric networks. The high power density ESS can meet the sudden power change requirements in the grid while the slower, high energy density ESS ramp up in power. This ensures that power quality is maintained in the grid while minimising degradation effects in the slow acting ESS. Afterwards long term energy imbalances will be met by high energy density ESS. The hybrid storage solutions offer lot of advantages for ESS deployment in electric grids which can be summed up as follows [37, 43, 44]

- Optimal solution in terms of total capital cost of investment
- Optimal solution in terms of ESS sizing
- Improved thermal management for ESS
- Reduction in rate of degradation and improved lifetime of ESS.

The Figure1.4 shows how different ESS technologies contribute in terms of power, discharge time and towards different functionalities in the grid. It enables a clearer understanding on the need for hybrid storage solutions to cover the entire spectrum of demands arising in the grid.

1.2.3 Current status of ESS integration in electric grids

As mentioned before there has been an increased deployment of ESS in electric grids of lately. Currently the installed capacity of ESS around the world is around 167 GW. The major share in this (160 GW) comes from PHS [3]. The higher contribution from PHS arises due to the fact that it was the widely considered storage mechanism in grid during the early days resulting in the wide scale deployment of them. Nevertheless, they are not considered as the main solution when it comes to implementing ESS in grids nowadays, due to their many disadvantages like high cost of investment, high lead times, lack of suitable sites and maturing of other storage technologies [5, 45]. This is also evident by the fact that PHS installation have been coming down in the last few years [3].

Electro-chemical storage currently accounts for 3.3 GW (considering only large grid connected system without accounting for smaller behind the meter installations) of total ESS installation in the world. The maturing of this technology has seen an increasing deployment of the same highlighted by the fact that 50% of the total ESS commissioned in 2018 is battery based systems. There has been an increased emphasis on combined renewable energy (PV, wind) and storage projects (battery) in 2018 [3]. Many such utility scale battery storage projects have been commissioned in 2018 like 25 MW (25 MWh) in Australia [46], 1 MW (1.3MWh) in Scotland [47], 48 MW (50 MWh) in Germany (single largest installation in Europe) [48] and cumulative 200 MW in the UK [49]. There are also plans on commissioning 568 MW (2.3 GWh) capacity battery storage in the United states [50] and 13 MW (40 MWh) battery system in Republic of Korea [3]. These utility scale installation have also shown to lower overall system costs in electric grids [51]. Apart from these large scale installations, the last few years has seen an increasing number of behind the meter installation in many European countries and Australia [3]. The battery technology considered in most of the above cases have been Li-ion based battery systems [3].

Hydrogen based storage using power to gas plants is also gaining in prominence [31]. The objective is to use surplus energy from renewable sources to generate hydrogen through processes like electrolysis which can then be utilised to develop clean power using technologies like fuel-cells (FC) for stationary applications [52]. Nevertheless currently most of the Hydrogen (95%) used for energy storage is generated from fossil fuels [53]. Despite this, the general consensus is that Hydrogen based storage will play an increased role in renewable generation integration and find extensive application in stationary and transport sectors. This also evident by the increased commitment from China and Japan towards the same [54,55]. Apart from high energy ESS, there has always been emphasis on using high power density ESS for power quality improvement in many countries [3].

1.3 The role of microgrids in modern electrical networks

Another impact of increased penetration of renewable sources is the shift from centralised to distributed generation (DG) utilising distributed energy resources (DER). DG is defined according to [56] as “An electric power source connected directly to the distribution network or on the customer side of the meter”. DERs need not be necessarily renewable sources, but the distributed nature of the renewable sources like wind

and solar energies have accelerated the shift to distributed generation [21]. Another major reason for the advent of DG is the ageing and saturated electric networks. In this context DGs can provide economic benefit through deferral of investments in larger generating units, transmission and distribution capacity enhancement. DERs also have lesser lead time in deployment, can contribute to power quality improvement, provide ancillary services and ensure enhanced reliability [21, 57, 58].

In order to facilitate the increased utilisation of DERs the concept of microgrids where put forward to manage locally the energy generated by the DERs and demand by forming subsections in the larger grid. In this context microgrid is defined according to the US Department of Energy as [59] "A microgrid is a group of interconnected loads and distributed energy resources within clearly defined electrical boundaries that acts as a single controllable entity with respect to the grid. A microgrid can connect and disconnect from the grid to enable it to operate in both grid-connected or island mode". As defined the microgrids have two modes of operation: a) grid connected mode where there is power exchange between the microgrid and main grid and b) islanded mode where microgrids support loads on its own and is disconnected from the main grid. The islanded mode is usually enforced during fault events in the main grid or in geographically isolated locations like islands where drawing long lines connecting to main grid is physical and economically not viable [60]. In the latter the microgrid is always operating in islanded mode. Traditionally intentional islanding in grids is something which was not allowed to avert any risk to maintenance operations. Nowadays new standards like IEEE Std 1547.4 [61] encourage islanded operation for microgrids and provide guideline for the same. Apart from DG, the factors which have driven the development of microgrids are summed up as [11]

- Economic Benefits- infrastructure cost saving through investment deferrals, fuel savings by eliminating transmission/distribution losses, ancillary services.
- Energy Security- Microgrids can supply critical facilities in their vicinity even when main grid is down from weather disruptions. Isolated operation of microgrid can override cascaded outages and are less vulnerable to cyber-physical attacks
- Aids increased penetration of renewable sources.

Microgrids, due to their smaller generation capacities and dependencies on DER tend to have very low inertia, resulting in need for a system which can emulate resilience.

Apart from this, in the islanded mode of operation microgrids need to be self sufficient in meeting their load demands. These requirements can be achieved to some extent using ESS in microgrids. This again highlights the relevance of ESS in modern grids.

1.4 Why the need for research in ESS integration??

Though the title of this subsection poses a question as to why the need for research in different aspects of ESS integration the answer should be fairly evident by now. ESS is going to play a major role in the future grids with the increasing penetration of RES and rise of microgrids. There is an ever increasing trend towards incorporating ESS in stationary grid connected applications as highlighted in Subsection1.2.3. This makes it imperative the need for research in these ESS technologies, their interfacing system (power converters) and control/management of these devices to ensure maximum benefit from the ESS integration.

In the area of research of ESS technology the focus is on developing newer more efficient ESS, improving the older ones in terms of their lifetime and round cycle efficiency which ensures economic benefit [62, 63]. In the case of interfacing power converters the research focusses mostly on developing newer power converter topologies which can be more efficient, more compact, requires lesser filtering requirement and utilisation of more efficient wide bandgap semiconductor devices [4, 63]. Finally in the area of control and management of ESS the research focusses on two aspects. The first, is in developing robust control systems for ESS and interfacing power converters to ensure a fast responding unit to load changes thus emulating grid resilience (synthetic inertia), provide active-reactive power (for AC grids) control and maintaining power quality. The second aspect of research is on developing algorithms which carries out energy management of ESS and various generating sources in the grid so that certain objectives are met. The objectives of these algorithms involves ensuring economic benefit from energy arbitrage, grid congestion relief, increased self consumption of renewable power or reduced degradation of ESS to name a few. Reducing the degradation rates of ESS and in turn the increase in lifetime through energy management will ultimately lead to economic benefit as it allows to get maximum returns from the investment made in ESS.

In this context, the general focus of the thesis is on the control and management of ESS in microgrids. The thesis will focus on both the aspect of robust control system

design and developing optimal energy management algorithm to meet some identified objectives (which will be discussed later). The specific problem statement will be presented in the subsequent section. Prior to that an overview of the entire control architecture and how the different aspects, robust control system and energy management stage, mentioned above is integrated into this architecture, will be presented.

1.4.1 Control and energy management architecture for ESS

As mentioned above there are two stages of developing a robust optimal control architecture for ESS in microgrids. The robust, real-time control side which takes care of system stability and power quality is defined as the power management side. The control action at this stage is fast, instantaneous, load following and results in real-time control of the power in the system. The energy management side as the name suggests manages energy stored in the ESS at any point of time. This needs to be done optimally based on some predefined objectives. As it is about energy management the intended control action is more long term and updated at a much slower rate in comparison to power management side [64].

The power and energy management stage, therefore, works in two time scales. The two stages are incorporated in the same system through a hierarchical control architecture. This hierarchical control scheme is classical in microgrid control [64, 65]. This makes sense as the control and energy management of the ESS in turn results in stability and energy exchange within the microgrid, effectively resulting in microgrid control. The hierarchical control scheme is now recognised in the IEEE Draft Standard for the Specification of Microgrid Controllers [66].

Adhering to the same, a hierarchical control architecture that will be adopted in this work as shown in Figure1.5. The power and energy management stages are clearly demarcated here. The control architecture presented here is a generic scheme for microgrid having RES generation, ESS and local loads. As can be seen the microgrid can be operated in islanded mode or in grid connected mode. The microgrid is modelled as an aggregated capacitance C_{grid} whereas the load is modelled as an aggregated resistance R_{load}. It should be noted that the ESSs are interfaced to the microgrid through power converters thereby ensuring controllability over the power that is being supplied. An overview of the different levels is provided next.

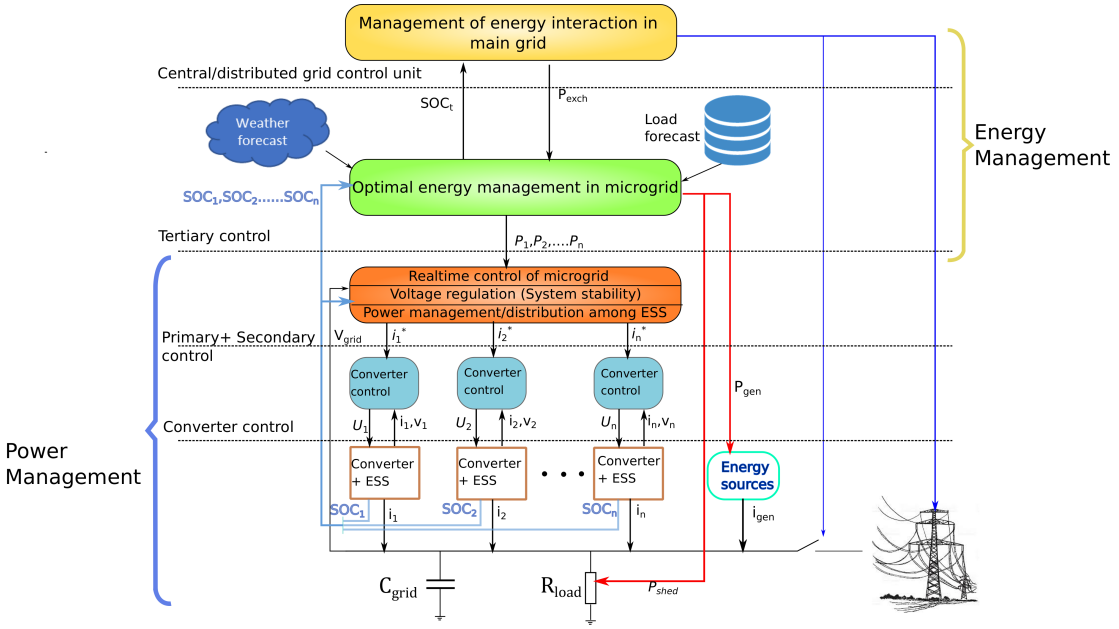

Figure 1.5: Hierarchical control architecture for ESS in grids.

Power Management stage

The power management as mentioned above, ensures the stability, power quality in the grid through the real time management of power among the ESS and within the grid. In this regards this stage is characterised by very small sample times ($ms - s$ range), instantaneous fast control actions being updated at a higher frequency and operates in real time. According to Figure1.5 this stage receives as input, the sampled value of grid voltage, frequency (AC network), currents from each interfacing converter and SOC of each ESS. The power management stage also receives set-points generated from the energy management level as inputs as shown in Figure1.5. The power management level is further distinguished into two parts: the converter control and the primary+secondary control part.

The converter control stage deals with the control of each interfacing power converters. The main objective is to regulate the power flow through the converter based on set-points generated from the higher levels. In this context, the objective of this control layer is to ensure robust set-point tracking by the power converters. The set point tracking in power converters can be achieved in many ways like using the classical PI controller [67], sliding mode controller [68] or differential flatness theory based controller [69]. This control layer is embedded in each interfacing converter and the set-point to each, is based on the output from energy management and primary+secondary level.

This control layer is also provided the sampled current from the output of individual converters as feedback input.

The primary + secondary layer of the power management level is tasked with the maintaining stability, power quality and distribution of power among the ESS in the microgrid. In the microgrid formed by the interconnection of the ESS, RES and loads, this control layer monitors the grid voltage, frequency (AC network). Based on their deviation from nominal value this control layer computes the necessary control action to keep these parameters within prescribed limits. These system parameter variations arise from unaccounted load or reactive (ac network) power variation and if not handled properly can make the microgrid unstable or affect the power quality. The control action generated by this layer needs to be split among the various ESS and dispatchable generating sources (if any available) appropriately. The power splitting is done by the primary side of the primary +secondary control layer. In ESS this can be done with frequency based splitting [70] or using droop control [71] based techniques. The maintenance of system parameters (voltage and frequency) within prescribed limits is achieved by the secondary control part of the primary +secondary control layer. Thus to sum up, when sudden load change induced grid parameter value deviation occurs, the primary+secondary control layer arrests this deviation and brings the system parameter values to prescribed level while splitting the control action to the various units in the microgrid (ESS or dispatchable generation unit) appropriately. This layer receives reference values from the energy management side and modifies them depending on the system behaviour to maintain stability/ power quality. This modified set-points are then passed on to the converter control layer. This primary+secondary layer is provided with the sampled value of system voltage and frequency (AC network) as feedback inputs. In the power management stage the converter control layer is always faster than the primary+ secondary layer.

Energy management stage

The energy management stage handles the energy scheduling among the different units like ESS and dispatchable sources This is done such that some objectives like system operation cost is optimised [72, 73], ESS degradation rate is minimised [74] or grid performance like congestion is alleviated [75]. The minimisation degradation of ESS is imperative as it allows maximum utilisation of the investments made in setting up the

ESS. If the energy handled by the ESS is not properly managed they can undergo rapid degradation which results in need for their replacement and more capital investment. The grid congestion as mentioned before arises from the RES integration. Integrating ESS will not simply solve the issues with RES. Inorder to ensure RES are grid friendly, the energy should be managed appropriately using the ESS so that they are supplied to the grid at right instances. These issues will be discussed in detail in later chapters. Nevertheless, it should be emphasised that the energy management state is crucial to achieving this. As this level deals with the energy interactions the control action is updated in longer time intervals. As such this stage tends to be slower than the power management side with sampling time in the range of minutes-hours. The input to this stage is abstract like the system states which in this case will be State of charge (SOC) or state of hydrogen (SOH) of the ESS. The grid parameters like voltage or frequency are not considered here as their control require faster action. This stage is also provided with prediction on RES generation and load profiles. The generated set-points from this stage is then send as input to power management side. The energy management side can be distinguished into two layers as well: the tertiary control layer and central/distributed grid control unit.

The tertiary control layer forms the centralised energy management unit for the microgrid. It can make the energy management decisions heuristically using rule based [76, 77], fuzzy inference methods [78] or analytically using optimisation based techniques [74] . The ESS states, predicted load and generation profile for the microgrid are provided as input to this layer. The output of this layer are the set-points for ESS and dispatchable generation sources which are applied to the power management side. The power management stage will then work around these set-points and compensate for the system variations that occur between the sampling instants of the tertiary layer, thereby maintaining system stability

The central/distributed grid control unit deals with the energy interaction in the main grid. The microgrid when viewed from the main grid can be abstracted as a energy unit for e.g aggregated as the total energy stored in all the ESS. This control layer will then allow the main grid to regulate this energy in a centralised or distributed way such that, when needed, the microgrid can aid the operation of the main grid. This layer forms the highest layer of the control architecture and is the slowest with sampling times in the range of hours.

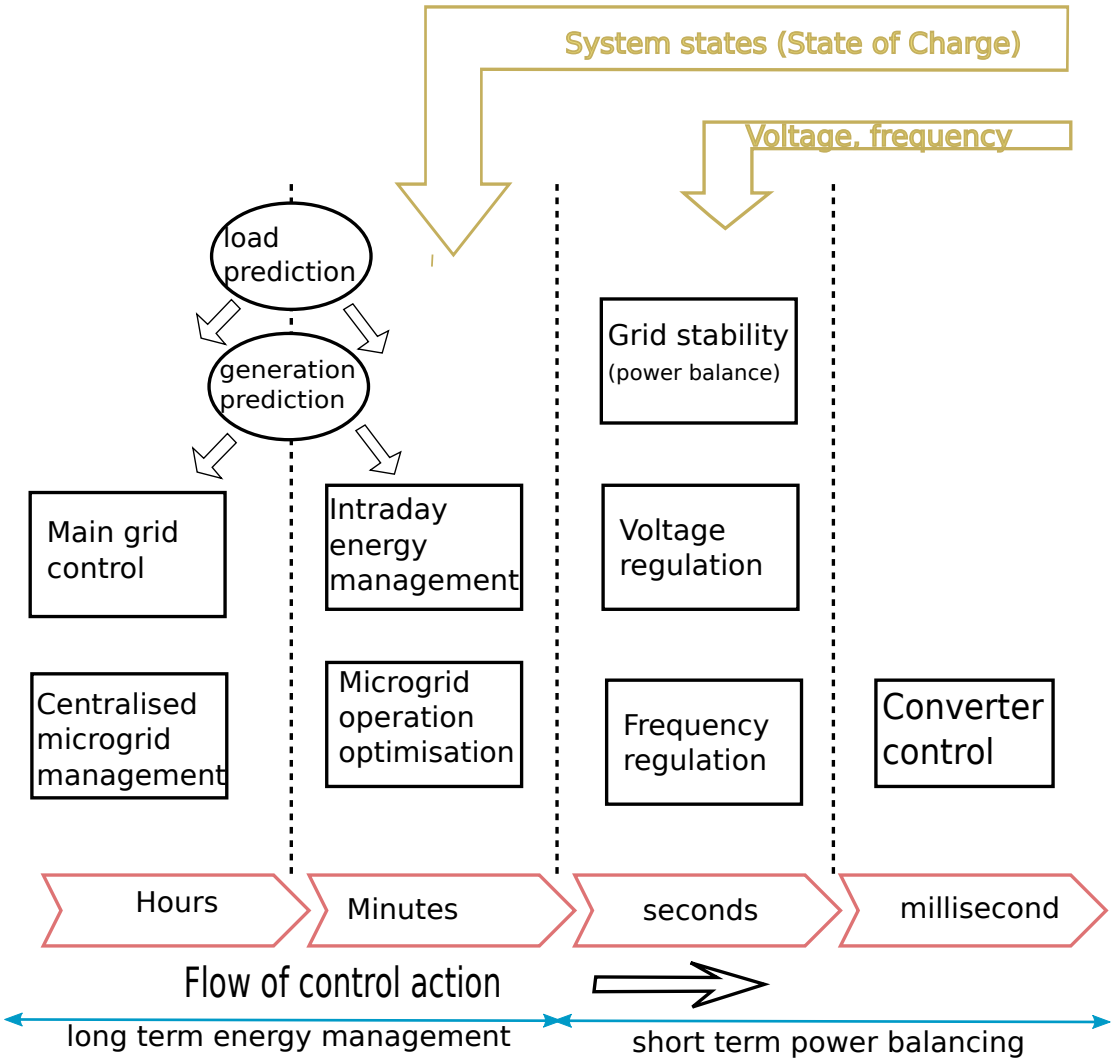

Figure 1.6: The hierarchical control architecture for the control of ESS in electric grids, represented from the perspective of the functions performed at each level. The flow of information from the grid and control action to the physical system is shown

Therefore, the different layers in the hierarchical control architecture are brought together, in a unified framework, to ensure the stable and optimal operation of the microgrids. The different levels operate at different time scales achieving short term power balance functionality and long term system operation optimisation. There is flow of system information from the lower to higher levels whereas there is flow of system control action from higher to lower levels. As the control action move down through each layer they are amended to shorter time intervals which will be finally executed by the converter control layer. The flow of system data, control action, the time scales and the functions carried out by each layers can be visualised in Figure1.6

1.5 Thesis objective

In light of all the above discussions the general objective of the thesis is defined as: "*Implement a control architecture for a hybrid ESS in a DC microgrid with RES such that it*

(a) *aids the increased penetration and self consumption of RES at all instances*

(b) *provides robust stable microgrid operation and improved power quality under intermittent, non-dispatchable renewable generation*

(c) *provides real time power management among the hybrid ESS*

(d) *provides optimal energy management of ESS such that the renewable generation remains grid friendly while maintaining efficient and economic microgrid operation under intermittent generation.*

(e) *minimises rate of degradation of ESS during the continuous operation so that maximum returns on the capital investment made can be achieved.*"

The general control architecture presented in Figure1.5 will be considered for the same. In achieving the general objective the following steps will be undertaken

- Identify the state of art and scope for improvement in each level of control architecture
- Improve converter control stage performance by proposing controllers for interfacing power electronic converters which will not significantly impact the grid power quality during ESS power interaction with the grid.
- Propose a primary + secondary scheme that provides a robust, stable control of microgrid under intermittent renewable generation and ensures improved voltage regulation performance. The proposed scheme will also include a optimal power splitting strategy of the control action among the ESS based on their characteristics. Special significance will be given to ensuring high operational efficiency and to ensure that a particular ESS is not overly stressed leading to excessive degradation.

- Develop a tertiary control layer based on the identification of some real world scenarios where RES poses issues to the current grid infrastructure. The developed tertiary scheme will implement state-of-the-art techniques to provide on-line optimal energy management of ESS to mitigate these issues while ensuring minimal ESS degradation. Critical to achieving this is having good predictions about generation and load profiles. To this end emphasis will be placed on surveying, developing forecasting techniques and identifying the most suited one for the considered scenario.
- Verify the proposed controllers through simulations and wherever possible through experimental validation.

It should be noted that this thesis will not deal with the aspects of central/distributed grid control layer discussed before.

1.6 Thesis outline

The rest of the thesis is outlined as follows. The Chapter 2 provides an overview of the hybrid storage system considered in this work, their operating principle-characteristics and general microgrid architecture for which the control and energy management solutions are developed in this work.

Chapter 3 will deal with the contributions in converter control stage. An overview of the existing state-of-the-art will be provided and a novel control strategy will be proposed for the converter control. The objective of this controller will be to improve the transient response of the converter system. This chapter will outline the design of proposed controller, development of simulation models and experimental validation of the same. Robustness and stability analysis will also be carried out in this chapter.

Chapter 4 will be about the primary+secondary control scheme. A novel power splitting strategy for the hybrid ESS will be presented in this section taking into consideration the degradation mechanism and physical characteristics of the different ESS. This chapter will also present an improved voltage regulation control for the DC microgrid with the aim to improve the power quality and transient behaviour. In this context the design of the proposed methodology will be presented and simulation models will be developed.

Chapter 5 will present the methodology employed for the predicting generation and load profiles. The chapter will present some forecasting methodologies which can be used in the tertiary level to enable better decision making in the energy management. The formulation of prediction system and the results obtained from the same will be presented.

Chapter 6 will outline the tertiary control layer. The main focus, as mentioned above, will be on presenting some real world issues due to RES integration and demonstrating how efficient energy management of ESS can be used to overcome the same. In this context some state of the art energy management techniques will be analysed and developed for the microgrid with hybrid ESS system, in this chapter. The proposed energy management system will be formulated to mitigate the issues in the grid arising from RES integration, promoting self consumption of RES power and minimising degradation of the ESS. An extensive analysis that demonstrates and quantifies the performance of the tertiary control stage will carried out in the chapter. The chapter also addresses the energy management problem in the grid connected and islanded mode of operation. The verification of the proposed energy management system will be carried out through simulations. Finally, the work in this Ph.D will be concluded through Chapter 7.

Chapter 2

Hybrid System Overview

This chapter introduces the DC microgrid and the hybrid ESS architecture considered in the work. A generic overview of the microgrid with hybrid ESS considered is presented along with a short discussion on the working principle, energy storage mechanism of the different ESS. An overview of the test setup used for experimental verification of various control strategies will also be presented. Finally a short overview of the design, simulation and experimental implementation tools considered will also be discussed.

2.1 System overview

The Figure 2.1 represents the generic aggregated scheme of the microgrid with the hybrid ESS considered in this work. In this work, the RES considered will be mostly PV system and as such the same is shown in the microgrid scheme. The generating source and the ESS are connected to a DC bus through its interfacing DC-DC converters. This ensures controllability over the power that is delivered by these systems. The DC bus supplies the microgrid load or interacts with the main grid through an DC-AC converter. The proposed microgrid is capable of both grid connected mode of operation or in islanded mode disconnected from the main grid. The different ESS considered in the work are SC, battery and hydrogen storage with fuel cell (FC) -electrolyser system with DC output.

It can be seen that the case considered in this work utilises two high energy density ESS for the microgrid system. Typically, a hybrid combination of one type of high energy

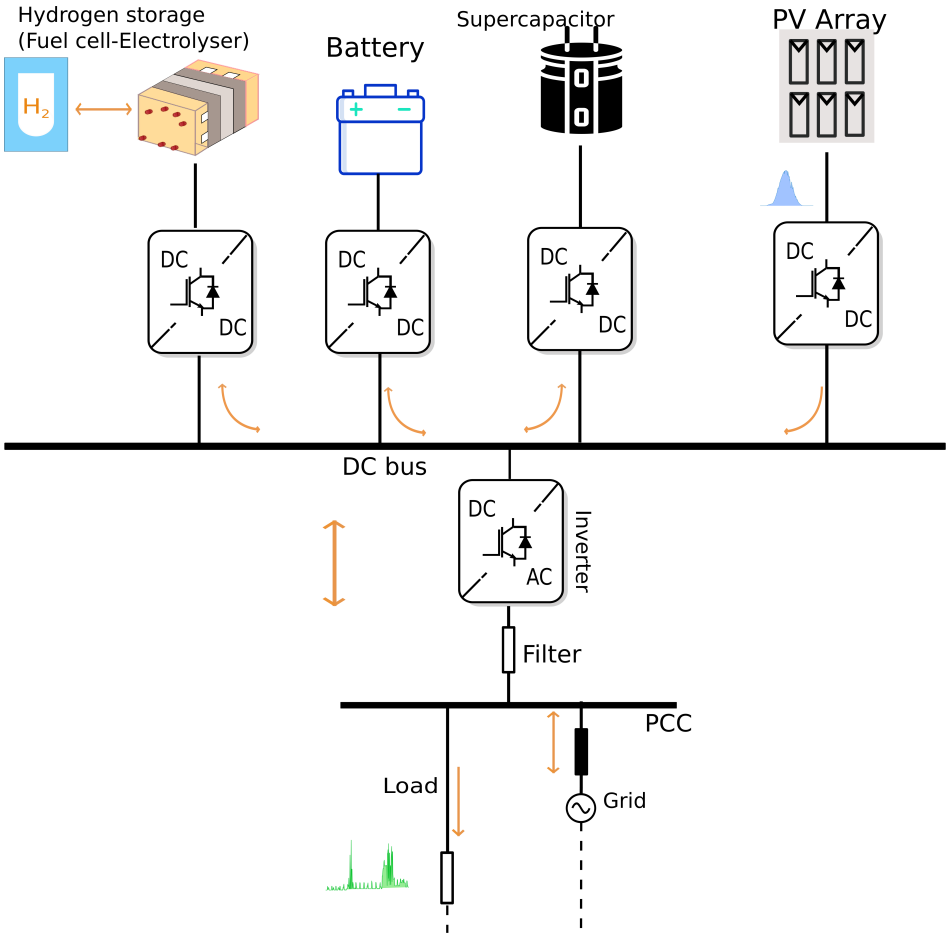

Figure 2.1: Schematic of microgrid with PV generation and the hybrid ESS considered.

and high power density ESS is capable of meeting all the requirements in the grid. In some scenarios like islanded operation a large energy storage capability will be beneficial to ensure increased utilisation of RES generation, self-sufficiency and reliability in grid operation. In this case, the capacity demanded from the high energy density ESS will be high. Conventional high energy density storage like PHS or CAES can easily meet this high capacity requirement in an efficient and economical manner [1]. Nevertheless, the utilisation of these ESS are nowadays limited due to their adverse impact on the environment and difficulty in obtaining suitable sites for their integration [5]. Battery systems provide a very good solution when there is a need for high energy density, especially from the perspective of operating efficiency. However, when large storage capacity is need batteries may not be economically viable. This is mainly due to the high storage costs associated with battery systems [37]. The reason for the same being, battery stores energy internally resulting in a very large capacity battery that will be expensive. Therefore, in scenarios where large storage capacity is needed the battery

needs to be used in conjunction with another ESS that has low storage cost. The FC-electrolyser system with hydrogen storage can ensure the same. The FC systems store energy externally in the form of fuel (like hydrogen). As a result, increasing the storage capacity only involves increasing the capacity of the external tanks storing the fuel and not the FC system itself. This results in low storage costs [37]. The FC system also presents an interesting choice among the other high energy density ESS due ti technological readiness [1]. However, FC systems have poor round cycle efficiency and using them alone as a high energy density storage device may not advantageous in terms of efficiency. Therefore, in situations that demand high energy storage capability, currently, a combination of battery and FC can provide optimal solution as a trade-off between operation efficiency and economic factors [1, 37].

In this type of hybrid combination, the battery typically cater to mid-term imbalance and hydrogen storage will take care of long term imbalances. Thus the imbalance spectrum (long and short term) presented in Figure 1.4 are met by the chosen hybrid ESS. This will be more evident through the discussion in the upcoming chapters

It should be emphasised that, in current scenario, most of the energy storage requirement can be achieved by using a battery alone. Nevertheless, in some case (especially islanded operation) both the battery and FC system need to be used in conjunction. In order to address all the scenarios, that can arise in the grid, the hybrid combination of SC, battery and FC system is considered in this work. Developing a control scheme accounting for all the characteristics of the three ESS, facilitates the development of a very generic versatile control strategy. The developed control system will be flexible, such that they can be easily modified to cater a less hybrid combination or even a single ESS. Finally, it should also be emphasize that this work does not claim that the combination of three ESS, as shown above, is the best possible. In some situations where PHS or CAES they can provide better solution, if they are an viable option. The operating principle, energy storage mechanism and characteristics of the ESS considered above (SC, Battery and FC system) is discussed next.

2.1.1 Supercapacitors

Supercapacitor, ultracapacitor or double layer capacitors as they are usually called are devices that store energy in an electro chemical double layer and are used in applications were fast charging, discharging is expected. In the physical structure, it is very similar to

that of a battery and might come across as an electrochemical storage device. However, unlike batteries these devices do not rely on a chemical process to store the energy but rather the electric field [1]. The idea of energy storage in an electrochemical double layer, used in SC, was put forward in [79]. The SC consists of two electrode plates immersed in an electrolyte containing positive and negative ions, separated by an ion permeable separator as shown in Figure 2.2. When an electric field is applied the energy storage in a SC happens through the charge accumulation along the surface separating the electrode and electrolyte as shown in Figure 2.2. There is no electron exchange happening between the electrode and electrolyte unlike a battery. This principle aids the faster charging and discharging of the SC. It can be seen in Figure 2.2 that the SC has charge accumulations at the two electrode thereby forming two capacitances C_1, C_2 connected in series and hence the name double layer capacitor. The total capacitance will therefore be $C_{eq} = \frac{C_1 \cdot C_2}{C_1 + C_2}$.

If C_1 and C_2 are the same it is called a symmetric supercapacitor. The large capacitance values are achieved by the SC due to two main factors: the large surface area of the electrode which is further enhanced using activated carbon and very low gap between the electrode and electrolyte (in the range of Å) [80] [81].

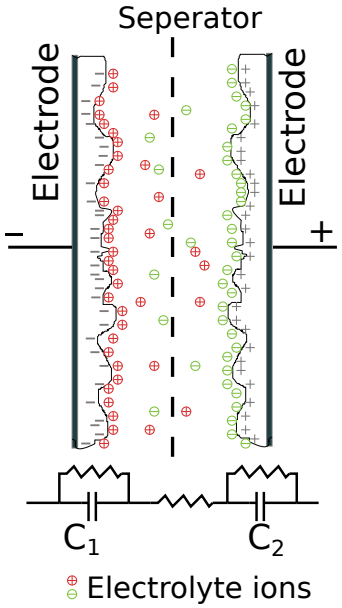

Figure 2.2: Supercapacitor internal assembly.

The charge accumulation at the electrodes under the influence of applied electric field is fast since the process only involves ions moving in and out. This allows the SC to respond to sudden changes in power requirement by charging and discharging quickly making it suited for catering sudden load variations. The absence of chemical reaction for energy storage in SC also results in lower degradation of electrodes under charge-discharge cycling [81]. Currently there are commercial SC from Maxwell that claim an energy density of 2.3-4 WH/kg and power density of 3600-6800W/kg for the modules. Apart from this commercial SC from Maxwell claim an estimated cycle lifetime in the range

of 1,000,000 cycles and a projected DC life (held continuously at the rated voltage) of 10 years at 25°C.

2.1.2 Batteries

Batteries are the oldest energy storage technology to be developed. The fundamental unit of a battery is an electrochemical cell formed by a positive electrode (anode) and negative electrode (cathode) separated by an electrolytic solution. In each cell redox reaction occur, which is responsible for electrical to chemical energy conversion and vice-versa. The electrolytic solution, formed by dissolved salts, forms a medium of ion transfer whereas an external electrical connection between the electrodes enables electron transfer and thus electrical power transfer [1, 27, 82]. A battery is formed by many such electrochemical cells connected in series.

There are different battery technologies used in stationary grid connected applications like Lead acid, Nickel cadmium, Sodium sulphur and Lithium ion. Among them, Lithium ion (Li-ion) batteries are increasingly utilised nowadays due to their higher energy densities, higher efficiencies, long cycle-life and rate capabilities [27]. This is also evident with the recent commissioning of many Li-ion battery based storage solutions for power grid and renewable sources like the Tesla Big battery in Australia [51], the Batwind (offshore wind with battery storage) project in Scotland [47], the 50 MWh battery storage in Germany [48] to name a few. The anode of the Li-ion battery is made of graphite with layering structure housing Li cells in it. The cathode is formed by Lithiated metal oxide like ($LiCoO_2, LiFePO_4$) and Li salt solutions make up the electrolyte. Li-ion batteries based on $LiFePO_4$ is increasingly used nowadays due to their higher safety and cost factor [1, 27, 82].

The ageing/degradation of the Li-ion batteries arises mainly from calender and cyclic ageing phenomenons. The calender ageing is the irreversible capacity loss in the battery occurring during the storage. In other words if a battery is kept in a charged state over a long period of time it is bound to lose its capacity. The rate of capacity loss is dependent on the operating conditions like temperature and charge (SOC) levels. Calender ageing in Li batteries are accelerated under high temperature and high charge storage. In high temperature operation, secondary reactions in the battery lead to loss of available Lithium in graphite electrode causing degradation. The high charge storage leads to huge potential disequilibrium at the electrode/electrolyte interface which accelerates

the degradation of the solid electrolyte interphase which is essential to the functioning of Li ion batteries. Therefore, high temperature and dwell times at high SOC levels are main scenarios to be avoided with Li-ion batteries to prevent rapid degradation in grid connected operation. The cycling ageing is the loss of capacity arising from the persistent charging and discharging of the battery during its operation. The cycling ageing is dependant on the factor ΔSOC, the cycle amplitude defined as the change in SOC undergone by the battery in one charge-discharge cycle. The larger the cycling amplitude the battery has to undergo, higher is the degradation. It should be noted that cycling ageing is a direct consequence of the battery utilisation and cannot be avoided entirely. Nevertheless care should be taken to limit, whenever possible, high magnitude cycles which can lead to increased degradation [83–85]. The end of life (EOL) of batteries is usually defined when the capacity fade arising from degradation reaches 80% of its rated value. The Li-ion batteries have an average lifetime of 5-15 years depending on the operating conditions or around 10,000 charge discharge cycles [1, 86]. The energy density of Li-ion batteries vary between 70-200 Wh/kg and power density between 150-315 W/kg [1].

2.1.3 Fuel cell-electrolyser system

The fuel cells and electrolyser, unlike batteries, is not an energy storage device. It facilitates conversion of chemical energy to electrical energy using hydrogen as a fuel and vice versa. Therefore, unlike batteries the energy storage is not done internally in the device but externally with the fuel (hydrogen). This enables the fuel cell based hydrogen storages to have a very high energy storage ability as this is directly dependant on the amount of hydrogen that can be stored. In other words they tend to have very low storage cost [37]. It should be noted that the fuel cell is simply a generator of electricity using hydrogen and unlike batteries cannot be used for taking in surplus power in the grid and the electrolyser is used to convert the surplus power to hydrogen.

First the fuel cell operation is discussed. The operation principle of fuel cell's energy conversion is very similar to that of a battery. It consists of two electrodes separated by an ion exchange layer and an external circuit which facilitates the electron exchange. The anode forms the negative and cathode forms the positive terminal in fuel cells unlike in batteries. In comparison to battery, the electrode material does not react and store the charge. Instead the external fuel undergoes redox reaction in the vicinity of the

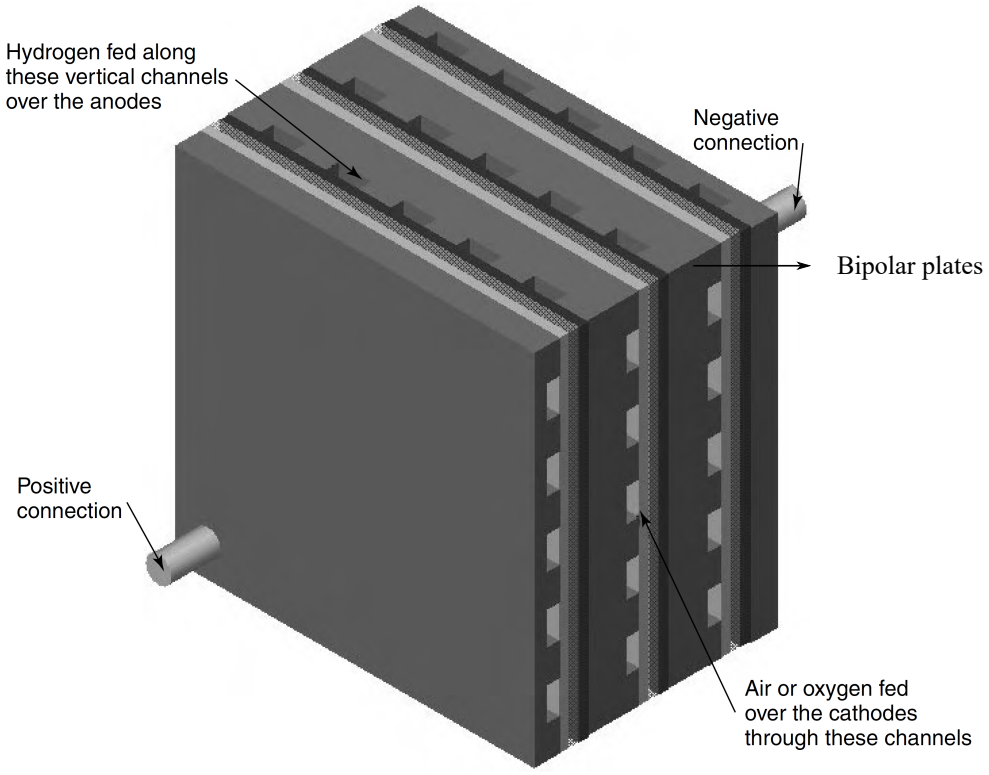

Figure 2.3: Fuel cell system with stacked bipolar plates and gas feeding channels (Source: [6]).

electrodes to generate the energy. The basic hydrogen fuel cell utilises hydrogen and oxygen as the fuels. At the anode hydrogen gas ionizes resulting in

$$2H_2 \longrightarrow 4H^+ + 4e^- \tag{2.1}$$

and the at the cathode oxygen reacts with the electrons and H^+ ions generated at the anode resulting in

$$O_2 + 4e^- + 4H^+ \longrightarrow 2H_2O. \tag{2.2}$$

The ion exchange layer will facilitate the movement of H^+ ions from anode to cathode whereas the external circuit allows the electron movement though the electrodes. The ion exchange layer can be either an acidic electrolyte solution, an alkaline solution or polymer membranes. Commercial fuel cells widely use polymer membranes also called as proton exchange membranes (PEM) in their fuel cell assembly. In most fuel cells, to facilitate faster reaction and thereby energy generation, catalyst material, usually

platinum, is used at the electrodes. As in the case with batteries, fuel cells also utilise series connection of multiple cells to achieve higher voltage output. This is usually done using bipolar plates stacked together to achieve an efficient series interconnection, higher voltage and physical robustness. The bipolar plates are also made porous to ensure gas diffusion and a high surface area of reaction. A typical PEM fuel cell with stacked bipolar plate assembly is shown in Figure 2.3 . It should also be noted that the fuel used in the fuel cell need not necessarily be hydrogen. A very attractive alternative that is considered lately is the direct methanol fuel cells which utilise methanol instead of hydrogen as the energy storage medium [6, 87].

The continuous operation of the fuel cell is bound to ensue in degradation resulting from water accumulation at gas diffusion pores affecting the surface area of reaction, platinum particle sintering and reduced proton conductivity of the membrane due to impurities in the supplied fuel [88,89]. Another major cause of degradation under dynamic operation of the fuel cell is that of the electrocatalyst under fuel starvation. Unlike the other degradation phenomena the electrocatalyst degradation is a direct consequence of the load behaviour supplied by the fuel cell system. The fuel cell system when subjected to sudden changes in load demand undergo fuel starvation at the membrane electrode assembly. This is because when there is a sudden increase in power output, the consumed fuel is not replenished at the same rate by the fuel delivery system, which has a slower response time. This fuel starvation will lead to reverse polarity at the cells as they are sourcing more current than what is possible with fuel delivery. This cell reversal has adverse effects on the catalyst material at the anode and cathode like surface areas loss, dissolution to name a few. The fuel starvation is associated with severe, non reversible damage in the fuel cells and should be avoided. Therefore, in fuel cell operation care should be taken to ensure that the fuel cell is not subjected to sudden load variations which can ultimately lead to fuel starvation and degradation.

The current target for fuel cells lifetime in stationary application (based on US department of energy) is 40000 hours or 15 years [90] though no conclusive study exists on how far this has been achieved. Commercial fuel cells from Ballard claim lifetime of above 20000 hours. The energy density of the fuel cell is the highest among all the ESS considered here at 800-10000 Wh/kg [1].

The electrolyser is nothing but a fuel cell working in the reverse mode, where surplus power from the grid is used to generate hydrogen. The operation principle and physical structure is same as that of the PEM fuel cells. However, the idea of its integration

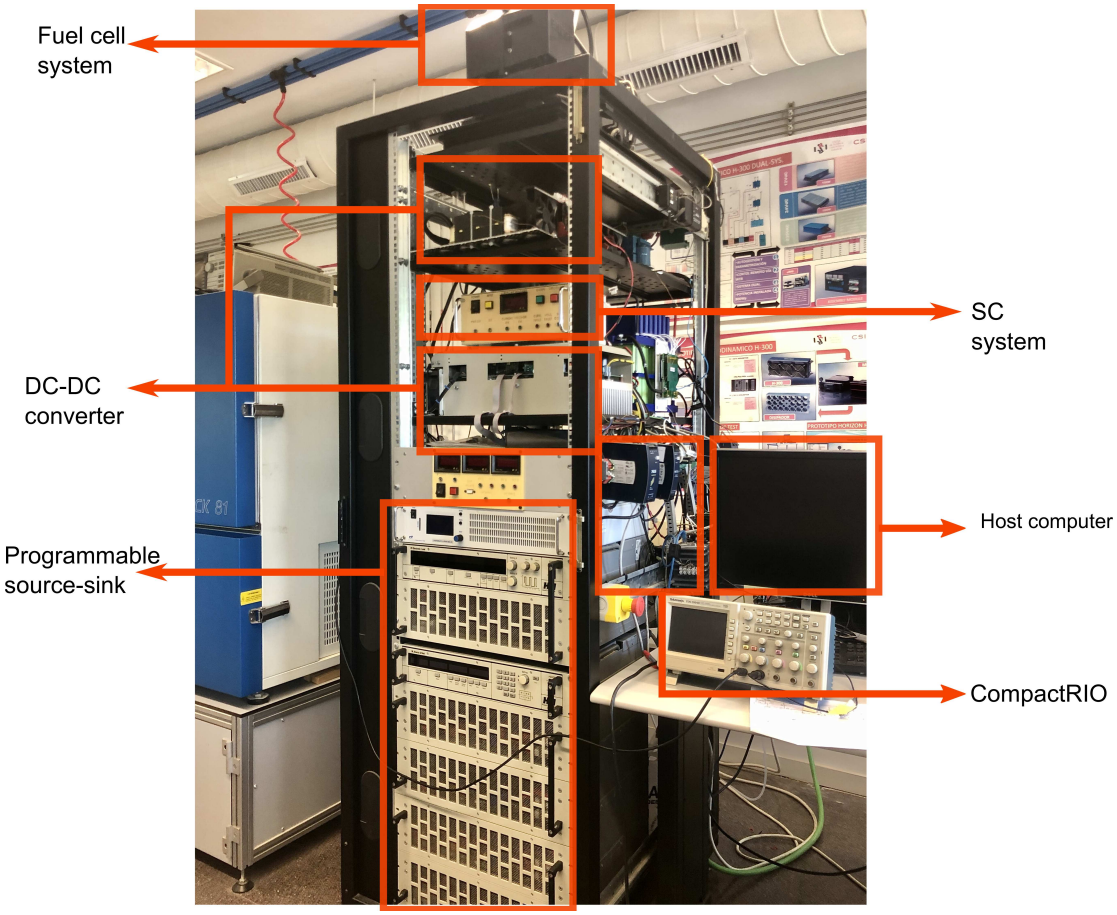

Figure 2.4: Test setup used for experimental verification in this work.

in stationary application is still at its early stage. There has been feasibility studies conducted on converting surplus wind energy to hydrogen by the national renewable energy lab (USA) [91]. A fuel cell system assembly having an electrolyser is also referred to as the regenerative fuel cell system.

2.2 Test setup description, design and experimental implementation tools

As discussed in Chapter 1 the control strategies proposed in this work will be verified experimentally wherever possible. The experimental setup considered in this work is shown in Figure 2.4. The experimental bench consists of a 1.2 KW Ballard Nexa fuel cell system. The supercapacitor from MAXWELL has a capacitance of 165 F with rated voltag eof 48 V and stored energy of 53 Wh. The storage systems are connected

to the DC bus through DC-DC converters utilising semistack converter system from Semikron. The DC-DC converters are switched at 20kHz. The experimental setup also houses The Höcherl & Hackl NLseries programmable DC source/sink and ZS series electronic load which can be programmed to emulate a renewable source, load behaviour. The real time controller developed in this work will be implemented in FPGA of the CompactRIO platform from national instruments. The setup also has a host computer which can communicate with the CompactRIO system.

The main simulation software used in this work has been Matlab and Matlab Simulink. The simulation of the power converter models and its controller verification was done in Simulink whereas the coding of energy management algorithms where done in Matlab. The FPGA programming was done with LabVIEW interface from national instruments. Python has also been used in this work to develop codes for the machine learning algorithm used in the prediction of generation and load profiles.

2.3 Assumptions and limitations

It should be noted that this work does not explicitly deal with the problem of sizing of hybrid ESS and focusses mostly on the aspects of the control and managing the ESS. It should also be noted that the choice of the ESS in the hybrid framework is not definitive. This can vary depending on the application. The author's objective is to develop a generic control and energy management framework when using ESS of all different characteristics (physical and application wise). In this context, the microgrid architecture shown in Figure 2.1 was considered. Depending on the application requirement the composition of hybrid ESS can vary and the generic control scheme that will be proposed in this work can be easily modified to cater the requirements of the system considered. The authors do not claim that this is the best configuration possible as it depends on the application requirement, location of hybrid ESS deployment and economic factors.

In experimental validation, the test setup shown in Figure 2.4 does not include an electrolyser and battery. The system comprises only of FC and SC. The experimental validation, wherever possible, will be carried out using the FC and SC hybrid system. Nevertheless, there exist the possibility of emulating the electrolyser, hydrogen storage or battery system using the CompactRIO platform and programmable source/sink.

The scheme considered above allows decoupling of the DC, AC side operation using

the DC-AC inverter. This allows utilisation of separate control systems for DC and AC bus control. The author would like to emphasis that in this work the real time control (power management stage) developed will focus on the DC bus control. As such in the power management stage, the focus will be on the voltage regulation problem of the DC bus since power imbalance affect the DC bus voltage. Nevertheless, the proposed control strategy can be easily extended to the AC grid case to incorporate both frequency and voltage regulation problem.

As highlighted the microgrid is capable of energy interaction with the main grid which can in turn be utilised for grid support. The decision on the energy exchange with the grid for grid support will be decided by the central/ distributed control unit depending on the main grid operation. This work will not consider the decision making strategies of the centralised/distributed grid control unit for controlling different microgrids and their power interactions with main grid. As a result the work considers only the converter, primary+secondary and tertiary control stages.

Finally, the microgrid considered in this work is an aggregated representation of multiple home applications. The control strategies and energy management developed will be for these small microgrids. In this scenario centralised control schemes will be mostly considered and developed in this work at the primary+secondary and tertiary levels. The distributed schemes for the larger power grid will be mostly incorporated at the central/ distributed control unit which is not considered here.

2.4 Concluding remarks

This chapter introduced the architecture of a microgrid with ESS integration to be used as a base system in developing the control and management strategies discussed in the upcoming chapters. The assumptions and limitations of this work has also been established. An overview of the ESS considered in this work, their energy storage and degradation mechanisms have also been highlighted. An overview of the important aspects have only been provided, for the sake of brevity. Finally, the chapter also introduced the test bench that will be used for the verification of control strategies developed. Having established these introductory concepts the next part of the thesis will focus on the development of power management stage of the control architecture.

Part II

Power management stage

Chapter 3

Converter control

This chapter discusses the converter control stage and contributions of this work in this level. In this context a reset controller framework for current control in converters is introduced. The advantages of the proposed controller will be discussed, along with the design criteria for the same. The chapter also deals with formal pre-input to state stability analysis for the proposed controller along with robustness analysis to parameter uncertainty and to measurement noise. Finally, the capability of proposed reset controllers will be demonstrated through simulation and experimental results.

The power management stage of the control architecture will be discussed in the next two chapters. As outlined before the power management stage forms the lower level of the control architecture and is characterised by real time, fast control actions triggered by events in the grid pertaining to load or generation variation (RES). This control level provides real time power balance thus maintaining the system stability under these events, power quality and real time load sharing among the different sources in the grid based on some predefined criteria. This stage comprises of two sub levels. The converter control and primary+secondary control level. This chapter discusses the converter control part of the power management stage and discusses the contributions of this work at this level.

The converter forms the fundamental interfacing unit between the energy sources (RES) or ESS to the grid. The increased penetration of RES and ESS has led to the increased utilisation of these converter systems in modern grids. These converters are

power electronic systems which, depending on the nature of the grid and sources can provide DC/DC, DC/AC or AC/DC power conversion [67]. Considering the DC nature of the grid and sources, DC/DC converters will be considered in this work.

3.1 Introduction and overview to converter control

The interfacing converters allow for regulation of the power flow from the RES or ESS to the grid. The converter control stage forming the lowest layer of the control architecture facilitates this power regulation. Unlike upper layers, the controllers' objective at this layer is reference tracking such that the individual converter supply the power defined from the higher levels to the grid as a current injection. The controller set points are a combination of the control actions from the energy management and primary+secondary stage thus accounting for optimal system operation and stability.

In the power management stage, to counteract sudden load or RES variations and to minimise their effects on voltage profile (power quality) the control action generated from the primary+secondary level needs to be executed by the converter control stage with minimum delay. This requires that the response of the reference tracking converter control level should be fast. In converters the reference tracking problem is widely addressed using PI controllers [67, 92]. In practical systems these PI controllers are tuned such that grid parameters are maintained within prescribed limits at any instance. Though robust PI controllers tend to produce high overshot and oscillatory behaviour at the output during transient period when tuned for a fast response. The injection of such oscillatory power into the DC bus of a weak microgrid can affect the power quality and also the system robustness. This highlights a scope for improvement in the converter controller performance.

An ideal behaviour from the converter system can be a fast response with improved transient behaviour in terms of output overshoot. Higher order sliding mode controls [68, 93, 94] and differential flatness theory based [69] control techniques have been investigated in converter systems to achieve these ideal responses. However, these require complex formulations in deriving their control law (sliding mode control) or requires that the system have differential flat behaviour for its application.

Resetting the integrator output of a PI control can provide an improved transient

performance. This idea of resetting the integrator output is not new and was first introduced by J.C Clegg thorough his seminal work [95]. This work proposed the Clegg Integrator (CI) which is a hybrid dynamical non-linear integrator that resets its output to zero when input becomes zero, thus providing improved performance and reduced overshoot. This was followed by many works which expanded the class of reset controllers to First Order Reset Elements (FORE) [96–100]. After the seminal works introducing the CI and the FORE, general single-input single-output reset controllers derived from linear and time invariant base system, were introduced in the late 90's (see [101, 102] and references therein). $PI + CI$ controllers [103–105] belong to this group. The reset controllers are capable of overcoming the limitations of its linear counterparts and provide improved performance [106]. A general background on reset control systems can be obtained from the monograph [102].

The $PI + CI$ is a reset controller derived from the classical PI controller. It employs the CI along with a PI to improve its performance. The CI on its own is not able to ensure zero steady-state error unless there is an integrator in the plant. The $PI + CI$ uses the integrator from the PI controller to eliminate the steady-state error and CI to achieve improved performance by allowing fast response with reduced overshoot. There has been many works done in the area of $PI + CI$ controllers involving laying out design criteria [104], [105] for different plants and stability analysis of such systems [103] [107] [108]. The application of such controllers in real world applications like pH in-line control [105], bilateral teleoperation [109], solar collector field [110], industrial wafer scanners [111] and control of industrial heat exchangers [112] have highlighted its ability for an improved transient performance over the classical PI controller.

This improvement in practical applications makes PI+CI reset controllers an interesting solution in converter control systems, considering the demands for fast response and improved transient behaviour. The idea for consideration of PI+CI at converter control level is further reinforced by the controller's proven ability to ensure a flat response to step inputs in first order plants as highlighted in [105]. This has prompted the use of PI+CI reset controller in this work at the converter control stage. The objective had been to improve the control system's transient performance when required to provide a fast response, as is the case here.

3.2 PI+CI reset controller based converter control system

3.2.1 Controller modelling and analytical representation

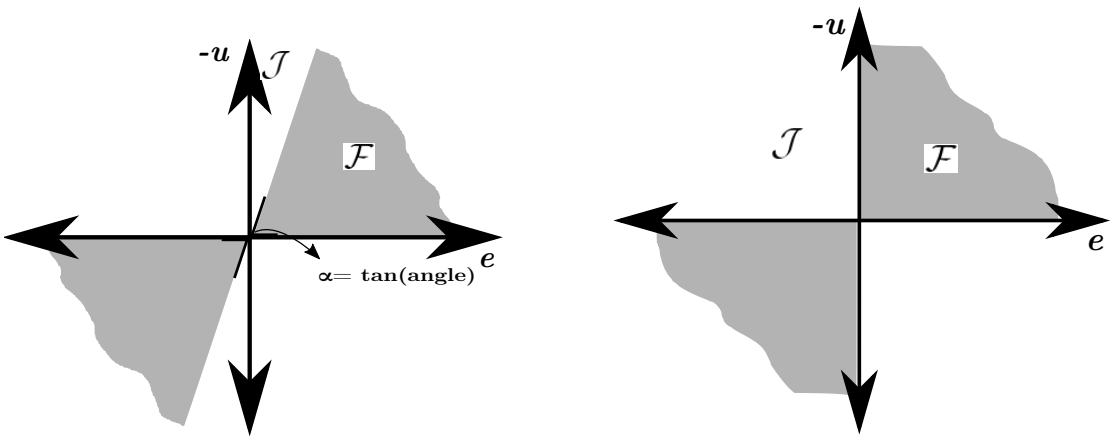

(a) General reset system (b) Clegg integrator(CI)

Figure 3.1: Sector condition representing the flow and jump set of (a), general reset controller and (b), PI+CI controller with $\alpha \to \infty$.

The analytical representation of a general reset controller can be done using the hybrid inclusions framework of [99,113] with a resetting law based on a sector condition over its input-ouput pairs. This modelling has been followed in many subsequent works including some generalizations, for example the model given in [114], which was adopted in this work. According to [114] a generalised reset controller $\mathcal{R}$ is given by

$$\mathcal{R} = \begin{cases} \dot{\mathbf{x}}_r & = \mathbf{A}_r\mathbf{x}_r + \mathbf{b}_r e, \quad if(e, -u_{\mathcal{R}}) \in \mathcal{F} \\ \mathbf{x}_r^+ & = \mathbf{A}_\rho\mathbf{x}_r, \qquad\quad if(e, -u_{\mathcal{R}}) \in \mathcal{J} \\ -u_{\mathcal{R}} & = \mathbf{c}_r\mathbf{x}_r \end{cases} \tag{3.1}$$

where $\mathbf{x}_r \in \mathbb{R}^{n_r}$, $\mathbf{A}_r, \mathbf{b}_r$ and $\mathbf{c}_r$ are the appropriate system matrices, $-u_{\mathcal{R}}$ is the output of the reset controller employed and e is the input. $\mathcal{F}, \mathcal{J}$ are the flow and jump sets of the system respectively. In the set defined by $\mathcal{F}$, the controller states flow according to linear differential equation whereas the states undergo a jump at the boundary of set $\mathcal{J}$. $\mathbf{x}_r^+$ represents the state of the controller after jump caused by the reset instance. The matrix $\mathbf{A}_\rho$ is the reset matrix which defines the system states after the reset instance.

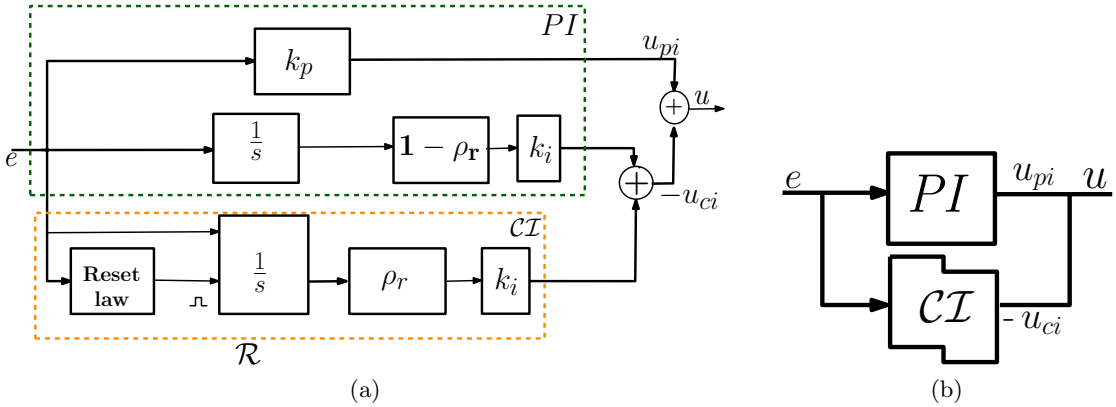

Figure 3.2: (a), PI+CI controller schematic with PI part highlighted in green and reset CI part highlighted in orange.(b), An equivalent representation of PI+CI with $\mathcal{R}$ representing CI.

The flow set $\mathcal{F}$ is given by

$$\mathcal{F} = \{(e, -u_\mathcal{R}) \in \mathbb{R}^2 | e u_\mathcal{R} \leq -\frac{1}{\alpha} u_\mathcal{R}^2\}, \tag{3.2}$$

while $\mathcal{J}$ is given by

$$\mathcal{J} = \{(e, -u_\mathcal{R}) \in \mathbb{R}^2 | e u_\mathcal{R} \geq -\frac{1}{\alpha} u_\mathcal{R}^2\} \tag{3.3}$$

where $\alpha > 0$ is as shown in Figure 3.1a The flow and jump sets defined using the above equations can be illustrated in a two dimensional plane as sectors shown in Figure 3.1a. The jump condition occurs along the boundary of $\mathcal{F}$ and $\mathcal{J}$ in Figure 3.1a [114]. The general reset controller expression in (3.1) can be used to express all the different reset controllers. For a detailed exposition to the hybrid inclusions framework, including definition of hybrid time and the solution concept for reset systems refer to [113].

A PI+CI controller is obtained by introducing a CI along with the classical PI controller and is schematically represented as in Figure 3.2. In this way the total integral action of a classical PI controller is split between a linear inetgrator and reset CI. The reset law in CI part is defined by the boundary of $\mathcal{J}$ with $\mathcal{F}$. The term ρ_r is the reset ratio and represents the percentage of the total integral action that gets reset through the CI. For example, if $\rho_r = 0$ it results in a classic PI controller, which will be referred henceforth as PI_{base}, whereas a $\rho_r = 1$ results in P+CI controller. Once the PI_{base} controller has been designed, usually to obtain a fast response, the PI+CI controller acts by removing (or minimizing) the overshoot (and hence the significance of negative output of reset part). The desired design specification (a fast response without overshooting) may be obtained simply by adjusting the parameter ρ_r. As such, in this

work, the design problem will be to find a ρ_r value between 0 and 1 which will ensure a improved transient performance over PI controller.

The PI+CI controller can be represented as in (3.1), using hybrid inclusion framework by

$$\begin{cases} \dot{\mathbf{x}}_r &= \mathbf{A}_r\mathbf{x}_r + \mathbf{b}_r e, & if(e, -u_{ci}) \in \mathcal{F} \\ \mathbf{x}_r^+ &= \mathbf{A}_\rho\mathbf{x}_r, & if(e, -u_{ci}) \in \mathcal{J} \\ u &= \mathbf{c}_r(\rho_r)\mathbf{x}_r + d_r e \end{cases} \tag{3.4}$$

where $\mathbf{x}_r = [x_i \ x_{ci}]^T$ are the states of the controller defined by the integrator (x_i) and CI (x_{ci}) states, and

$$\mathbf{A}_r \triangleq \begin{bmatrix} 0 & 0 \\ & \\ 0 & 0 \end{bmatrix}, \quad \mathbf{b}_r \triangleq \begin{bmatrix} 1 \\ \\ 1 \end{bmatrix}, \quad \mathbf{c}_r \triangleq k_i \begin{bmatrix} 1-\rho_r & \rho_r \end{bmatrix} d_r \triangleq k_p, \quad \mathbf{A}_\rho \triangleq \begin{bmatrix} 1 & 0 \\ & \\ 0 & 0 \end{bmatrix}. \tag{3.5}$$

Note that the dependence of $\mathbf{c}_r$ on ρ_r has been explicitly shown in (3.4),(3.5). The sets $\mathcal{F}$ and $\mathcal{J}$ for the PI+CI controller are defined as in (3.2, 3.3), where $\alpha > 0$ typically takes a large value (note that for $\alpha \to \infty$ the CI developed in [99] is recovered and this PI+CI controller is equivalent to that developed in [104], as far as its initial conditions are taken in the set $\mathcal{F}$). The $-u_{ci}$, u_{pi} are outputs of CI, PI part respectively and u the total output of PI+CI as shown in Figure 3.2b. The resulting $\mathcal{F}$ and $\mathcal{J}$ for PI+CI is represented as in Figure 3.1b. Although the PI+CI controller can also be built using a variable ρ_r, see [105], for the purposes of this work variable reset ratio is not considered and ρ_r will be a constant parameter.

3.2.2 Hybrid dynamical reset control system

The Figure 3.3 shows a general reset control system where a plant , P, is controlled using $PI+CI$ controller. The additive input in the feedback path represents the measurement noise, n. The reference to the closed-loop system is represented by an exogenous signal $\mathbf{w}_1$ in Figure 3.3. It is assumed that $\mathbf{w}_1$ is a Bohl function and is represented as

$$\begin{aligned} \dot{\mathbf{w}}_1 &= \mathbf{A}_1\mathbf{w}_1, \mathbf{w}_1(0) = w_{10} \\ r &= \mathbf{c}_1\mathbf{w}_1 \end{aligned} \tag{3.6}$$

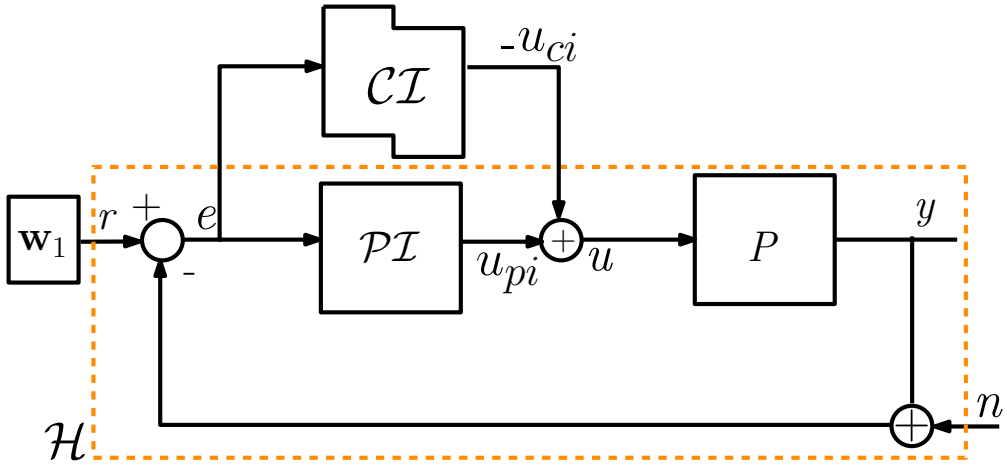

Figure 3.3: Reset control system with a PI+CI controller and exogenous inputs in reference $\mathbf{w}_1$ and measurement noise n.

where $\mathbf{w}_1 \in \mathbb{R}^{n_1}$, $\mathbf{A_1}$ and $\mathbf{c_1}$ are appropriate system matrices. The plant, P, is represented in the state-space form as

$$\begin{aligned} \dot{\mathbf{x}}_p &= \mathbf{A}_p\mathbf{x}_p + \mathbf{b}_p u, \\ y &= \mathbf{c}_p\mathbf{x}_p \end{aligned} \tag{3.7}$$

where $\mathbf{x}_p \in \mathbb{R}^{n_p}$. Therefore, using (3.4), (3.6), (3.7) the closed-loop control system with reset controller can be represented as a hybrid dynamical system (note that ρ_r is a constant parameter, explicit dependence on it is shown) given by

$$\begin{cases} \dot{\mathbf{x}} &= \mathbf{A}(\rho_r)\mathbf{x}, & \mathbf{x} \in \mathcal{F}_\mathcal{C} \\ \mathbf{x}^+ &= \mathbf{A}_R\mathbf{x}, & \mathbf{x} \in \mathcal{J}_\mathcal{C} \\ y &= \mathbf{c}\mathbf{x} \end{cases} \tag{3.8}$$

where $\mathbf{x} \in \mathbb{R}^{n_p+2+n_1}$ is the state of closed-loop system defined by $[\mathbf{x}_p, \mathbf{x}_r, \mathbf{w}_1]^T$. The matrices $\mathbf{A}$,$\mathbf{c}$,$\mathbf{A}_R$ are defined as

$$\mathbf{A}(\rho_r) \triangleq \begin{bmatrix} \mathbf{A}_p - \mathbf{b}_p d_r \mathbf{c}_p & \mathbf{b}_p \mathbf{c}_r(\rho_r) & \mathbf{b}_p d_r \mathbf{c}_1 \\ -\mathbf{b}_r \mathbf{c}_p & \mathbf{A}_r & \mathbf{b}_r \mathbf{c}_1 \\ 0 & 0 & \mathbf{A}_1 \end{bmatrix} \tag{3.9}$$

$$\mathbf{c} \triangleq (\mathbf{c}_p\ \mathbf{0}_2\ \mathbf{0}_{n1}), \quad \mathbf{A}_R \triangleq diag(\mathbf{I}_{n_p}, \mathbf{A}_\rho, \mathbf{I}_{n_1})$$

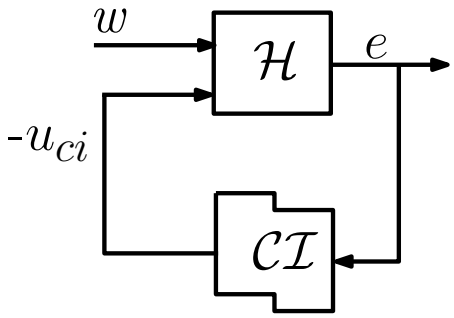

Figure 3.4: Reduced feedback interconnection from Figure 3.3 of LTI dynamical system ($\mathcal{H}$) and CI controller.

where $\mathbf{I}$ is unit matrix and $\mathbf{0}$ is a zero vector of appropriate order. The set $\mathcal{F}_\mathcal{C}, \mathcal{J}_\mathcal{C}$ is the same as that in (3.2)-(3.3) but reformulated as a function of system states given by

$$\mathcal{F}_\mathcal{C} = \{\mathbf{x} \in \mathbb{R}^{n_p+2+n_1} | \mathbf{x}^T \mathcal{M} \mathbf{x} \leq 0\} \tag{3.10}$$

while $\mathcal{J}$ is given by

$$\mathcal{J}_\mathcal{C} = \{\mathbf{x} \in \mathbb{R}^{n_p+2+n_1} | \mathbf{x}^T \mathcal{M} \mathbf{x} \geq 0\} \tag{3.11}$$

where $\mathcal{M} = \mathbf{C_{\mathcal{F}1}}^T \mathbf{C_{\mathcal{F}2}} \alpha + \mathbf{C_{\mathcal{F}2}}^T \mathbf{C_{\mathcal{F}2}}$
with $\mathbf{C_{\mathcal{F}1}} = \begin{bmatrix} -\mathbf{c}_p & \mathbf{0}_2 & \mathbf{C}_1 \end{bmatrix}$ and $\mathbf{C_{\mathcal{F}2}} = \begin{bmatrix} \mathbf{0}_{np} & 0 & -k_i \rho_r & \mathbf{0}_{n1} \end{bmatrix}$.

As the converter control focusses on reference tracking problem, the disturbance inputs are not considered in the reset control considered in this chapter.

3.2.3 Robustness against sensor noise and stability for reset systems

The reset control system (3.8) trivially satisfies the so-called basic hybrid conditions [113], since the flow and jump maps are continuous and the sets $\mathcal{F}$ and $\mathcal{J}$ are closed. This gives us some desirable properties like robustness against sensor noise, and also robustness in stability, see [113] for detailed results. In this work, the stability analysis for reset system is based on [114]; and according to it, the stability notion is pre-input to state stability (pre-ISS). Since developing an ISS Lyapunov function which can verify the stability can be cumbersome in the case of hybrid systems like reset controllers, in [114] a nice frequency domain based stability result for reset system is used.

In order to introduce this stability concept consider the Figure 3.4. It shows the feedback interconnection of a dynamical system ($\mathcal{H}$) and the CI controller. The system

$\mathcal{H}$ includes all the linear part of the reset control system discussed in the previous section and is represented by the highlighted region (orange) in Figure 3.3. The system is considered minimal with

$$\mathcal{L}\{e\} = \mathcal{G}_{eu}(s)\mathcal{L}\{u_{ci}\} + \mathcal{G}_{ew}(s)\mathcal{L}\{\mathbf{w}_1\} \tag{3.12}$$

where $\mathcal{G}_{eu}, \mathcal{G}_{ew}$ are the transfer functions of the system from u_{ci} to e and $\mathbf{w}_1$ to e respectively.

The stability of reset system can be guaranteed if it satisfies the following criteria [114]:

1. The system matrix $\mathcal{H}$ is Hurwitz, that is its eigenvalues are strictly in the left half side of complex plane.

2. The transfer function $\mathcal{G}_{eu(s)}$ as in (3.12) satisfies

$$\frac{1}{\alpha} + Re(\lim_{w\to\infty} \mathcal{G}_{eu(s)}) > 0 \tag{3.13}$$

and

$$\frac{1}{\alpha} + Re(\mathcal{G}_{eu(s)}) > 0 \quad \forall w \in \mathbb{R} \tag{3.14}$$

provided matrices $\mathbf{A}_r, \mathbf{c}_r$ in (3.5) is detectable. Satisfying the above criteria will guarantee the existence of a pre-ISS Lyapunov function which is smooth with negative derivative between reset instants and decreases in value after a reset instance.

3.2.4 Design criteria of PI+CI reset controller

As mentioned before the PI+CI controller is capable of a flat response in first order system subjected to step inputs. The selection criteria of ρ_r which ensure this flat response will be used in this work to improve the performance of converter control stage.

The solution of (3.8), unlike linear system, is expressed as a sequence of LTI system responses [105] existing between reset intervals $(t_k, t_{k+1}]$ given by

$$\mathbf{x}(t) = e^{\mathbf{A}(\rho_r)(t-t_k)}\mathbf{x}(t_k^+) \tag{3.15}$$

where t_k is the reset instant and $\mathbf{x}(t_k^+) = \mathbf{A}_R\mathbf{x}(t)$. For a given $k \in \{0, 1, 2...\}$ it can also be defined as

$$\mathbf{x}_k(t) \triangleq \mathbf{x}(t + t_k) = e^{\mathbf{A}(\rho_r)t}\mathbf{x}(t_k^+), \quad \forall \quad t \geq 0. \tag{3.16}$$

The Laplace transform for the same is written as

$$\mathbf{X}_k(s) = (s\mathbf{I} - \mathbf{A}(\rho_r))^{-1}\mathbf{x}(t_k^+). \tag{3.17}$$

The resulting solution for (3.17) as a sequence of LTI system response is obtained by inverse Laplace transform as

$$\mathbf{x}(t) = \begin{cases} \mathbf{x}_0(t) & t \in [0, t_1] \\ \mathbf{x}_1(t - t_1) & t \in (t_1, t_2] \\ \mathbf{x}_2(t - t_2) & t \in (t_2, t_3] \\ ..... \end{cases} \tag{3.18}$$

The closed-loop system error can also be expressed in a similar way. The system error for the reference tracking problem is defined as

$$e(t) = \mathbf{c}_E\mathbf{x}(t) \tag{3.19}$$

where $\mathbf{c}_E = (-\mathbf{c}_p\ \mathbf{0}_2\ \mathbf{c}_1)$. The Laplace transform of (3.19) is then

$$E_k(s) = \mathbf{c}_E(s\mathbf{I} - \mathbf{A}(\rho_r))^{-1}\mathbf{x}(t_k^+). \tag{3.20}$$

The solution to (3.20) is also a sequence of LTI system responses of the form (3.18).

Consider a first order plant $P(s)$ given by

$$P(s) = \frac{b_0}{s + a_0}, \tag{3.21}$$

subjected to an exogenous input $\mathbf{w}_1$ represented by a step signal of amplitude w_{10}. The solution for the closed-loop error is obtained by solving (3.20) using (3.21). The resulting error equation, defined between the reset instances, is given by [105]

$$E_k(s) = \frac{a_0 w_{10} - b_0 k_i(1 - \rho_r))x_i t_k}{s^2 + (a_0 + b_0 k_p)s + b_0 k_i} \tag{3.22}$$

where, k_p and k_i are the PI controller constants shown in Figure 3.2a. Based on (3.22), the value of ρ_r which forces the system error to zero at the first instance of zero crossing and maintains it there, thus ensuring a flat response, is given by

$$\rho_r = 1 - \frac{a_0 w_{10}}{b_0 k_i x_{I,1}} \tag{3.23}$$

where $x_{I,1}$ is the value of the aggregated integrator state $(x_i + x_{ci})$ at the first reset instance. It should be noted that the value for ρ_r defined in (3.23) is dependant on the nature of exogenous signal applied at the input of the system. The above expression gives is an optimal value of ρ_r only for the step input.

3.3 Converter overview and modelling

Grid connected converters can be classified into grid-feeding, grid-supporting or grid forming systems depending on their mode of operation [115–117]. The grid forming converters act as an ideal voltage source in the DC bus and sets the nominal voltage, frequency (AC grids) level for the grid. The grid feeding power converters are tasked with delivering power to an already energised grid. They act like a power source connected to the grid and follows a power reference through proper control. The grid supporting converters are responsible for maintaining their grid voltage, frequency (AC grids) within prescribed limits by regulating their output. In this work, the grid forming functionality is not considered and the converters are typically operating either in grid feeding or grid supporting mode. Considering DC microgrid, DC/DC converters are analysed in this work. In general DC/DC converters can be either buck, boost or buck-boost type [67]. All these converter types can be modelled in the first order form of (3.21), when operated in the grid feeding or grid supporting mode. This makes PI+CI controller ideal for the converter control systems, wherein the design criteria for ρ_r given by (3.23) can be directly utilised to obtain a near flat response to step inputs.

However, in practical applications additional filters can be incorporated in the converter system. This is done mainly for smoothing the current drawn from the power sources, so as to protect them, or for improving the power quality at the output. In any case, this will result in deviation of the plant model from the first order form as shown in (3.21). In this scenario, additional design considerations should be undertaken to ensure that the PI+CI controller is still capable of flat response to step inputs.

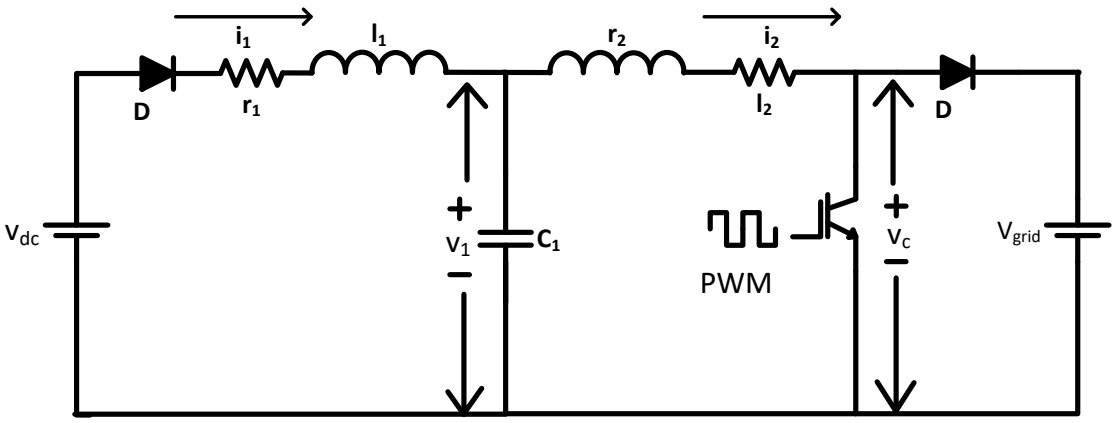

Figure 3.5: Schematic of the DC-DC boost converter.

An example of the same can be the FC converter, which is usually designed with an input filter to protect the FC from high ripple input current demanded by the switch mode converter system. This is vital to reduce the degradation in FC system due to the high ripple current. A boost converter topology with input filter used for interfacing a FC to DC microgrid is shown in Figure 3.5. The FC system is modelled as the DC voltage source v_{dc} in the above figure and the grid is represented as v_{grid}. The inductor l_1 and capacitor c_1 in Figure 3.5 form the input filter. The inductor l_2 enables the boosting of input voltage. The resistors r_1 and r_2 are the effective series resistances of l_1 and l_2 respectively.

The averaged large signal modelling approach [118, 119] can be used to model these converter systems. Defining the average voltage across the power electronic device (MOSFET, IGBT) as $v_c = d'v_{grid}$ where $d' = 1 - d$, the averaged converter model can be developed neglecting the switching ripple. Applying the Kirchoff's voltage and current laws the averaged state equations are given as

$$\begin{aligned} l_1\frac{i_1}{dt} &= v_{dc} - v_1 - r_1 i_1 \\ l_2\frac{i_2}{dt} &= v_1 - v_c - r_2 i_2 \\ c_1\frac{v_1}{dt} &= i_1 - i_2. \end{aligned} \tag{3.24}$$

The converter model can then be defined as

$$I_2(s) = \frac{V_{dc}(s) - (c_1 l_1 s^2 + c_1 r_1 s + 1)V_c(s)}{l_1 l_2 c_1 s^3 + c_1(l_1 r_2 + l_2 r_1)s^2 + (c_1 r_1 r_2 + l_1 + l_2)s + (r_1 + r_2)}. \tag{3.25}$$

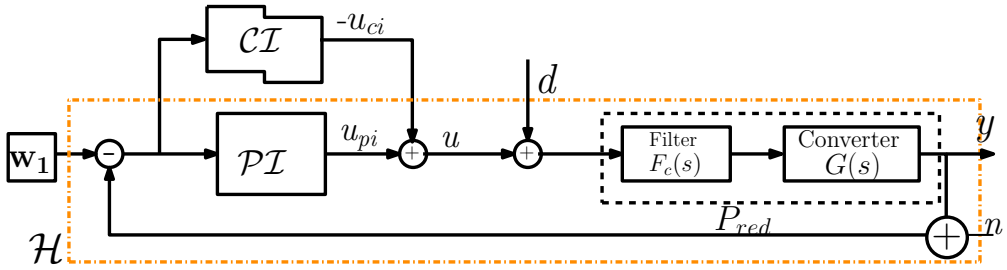

Figure 3.6: The closed-loop reset control system employed for the boost converter.

A variable change is proposed for (3.25) as shown below

$$V_{m2}(s) \triangleq \frac{V_{dc}(s)}{l_1c_1s^2 + r_1c_1s + 1} - V_c(s) \tag{3.26}$$

resulting in a model given by

$$G(s) = \frac{I_2(s)}{V_{m2}(s)} = \frac{c_1l_1s^2 + c_1r_1s + 1}{l_1l_2c_1s^3 + c_1(l_1r_2 + l_2r_1)s^2 + (c_1r_1r_2 + l_1 + l_2)s + (r_1 + r_2)}. \tag{3.27}$$

This variable change is important to ensure that at start up the voltage v_c is same as v_{dc} thereby eliminating large in-rush currents. The above model for the converter system does not conform with the first order model used for the reset controller gain (ρ_r) determination.

3.3.1 PI+CI reset control design considering higher order converter models

In the event converter systems are represented using higher order models, as given by (3.27), the design process of PI+CI controllers should be modified to account for the same. The calculation of reset gain using (3.23) is applicable only when the plant model seen by the PI+CI controller is first order. Therefore, some compensation technique should be introduced, so that from the controller's perspective the higher order converter model appears first order. This will ensure that (3.23) can be used to determine the reset gain which will eventually guarantee a flat response to step inputs using the PI+CI controller.

This can be achieved using a compensating filter transfer function added to the control loop as a shown in Figure 3.6. The generic converter model $G(s)$ can be represented

in terms of poles and zeros of transfer function as

$$G(s) = \frac{k(s - z_1)(s - z_2)...}{(s - p_1)(s - p_2)(s - p_3)...} \tag{3.28}$$

where the zeros $z_1, z_2...$ and higher order poles $p_2, p_3...$ are contributed by the input or output filters in the converter circuit. The DC/DC converter of the buck, boost, buck-boost topologies working in grid feeding mode and having input or output filters can be expressed in this form. The order of $G(s)$ will be decided by the order of the filter used. In the example case shown above, the second order input filter resulted in the third order plant model. Under this scenario compensating filter of the control loop will be chosen as:

$$F_c(s) = \frac{(s - p_2)(s - p_3)...}{k(s - z_1)(s - z_2)...} \tag{3.29}$$

such that the equivalent plant (P_{red} as shown in Figure 3.6) seen by the PI+CI reset controller will be

$$P_{red}(s) = \frac{k}{(s - p_1)}. \tag{3.30}$$

The $P_{red}(s)$ has the similar form as (3.21). Therefore, $P_{red}(s)$ can be used for the calculation of ρ_r as discussed in the previous section, for a flat response.

3.4 Reset control system design for the FC converter

The design criteria having been laid out, the FC converter represented by (3.27) will be used to demonstrate the design procedure and highlight the improvements achieved with reset control system employing PI+CI controller. The FC converter has been selected for the same since they are usually working in the grid feeding mode following step reference making them ideal for PI+CI controller implementation.

The converter parameters and passive component values used in the converter system design is given in Table.3.1 and is the same as that shown in the test set up of Figure 2.4. The transfer function $G(s)$ for the values shown in Table.3.1 is given by

$$G(s) = \frac{I_2(s)}{V_{m2}(s)} = \frac{1742 \cdot (s + 35.70 \pm 1800i)}{(s + 87.1)(s + 38.20 \pm 2070i)}. \tag{3.31}$$

Component name	Value
l_1	140 μH
l_2	434.3 μH
c_1	2.2 nF
r_1	10 mΩ
r_2	42 mΩ
Switching frequency, f_s	20 kHz
Input voltage, V_{dc}	32.5 V
Output voltage, V_{grid}	75 V
Converter rated power	1kW

Table 3.1: Component value used in DC-DC converter.

The compensating filter for the same will then be chosen as

$$F_c(s) = \frac{s + 38.20 \pm 2070i}{s + 35.70 \pm 1800i} \tag{3.32}$$

so as to cancel the effect of the zeros and poles from input filter. The same is demonstrated through the bode plot of converter and compensating filter shown in Figure 3.7. The resulting equivalent first order representation of the plant seen by the controller is then given by

$$P_{red}(s) = G(s) \cdot F(s) = \frac{1742}{s + 87.1}. \tag{3.33}$$

This P_{red} is now considered for the calculation of ρ_r value. The design of the $PI + CI$ is then carried out as follows. First, the PI_{base} parameters k_p and k_i are calculated. A base selection of these parameters were carried out using the AMIGO design technique outlined in [120]. The k_p, k_i values of this base design were then tuned to improve the system performance towards noise entering through plant input, as the AMIGO design considers only output noise. This was done since in the DC-DC converter, switching noise is introduced at the plant input by converting the control action u in Figure 3.6 to 20 kHz gate pulses for the IGBTs. A set of PI_{base} parameters were considered and the one with better performance in the DC-DC converter set up was chosen. The k_p, k_i used in the PI_{base} were 0.03316, 19.39 respectively resulting in a settling time of 0.055s.

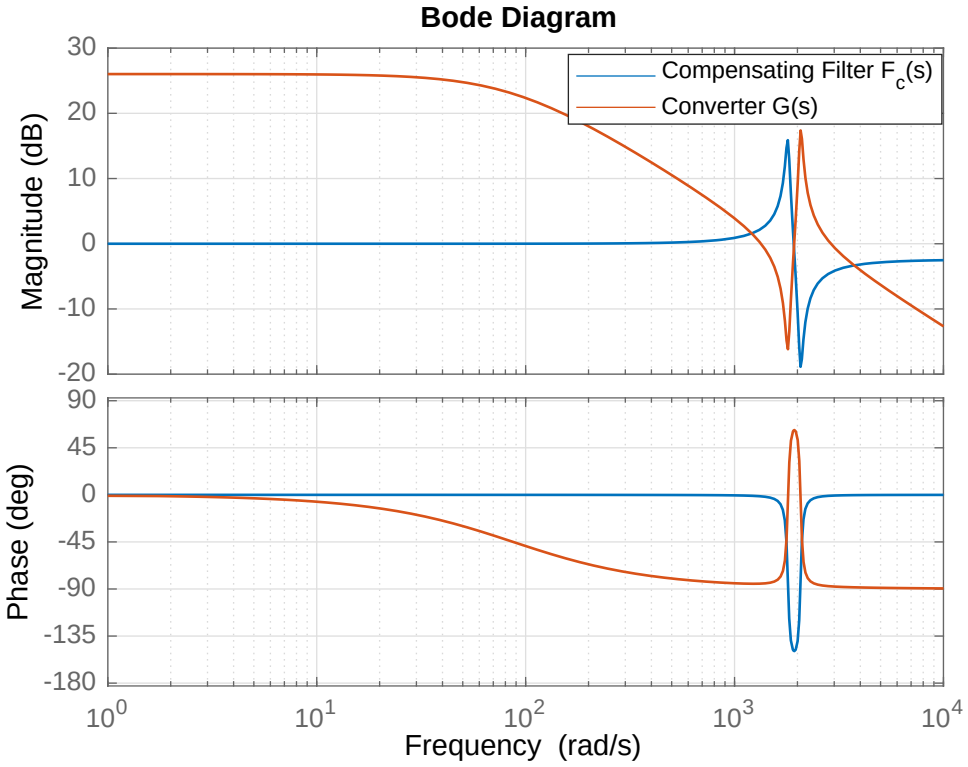

Figure 3.7: Bode plots showing the frequency response of the converter $G(s)$ and compensating filter $F_c(s)$ highlighting the pole-zero compensation.

The fast settling time though results in a peak overshoot of 28%. The next step is to calculate the value of ρ_r using (3.23) to obtain the flat response. The $k_i x_{i,1}$ term in (3.23) is the output of the PI_{base} integrator at the instance of first zero crossing of system error. The value for $k_i x_{i,1}$ was calculated off-line using a simulated model of system controlled by PI_{base} and used in the calculation of ρ_r. This resulted in a value of $\rho_r = 0.4889$ given by (3.23).

3.4.1 Stability analysis of proposed PI+CI control system

Stability of the DC-DC boost converter control system is analysed using the results in Section 3.2.3. In the case of $PI + CI$ controller employed for boost converter in this work, the transfer function $\mathcal{G}_{eu}(s)$ is

$$\mathcal{G}_{eu}(s) = \frac{P_{red(s)}}{1 + P_{red(s)} PI(s)} = \frac{1742s}{s^2 + 144.9s + 33780}. \tag{3.34}$$

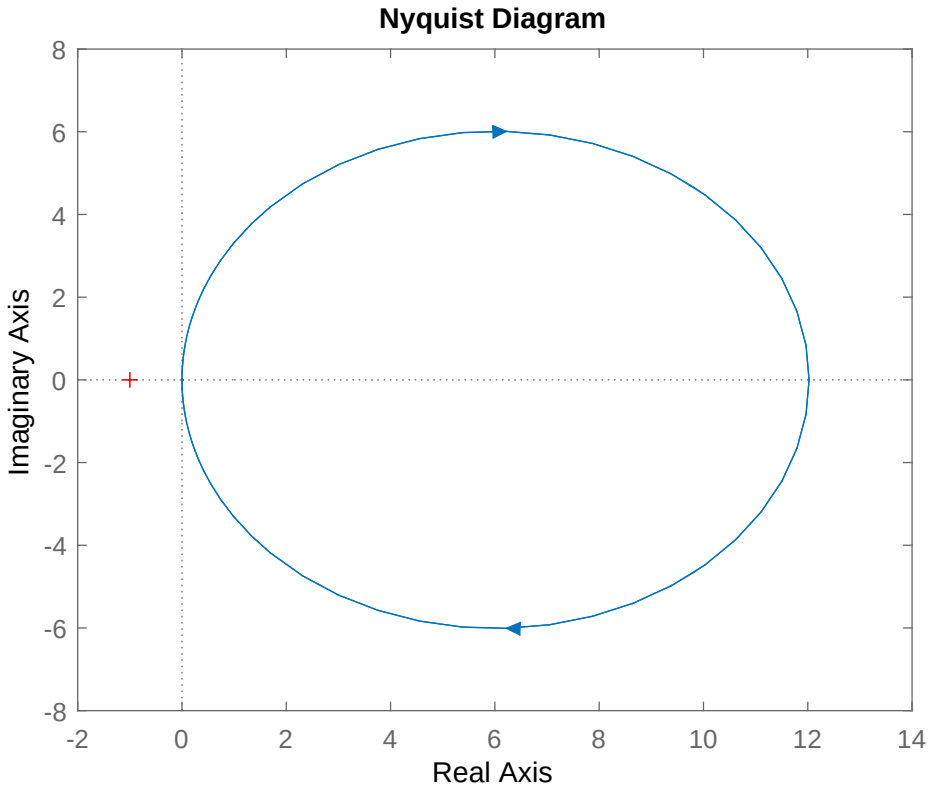

Figure 3.8: Nyquist plot for the transfer function $\mathcal{G}_{eu}(s)$.

.

The first criteria of the stability condition will be satisfied by designing a stabilizing PI_{base} such that the linear system represented by $\mathcal{H}$ is stable which is also the case here. The transfer function $\mathcal{G}_{eu}(s) \to 0$ as $w \to \infty$ is trivial thereby, satisfying (3.13). Finally the fulfilment of (3.14) is explained through Figure 3.8. This shows the Nyquist plot of the transfer function $\mathcal{G}_{eu}(s)$. The sector condition for CI controller is defined for $\alpha \to \infty$ resulting in the $Re(\mathcal{G}_{eu(s)})$ to lie on the right half side of the complex plane in the Nyquist plot to ensure condition 2. This can also be observed in Figure 3.8. As a result, it is shown that closed-loop system is stable according to Section 3.2.3.

The $PI + CI$ controller used in this work is a hybrid controller and unlike linear systems robustness analysis may not be straightforward. Well-posedness of the reset control systems, as well as robustness to measurement noise and stability easily follow by using the formal methods developed in [113]. The sense of robustness in [113] is related with keeping a desired property, e. g. stability, for arbitrarily small values of for example sensor noise. It is also interesting to analyze if the stability is maintained under

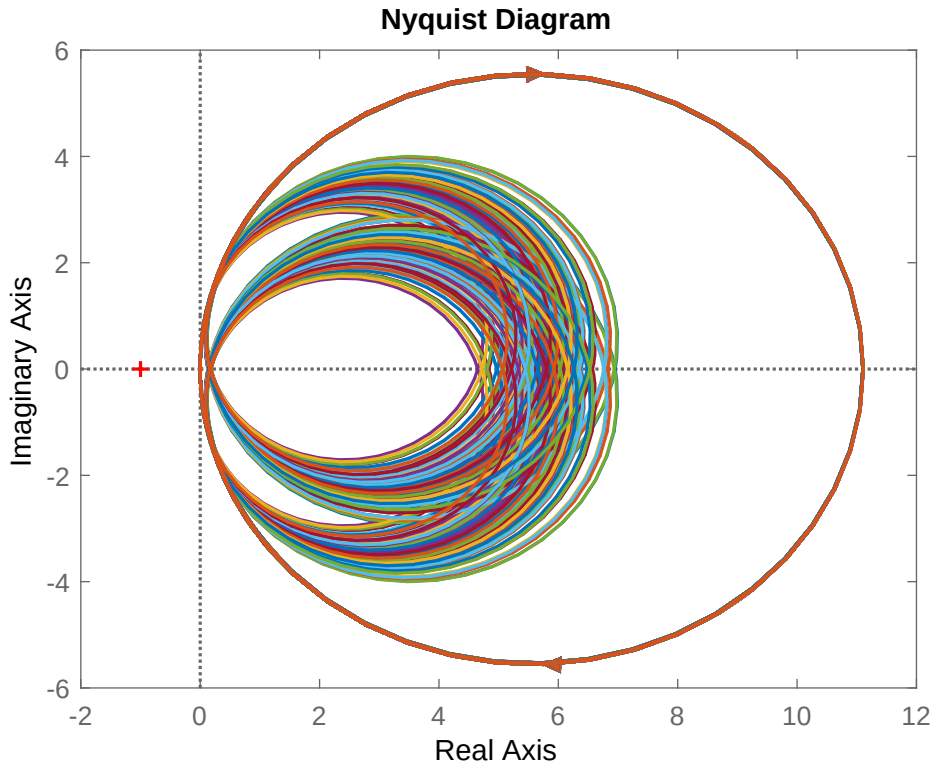

Figure 3.9: Nyquist plots of $\mathcal{G}_{eu}(s)$ for the varying values of the boost converter l_1, l_2, c_1.

parameter uncertainty, which is also a basic issue in control practice. An additional advantage of frequency domain analysis of Section 3.2.3 is that it easily allows this type of parameter uncertainty analysis to be carried out efficiently. The values of inductors and capacitors are usually mentioned within a range defined as a percentage of the nominal value. Under such conditions an exact pole zero cancellation may not be possible and the system may not be exactly first order. The stability of the system under such scenario needs to be ascertained. The uncertainty in the nominal value of the components l_1, l_2 and c_1 considered here is 10%, based on the data-sheet of these components. The stability under uncertainty is ascertained using the results of Section 3.2.3. Satisfying first condition of stability criteria and (3.13) is trivial. The effect of uncertainty on the condition (3.14) is highlighted in Figure 3.9. The plot in Figure 3.9 is generated using 100 random values of the components l_1, l_2 and c_1 within the uncertainty range. It can be noted that despite uncertainty, the Nyquist plots are always positioned on the right half of the complex plane ensuring that (3.14) is always satisfied. This establishes stability under uncertainty of parameter values.

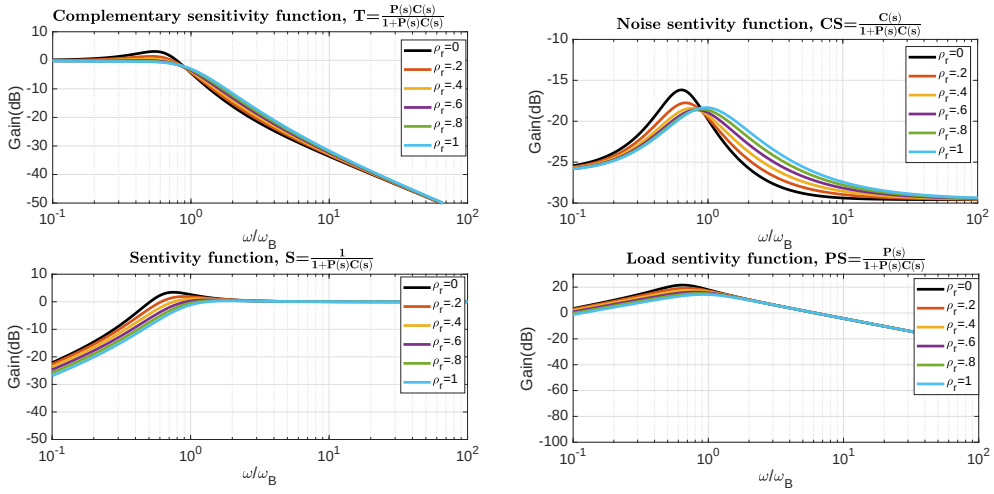

Figure 3.10: Magnitude plots of the system closed-loop transfer function (TF), Noise sensitivity Function (CS), sensitivity function (S) and load sensitivity function (PS) plotted for linear base system $(\rho_r) = 0$ and different reset ratios.

3.4.2 Describing function based robustness analysis

Having already established closed-loop stability of the system the analysis in this section allows a heuristic understanding of the reset system robustness in comparison to linear base system. This is done using describing function (DF), which will otherwise be impossible by any other means. Although an approximated analysis, in control practice it gives an adequate characterization of both stability margins and sensor noise effect since the feedback loop has the necessary low-pass property. In this context, DF analysis can present itself as a simple tool for a designer to provide an intuition on the robustness of the designed reset controller using well established frequency domain techniques. Whilst DF analysis have been found to fail in some cases it can still be an important tool and its use in non-linear systems have been justified through the works in [121–123]. The describing function of a $PI + CI$ is given by [102]

$$PI + CI(\omega) = k_p \frac{j(w\tau_i + \frac{4}{\Pi}\rho_r) + 1}{j\omega\tau_i} \tag{3.35}$$

where $\tau_i = \frac{kp}{ki}$. The important characteristic of DF of the $PI + CI$ controller is that the function does not depend on the amplitude of the input but solely on the frequency of input. This allows the use of frequency domain methods for robustness analysis.

The $PI + CI$ controller has been proposed to overcome the inherent limitation of its linear counterparts. Nevertheless it is necessary to investigate whether this is achieved

without increasing the cost of feedback (sensitivity to sensor noise) or sensitivity to load disturbance so that its application is justified. An understanding of this can be achieved using the system transfer functions mentioned in [124], which are constructed using the DF for $PI + CI$ given by (3.35). The four system transfer functions considered for the same [124] are system complementary sensitivity transfer function (T), sensitivity function (S), noise sensitivity function (CS) and load sensitivity function (PS) given by

$$T(w) = \frac{Y(w)}{w_1(w)} = \frac{PI + CI(w) \cdot P_{red}(jw)}{1 + PI + CI(w) \cdot P_{red}(jw)} \tag{3.36}$$

$$S(w) = \frac{Y(w)}{N(w)} = \frac{1}{1 + PI + CI(w) \cdot P_{red}(w)} \tag{3.37}$$

$$CS(w) = \frac{U(w)}{N(w)} = \frac{PI + CI(w)}{1 + PI + CI(w) \cdot P_{red}(w)} \tag{3.38}$$

$$PS(w) = \frac{Y(w)}{D(w)} = \frac{P_{red}(w)}{1 + PI + CI(w) \cdot P_{red}(w)}. \tag{3.39}$$

The Figure 3.10 shows Bode plots of (3.36),(3.37),(3.38),(3.39) for varying values of ρ_r. The frequency axis is normalised using the cut-off frequency w_b. It can be observed from Figure 3.10 that gains the system reference to output transfer function (T) are very similar for the linear ($\rho_r = 0$) and reset system in the entire frequency range. The linear system though will exhibit a higher overshoot compared to reset system based on the plots. This is to be expected as the reset action ensures flat response. The closed-loop bandwidth remains the same ($w/w_b = 1$) and the reset system performance is very similar to the base system at high frequencies.

The DC/DC converter, presented in this work, is a system where the noise will enter through the plant input d (Figure 3.6) in the form of switching noise. The control input u will be converted to 20 kHz gate pulses for the IGBTs using pulse width modulation (PWM). Therefore an interesting plot to study will be the effect of plant output to noise input d which is given by load sensitivity function (PS). This also allows understanding of load disturbance rejection capability of the plant. It can be seen from Figure 3.10 that the addition of reset action has actually reduced the sensitivity of the system towards input disturbance. Nevertheless at switching frequency of 20 kHz the gain plots are same showing similar performance. Finally, the effect of measurement (output) noise on the plant performance is studied through the noise sensitivity (CS) and sensitivity (S) functions. The linear base system still exhibits a higher sensitivity in comparison to the reset systems. It should also be noted that in all the above cases higher the reset ratio

lesser is the sensitivity of the functions. Therefore, a general consensus that can be drawn from here is that the reset action does improve the system performance by producing a fast flat response and provides a marginal improvement in system robustness, observed by reduced gains in the sensitivity functions.

Nevertheless, it should be noted that the DF analysis only provides a heuristic understanding of system robustness and may not be truly reflective of the actual system performance. The real impact of the reset system will be verified in the next section where results from an actual converter system subjected to measurement and switching noises will be presented.

3.5 Results

3.5.1 Simulation results

The simulation results obtained using models developed with Matlab-Simulink are presented first. First, the results with the averaged models developed for the converter without using the switching elements and associated data acquisition systems are presented so as to effectively demonstrate the capabilities of the $PI + CI$ reset controllers The Figure 3.11 shows reference tracking performance of the plant controlled by the PI_{base} and $PI + CI$ controllers when subjected to a step change in reference value from 10A to 20 A. The ability of reset controller in improving the tracking performance is clearly observable by the flat response that it produces in Figure 3.11(a). The maximum overshoot with PI controller is around $22.8A$ and this was eliminated by the $PI + CI$ controller which resulted in 12 % reduction in overshoot.

The control action generated by the PI and $PI + CI$controller is shown in Figure 3.11(b). The reset action of the integrator state, at the instance of first zero crossing of error is clearly visible here. This also gives an understanding of how the reset controller achieves the flat response. It can be observed from Figure 3.11(b) that with classical PI controller the integrator state, after the first zero crossing, takes a finite amount of time to reach its steady state value which ultimately leads to large overshoot and oscillatory response. In the $PI + CI$controller based system, this is avoided through reset action which forces the integrator to its steady state value at first zero crossing.

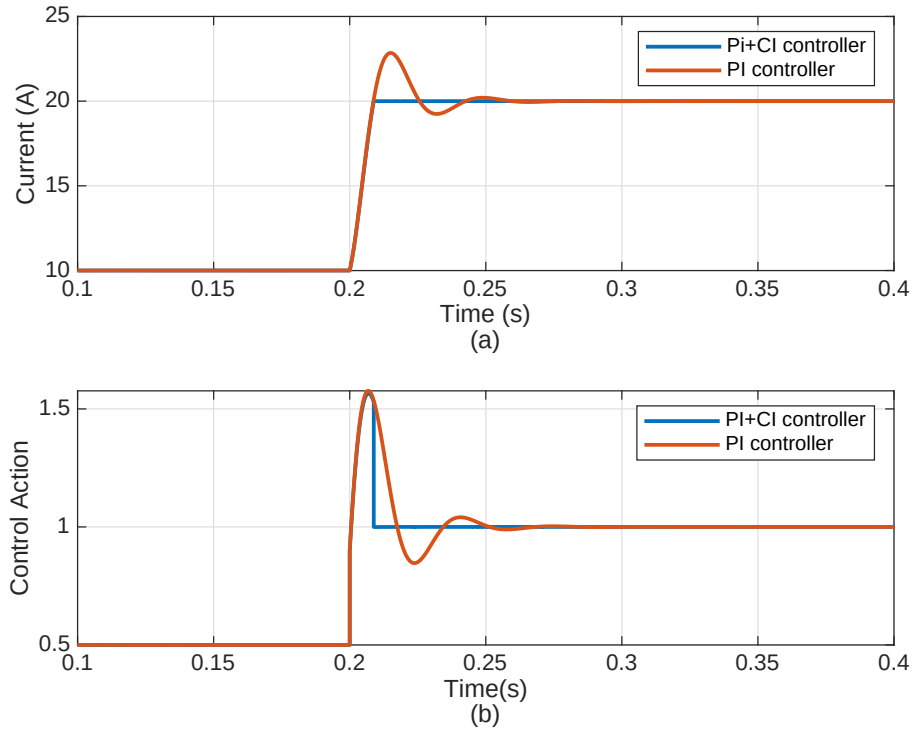

Figure 3.11: A comparison in simulation of (a) step response of the linear PI and the reset $PI + CI$ controllers showing the flat response that can be achieved and (b) the control action.

The utilisation of reset ratio ρ_r obtained from (3.23) ensures that integrator output is driven to its steady state value faster and oscillatory response at the converter output is eliminated.

The DC-DC boost converter, in the application considered here, is operated in the grid feeding mode with the objective to deliver a reference value of current (power) to the microgrid. Under this scenario, the robustness of $PI + CI$ controller can be ascertained by assessing whether it can ensure a flat response to a step change in reference, while also being subjected to a varying input voltage in v_{dc}. This analysis is essential since the input power source in grid connected DC-DC converters, like storage systems (batteries, fuel cell etc) are subjected to voltage variations at their output. This voltage variation exhibited by these sources tend to be of slow dynamics and can be emulated using a DC voltage source superimposed with a low frequency sine wave as shown in Figure 3.12.(b). The converter response when subjected to such a varying power source, while using $PI + CI$ controller, is shown in Figure 3.12.(a) It can be seen that the $PI + CI$

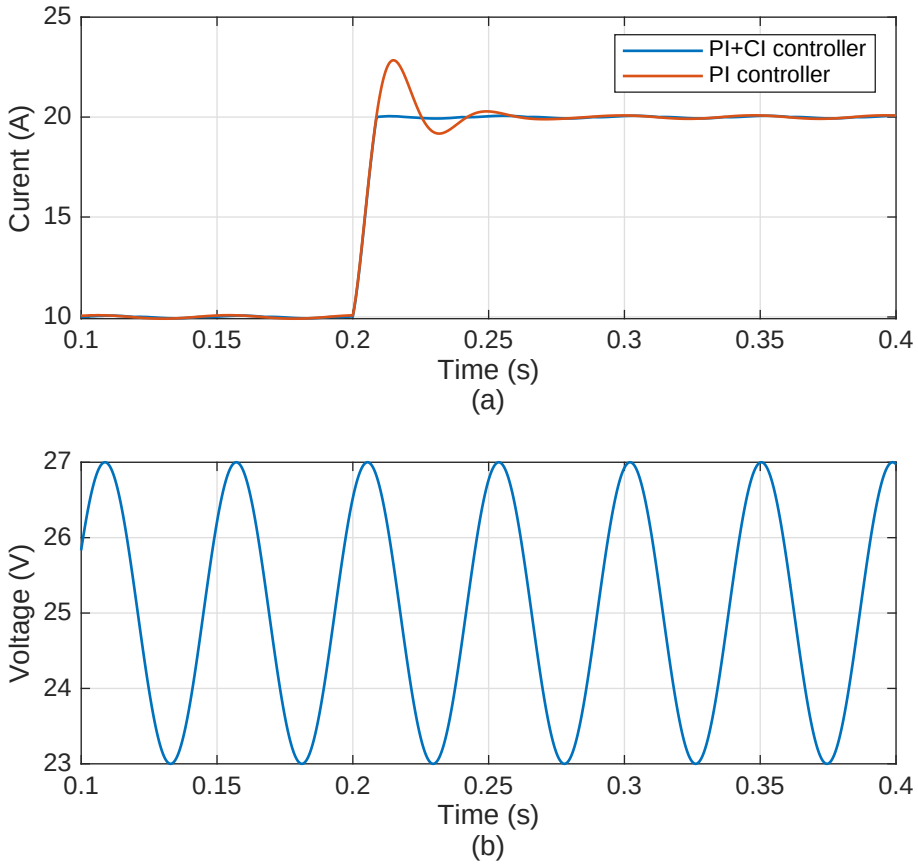

Figure 3.12: Step response of the controller under a varying input voltage (v_{dc}) (a) Step response comparison between PI and $PI+CI$ controller (b) varying input voltage (v_{dc}).

controller is still capable of eliminating the overshoot, in comparison to PI controller, under input voltage variation. Nevertheless, it should be noted that in the steady state both controllers exhibit a small oscillatory behaviour due to the input voltage variation. This is to be expected as the $PI + CI$ controller only targets and improves the transient response by eliminating the overshoot and ensuring a fast settling to steady state value. The robustness of controller to measurement noise will be discussed through the experimental results presented in the next section.

Finally, in order to highlight the robustness of the $PI + CI$ controller to parameter uncertainty the results in Figure 3.13 are presented. This shows the step response of the $PI + CI$ based control system under parameter uncertainty. As is the case before the uncertainty range considered in 10% the nominal value of the passive components. The step responses shown in Figure 3.13 when employing reset control system based

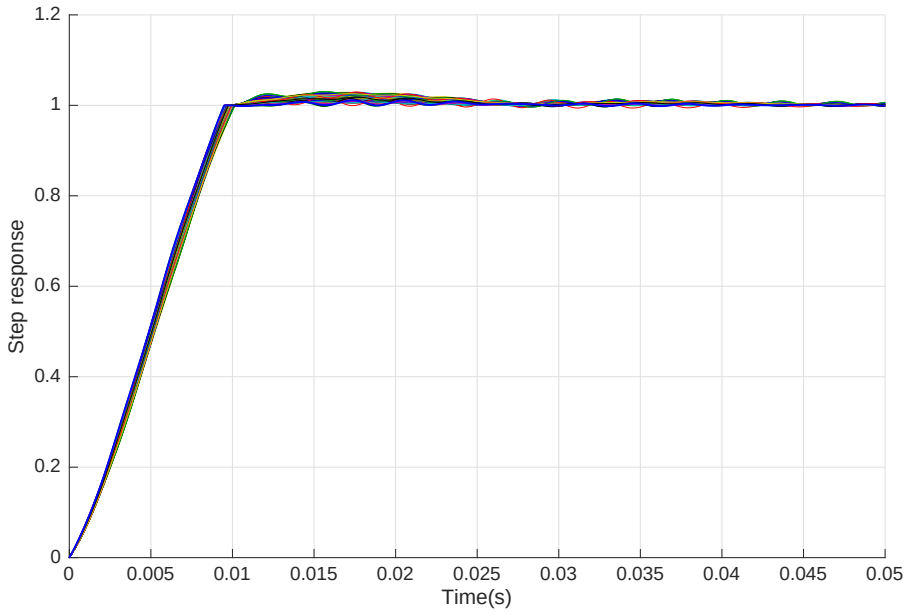

Figure 3.13: Step responses of the designed system for parameter variations in l_1, l_2, c_1 for the designed value of $\rho_r = 0.4889$.

boost converter is obtained by taking 100 random samples within the uncertainty range. Based on the results it is further evident that $PI + CI$ can ensure a stable, near flat response even under parameter uncertainty and highlights its robustness.

3.5.2 Experimental results

The experimental verification of the PI+CI controller for converter control was carried out in the experimental setup shown in Figure 2.4. The controller was programmed in the FPGA of CompactRIO from National instruments using LabVIEW. The data acquisition is carried out using NI 9201 C series voltage input modules which captures hall sensor outputs and samples at 16 μs per channel. The experimental results shown here are based on the output of these modules obtained through LabVIEW interface.

The Figure 3.14 shows the reference tracking performance of the converter under a varying reference alternating between 10A and 20A when used with PI_{base} (fast PI) controller. The higher overshoot which arises at converter output due the fast control action from the PI_{base} can be noticed in Figure 3.14 and is emphasised in Figure 3.15 where the rising edge of the step response is zoomed into. It is this overshoot that can be negated with well designed reset control.

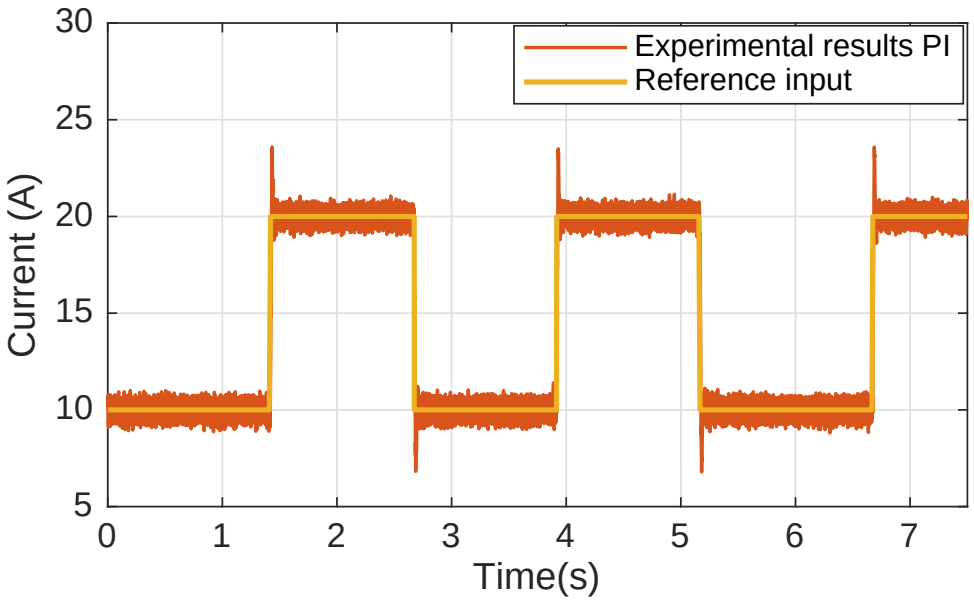

Figure 3.14: Reference tracking performance of the converter (red) when used with PI_{base} controller for reference input (orange). The overshoot with PI_{base} controller can be observed here.

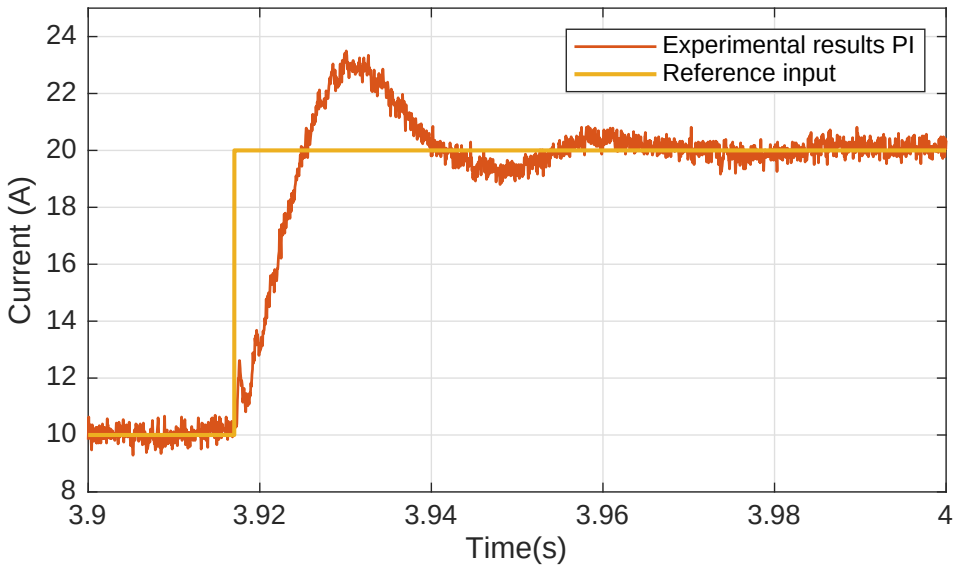

Figure 3.15: Zoom in near a rising edge of the step response in Figure 3.14 highlighting the overshoot resulting from PI_{base} controller.

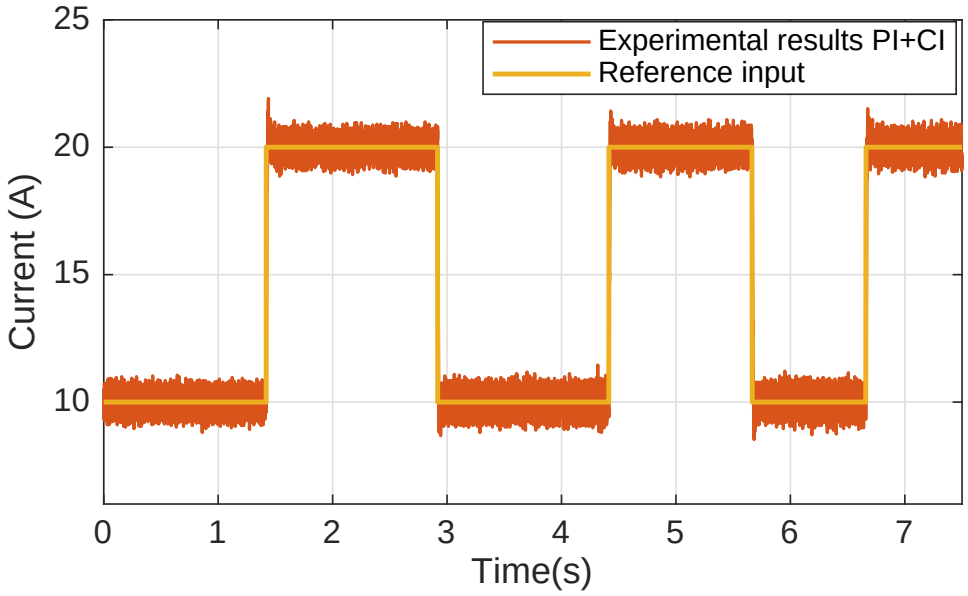

Figure 3.16: Reference tracking performance of converter set up (red) when used with $PI + CI$ reset controller. The flatter response from reset control is observed.

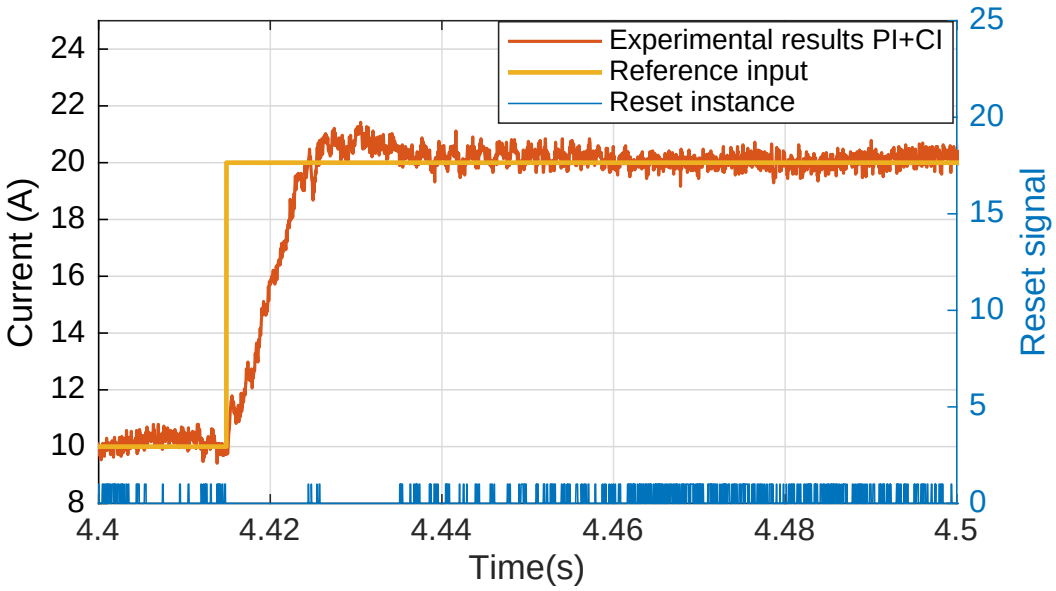

Figure 3.17: Zoom in at rising edge of the step response from Figure 3.16 emphasizing the flat trajectory achieved with reset control and the reset instances (blue).

The Figure 3.16 shows reference tracking of the converter when using the $PI + CI$ controller under a reference value alternating between 10A and 20A. In comparison to Figure 3.14 the tracking performance under $PI + CI$ is devoid of overshoots as shown in Figure 3.16 when subjected to step change in reference value. The absence in overshoot is clearly observed in Figure 3.17 where the response in Figure 3.16 is zoomed at a rising edge. The peak value at the transient period for the $PI + CI$ controller based system shows an almost 10 % reduction in overshoot in comparison to that of the PI controller in Figure 3.15. This is in close accordance with the simulation results presented in Figure 3.11 where a 12% reduction in peak overshoot was observed. The slight discrepancy in the values between simulation and experimental results arise from the unmodelled dynamics of filters in data acquisition side, A/D converters and switching dynamics which where not considered in the simulation models. The Figure 3.17 also shows the reset signals (violet) which resets the CI at the lower portion of figure. In comparison to PI_{base} the absence of output oscillation and faster settling time is evident from the results in Figure 3.15, Figure 3.17 for $PI + CI$ controller.

It is observed that the plot of converter response in Figure 3.14 and Figure 3.16 when using both PI and $PI + CI$ controller appears noisy. This is contributed mainly by the measurement noise of high bandwidth Hall sensors used in the current measurement. The effect of measurement noise on the reset action is observable in Figure 3.17 through the reset signals. The noise corrupted signal used in FPGA causes the CI part of the reset controller to be reset multiple times during steady state condition as evident by the large number of reset signals in Figure 3.17. Nevertheless, it should be noted that the reset signals are well posed (well-defined and are distinct). It should also be noted that the effect of noise inherent to the hall sensor has negligible impact on the stability of the system as evident by the response of PI+CI controller based system in Figure 3.16. This highlights the robustness of the proposed technique under measurement noise. This is also in accordance with the conclusions drawn based on the DF analysis in Section 3.4.2.

3.6 Concluding remarks

The study conducted in this chapter highlights the effectiveness of utilisation of PI+CI controller in converter control stage. The design procedure for the PI+CI control can be utilised in the classical DC/DC converter configurations including the buck, boost or buck-boost systems when subjected to step input. This makes PI+CI controllers suited

for utilisation in DC/DC converters interfacing the FC or battery based systems to grids which are predominantly provided with step references (demonstrated in subsequent chapters) in their current loops. The suitability of PI+CI controllers in the scenario when the reference to the current loop deviates from the step input need to be studied and assessed in the future work. Apart from this, developing design criteria for $PI+CI$ controller under this condition should also be investigated.

The advantage of the PI+CI controllers lies in their simplicity in design and implementation. The designing phase is very similar to the classical PI controller with additional decision needed to be made on determining the reset ratio, ρ_r. Nevertheless, this can be easily carried out using the formulations highlighted in this chapter. Despite their non-linear hybrid nature, simple frequency domain techniques can be utilised in verifying their stability and intuition towards system robustness can be build through describing function analysis. Finally, from a practical perspective implementing these controllers are not computationally expensive. Realising them in FPGA involves adding an additional integrator that reset at the zero crossing of the error signal in parallel to the classical PI controller. The simulation and experimental results highlights the viability, robustness of the controller in converter applications.

In terms of objectives pertaining to converter control stage defined in Chapter 1 the PI+CI controller provides an improvement in dynamic performance of converters, operating in grid feeding mode, by eliminating the overshoot in the power that is being injected into the grid. This elimination of the overshoot also aids in improving the quality of power being injected as well. Finally to conclude, the major publications based on the work carried out in this chapter is given below:

C1 Nair, Unnikrishnan Raveendran, Ramon Costa-Castelló, and Alfonso Baños. "Reset control of boost converters." In 2018 Annual American Control Conference (ACC), pp. 553-558. IEEE, 2018.

J1 Nair, Unnikrishnan Raveendran, Ramon Costa-Castelló, and Alfonso Baños. "Reset Control for DCDC Converters: An Experimental Application." IEEE Access 7 (2019): 128487-128497.

Chapter 4

Primary+secondary control

This chapter presents the work done in this thesis as part of the real-time control of the microgrid system with interconnected hybrid ESS. The control level considered in this chapter is the primary+secondary control from the power management stage. One of the main objective of this chapter will be developing improved voltage regulation and stable control for microgrid under disturbances. Another objective is the development of the real-time power distribution strategy among the hybrid ESS considering operating efficient and ESS degradation. The design methodology of the proposed controls will be discussed and performance will be verified through simulations.

The next level in the power management stage is the primary+secondary control. In the hierarchical control scheme, this is placed above the converter control level presented in the previous chapter and generates set points for the converter systems. As this level is part of the power management stage the control actions are fast and sampling times are small. Prior to developing the primary+secondary control for microgrids with high RES integration and hybrid ESS, an overview of the control strategy employed in the conventional grids is discussed first.

The control system in the conventional power grids is characterised by 3 levels of response. In the event of a sudden load change in the grid, the inertial response is instigated first. In this, the kinetic energy stored in the rotating masses of the generating systems will be used to counter the load variation. The generators in conventional systems are slow acting devices and this kinetic energy acts as a buffer between the

instance of load variation and the generator response. As the kinetic energy is used to counter the load variation, due to the synchronous nature of the sources, the system parameters like voltage or frequency will deviate from the nominal value. The magnitude of the deviation is inversely proportional to moment of inertia associated with the system. Due to the presence of large rotating masses these systems tend to have high inertia associated with them, leading to smaller variations in system parameters and a higher resilience in the grid.

Following inertial response the primary response kicks in which conventional generators ramp up their power output to ensure the power balance in the grid and arrest the deviation of system parameters from nominal value. The primary response tends to be slower. In weak grids, with lesser inertia, the delay in the onset of primary response can cause the grid parameters to deviate significantly from the nominal values to activate the protection relays leading to collapse of the power network.

The primary response only ensures the power balance in the grid but does not bring the system parameters like voltage or frequency back to nominal value. This is because, as said above, due to the synchronous nature of the grid the parameter values are closely related to the kinetic energy of the rotating generating sources. As a portion of this has been utilised in the inertial response they need to be replenished to bring the system parameters back to nominal values. This is achieved by the secondary response in conventional grid. The secondary response is usually directed by the local area operator, who varies the power output of the generating sources so that the system parameters are brought back to nominal value and thus replenishing the used inertial energy. This restoration of the inertial energy is essential so as to ensure the stability and resilience of the grid under load variations in the future.

As discussed in the Chapter 1, modern grid with high RES generation suffer from low system inertia which can be detrimental to the network stability. The ESS can be used to increase the inertia, grid resilience and address the power imbalances arising from the mismatch of RES generation and load demand. In this context, ESS provide dispatchable energy reserves. However, these dispatchable reserves formed by the ESS need to be controlled in real-time to emulate the inertial, primary and secondary responses occurring in conventional grids. Therein lies the objective of the primary+secondary control, developed in this chapter. It will ensure the stability of the weak microgrids though the real-time power management of hybrid ESS and emulation of inertial, primary and secondary responses of the conventional grids.

Therefore, to sum up, the primary+secondary control developed will ensure:

- Stability and voltage regulation in a weak DC microgrid under power imbalances caused by mismatch between non-dispatchable RES generation and load demand.

- Real time power management, splitting among the hybrid ESS such that the inertial, primary and secondary responses of the conventional grid is emulated.

The power management or splitting functionality of the primary+secondary control will be developed to address a very generic hybrid ESS architecture comprising of high power density (SC) and multiple high energy density ESS (battery and regenerative FC) as discussed in Chapter 2. The power splitting will also address the scenario where the total capacity of a single ESS (battery or SC or regenerative FC) is realised using multiple smaller capacity ESS of same type. The design criteria for different stages will also be outlined in this chapter. The developed primary+secondary control will be easily scalable to address any hybrid ESS combination.

The functionalities pertaining to power quality improvement like the harmonics performance, associated resonant behaviour or electromagnetic interference (EMI) /electromagnetic compatibility (EMC) considerations are not accounted here. These aspects will be dealt mostly through the hardware design of converters and their filters which are beyond the scope of this work.

It should be noted that the set points for the ESS generated by the primary+secondary stage will be augmented with the output from tertiary stage, discussed later. The set points from the tertiary stage are updated at a slower rate in comparison to the primary+secondary stage as discussed before. In this scenario the control action from primary+secondary controller modifies these tertiary level set points between the intervals that they are being updated (from tertiary level), such that the stability of the microgrid is maintained.

In the rest of the chapter the primary+secondary control will be developed in two stages. The first stage deals will robust control of microgrid to ensure stability and voltage regulation in the system. The second stage addresses the power management/splitting among the hybrid ESS.

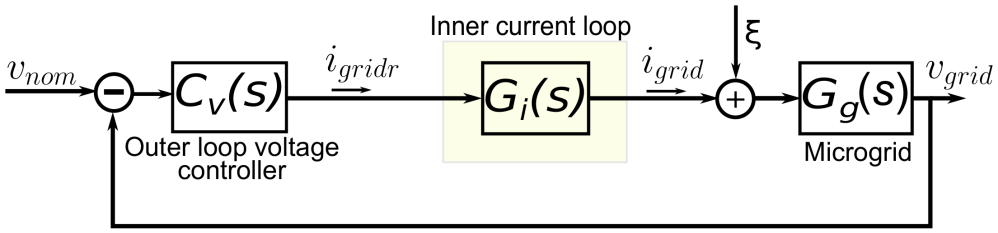

Figure 4.1: Dual loop scheme for voltage regulation control.

4.1 Microgrid stability and voltage regulation with primary+secondary control

Microgrids integrated with high share of RES generation are prone to frequency power imbalances due to the mismatch between generation and load demand. This coupled with the weak nature of the grid will lead to frequent, significant, deviation in grid voltage (DC grid) from the nominal value. The control action from the primary+secondary control cater to these imbalances, to maintain the stability of grid and regulate the grid voltage around a nominal value. In turn, this ensures that the real-time operation of the grid is reliable. The power imbalances occurring in the grid can be considered akin to an external disturbance acting on a system. In this context, the stability and voltage regulating functionality of the primary+secondary control can be considered similar to a disturbance rejection control scheme. The objective will be to develop a robust disturbance rejection scheme with improved dynamic behaviour during voltage regulation. Improving the dynamic behaviour during voltage regulation can also improve the power quality in the grid.

The widely used control architecture for ensuring stability and voltage regulation in microgrids, irrespective of centralised or decentralised schemes, is the dual loop architecture shown in Figure 4.1. This scheme employs an outer loop for voltage and inner loop for current control [64, 125–127]. The inner loop typically represents the converter control stage, discussed in the previous chapter, and performs reference tracking. In the centralised schemes, as considered here, the inner loop represented by $G_i(s)$, in Figure 4.1, represents the equivalent dynamics of the parallel connected converter control stages of the different ESS in the hybrid scheme. An analysis of this inner loop dynamics of the primary+secondary stage will be be presented later on in this chapter. In Figure 4.1 the $C_v(s)$ represents the voltage loop controller whereas the $G_g(s)$ represents the dynamics of the microgrid.

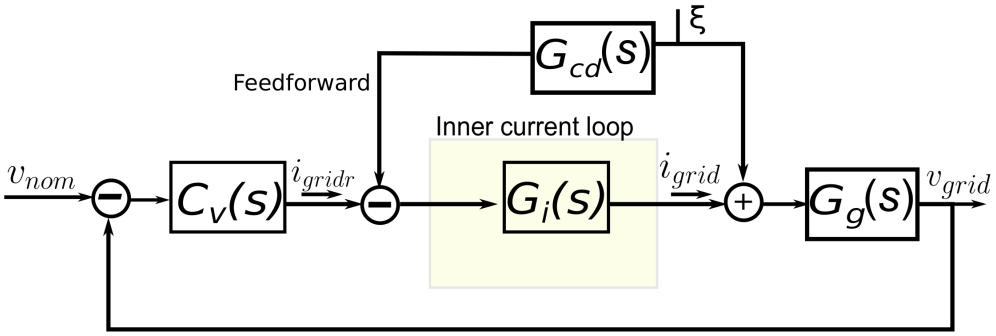

Figure 4.2: Dual loop scheme augmented with disturbance feed-forward for improved transient behaviour.

The voltage loop, in the double loop architecture, is always tuned to be slower than that of the current loop in order to ensure a stable grid behaviour. In the case of weak grids, primary+secondary control should ensure a fast response from the hybrid ESS system to the disturbance, so as to maintain the system stability. Therefore, faster dynamics are expected from the voltage regulation control. Tuning the outer loop controller to ensure faster response has its limitations in terms of system stability. Another method for improving the dynamics of dual loop control is the feed forwarding of the measured disturbances [128, 129] using a feed-forward control scheme of Figure 4.2. However, this requires a complete knowledge of the disturbances through measurements that has to be communicated to the centralised control unit. This leads to an increased utilisation of sensors and high bandwidth communications which can drive up the cost of the control system and in some cases tend to be impractical.

Observer based control systems can help overcome this issue. These observers can provide an estimation of the disturbances using a system model and without relying on high bandwidth communication or extensive metering. This can be achieved using a class of observers derived from the Luenberger observer, called the Disturbance observer [130]. Disturbance observers (DO) utilise an approximate disturbance model, proposed based on prior knowledge of the system behaviour, to provide an estimation of the disturbance acting on the system [131] [132]. These observers are also referred to as an extended state observer (ESO) as it considers disturbance as an additional state of the system. The application of observers in improving the voltage regulation performance of electrical systems have been explored. In [133] an application of ESO is shown for input DC link voltage regulation of a two level, three phase converter. In the above work, the DO is utilised to provide an estimation of the load variations (considered as disturbance) at the converter output. This estimation will then be used in the input DC link voltage

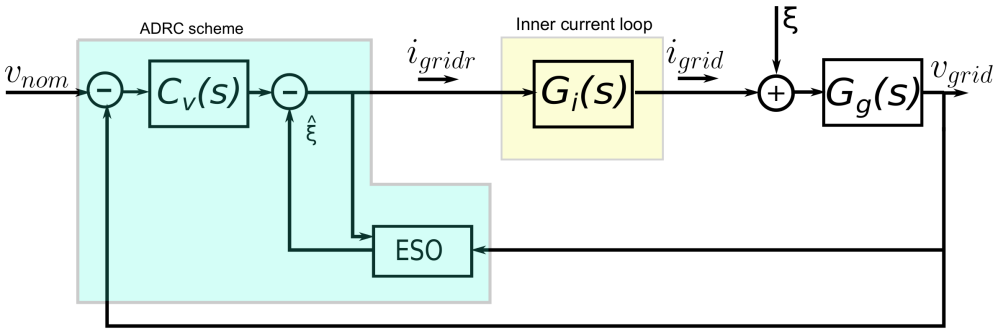

Figure 4.3: The ADRC scheme for voltage regulation and disturbance rejection.

regulation. A similar approach is investigated in [134] where a non-linear observer is used in the regulation of the DC bus voltage in a hybrid AC/DC system. The observer in this work provides an estimation of the load demand at the DC side of the hybrid AC/DC system. The load estimate is then used in the control of the AC/DC converter interfacing the AC side to DC side so as to counteract the Dc side load demand. Finally, the work in [135] proposes the use of an ESO in the DC bus voltage regulation of a cascaded power converter system formed by an AC/DC and DC/DC converters.

The previous applications of ESO in electrical systems have focussed on utilising them for the control in stand alone converter systems. In an interconnected system like microgrid, with high RES generation and multiple energy sources, observers can be used for estimating the disturbances (power imbalance) arising in the microgrid. This estimation can then be used in improving the dynamics of the voltage regulation just like the feed forward control but without using additional sensors to measure the disturbances. In this work the same will be considered by using a linear ESO for the disturbance estimation in the DC microgrid. The estimated disturbance will be used as an additional input to the outer loop, of the dual loop scheme, to improve its transient response and ensure robust grid stability. This proposed voltage regulation architecture using the ESO will henceforth be referred to as the adaptive disturbance rejection control (ADRC) scheme.

4.1.1 The ADRC scheme

The ADRC scheme used for the voltage regulation part of primary+secondary control is shown in Figure 4.3. The ESO will provide an estimation of the disturbance (imbalance power), ξ, in the system. The estimation from the ESO will be augmented with the control action from the outer loop controller ($C_v(s)$) as shown in Figure 4.3. The $G_g(s)$,

in the above figure, is considered as

$$G_g(s) = \frac{1}{s \cdot C_{grid}} \tag{4.1}$$

where C_{grid} is the equivalent capacitance of the grid expressed as a lumped parameter.

Extended State observer (ESO)

The ESO achieves the disturbance estimation by monitoring the grid voltage (v_{grid}), as shown in Figure 4.3, without the need for additional measurements. In order to develop the ESO architecture the relationship between grid voltage and the disturbance is defined. The dynamic equation defining the same is given by

$$C_{grid}\frac{dv_{grid}}{dt} = \xi + i_{grid}, \tag{4.2}$$

where ξ (not known a priori) is defined as

$$\xi = i_{ren} - i_{load}, \tag{4.3}$$

where i_{ren} represents the current injected to the grid by renewable sources and i_{load} represents the current drawn by loads from the grid.

Equation (4.2) can be rewritten as

$$\frac{dv_{grid}}{dt} = k\xi + ki_{grid}, \tag{4.4}$$

where $k = \dfrac{1}{C_{grid}}$ and i_{grid} is the total current supplied to the grid by all the ESS. As discussed before, the ESO incorporates disturbance as an additional state of the system. This requires that a disturbance model be chosen to be augmented with the grid voltage model. The disturbance model considered in this work is given by

$$\frac{d^m\xi}{dt} \approx 0, \tag{4.5}$$

where m is chosen large enough to represent most of the disturbances arising in the microgrid. Additionally, ξ is also assumed to be class C_{m-1}, i.e. the first m-1 derivative of ξ exist and are continuous. The resulting augmented system model incorporating

(4.4) and (4.5) is given by

$$\begin{aligned} \dot{\mathbf{x}}_\mathbf{o} &= \mathbf{A_o}\mathbf{x_o} + \mathbf{b_o}i_{grid} \\ v_{grid} = y &= \mathbf{c_y}\mathbf{x_o} \end{aligned} \tag{4.6}$$

where

$$\mathbf{x_o} = \begin{bmatrix} x_1, x_2, ..., x_{n_o-1}, x_{n_o} \end{bmatrix}^T, \tag{4.7}$$

$$\mathbf{A_o} = \begin{bmatrix} 0 & k & 0 & . & . & . & 0 \\ 0 & 0 & 1 & . & . & . & 0 \\ . & . & . & . & & & . \\ . & . & . & & . & & . \\ . & . & . & & & . & . \\ 0 & 0 & 0 & . & . & . & 1 \\ 0 & 0 & 0 & . & . & . & 0 \end{bmatrix}, \quad \mathbf{b_o} = \begin{bmatrix} k \\ 0 \\ . \\ . \\ . \\ 0 \\ 0 \end{bmatrix}$$
$$, \mathbf{c_y} = \begin{bmatrix} 1 & 0 & . & . & . & 0 & 0 \end{bmatrix}. \tag{4.8}$$

The $\mathbf{x_o} \in \mathbb{R}^{n_o}$ is the state of augmented system such that $x_1 = v_{grid}$, $x_2 = \xi$, $x_{n_o} = \frac{d^m \xi}{dt^m} = 0$ and $\mathbb{R}$ is the set of real numbers. The augmented model of the system having been defined the ESO is model is represented using the same architecture as that of the Luenberger observer [136] given by

$$\dot{\hat{\mathbf{x}}}_\mathbf{o} = \mathbf{A_o}\hat{\mathbf{x}}_\mathbf{o} + \mathbf{b_o}i_{grid} + \mathbf{l_o}(y - \hat{y}), \tag{4.9}$$

where $\hat{\mathbf{x}}_\mathbf{o}$ represents the estimated states of (4.7), $\hat{\mathbf{x}}_\mathbf{2} = \hat{\xi}$ the disturbance estimation, $\hat{y}$ is the estimated value of v_{grid} by ESO and $\mathbf{l_o}$ is the observer gain.

4.1.2 Control law

A generalised control law in $C_v(s)$ for voltage regulation, with $\hat{\xi}$, is given as

$$i_{gridr} = \frac{1}{k}[\dot{v}_{nom} + k_{pv}e_b + k_{iv}\int e_b - \hat{\xi}]. \tag{4.10}$$

where, v_{nom} is the nominal grid voltage, e_b is the tracking error of the grid voltage ($v_{nom} - v_{grid}$), k_{pv}, k_{iv} are the gains of the voltage loop controller ($C_v(s)$) and i_{gridr} is the reference value for inner current loop. If the inner loop in Figure 4.3 is designed with faster dynamics than that of the outer loop, which is usually the case, then the delay introduced by the current loop dynamics from i_{gridr} and i_{grid} will be small and insignificant w.r.t.o the outer loop. In this scenario the following assumption, $i_{gridr} \approx i_{grid}$ can be justified. Under this assumption, substituting (4.10) in (4.4) results in

$$\dot{e}_b + k_{pv}e_b + k_{iv}\int e_b = \hat{\xi} - \xi. \tag{4.11}$$

A properly tuned ESO will be capable of estimating the disturbance with negligible error, resulting in the right hand side of (4.11) tending to zero. Therefore, (4.11) will be dominated by the dynamics of the following characteristic polynomial

$$p_{eb} = s^2 + k_{pv}s + k_{iv}. \tag{4.12}$$

A suitable selection of k_{pv} and k_{iv} will ensure that the voltage regulation loop be Hurwitz with required dynamical characteristics. This guarantees that the tracking error e_b will lie in the vicinity of zero, disregarding the disturbance function ξ. It should be noted that in the control law defined by (4.10) there is a feedback back part formed by k_{pv} and k_{iv} which is incorporated in C_v and a feed forward path formed by $\dot{v}_{nom}$. In the case of the voltage regulation of grid connected system, presented in this work, the nominal grid voltage is constant causing the feed forward term being zero. This results in the classical PI controller being implemented as C_v.

4.1.3 Static gain determination in the ESO

The ADRC part of the primary+secondary stage ensures improved grid voltage regulation (dynamically). This is due to the feed forwarding of the disturbance estimate which

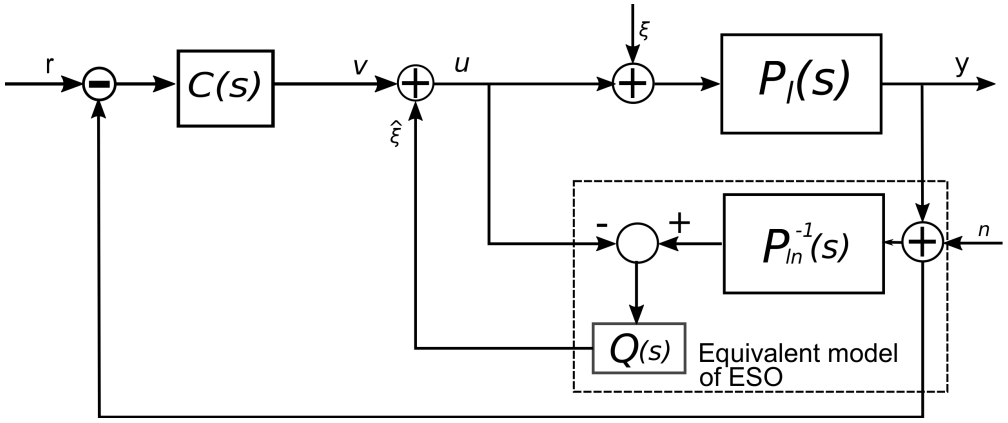

Figure 4.4: Simplified schematic of a generic disturbance rejection control using ESO, with ESO represented using its equivalent model.

is then augmented with the control action from the outer loop controller. Nevertheless, the addition of another dynamic system in the form of ESO in the ADRC scheme can affect the robustness of the voltage regulation control and in turn adversely affect the stability of the microgrid. Therefore, the ESO should be defined cautiously such that the overall robustness of the voltage regulation control is not significantly affected.

The degree of freedom available in defining the ESO, lies in the selection of an appropriate value for the static gain $\mathbf{l_o}$. Considering the Luenberger architecture of the ESO, a straightforward approach for determining $\mathbf{l_o}$ the pole placement technique [137]. In this method, the gains of the observer are determined such that the poles of the observer system are at a position defined prior to by the designer. Typically, the criteria for defining the location of observer poles is such that the observer dynamics are faster than the control loop dynamics. Though the pole placement provides a simple, straightforward method for the determining the static gain $\mathbf{l_o}$, it cannot analytically guarantee that the robustness of the close-loop control is not adversely affected. This drawback is not addressed in the previous works [133–135] which incorporated observers for disturbance rejection in electrical systems.

In order to identify the impact of the ESO on the closed-loop system an understanding of the equivalent behaviour of the ESO needs to be developed first. The Figure 4.4 represents a simplified schematic of a disturbance rejection control using ESO for a generic plant, $P_l(s)$. Unlike the ADRC scheme presented in Figure 4.3 inner loop dynamics are not shown in the simplified representation of Figure 4.4. In Figure 4.4 the ESO is represented through its equivalent model [135, 138] highlighted within the

dotted square region. The v represents the control action from a generic outer loop compensator $C(s)$, r is the reference input, n is the measurement noise and y is the output of the generic plant. The $P_{ln}(s)$ is the nominal model of the plant which is used in the observer design. The nominal model will be a lower order approximation capturing the dominant plant dynamics as is the case with any control problem. The $Q(s)$ represents a proper transfer function and is defined based on the static gain value, $\mathbf{l_o}$, of the observer. Based on the equivalent representation of the ESO, the disturbance estimate can be written, assuming $n = 0$, as

$$\hat{\xi} = -Q(s)u + Q(s)P_{ln}^{-1}(s)y \tag{4.13}$$

where u is as shown in Figure 4.4. Considering the Luenberger structure of the ESO given by (4.9) and the equivalent representation of Figure 4.4, the ESO model can expressed in state space form as

$$\begin{aligned} \dot{\hat{\mathbf{x}}}_\mathbf{o} &= (\mathbf{A_o} - \mathbf{l_o}\mathbf{c_y})\hat{\mathbf{x}}_\mathbf{o} + \begin{bmatrix} \mathbf{b_o} & \mathbf{l_o} \end{bmatrix} \begin{bmatrix} u \\ \\ y \end{bmatrix} \\ \hat{\xi} &= \mathbf{c}_o\hat{\mathbf{x}}_\mathbf{o} \end{aligned} \tag{4.14}$$

where $\mathbf{A_o}, \mathbf{b_o}, \mathbf{c_y}$ are the matrices of ESO consisting of the augmented plant and disturbance model. $\mathbf{c}_o$ is the ESO output matrix which is used to provide disturbance estimate as the output from ESO. Comparing (4.14) and (4.13) $Q(s)$ is given as

$$Q = \left[\begin{array}{c|c} \mathbf{A_o} - \mathbf{l_o}\mathbf{c}_y & -\mathbf{b_o} \\ \hline \mathbf{c_o} & 0 \end{array}\right].$$

The above shows the relationship between $Q(s)$ and $\mathbf{l_o}$. In order to understand the nature of the dynamic behaviour of $Q(s)$ consider the output y of $P(s)$ defined as

$$y = G_{yr}(s)r + G_{y\xi}(s)\xi + G_{yn}(s)n \tag{4.15}$$

where $G_{yr}(s), G_{y\xi}(s), G_{yn}(s)$ are the transfer functions from inputs r, u, n to output y for the schematic shown in Figure 4.4. As $P_{ln}(s)$ defines the dominant dynamics of the

plant, the assumption that $P_l(s) \approx P_{ln}(s)$ can be used and these transfer functions can be given as

$$\begin{aligned} G_{yr}(s) &= \frac{P_l(s)C(s)}{1 + P_l(s)C(s)} \\ G_{y\xi}(s) &= \frac{P_l(s)(1 - Q(s))}{1 + P_l(s)C(s)} \\ G_{yn}(s) &= \frac{P_l(s)C(s) + Q(s)}{1 + P_l(s)C(s)} \end{aligned} \tag{4.16}$$

In the above the $G_{y\xi}$ is the load sensitivity transfer function and G_{yn} is the sensitivity transfer functions [124] of the plant $P_l(s)$. If $Q(s) \approx 1$, it will result in $G_{y\xi} = 0$ making the disturbance input having no effect on the output y. On the other hand if $Q(s) \approx 0$, it will result in $G_{yn}(s) = G_{yr}(s)$. This makes the impact of measurement noise on plant output similar to that of the conventional double loop control architecture, thus eliminating any effect of the ESO on the sensitivity of the closed-loop system to noise. Since the load disturbance tends to be in the lower frequency and measurement noise occupies the high frequency spectrum, the above conditions will be satisfied if $Q(s)$ is a low-pass filter. This will result in unity gain at low frequency and gain roll off at high frequencies, depending on the order of $Q(s)$, thus satisfying both the above conditions. Another important characteristic of $Q(s)$ is that, it always has an order higher than that of the nominal plant model, $P_{ln}(s)$.

The above transfer functions also highlight the need for considering the closed-loop system behaviour into account while determining the gain $\mathbf{l_o}$. As expected the ESO affects the disturbance rejection performance of the closed-loop control as shown in (4.16). Apart from this, if the gain $\mathbf{l_o}$ is not chosen properly it can affect the sensitivity of the closed-loop system to measurement noise. Designing the ESO accounting for the closed-loop behaviour will also ensure that the closed-loop system has certain behavioural characteristics. This allows for easiness in establishing properties of the closed-loop system pertaining to robustness and stability. Considering the above aspects, the gain $\mathbf{l_o}$ of the ESO in the ADRC scheme will be determined accounting for the closed-loop system behaviour in this work.

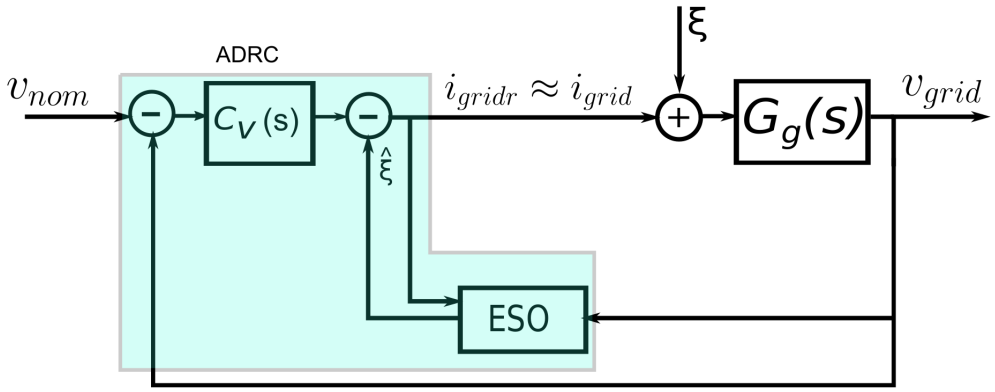

Figure 4.5: The equivalent representation of Figure 4.3 under the approximation of (4.17).

ESO gain determination considering closed-loop system behaviour

In the ADRC scheme represented using Figure 4.3 the inner loop dynamics represented by $G_i(s)$ will be significantly faster than the outer voltage regulation loop dynamics. This will be further evident through the analysis on the inner loop behaviour presented later on in this chapter. In this scenario, from the perspective of the outer loop the delay introduced by $G_i(s)$ will be very small and as such

$$i_{gridr} \approx i_{grid} = u \tag{4.17}$$

presents a valid approximation. Based on this approximation, the ADRC scheme of Figure 4.3 can be represented as Figure 4.5. This approximate representation is similar to the simplified disturbance rejection scheme with ESO given by Figure 4.4.

Considering the above, the ESO model defined in (4.9) can be written in state space notation as

$$\begin{aligned} \dot{\hat{\mathbf{x}}}_\mathbf{o} &= (\mathbf{A_o} - \mathbf{l_o c_y})\hat{\mathbf{x}}_\mathbf{o} + \begin{bmatrix} \mathbf{b_o} & \mathbf{l_o} \end{bmatrix} \begin{bmatrix} i_{gridr} \\ y \end{bmatrix} \\ \hat{\xi} &= \mathbf{c}_o \hat{\mathbf{x}}_\mathbf{o} \end{aligned} \tag{4.18}$$

where $\mathbf{c}_o = \begin{bmatrix} 0 & 1 & . & . & . & 0 & 0 \end{bmatrix}$ and $y = v_{grid}$. In order to determine the gain $\mathbf{l_o}$ of the ESO the closed-loop disturbance rejection transfer function, $G_{y\xi}(s)$, is used. The

$G_{y\xi}(s)$, defined in (4.16), for the approximated closed-loop system of Figure 4.5 is given by

$$G_{y\xi}(s) = \frac{P(s)(1-Q(s))}{1+P(s)C(s)} = \frac{G_g(s)(1-Q(s))}{1+G_g(s)C_v(s)}. \tag{4.19}$$

In order to ensure closed-loop stability under external disturbances the following condition has to be ensured by $G_{y\xi}(s)$ [139]

$$|W_d(s)G_{y\xi}(s)| < 1 \quad \forall s = j\omega \tag{4.20}$$

where $W_d(s)$ is a weighting function chosen such that the dynamic performance of the closed-loop system has certain characteristics. Substituting (4.19) in (4.20) and rewriting as

$$\left| W_d(s)\frac{G_g(s)}{1+G_g(s)C_v(s)} \cdot (1-Q(s)) \right| < 1 \quad \forall s = j\omega \tag{4.21}$$

facilitates treating (4.21) as a constraint in (1-Q(s)). Based on this, using a weighting function $W_\xi(s)$ such that

$$\left| W_d(s)\frac{G_g(s)}{1+G_g(s)C_v(s)} \right| < |W_\xi(s)| \quad \forall s = j\omega \tag{4.22}$$

allows (4.21) to be represented in a simplified form given by

$$|W_\xi(s) \cdot (1-Q(s))| < 1 \quad \forall s = j\omega. \tag{4.23}$$

This simplified condition ensures two aspects. Firstly, it bounds the frequency response of the closed-loop disturbance rejection transfer function, thereby ensuring system stability under external disturbances. Secondly, based on Figure 4.4, the $Q(s)$ is the transfer function from ξ to $\hat{\xi}$. Therefore, $1-Q(s)$ will represent the dynamics of the disturbance estimation error $(\xi - \hat{\xi})$. Therefore, by choosing a proper $W_\xi(s)$, the error dynamics of the ESO disturbance estimation can be controlled and in turn the dynamics of the disturbance rejection performance. Based on the low-pass nature of $Q(s)$, the $1-Q(s)$ will exhibit a high-pass characteristic and W_ξ can used to establish a lower bound on the cut-off frequency of $1-Q(s)$. Representing $1-Q(s)$ as the transfer function $G_{\hat{\xi}\xi}(s)$, the condition in (4.23) can be equivalently represented using the $\mathbf{H}_\infty$

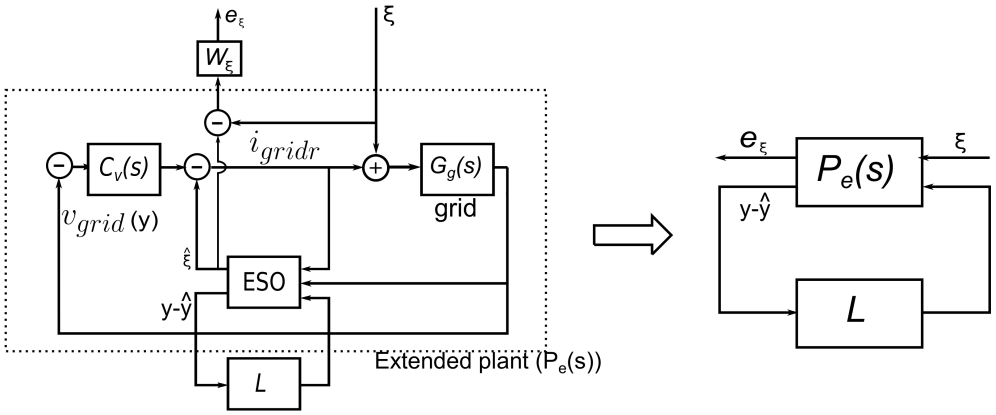

Figure 4.6: Equivalent representation of Figure 4.5 as a feedback interconnection of an extended plant and static gain.

norm [140] as a bound given by

$$\|W_\xi(s)G_{\hat{\xi}\xi}(s)\|_\infty < 1. \tag{4.24}$$

A detailed discussion on the transfer function norms will be provided in Appendix A.

The gain determination in the ESO can now be defined as a $\mathbf{H}_\infty$ bound problem given by

$$\begin{aligned} &\text{Find } Q(s) \text{ such that} \\ &\|W_\xi(s)G_{\hat{\xi}\xi}(s)\|_\infty < 1 \end{aligned} \tag{4.25}$$

Solving the above problem involves finding a $Q(s)$ with low-pass characteristics and higher order than the nominal plant model, in the rational transfer function space. Searching for such a $Q(s)$ in the infinite dimensional rational transfer function space is a difficult problem to solve. However, $Q(s)$ can be represented in terms of static gain $\mathbf{l_o}$ as shown (4.1.3). The utilisation of the same can be used to transform (4.25) into a search for static gain $\mathbf{l_o}$ given by

$$\begin{aligned} &\text{Find } \mathbf{l_o} \in \mathbb{R}^{n_o} \text{ such that} \\ &\|W_\xi(s)G_{\hat{\xi}\xi}(s)\|_\infty < 1 \end{aligned} \tag{4.26}$$

where n_o is the order of ESO as given in (4.7). The fixing of the disturbance model facilitates limiting the dimension of $\mathbf{l_o}$ and thus convert the (4.26) to a search in the finite dimensional vector space. Extracting the gain, $\mathbf{l_o}$ out of the closed-loop system,

the ADRC scheme of Figure 4.5 can be equivalently represented by Figure 4.6 as a feedback connection of a static gain with an extended plant $P_e(s)$ (shown inside the dotted region). This is further reduced to the abstract feedback interconnection form (F_{bl}) [124], given in Figure 4.6. The optimisation problem in (4.26) can be equivalently transformed into a synthesis problem of finding optimal static feedback gain $\mathbf{l_o}$ for the extended plant $P_e(S)$ such that the $\mathbf{H}_\infty$ norm of closed-loop system is less than 1. This is analytically written as

$$\|F_{bl}(P_e(s), \mathbf{l_o}), \mathbf{l_o}\|_\infty < 1. \tag{4.27}$$

The system matrices of the ESO, $P_e(s)$ for the representation shown in Figure 4.6 are

$$ESO = \left[\begin{array}{c|ccc} \mathbf{A_o} & \mathbf{b_o} & 0 & I \\ \hline \mathbf{c}_o & 0 & 0 & 0 \\ \mathbf{c}_y & 0 & -I & 0 \end{array}\right], P_e(s) = \left[\begin{array}{c|cc} \mathbf{A_e} & \mathbf{B}_{e1} & \mathbf{B}_{e1} \\ \hline \mathbf{C}_{e1} & \mathbf{D}_{e11} & \mathbf{D}_{e12} \\ \mathbf{C}_{e2} & \mathbf{D}_{e21} & \mathbf{D}_{e22} \end{array}\right] \tag{4.28}$$

where $\mathbf{A_e} \in \mathbb{R}^{n_e \times n_e}$ with n_e is the order of $P_e(s)$. The $\mathbf{D}_{e11} \in \mathbb{R}^{1\times 1}$ and $\mathbf{D}_{e22} \in \mathbb{R}^{1\times(n_o)}$.

The gain synthesis problem that satisfies the condition (4.27), for the system represented in Figure 4.6, can now be represented as a linear matrix inequality (LMI) problem, based on the theorem defined in [141]. If the following conditions

- W_ξ is a stable transfer function
- The pair (A_o, B_{e2}) is stabilisable
- The pair (A_o, C_{e2}) is observable
- $D_{e22} = 0$

are satisfied, the Theorem 4.1 can be stated as below

Theorem 4.1. *[141] There exists a stabilizing gain $\mathbf{l_o}$ for the plant $P_e(s)$, with minimal realisation, such that $\|F_{bl}(P_e(s), \mathbf{l_o}), \mathbf{l_o}\|_\infty < \gamma$, if and only if there exists two symmetric*

matrices $\mathbf{S}$ *and* $\mathbf{R}$ *such that*

$$\begin{bmatrix} N_R^T & 0 \\ 0 & I \end{bmatrix} \begin{bmatrix} \mathbf{A}_e\mathbf{R} + \mathbf{R}\mathbf{A}_e^T & \mathbf{R}\mathbf{C}_{e1}^T & \mathbf{B}_{e1} \\ \mathbf{C}_{e1}\mathbf{R} & -\gamma I & \mathbf{D}_{e11} \\ \mathbf{B}_{e1}^T & \mathbf{D}_{e11}^T & -\gamma I \end{bmatrix} \begin{bmatrix} N_R & 0 \\ 0 & I \end{bmatrix} \prec 0 \tag{4.29}$$

$$\begin{bmatrix} N_S^T & 0 \\ 0 & I \end{bmatrix} \begin{bmatrix} \mathbf{A}_e^T\mathbf{S} + \mathbf{S}\mathbf{A}_e & \mathbf{S}\mathbf{B}_{e1} & \mathbf{C}_{e1}^T \\ \mathbf{B}_{e1}^T\mathbf{S} & -\gamma I & \mathbf{D}_{e11}^T \\ \mathbf{C}_{e1}^T & \mathbf{D}_{e11} & -\gamma I \end{bmatrix} \begin{bmatrix} N_S & 0 \\ 0 & I \end{bmatrix} \prec 0 \tag{4.30}$$

$$\begin{bmatrix} \mathbf{R} & I \\ I & \mathbf{S} \end{bmatrix} \prec 0 \tag{4.31}$$

$$Rank(RS - 1) = 0 \tag{4.32}$$

where N_R, N_S *are bases of the null space of* $\begin{bmatrix} \mathbf{B}_{e2}^T & \mathbf{D}_{e12}^T \end{bmatrix}$ *and* $\begin{bmatrix} \mathbf{C}_{e2}^T & \mathbf{D}_{e21}^T \end{bmatrix}$ *respectively.*

The condition $D_{e22} = 0$ is trivially satisfied based on (4.28). In the above LMI problem, the conditions (4.29), (4.30), (4.31) are convex constraints on $\mathbf{S}$ and $\mathbf{R}$. However, the constraint (4.32) is non-convex resulting in the above problem being difficult to solve. The reason for the same being that the dimension of the static gain $\mathbf{l_o}$, given by n_o, is less than the order n_e of the extended plant. In the scenario where the dimension of $\mathbf{l_o}$ is less than the order of $P_e(s)$, the LMI feasibility problem of Theorem 4.1 can be replaced with the trace minimisation problem according to [142].

The equivalent trace (tr) minimisation problem is given by

$$\begin{aligned} &\min_{\mathbf{R},\mathbf{S}\in\mathbb{R}^{nl\times nl}} tr(\mathbf{RS}) \\ &\text{Subject to } : (4.29), (4.30), (4.31). \end{aligned} \tag{4.33}$$

Though the above objective function is still not convex, the cone complementary linearisation algorithm defined in [143] can now be used for solving this optimisation problem

in an iterative manner. According to the algorithm the linearised representation of (4.33) is given by

$$\begin{aligned} &\min_{\mathbf{R}_{k+1},\mathbf{S}_{k+1}} \; tr(\mathbf{R}_{k+1}\mathbf{S}_k + \mathbf{R}_k\mathbf{S}_{k+1}). \\ &\text{Subject to } : (4.29), (4.30), (4.31) \end{aligned} \tag{4.34}$$

The above presents a convex optimisation problem which can be easily solved. The iterative process of solving the above optimisation problem to find the $\mathbf{R}, \mathbf{S}$ matrices is given as the following steps

1. Define the system matrices for $P_e(s)$
2. Solve LMI feasibility problem for the conditions (4.29), (4.30), (4.31) to find an initial $\mathbf{R}_0, \mathbf{S}_0$
3. If no feasible $\mathbf{R}_0, \mathbf{S}_0$ exists. Exit the iterative process. Else set k=0
4. Solve the convex optimisation problem (4.34) for $\mathbf{R}_{k+1}, \mathbf{S}_{k+1}$.
5. Check if stopping criteria has reached. If the criteria is satisfied exit the iterative process, else go to Step 4.

Solving the cone complementary linearisation algorithm described above will result in obtaining $\mathbf{R}$ and $\mathbf{S}$ that satisfies (4.34). The static gain, $\mathbf{l_o}$, that satisfies $\|F_{bl}(P_e(s), \mathbf{l_o}), \mathbf{l_o}\|_\infty < \gamma$ can now be found by solving the following LMI

$$\begin{bmatrix} \mathbf{A}_e^T\mathbf{S} + \mathbf{S}\mathbf{A}_e & \mathbf{S}\mathbf{B}_{e1} & \mathbf{C}_{e1}^T \\ \mathbf{B}_{e1}^T\mathbf{S} & -\gamma I & \mathbf{D}_{e11}^T \\ \mathbf{C}_{e1}^T & \mathbf{D}_{e11} & -\gamma I \end{bmatrix} + \begin{bmatrix} \mathbf{C}_{e1}^T \\ \mathbf{D}_{e21}^T \\ 0 \end{bmatrix} \mathbf{l_o}^T \begin{bmatrix} \mathbf{B}_{e2}^T\mathbf{S} & 0 & \mathbf{D}_{e12}^T \end{bmatrix} \tag{4.35}$$

$$+ \begin{bmatrix} \mathbf{S}\mathbf{B}_{e2} \\ 0 \\ \mathbf{D}_{e12} \end{bmatrix} \mathbf{l_o} \begin{bmatrix} \mathbf{C}_{e1} & \mathbf{D}_{e21} & 0 \end{bmatrix} \prec 0. \tag{4.36}$$

The design of static gain, $\mathbf{l_o}$, considering the $\mathbf{H}_\infty$ norm of the closed-loop disturbance rejection transfer function presents another advantage. Through the bounding of $\mathbf{H}_\infty$ norm the design allows to bound the $\mathbf{L}_2$ norm of the system output y under a disturbance. If the $\mathbf{L}_2$ norm of the disturbance signal ξ is $\|\xi\|_2$ then the $\mathbf{L}_2$ norm of output, $\|y\|_2$, can be bounded as [140]

$$\|y\|_2 \leq \|G_{y\xi}\|_\infty \|\xi\|_2 \tag{4.37}$$

where $\|G_{y\xi}\|_\infty$ is the $\mathbf{H}_\infty$ norm of the disturbance rejection transfer function. The $\mathbf{L}_2$ norm of a signal gives an indication about the energy associated with the same [140] (see Appendix). Therefore by bounding the $\mathbf{L}_2$ norm of the output response under the disturbance, the energy associated with the output is bounded and in turn the system stability. A detailed discussion on the $\mathbf{L}-$ norms for signals and their physical implications can be found in Appendix A.

This concludes the part of the primary+secondary control that ensure the stability and improved voltage regulation in weak microgrids during frequent power imbalances that occur in the system. The ADRC scheme, proposed for the same, ensures the stability of microgrid and faster dynamics in the voltage regulation through feed forwarding of the disturbance estimate. The design methodology using LMI, for the gain determination in the ESO of the ADRC scheme, accounting for closed-loop behaviour guarantees that the faster voltage regulation dynamics are achieved without compromising on the robustness of the control system.

4.2 Power management among hybrid ESS with primary+secondary control

The control action from the outer loop, i_{gridr}, is the reference value for sum total of current (power) to be injected or absorbed from the grid to ensure the system stability. This power catered to the microgrid should be distributed, in real-time, by the primary+secondary control among the different ESS in the hybrid scheme. As discussed before, in the event of a power imbalance, another objective of the primary+secondary control is to emulate the inertial, primary and secondary responses of the conventional grid. The power splitting strategy in the primary+secondary control tries to emulate the above responses so that a reliable operation of the weak microgrid is achieved.

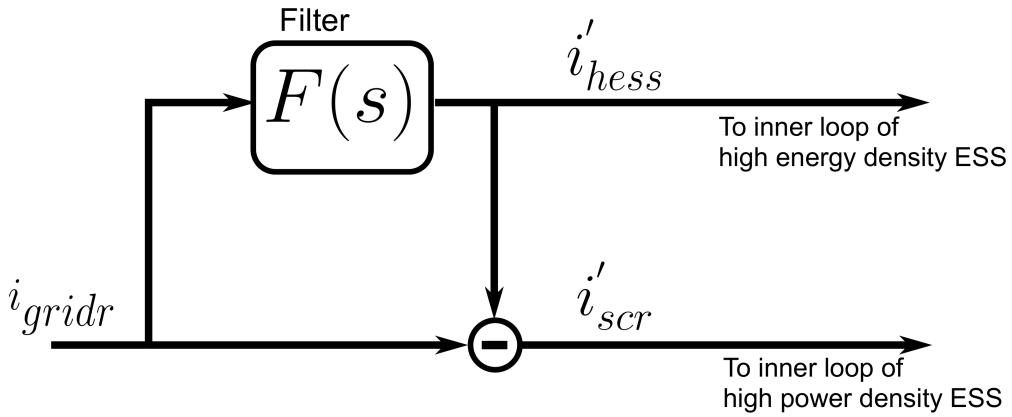

Figure 4.7: Splitting of the outer loop control action (i_{gridr}) among high power and energy density ESS using a low-pass filter to emulate inertial and primary responses.

4.2.1 Power splitting between high power and energy density ESS

In the event of a power imbalance, the inertial response is the first and the fastest acting reaction to the imbalance. As discussed before, in the hybrid ESS system of high power and energy density ESS the former is capable of such fast reactions. Therefore, the inherently fast acting SC (high power density ESS) should be tasked with emulating the inertial response and improving the grid resiliency. The high energy density ESS (Batteries, FC) with their large storage capacity can ensure power balance in the long run. These ESS tend to be slow acting and as such have slower reaction times. As a result, the high energy density ESS can be used to emulate the primary response.

This kind of a response from the high power and energy density ESS can be achieved using a frequency based splitting of the control action from the outer loop using a filter. The high frequency portion of the control action (i_{gridr}) will be directed to the high power density ESS and the low frequency portion will be directed to the high energy density ESS using a low-pass filter $F(s)$ as shown in Figure 4.7. The previous literatures on power splitting schemes in a hybrid ESS framework also used a similar approach. These works used either a filter [70, 144–147] or wavelet transformations [148–150] to split the power among the different ESS in a hybrid architecture.

The filter based power splitting approach have been considered in this work over the wavelet transformation mainly from the perspective of easiness in practical implementation. Based on the power splitting presented in Figure 4.7, the reference value of

current (power) to be catered by the high energy ($i^{'}_{hess}$) and power density ESS ($i^{'}_{scr}$) is given by

$$i^{'}_{scr}(s) = i_{gridr}(s)(F(s) - 1) \tag{4.38}$$

$$i^{'}_{hess}(s) = i_{gridr}(s) \cdot F(s). \tag{4.39}$$

In the case where multiple different ESS constitute the total capacity formed by the high energy density ESS, like battery and regenerative FC as considered here, the $i^{'}_{hess}$ is indicative of the total power that has to be contributed by all the ESS together. The design consideration of the low-pass filter, $F(s)$, will be presented later on this section after introducing other aspects of the real-time power management in the primary+secondary level.

Power management among high energy density ESS

As shown above, $i^{'}_{hess}$ is the total current to be provided by the high energy density ESS. In many practical cases a single storage device like battery will be sufficient to meet the energy storage capacity demanded of the high energy density ESS. In such scenarios the $i^{'}_{hess}$ will be catered entirely by the battery system. However, in some applications (like islanded operation) the amount of energy to be stored in high energy density ESS is very large. In this scenario, the total energy to be stored needs to be distributed among the battery and another high energy density ESS, like the FC-electrolyser system. This is done considering economic factors involved in the integration of storage systems and operation efficiency of the same, as discussed in Chapter2. Typically the usage of both battery and FC-electrolyser system is done when the PHS or CAES is not considered as a viable solution for high energy density ESS. In these situations, the primary+secondary control should also make the power management decision between the different high energy density ESS.

As discussed in Chapter1, the battery has higher round cycle efficiency compared to the FC-electrolyser system. Therefore, from the standpoint of operational efficiency of the microgrid the utilisation of battery is more preferential. Nevertheless, care should also taken to ensure that the battery is not highly charged or deep discharged, as this can degrade the battery [83]. In the case of FC-electrolyser system, apart from low operational efficiency, care should also be taken to ensure that these systems are not subjected to sudden changes in the power demanded from them. This can lead to degradation in

FC systems from fuel starvation [88]. Therefore, the real-time management of power among the high energy density ESS should be carried out, by the primary+secondary control, considering the operational efficiency of the microgrid and degradation mechanism of the different ESS.

In this scenario, a straightforward approach will be to utilise the battery as long as the battery is within the safe SOC limits. The FC-electrolyser system will then be utilised only when the battery is fully charged or discharged. In this way both operational efficiency and battery degradation is accounted. A similar approach was proposed in [146] where an adaptive filter with varying cut-off frequency, depending on battery SOC (SOC_b), was used to facilitate the power split between battery and FC system. However, ensuring the system stability when utilising a filter with varying cut-off frequency (depending on the SOC_b) can be tedious.

In this work, to avoid this, a threshold based approach utilising SOC_b is considered. As long as the SOC of battery is within the allowed limits, the $i^{'}_{hess}$ will be catered by battery and thereafter by the FC system. This can be achieved with a classical threshold function as shown in Figure 4.8. However, such a splitting can result in an abrupt switch of the outer loop control action from battery to the FC side. This is not advisable as the sudden switch to FC side will result in a abrupt change in the setpoint to the FC system. As discussed before the FC is not capable of delivering a sudden change in its output power and should not be forced to do the same. Therefore to overcome this, the threshold based approach is modified to ensure a gradual transition from the battery to FC side using the SOC_b as defining criteria for the transition.

This can be achieved with a sigmoid function instead of the classical threshold function. The sigmoid is any S shaped function, typically defined using the logistic function

$$\mathcal{S}(x) = \frac{1}{1 + e^{-a_s(x-c_s)}} \tag{4.40}$$

where a_s, c_s are constants that define the steepness, offset of the sigmoid function respectively. Unlike the threshold function, the advantage of the sigmoid function is that it is differentiable at every point, thus ensuring a smooth transition between the ESS.

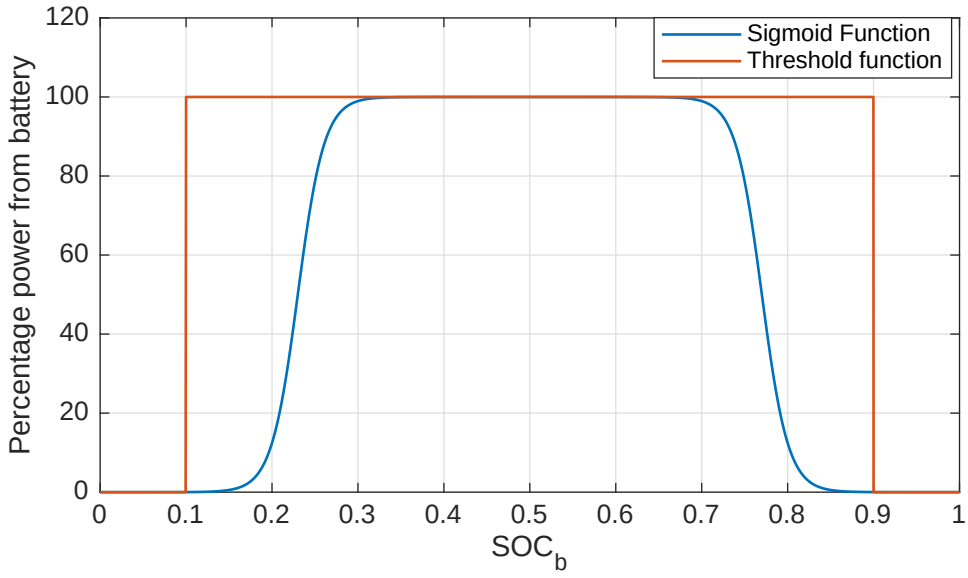

Figure 4.8: Comparison of power splitting strategy between high power density ESS using hard threshold and sigmoid function. The smoother behaviour of the sigmoid compared to hard threshold is evident.

In the primary+secondary control, to facilitate the splitting of i'_{hess} between the battery and FC system a double sigmoid function of the form

$$\mathcal{S}(SOC_{\mathrm{b}}) = \left(\frac{1}{1 + e^{-a_s(SOC_{\mathrm{b}} - c_{s1})}} + \frac{1}{1 + e^{a_s(SOC_{\mathrm{b}} - c_{s2})}} \right) \cdot 100(\%) \tag{4.41}$$

will be used. The output of the double sigmoid function is shown in Figure 4.8 and represents the percentage of i'_{hess} catered by the battery system. The remaining portion will be catered by the FC system. This splitting of i'_{hess} using the sigmoid function, to generate the set points for the inner loops of battery and FC system is schematically represented using Figure 4.9. According to Figure 4.8, it can be seen that as SOC_{b} is getting too low or high, the sigmoid progressively reduces the power catered by the battery and shifts it to the FC. Therefore, even before the limits of SOC_{b} are reached the battery power is shifted to the FC providing further protection to the battery. The rate at which the FC takes over the power demand is adjusted by choosing a proper value for a_s in (4.41). The c_{s1}, c_{s2} in (4.41) determine the values of SOC_{b} at which the power delivery start to switch from battery to FC system. Typically the lower and upper limits of SOC_{b} are 0.1 and 0.9 respectively. As a result, the selection of c_{s1}, c_{s2} as 0.2 and 0.8 should ensure adequate protection to the battery against deep discharge and over charging. Based on the power splitting schematic shown in Figure 4.9 the set

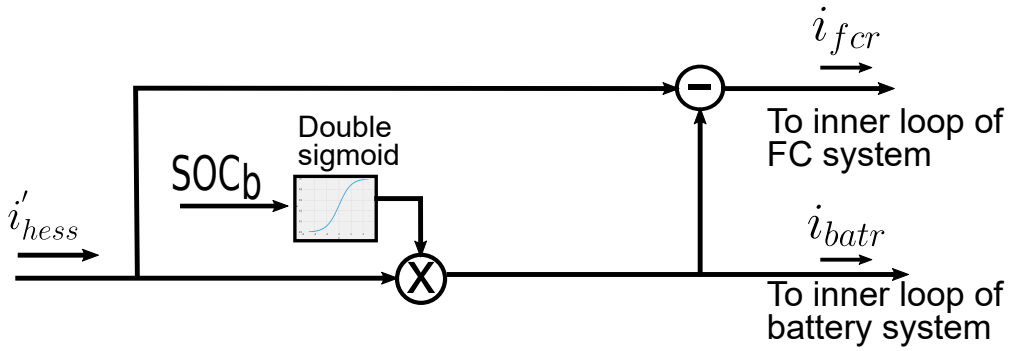

Figure 4.9: Schematic of power splitting among the high energy density ESS (battery and FC-electrolyser system).

points for the battery (i_{batr}) and FC current (i_{fcr}) inner loops are given by

$$i_{batr} = i_{hess} \cdot \mathcal{S}(SOC_{\mathrm{b}}) \tag{4.42}$$

$$i_{fcr} = i_{hess} \cdot (\mathcal{S}(SOC_{\mathrm{b}}) - 1). \tag{4.43}$$

In practical implementation, the double sigmoid function can be realised in a microcontroller or FPGA either using its piece wise linear approximations [151] or using MATLAB which can generate a HDL compatible look-up table of the sigmoid function that can be programmed into an FPGA.

4.2.2 Charge restoration in SC

The inertial response from the SC will result in an increase or decrease of the energy stored in these systems. This change in stored energy can affect the ability of the SC to effectively handle the future power imbalances that can arise in the microgrid, thus affecting the grid resiliency. Therefore, corrective measures should be incorporated in the primary+secondary control to ensure that the energy change occurring in the SC after an inertial response is addressed. It is always beneficial to maintain the energy levels in the SC around a nominal value such that the SC is always capable of effectively addressing future power imbalance scenarios arising in the grid. A good practice will be to ensure that the SC is always in a half charged state. This ensures that there is always half the capacity of SC for absorbing surplus power from grid or meet the demands of the grid. Ensuring that the SC is always half charged, throughout the operation, can be ensured through an additional control stage implemented in the primary+secondary level. This process of bringing the stored energy in SC back to a nominal value after

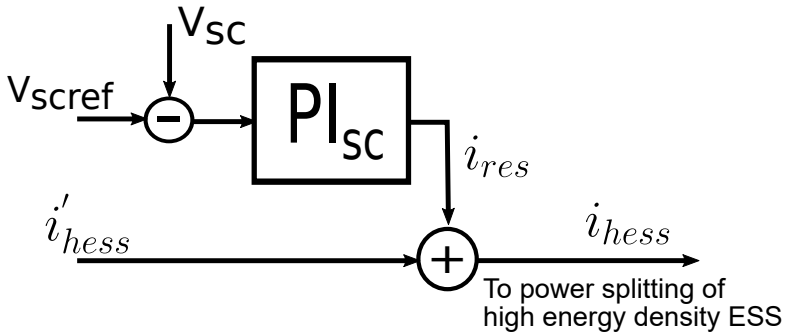

Figure 4.10: Charge restoration control for SC in the primary+secondary level.

every inertial response is similar to emulating secondary response in conventional grid, where the inertial energy of rotating masses are restored.. This charge restoration in SC is very important, as it always ensures that the weak microgrid has sufficient resiliency to handle future power imbalances.

Unlike the conventional grid, utilisation of the inertial energy from the SC will not be reflected in any of the grid parameter like voltage or frequency. This is because, these ESS are interfaced to grid in a decoupled manner through the power converters. Therefore, unlike conventional grids, monitoring system parameters like voltage or frequency will not give an indication of the amount of inertial energy that needs to be replenished. In this scenario a different approach is used for the energy restoration in SC. The supercapacitors have an almost linear relationship between the SOC and output voltage [152]. This enables the usage of measured output voltage of SC for the charge restoration purpose. This is highlighted in Figure 4.10 where the SC output voltage is compared with the a reference value, pertaining to the half SOC level in SC, to generate a control action. The control action, i_{res}, will be added to $i^{'}_{hess}$ and will be catered either by the battery or FC depending on the criteria defined in the previous section. It should be noted that the exact value of the voltage that ensures the half-charged state of SC will not be easily obtainable. Nevertheless, a judicious choice can be made by studying the SOC vs voltage curve of the SC. This ensures that the SC is always near the half charged region. Based on the SC charge restoration control the total reference current for the high energy density ESS (i_{hess})is given by

$$i_{hess} = i_{res} + i^{'}_{hess}. \tag{4.44}$$

It should be noted that in the discussion for power splitting among battery and FC system $i^{'}_{hess}$ was considered as the reference value for the total current to be catered by

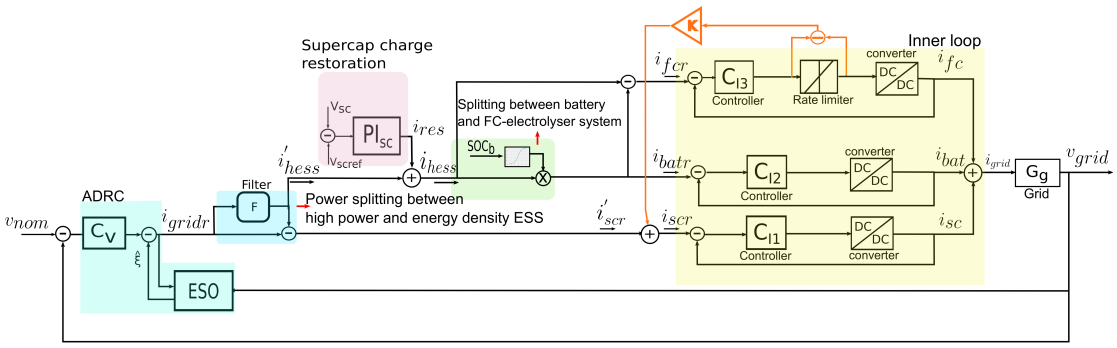

Figure 4.11: Schematic of the power splitting strategy among the SC, battery and FC electrolyser system along with the charge restoration in SC.

the high energy density ESS. However, i'_{hess} does not account for SC voltage restoration control. Accounting for the same, i_{hess} will be reference for total current catered by the high energy density ESS and will be used in (4.42).

The discussion above have introduced, in stages, the methodology utilised in the primary+secondary control to ensure the real-time power management among the different ESS in the hybrid scheme and emulation of different responses. The generation of set-points for the inner loops of the different ESS have also been identified. A unified primary+secondary control schematic incorporating the ADRC scheme and the power management strategies presented through Figure 4.7 , Figure 4.9 and Figure 4.10 is provided in Figure 4.11. The C_{I1}, C_{I2}, C_{I3} are the controllers for the converter control loop for SC, battery and FC systems. There are some aspects in Figure 4.11 which has not been discussed before. The inner loops are no longer represented using the equivalent dynamics given by $G_i(s)$. Instead, an elaborated representation of the individual inner converter control loops of the different ESS are provided. It can be noticed that the current loop of the FC-electrolyser system is provided with a rate limiter. This is done to further ensure that the FC system is protected from sudden setpoint changes and thus reduce the rate of degradation. The current mismatch between the i_{fcr} and i_{fc} (actual current injected to grid from FC system) due to the effect of ramp limiter will be catered by the SC as shown in Figure 4.11, to ensure power balance in the grid.

4.2.3 Design consideration for the power splitting filter

As discussed in Section 4.2.1 the low-pass filter ($F(s)$) provides a power split between the high power and energy density ESS. In order to introduce the design consideration for $F(s)$ consider the real-time power management part of the primary+secondary control

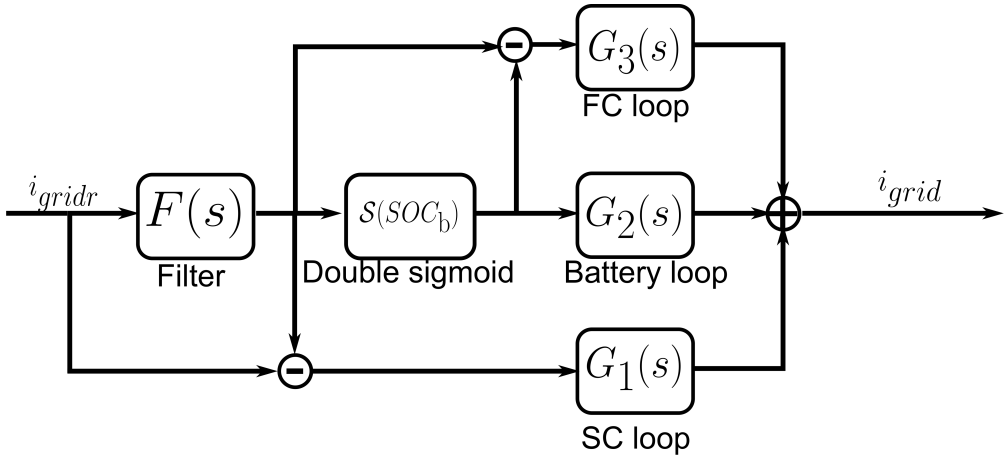

Figure 4.12: Equivalent representation of the inner current loop of the primary+secondary control scheme with the filter ($F(s)$).

shown in Figure 4.12. This shows the portion from i_{gridr} to i_{grid} of Figure 4.11 with the inner converter control loops of the different ESS represented by their closed-loop transfer functions. The $G_1(s), G_2(s)$ and $G_3(s)$ are the transfer functions of the converter control loops of the SC, battery and FC-electrolyser system respectively. The SC charge restoration control is omitted in the above as it does not contribute dynamically to inner loop from i_{gridr} to i_{grid}. It should also be noted that the double sigmoid function, $\mathcal{S}(SOC_\mathrm{b})$, is a static function in SOC_b and does not introduce any dynamic behaviour on its own. Based on the Figure 4.12 the equivalent dynamics of the inner loop from i_{gridr} to i_{grid}, represented by $G_i(s)$, is given as

$$G_i(s) = \frac{i_{grid}(s)}{i_{gridr}(s)} = G_1(s) - F(s)(G_3(s) - G_1(s) + \mathcal{S}(SOC_\mathrm{b})(G_2(s) - G_3(s))). \quad (4.45)$$

It can be noticed that the value of the second term in the above equation varies depending on the values of $\mathcal{S}(SOC_\mathrm{b})$ which in-turn is dependent on SOC_b. This scenario where the equivalent inner loop dynamics varies depending on SOC_b is not ideal. The varying inner loop dynamics can affect the performance of the overall primary+secondary control and makes the analysis of the system stability, robustness problematic. Therefore, a desirable property of the inner loop dynamics, $G_i(s)$, is that it is invariant. The design consideration for $F(s)$ aims to achieve the same. Based on (4.45) if

$$F(s) \to 0, \forall s = j\omega \quad (4.46)$$

it will result in $G_i(s) \approx G_1(s)$, resulting in inner loop dynamics being dominated by the SC current control loop dynamics. This can result in the inner loop achieving significant invariance in terms of dynamic behaviour. However, satisfying the above condition for $F(s)$, in the entire frequency spectrum, is not possible. Nevertheless, by setting the cut-off frequency of the low-pass filter, $F(s)$, as a very low value, it can be ensured that for a major portion of the frequency spectrum the above condition will be satisfied. This ensures that the contribution of the second term in (4.45) becomes negligible throughout the frequency spectrum resulting in $G_i(s) \approx G_1(s), \forall s = j\omega$.

If the $F(s)$ is chosen as a first order filter

$$F(s) = \frac{1}{\tau_f s + 1}, \tag{4.47}$$

by choosing $\tau_f >> 1$, the condition in (4.46) can be easily satisfied. This means that the cut-off frequency of $F(s) << 1\ rad/s$ and that the filter has unity gain only below this frequency. This typically corresponds to very low frequency region of the frequency spectrum. In this region the closed-loop transfer functions, $G_1(s), G_2(s), G_3(s)$, will have a gain of almost 1 resulting in the second term of (4.45) being almost zero. At values greater than 1 rad/s the gain of $F(s)$ is low and as a result the second term of (4.45) tends to zero. Therefore, throughout the frequency spectrum it can be guaranteed that the contribution from the second term in (4.45) is negligible, thus ensuring inner loop dynamics ($G_i(s)$) are invariant and dominated by the SC current loop dynamics ($G_1(s)$). It should noted that the filter $F(s)$ need not necessarily be first order. Higher order filters will also achieve similar results by choosing their cut-off frequency as shown above.

Since the dynamics from i_{gridr} to i_{grid} is now dominated by the $G_1(s)$, the Figure 4.11 can be equivalently represented as Figure 4.13. The dominance of the inner loop dynamics by the SC current loop dynamics has another advantage. The SC is the fastest acting ESS and typically the converter control loop, of the same, is designed to be the fastest among all the ESS. As a result, since $G_i(s) \approx G_1(s)$, from the perspective of the outer loop the inner loop appears to be very fast. This further justifies the assumption (4.17), used in the gain determination of the ESO. It should also be noted that the invariance can ensured only as long as the SC has sufficient to meet the demands arising in the grid. This further stresses the importance of the SC charge restoration control.

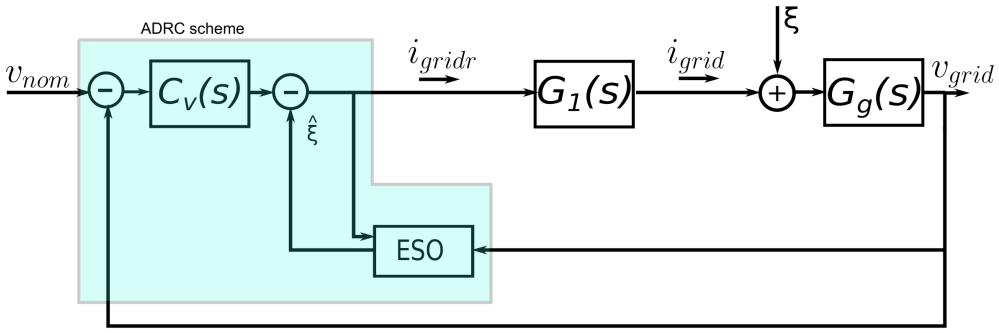

Figure 4.13: Equivalent representation primary+secondary control scheme of Figure 4.11 under model invariance and dominance of inner loop dynamics by SC current loop.

This concludes the part of the primary+secondary control where the real-time power management among the different ESS are handled and the inertial, primary and secondary responses of the conventional grid are emulated.

4.3 Power splitting among ESS of same type

In many practical scenarios pertaining to grid connected ESS the capacity demanded from a single storage device, for example battery, may not be realised by one battery of large capacity but through several batteries of smaller capacities n a distributed manner. This is done mainly for economical as well as operational reasons. In this scenario, the primary+secondary control should make the decision on how the total power demanded from the battery storage be handled by the smaller capacity batteries. The same should be considered for SC and FC-electrolyser system. The power management strategy discussed in this section is to address this generic scenario that can arise in the grid. The objective will be to decide how i_{batr}, i_{scr} and i_{fcr} (Figure 4.11) be divided among the smaller capacity batteries or SC or FC electrolyser systems, if they exist in a microgrid.

The discussions in the previous sections have already addressed the issues of stability and voltage regulation along with emulating inertial, primary and secondary responses using the ESS in weak grids, utilising the primary+secondary control level. The control architecture for the same was shown in Figure 4.11. As a result, the power splitting among ESS of same type, discussed here, do not have to account for these functionalities.

As aspects of stability or emulating the responses occurring in conventional grid are not considered, the power splitting will focus on trying to minimise scenarios that

can degrade an ESS. First the power splitting among the distributed battery storage is discussed. In this case, the objective should be to ensure that all the individual batteries get equally utilised. This ensures that one particular battery do not get over-charged or deep-discharged frequently, over the others, thus speeding up its ageing process. This scenario can be avoided by using the SOC of the individual batteries as an input feature, for deciding the power splitting criteria among the batteries. A straightforward approach, in the event of distributed battery storage, will be to ensure that an individual battery with higher SOC should cater to a higher percentage of total power demanded from the entire battery storage. This ensures that a battery with lower SOC is not over utilised and goes into deep discharge. It also ensures that a battery with higher charge is not kept in a charged state thus minimising dwell times at high SOC levels and in-turn calender ageing effects. Similarly, in the event where surplus power from the grid needs to taken in, the battery with the lower SOC should absorb a higher percentage of the total surplus power. This ensures that the battery with higher SOC levels are not pushed into an overcharged state.

This approach of utilising the measured SOC, of the individual battery, as a feature to decide the power splitting has been considered in previous works as well [71, 153–156]. These works focussed on the decentralised droop control for power splitting and the SOC of the individual batteries where used to determine the droop control gains. The aspects of droop control will not be discussed in detail in this thesis as they are beyond the current scope. Interested readers in droop control techniques are directed to [64]. Nevertheless, the above works presented an interesting solution for power splitting among ESS of same type which can adopted to the centralised control scheme considered here.

Specifically the idea presented in [154] will be adapted to the centralised primary+secondary control scheme, for battery systems. In this approach, the power catered by each battery in the distributed storage should be proportional to SOC^n during discharge and $\frac{1}{SOC^n}$ while charging. Considering the same, i_{batr} (the total current reference for the cumulative battery storage) will be split in the ratio $\mathcal{F}_{bat}$ defined as

$$\mathcal{F}_{bat}(SOC_z) = \begin{cases} \dfrac{(SOC_z)^b}{\sum_{a=1}^{l}(SOC_a)^b}, \text{for discharging} \\ \\ \dfrac{(DOD_z)^b}{\sum_{a=1}^{l}(DOD_a)^b}, \text{for charging.} \end{cases} \tag{4.48}$$

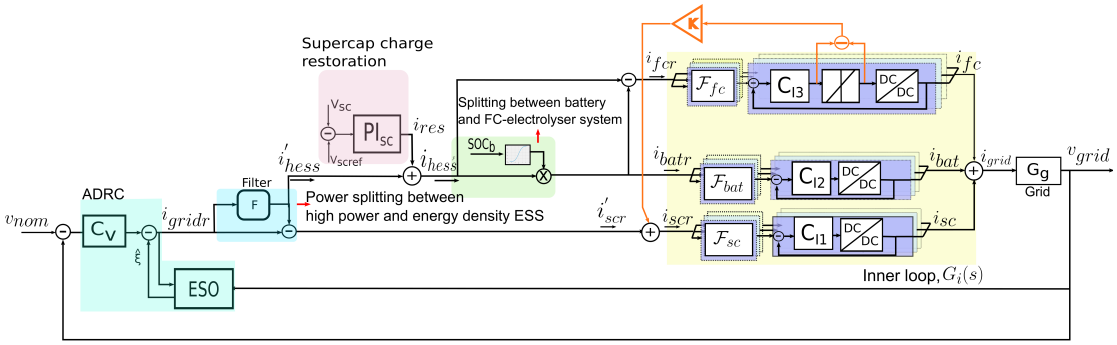

Figure 4.14: Complete primary+secondary control stage schematic. The power splitting among ESS of same type is also highlighted here.

where $z = 1, 2, 3...l$ is the number of batteries in the distributed storage and DOD is the depth of discharge given by $1 - SOC$. Depending on the whether the battery is charging on discharging one of the above conditions will be activated and the i_{batr} will be split accordingly, which will then serve as the reference input for the converter control loops of the individual battery systems. the schematic in Figure 4.14 shows the same. In a scenario, where at the start of microgrid operation, the individual batteries are at different SOC levels the power splitting using (4.48) will also ensure charge equalisation in batteries after sustained operation, provided the batteries are of same capacity. The time taken to achieve the charge equalisation is determined by the value chosen for the exponential, b, in (4.48). Higher the value of b, faster the batteries acquire charge equalisation.

Another important aspect that needs to be analysed, is the equivalent dynamics from i_{batr} to i_{bat} in Figure 4.14. Typically all the converter control loops of the individual battery systems are designed to have similar dynamics. If the closed-loop dynamics of each individual loop of battery is chosen as $G_2(s)$ the equivalent dynamics from i_{batr} to i_{bat} during discharging state is given by

$$\begin{aligned}\frac{i_{bat}(s)}{i_{batr}(s)} &= \mathcal{F}_{bat}(SOC_1)\cdot G_2(s) + \mathcal{F}_{bat}(SOC_2)\cdot G_2(s)....\mathcal{F}_{bat}(SOC_l)\cdot G_2(s) \\ &= \left(\frac{(SOC_1)^b}{\sum_{a=1}^{l}(SOC_a)^b} + \frac{(SOC_2)^b}{\sum_{a=1}^{l}(SOC_a)^b}..... \frac{(SOC_l)^b}{\sum_{a=1}^{l}(SOC_a)^b}\right)\cdot G_2(s) \\ &= G_2(s).\end{aligned} \tag{4.49}$$

The above holds during charging state of battery as well. This ensures that irrespective of the number of batteries in distributed storage, the dynamical behaviour from i_{batr} to i_{bat} will be invariant when using the power splitting strategy as in (4.48).

In the case of SC, the similar approach as that of the battery using the SOC of the SC can be used for the power splitting. The objective is same as that in the case of battery, to ensure equal utilisation of the different SC. The i_{scr} will be split in the ratio $\mathcal{F}_{sc}$ as

$$\mathcal{F}_{sc}(SOC_z) = \begin{cases} \dfrac{(SOC_z)^b}{\sum_{a=1}^{l}(SOC_a)^b}, \text{for discharging} \\ \\ \dfrac{(DOD_z)^b}{\sum_{a=1}^{l}(DOD_a)^b}, \text{for charging.} \end{cases} \tag{4.50}$$

In the case of ESS like FC-electrolyser systems, the energy is stored externally in the form of a fuel like hydrogen. In these kind of ESS the storage costs are very low, in comparison to battery, as discussed in Chapter 2. Therefore, when a larger capacity is needed in the case of FC systems they can be easily achieved by increasing the capacity of hydrogen storage tanks unlike batteries where the a larger capacity battery has to be installed. As a result, the larger capacity requirement in an FC-electrolyser system can be easily handled with a single large storage. Nevertheless, scenarios can arise where a single large storage is fed using multiple FC-electrolyser system. In this case, splitting of i_{fcr} among the different FC-electrolyser system converter control loops should be done. The i_{fcr} can be split in the ratio $\mathcal{F}_{fc}$ as

$$\mathcal{F}_{fc}(P_z) = \frac{P_z}{\sum_{i=1}^{l} P_i} \tag{4.51}$$

where P_z is the rated power capacity of each FC-electrolyser system and $z = 1, 2, 3...l$ is the number of FC systems considered. It should be noted that in the case of FC-electrolyser system, the rated power capacity of individual FC system is used for power splitting, unlike the case of battery or SC. This is because the FC works mostly like a generator using hydrogen as fuel. In the case of distributed generator units, conventionally the total power is distributed based on the power rating of the individual generators. This ensures that units having higher power rating provides a larger power output. The similar approach has been used for the FC-electrolyser system here. The (4.51) does not involve any term which needs to be measured at every sampling instant and as a result the value of the same remains constant through out the operation. Similar to (4.49), the dynamics from i_{fcr} to i_{fc}, of Figure 4.14, can be proved to be invariant.

Finally, based on the above discussions the dynamics from i_{batr} to i_{bat},i_{scr} to i_{sc} and i_{fcr} to i_{fc} of Figure 4.14 is always invariant. As a result, the power splitting strategy

discussed in this section will not in any way influence the analysis carried out in the previous sections pertaining to the ADRC scheme or Filter design criteria. It should be noted that, in the event multiple smaller capacity batteries are considered, the SOC_{b} used as the input of the double sigmoid function will be average SOC of all the smaller capacity battery system.

This concludes the discussion on the functionalities incorporated in the primary+secondary control scheme, considered in this work. In the subsequent section, the results of the performance of the primary+secondary control level will be discussed.

4.4 Results and analysis of primary+secondary control

In order to assess the performance of the primary+secondary control, a microgrid with hybrid storage system comprising of SC, battery and FC electrolyser system will be used. The total capacity required of the battery will be realised using two lower capacity battery systems. Similarly the total power rating demanded from the FC-electrolyser system will be realised using two lower power rated units. This specific test system was chosen so that all the functionalities incorporated in the primary+secondary control can be assessed. The assessment will carried out using simulation results of the primary+secondary control acting on the microgrid developed with MATLAB Simulink. The power semiconductor switches used in the interfacing converters, for the different ESS, were realised using the IGBT models available in the Simscape library of Simulink.

Considering the DC nature of the microgrid the ESS are interfaced to the grid through bi-directional DC/DC converters. The Figure 4.15 shows the schematic of the converter systems, used in this study, for interfacing the different ESS to the DC microgrid. The converters used for battery and SC systems are of the same topology, with the exception of the values of the passive components used. The FC-electrolyser system's converter have an additional input filter as shown in Figure 4.15b to enable a smooth input current profile. The authors do not claim that the converter topologies shown here are the most efficient for the respective ESS. Nevertheless, it provides a good starting point for demonstrating the improvements and performance of the primary+secondary control strategy proposed in this chapter.

The control parameters of the inner converter control loops are designed using the passive component values of the converters used in the experimental setup of Figure2.4.

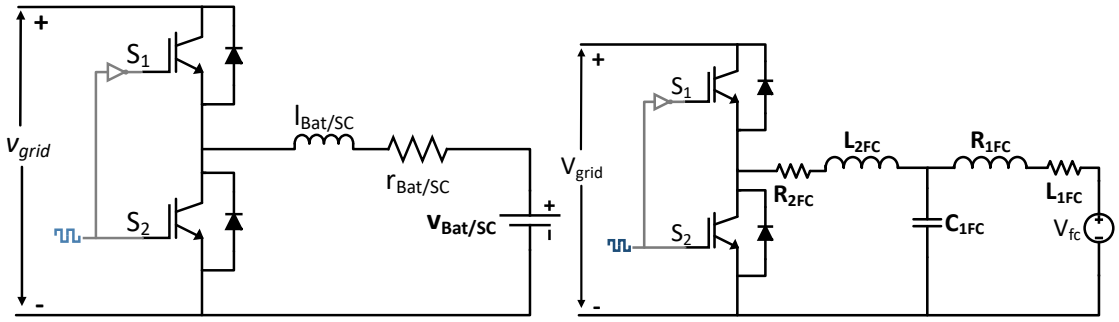

Figure 4.15: Converter topologies used in the interfacing of the ESS to the DC grid (a) Battery and SC converter (b) FC electrolyser system converter.

The FC converter of the the experimental setup is a unidirectional boost converter. In the simulations, as the FC-electrolyser system is considered the boost converter is replaced with the bidirectional scheme of Figure 4.15 but the values of the passive components (inductors and capacitors) are the same as that of the experimental setup.

The inner converter control loops where designed accounting for the physical capability of the ESS respective converter is interfacing. The SC converter loop was designed to be fastest. As the SC has to emulate inertial response which is inherently fast it was logical to design the SC converter control loop to be fastest. The inner loop of the FC electrolyser system was designed to be slowest. This is considering the physical limitation of the FC system which is prone to fuel starvation at its electrodes when subjected to sudden changes in power demand. Finally, the inner loop of the battery system was designed to have response speed in between the SC and FC system. Among the controllers used for converter control loop, the SC and FC-electrolyser inner loops used the classical PI control. As discussed in Section 4.2.1, the high frequency component of the control action from the outer voltage loop forms the reference for the SC inner loop. This results in a reference signal that will not be a step input. Based on the discussion in Chapter 3, the proposed PI+CI controller design was best suited for step references. Considering the same, the PI controller was used for the SC current loop. In the case of FC-electrolyser system, the presence of the rate limiter in the control loop, as shown in Figure 4.14, results in the reference signal having a ramping behaviour and hence PI controller was considered for the FC current loop. The inner loop of the battery used PI+CI controllers.

The values of the control parameters used in the primary+secondary stag, calculated based on the design criteria discussed in the previous section, is shown in Table.4.1. The

Parameter / Component	**Values**
Grid capacitance, C_{grid}	2.72 mF
Supercapacitor c_{sc}, ESR_{sc}	165 F, 6.3 $m\Omega$
SC converter - l_{sc}, r_{sc}	34.3 μH, 0.043 Ω
Battery converter - l_{bat}, r_{bat}	192 μH, 0.04 Ω
FC converter - $l_{1fc}, r_{1fc}, L_{1fc}, r_{1fc}, c_{1fc}$	140 μH, 0.01 Ω, 192 μH, 0.04 Ω, 2200 μF
SC current loop PI- k_{psc}, k_{isc}	0.134,96.231
Battery current loop PI - k_{pbat}, k_{ibat}	0.0138,17.222
FC current loop PI - k_{pfc}, k_{ifc}	0.0142, 16.321
Filter, τ_f (First order)	2.5
Outer loop PI - k_{pv}, k_{iv}	2, 20
Disturbance model order- m	2
γ	1
ESO gain- $\mathbf{l_o}$	$\begin{bmatrix} 8218.131 & 3453.284 & 22.240 \end{bmatrix}^T$

Table 4.1: Parameter values used in the primary+secondary control stage

FC current loop was designed to be the slowest with a settling time of $0.037s$ and peak overshoot of 26% (without considering the rate limiter). The battery current loop was designed to have a settling time of $0.2s$ and a peak overshoot of 19%. The SC current loop was designed to be the fastest with a settling time of $0.0033s$. It should be noted in the case where multiple ESS of same type are used the inner loops of the ESS of the same type are designed to be identical. The inner loops of the of the two battery systems and two FC systems, considered in the microgrid, was designed identically.

4.4.1 Verification of model invariance in inner loop

As discussed before, the filter design aimed at establishing model invariance in the inner loop. Based on the design criteria outlined in Section 4.2.3 the value of τ_f, in the case of a first order filter, should be chosen greater than 1 to ensure this model

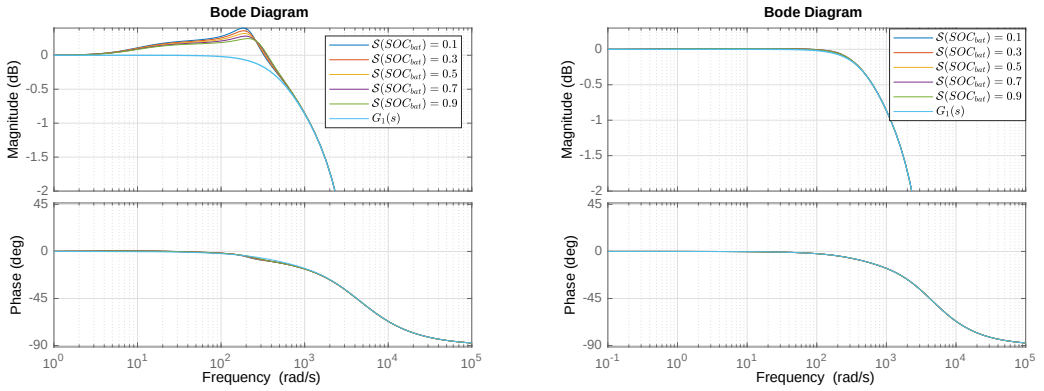

(a) (b)

Figure 4.16: Model invariance of the inner loop demonstrated through comparison of bode plots of inner loop transfer function with transfer function of SC current loop (a) $\tau_f = 0.1$ (b) $\tau_f = 2.5$.

invariance. In accordance with the same, the simulation models were developed using a filter with $\tau_f = 2.5$ as shown in Table 4.1. The model invariance of the inner loop can be verified through Figure 4.16. The figure shows the bode plots of the equivalent inner loop transfer function ($G_i(s)$) for various values of $\mathcal{S}(SOC_{\mathrm{b}})$ (double sigmoid function). According to (4.45) the dynamics represented by $G_i(s)$ should vary for different values of $\mathcal{S}(SOC_{\mathrm{b}})$. However, it can be seen from Figure 4.16b that the $G_i(s)$ remain invariant when using an $F(s)$ with $\tau_f = 2.5$, for the power splitting. This verifies the invariance property of the inner loop achieved by the filter design criteria outlined in Section 4.2.3. It can also be seen in Figure 4.16b that the equivalent inner loop dynamics ($G_i(s)$), for different values of $\mathcal{S}(SOC_{\mathrm{b}})$, is equivalent to the dynamics of the converter control loop the SC system, given by $G_1(s)$. This is also in agreement with the discussion outlined in Section 4.2.3.

The Figure 4.16a shows the same analysis but for filter with $\tau_f = 0.1$. In this case, the $\tau_f < 1$ and as a result the cut-off frequency tends to be greater than one leading to inability in establishing the invariance of inner loop dynamic behaviour as shown in Figure 4.16a. It can be seen that the inner loop dynamics are no longer equivalent to $G_1(s)$.

The value of τ_f was chosen to be 2.5 as it was possible to establish invariance and equivalence of $G_i(s)$ to $G_1(s)$ with this value. A value higher than 2.5 will also ensure the same, but resulting in an increased utilisation of SC. This in turn will require increased

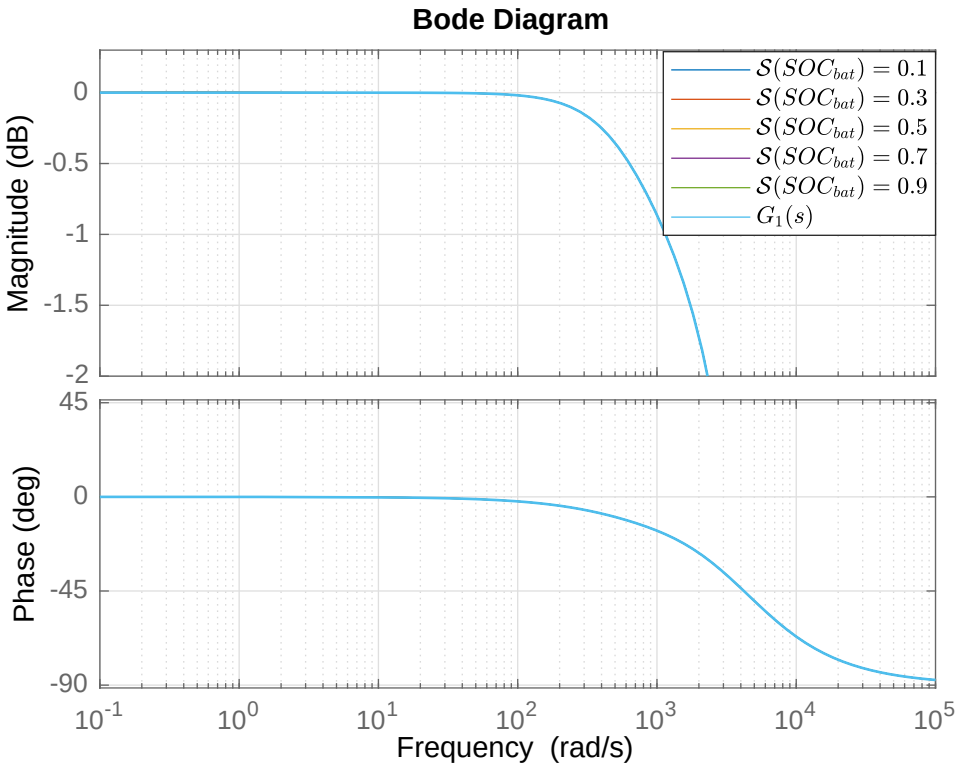

Figure 4.17: Invariance in dynamic behaviour of $G_i(s)$ for varying values of $\mathcal{S}(SOC_{\mathrm{b}})$ when using a second order $F(s)$. Higher order filter demonstrates similar behaviour as that of first order $F(s)$.

control action from the SC charge restoration control. The increased utilisation and subsequent depletion of SC charge can also affect the model invariance achieved by the inner loop, as discussed before. Therefore as a trade-off τ_f was chosen to be 2.5.

Finally, the invariance and equivalence of inner loop dynamics to that the SC converter loop can also be achieved with higher order filters. This is shown in Figure 4.17, which demonstrates the invariance of $G_i(s)$ to varying values of $\mathcal{S}(SOC_{\mathrm{b}})$ when using a second order filter in $F(s)$. The second order filter was chosen to have a natural frequency, ω_n, of 0.4 (equivalent to that of first order filter chosen above) and damping ratio of 1. Comparison of Figure 4.17 and Figure 4.16b does not reveal significant difference in the dynamical behaviour of $G_i(s)$, resulting in a similar performance with a higher order filter. The same is the case with even higher order filters. Since there is no significant improvement in the invariant dynamic behaviour of $G_i(s)$ with higher order filter, the rest of the discussion in this chapter will carried out using a first order $F(s)$.

4.4.2 Analysis of voltage regulation and ESO performance in ADRC

The first step in developing the ADRC scheme is determining the parameters , k_{pv}, k_{iv}, of the outer loop controller $C_v(s)$. These parameters are first determined without considering the ESO. As discussed before, the controller $C_v(s)$ is designed to ensure that the outer loop has slower dynamics than that of the slowest inner loop dynamics (FC loop). The objective of the outer loop is to ensure voltage regulation through disturbance rejection. Therefore, the parameters of $C_v(s)$ are determined using the closed-loop disturbance rejection transfer function, without considering the ESO. As the inner loop dynamics, $G_i(s)$, is equivalent to SC converter control loop dynamics, the equivalent representation of primary+secondary scheme shown in Figure 4.13 will be used to determine the closed-loop transfer functions. The transfer function from disturbance to output y, without the ESO, is then given by

$$G'_{y\xi}(s) = \frac{G_g(s)}{1 + G_g(s)C_v(s)G_1(s)} \tag{4.52}$$

This case without the ESO represents the classical double loop control scheme shown in Figure 4.1. The parameter values of k_{pv}, k_{iv} given in table 4.1 is obtained using the above transfer function. They were chosen such that the outer loop has a settling time of 0.38 s, almost ten times slower than the FC current loop.

The next step in the development of ADRC scheme is determining the ESO gain, $\mathbf{l_o}$, using the LMI based design methodology outlined in Section 4.1.3. As discussed before the $\mathbf{l_o}$ is determined considering the closed-loop disturbance rejection performance. According to (4.26), a degree of freedom available in the gain determination process is the ability to pre-define the weighting function,$W_\xi(s)$. Through proper selection of $W_\xi(s)$, according to (4.23), the error dynamics of ESO disturbance estimation $(\xi - \hat{\xi})$ can be controlled. This error dynamics represented by $1 - Q(s)$ have high-pass characteristics and hence acoording to (4.23) the $W_\xi(s)$ is chosen as a low-pass filter. The cut-off frequency of $W_\xi(s)$ will in turn define the dynamics of the ESO.

Another criteria in any observer design is to ensure that the observer dynamics is faster than the control loop dynamics. In the primary+secondary stage the ESO dynamics should, therefore, be faster than the outer loop dynamics. As the cut-off frequency of $W_\xi(s)$, ω_ξ, is increased the knee point of $1 - Q(s)$ is decreased according (4.23). Due

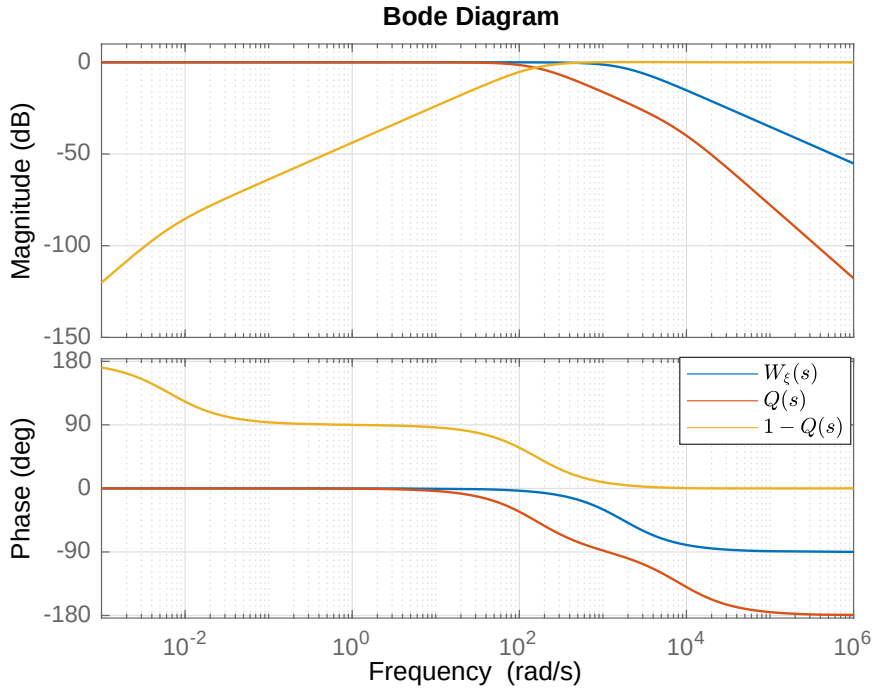

Figure 4.18: Bode plots of $W_\xi(s)$, $1-Q(s)$ and $Q(s)$ of the ESO for the value of $\mathbf{l_o}$ given in Table 4.1.

to the high-pass nature of $1-Q(s)$ this leads to faster dynamics of the disturbance estimation error. As a result, an increase in ω_ξ will result in faster disturbance estimation by ESO and improved disturbance rejection performance by ADRC scheme.

The other parameters that need to be defined before solving the LMI problem was the bounding $\mathbf{H}_\infty$norm value γ (defined in Theorem 4.1) and the order of the disturbance signal (m) to be used in the ESO model. The value of gamma was chosen as 1 based on the condition defined in (4.20). the order of the disturbance was chosen as 2. The second order model is considered as most of the disturbances occurring in the grids can be sudden (step) or gradual variation (ramp) in the generation or load profile. Considering all these aspects the $\mathbf{l_o}$ value, given in Table 4.1, was obtained for a $W_\xi(s) = \dfrac{1750}{s+1750}$ by solving the LMI problem. The above $W_\xi(s)$ was chosen, as beyond the $\omega_\xi = 1750$ the LMI feasibility problem used in the determination of $\mathbf{l_o}$ was not feasible for a $\gamma < 1$. The Figure 4.18 shows the bode plots of $W_\xi(s)$, $1-Q(s)$ and $Q(s)$ of the ESO for the value of $\mathbf{l_o}$ given in Table 4.1. The bode plots clearly show the high-pass of $1-Q(s)$ and the low-pass nature of $Q(s)$. The Q(s) has a cut-off frequency around 100 rad/s and a gain roll-off beyond this value. As a result, this satisfies the condition required

from Q(s) as highlighted using (4.16). The low cut-off frequency from $Q(s)$ also ensures that the disturbance estimation is less sensitive to measurement noise.

Prior to presenting voltage regulation and power splitting performance achieved with primary+secondary control, an assessment of the improvement in disturbance rejection performance with the ADRC scheme is carried out first. In order to effectively highlight this, the step response of the closed-loop disturbance rejection transfer function of the primary+secondary scheme is compared with and without the ESO. The transfer function without ESO, for the closed-loop system, $G'_{y\xi}(s)$ was already given in (4.52).The closed-loop transfer function with ESO, considering model invariance, for the primary+secondary scheme represented in Figure 4.13 is given as

$$G''_{y\xi}(s) = \frac{G_g(s)(1 - Q(s))}{1 + G_g(s)C_v(s)G_1(s) + Q(s)(G_1(s) - 1)}. \tag{4.53}$$

It should be noted for assessing the improvement with the ADRC scheme the approximate closed-loop transfer function, $G_{y\xi}(s)$, used in LMI based gain determination of ESO was not used. The $G_{y\xi}(s)$ was used only to facilitate a simpler formulation of the LMI problem for determining the $\mathbf{l_o}$. The Figure 4.19 compares the step responses of the closed-loop disturbance to output transfer function of the primary +secondary control with and without ESO. The response shown here is for a step input of value -1. It can be clearly observed that the disturbance estimate with the ESO and subsequent feedforward of the same, has resulted in a significant reduction in settling time of the step response with the ADRC scheme. The settling time was reduced from $0.388s$ to $0.153s$ using the ADRC scheme. This represents an almost 50% faster disturbance rejection performance. It should also be noted that the faster disturbance rejection achieved with the ADRC scheme is without an increase in the overshoot (undershoot in this case). It can be observed that the undershoot in the case of the ADRC scheme is actually lower than the case without ESO. This is further implied through the comparison of the $\mathbf{H}_\infty$ norms calculated for ADRC and conventional nested loop schemes. The value of $\mathbf{H}_\infty$ norm for ADRC scheme was 0.475 while that for the conventional nested loop scheme was 0.504. This further highlights the improvement with the ADRC scheme.

The Figure 4.20 shows the comparison of bode plots of the closed-loop transfer function, from disturbance to output, with and without ESO. This comparison provides an understanding of the robustness of the ADRC control scheme. It can be seen from Figure 4.20 that the bode plot of closed-loop system has a more low frequency bandpass

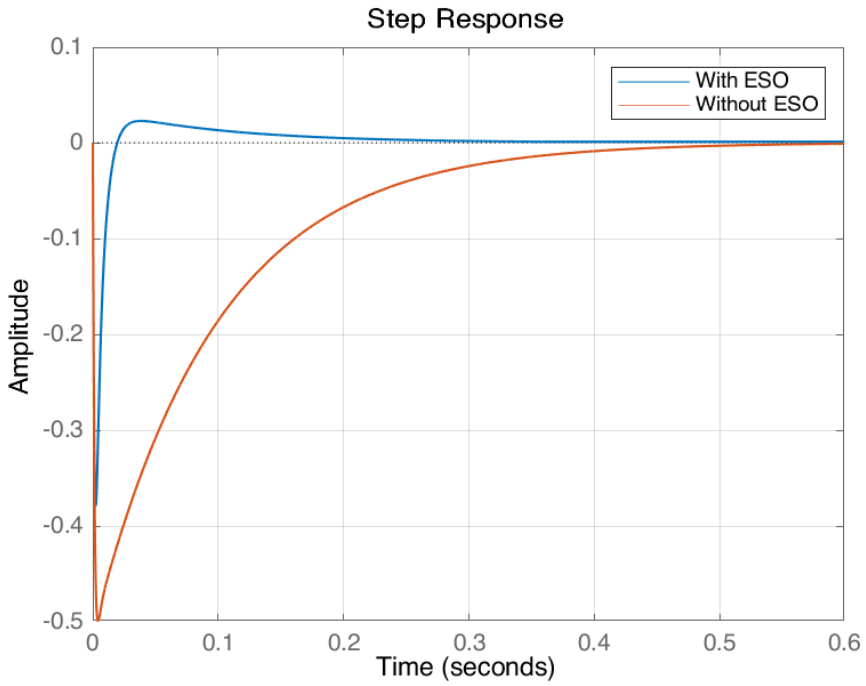

Figure 4.19: Step response comparison of the disturbance rejection performance by primary+secondary control with and without ESO (ADRC scheme).

characteristic with the classical dual loop control scheme (without ESO). In comparison, the ADRC scheme has a lesser bandpass characteristic. This explains the slower dynamics of the disturbance rejection performance in the dual loop control scheme, as it allows lower frequencies to affect its response. In terms of system robustness, the dual loop control scheme has infinite gain and phase margins whereas the ADRC scheme has a gain margin of 94 while the phase margin is infinity. Therefore, it can be concluded that the ADRC scheme can ensure na improved transient performance over the classical dual loop control without compromising on the control system robustness.

Voltage regulation performance

The voltage regulation performance in the microgrid using the ADRC scheme is discussed next. As discussed before the simulation models were developed using Simulink. The results discussed in the upcoming sections will be for a microgrid with one SC, two batteries and two FC-electrolyser system so as to asses all the power splitting strategies. The interfacing DC-DC converters were also incorporated in the Simulink models and

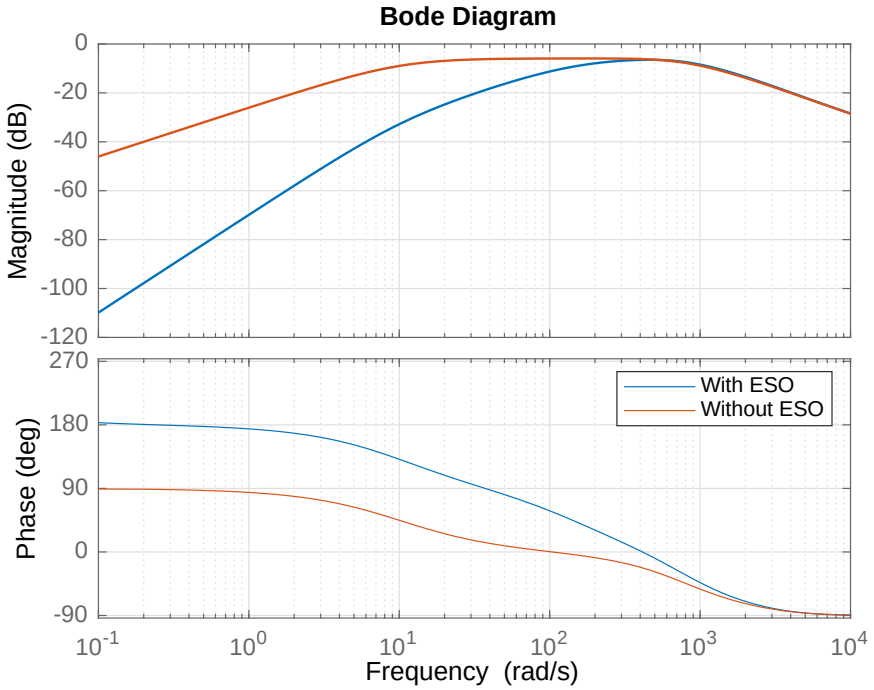

Figure 4.20: Comparison of Bode plots of the disturbance rejection performance by primary+secondary control with and without ESO (ADRC scheme).

were switched at 20 kHz. The Figure 4.21 shows the voltage regulation performance in the microgrid with the ADRC scheme. The results were generated when the microgrid was subjected to an imbalance power in the form of the step waveform shown Figure 4.21b. In Figure 4.21 this imbalance power is represented through the equivalent current profile. The Figure 4.21b shows the disturbance estimation (imbalance power) by the ESO in the ADRC scheme. It can be seen that the disturbance estimated by the ESO is higher than the imbalance power in the grid. This is because, in the actual microgrid there are losses in the interfacing DC/DC converters and the equivalent stray resistances in the passive components. Therefore, the power supplied to the grid by the ESS is higher than the actual imbalance power. The ESO is still capable of estimating this additional power demand arising from the losses despite the same not being considered in the ESO design. The Figure 4.21c shows the control action from the outer control loop, i_{gridr} which is the sum of the output from $C_v(s)$ and ESO.

In terms of voltage regulation performance, the improvement achieved with ADRC can be clearly observed through comparison between Figure 4.21 and Figure 4.22. The Figure 4.22 shows the performance with the conventional dual loop scheme without

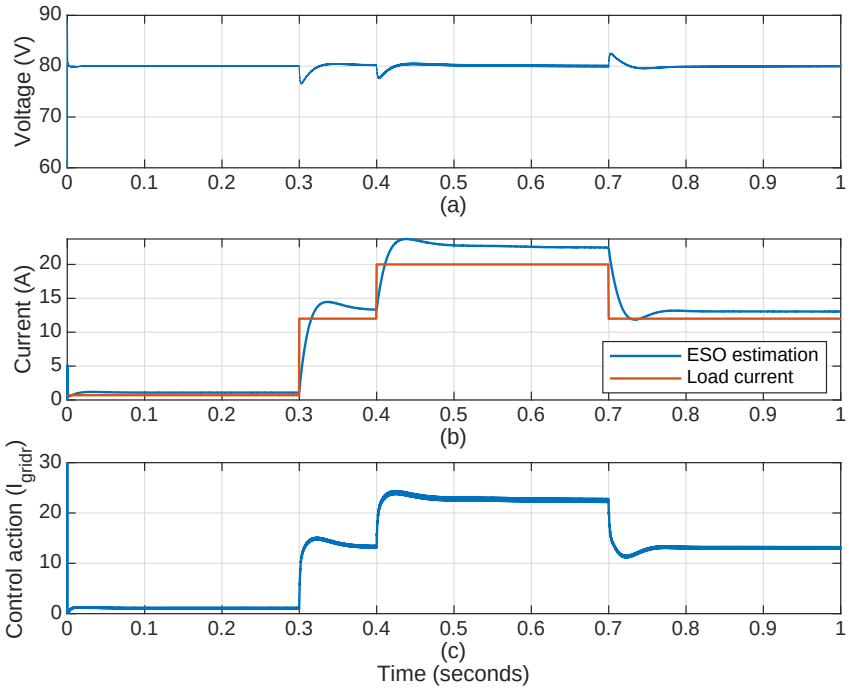

Figure 4.21: Voltage regulation performance in the microgrid with the ADRC scheme (a)Grid voltage profile (b) Disturabnce estimation from ESO and actual imbalance current to the grid (c) Control action i_{gridr}.

ESO. The longer time taken by the controller to bring the voltage back to the nominal value of 80 V, in the case of conventional dual loop architecture, highlights the capability of the ADRC scheme. The estimation from the ESO in the ADRC scheme allows the controller to bring the voltage back to nominal value faster as shown in Figure 4.21a. The ADRC scheme is capable of restoring the voltage back to nominal value in 0.12 seconds whereas the conventional control takes 0.32 seconds. This is very similar to the values seen when analysing the disturbance to output transfer function in the previous section. There is a slight difference in the settling times obtained from the Simulink models and the transfer function analysis carried out in the previous section. This is because the Simulink models where developed to mimic real world system as close as possible. As a result, the model incorporated data acquisition filters which will be used in real world applications when measuring the system parameters. These were not considered in the transfer function analysis represented in the previous section. The filters were modelled based on the actual filters used in the experimental setup of Figure 2.4. Due to the unmodelled effect of the same there exists slight difference between the simulation results of microgrid and the transfer function analysis. Nevertheless, the improvement with ADRC scheme can be clearly comprehended.

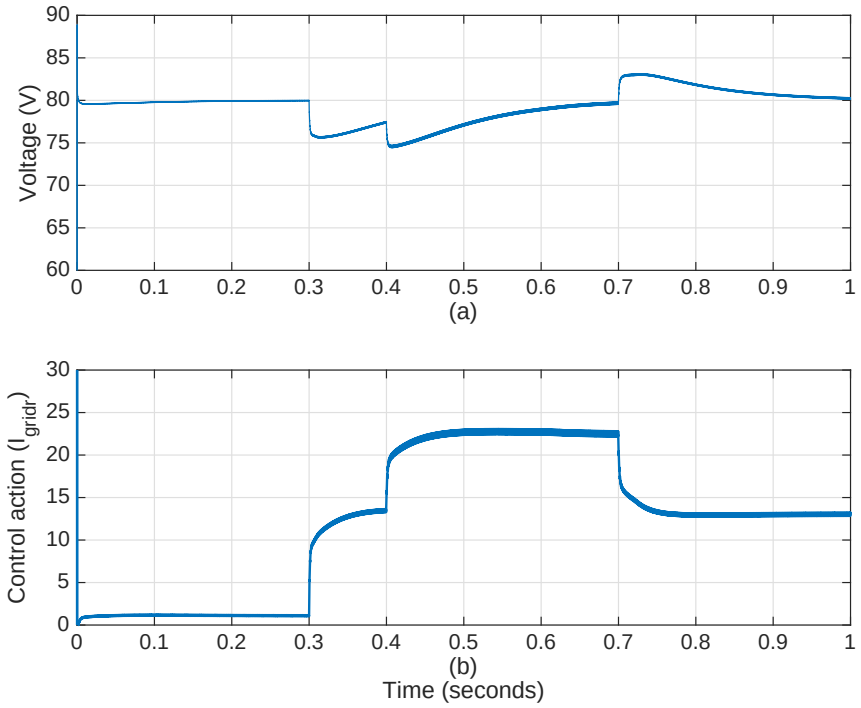

Figure 4.22: Voltage regulation performance in the microgrid with conventional dual loop control scheme (a)Grid voltage profile (b) Control action i_{gridr}.

4.4.3 Power splitting among hybrid ESS and ESS of same type

The Figure 4.23 shows the real-time power splitting among the different ESS achieved by the primary+secondary control, during power imbalances in the grid. The results are obtained from the simulation of the same microgrid architecture described in the previous section. In order to demonstrate the power splitting among the hybrid ESS (SC, battery and FC) and also among the ESS of same type the initial condition for the battery SOC was taken as 0.5 and 0.6 for battery one and two respectively. The ESS were sized such that in the time frame shown in Figure 4.23, there can be significant change in the energy stored in the ESS to facilitate switching from one ESS to another (from battery to FC) in order to cater the power imbalance in the system. This enables to assess the different power transitions. The two FC systems where chosen to have different power ratings in the simulation so as to highlight the power splitting among the two FC systems as well.

As shown in Figure 4.23, when there is a change in the power imbalance in the grid the first response is from the SC, as expected. This arises from the power splitting

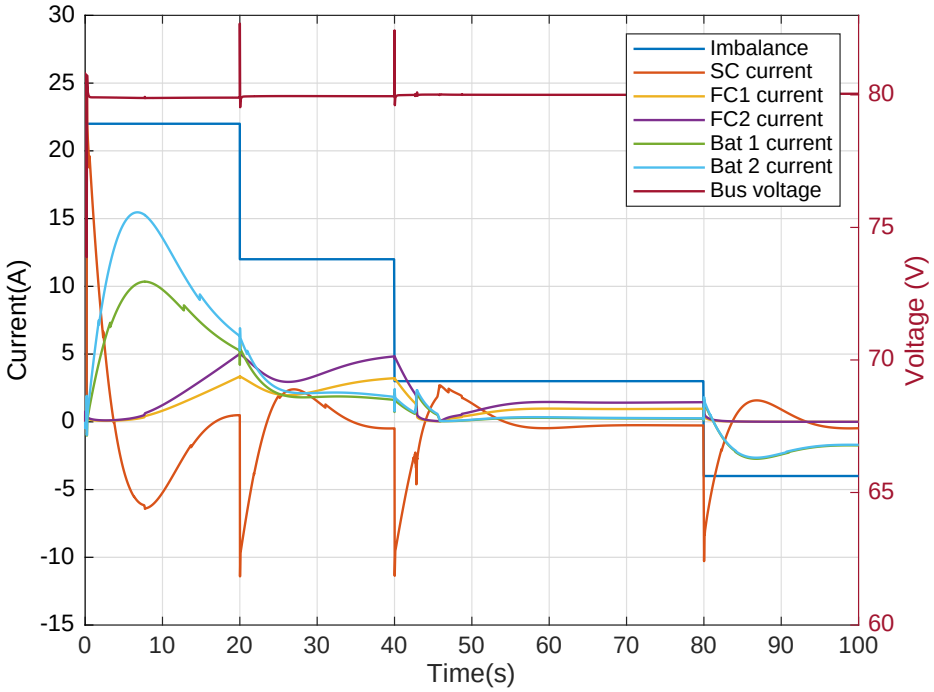

Figure 4.23: Power splitting among the ESS and voltage by the primary+secondary stage under power imbalance in the microgrid.

carried out by the filter between the high power density and high energy density ESS. The control action from the outer loop, i_{gridr}, will be split by the filter into high and low frequency components. The inner loop of the SC system will be provided with the high frequency part which initiates the initial response from the SC system to power imbalances. As discussed before, this initial response demonstrates the emulation of the inertial response by the SC system. This response from the SC arrests the bus voltage deviation and brings it back to the nominal value quickly as shown in Figure 4.23. Thus, this result highlights the ability of the SC system in ensuring a degree of inertia in the weak microgrid towards power imbalance.

The filter action results in high energy density ESS catering the low frequency component of the outer loop control action. As mentioned before, to ensure a higher operating efficiency of the grid the battery is made to cater imbalance power when there is sufficient charge in them. In this case, at the start of simulation Battery 1 and 2 have 0.5 and 0.6 SOC respectively resulting in the power being catered by batteries. As the two batteries have different SOC, based on the discussion in Section 4.3, the battery with the higher SOC will provide a higher power output. This is clearly observable in

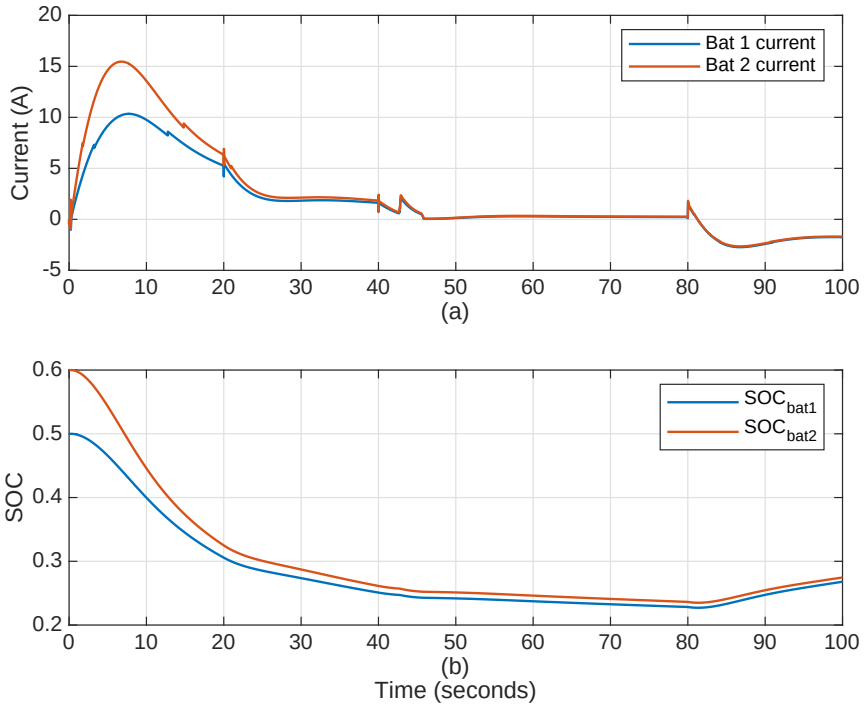

Figure 4.24: The battery system behaviour for the scenario in Figure 4.23 (a)battery current profiles (b) battery SOC profiles.

Figure 4.23 where battery 2, which has a higher initial SOC has higher power (current) output initially. The rate at which the battery power output ramps up depends on filter, $F(s)$. This ramping up in power from the higher energy density ESS is analogous to the primary response in the conventional system.

After continued operation of the batteries, the SOC levels start coming down. This will result in a shifting of power being catered to the microgrid from batteries to the FC systems as shown in Figure 4.23. As discussed before, this is essential to avoid deep discharge of battery and the subsequent degradation that arises from it. The FC systems start catering to the power imbalance at around $10s$ as shown in Figure 4.23. The shifting of the power output from the battery to FC will be carried out based on the methodology discussed in Section 4.2.1, using the double sigmoid function. In the case considered here, since there are two battery systems the average SOC of the batteries will be used as input to the double sigmoid function to determine the power being catered by the FC system. The FC starts catering to the power demand even before the battery SOC reaches the lower permissible limits. This can be observed in Figure 4.24b, where the average SOC of the two batteries is still 0.4, at $10s$, when the

FC starts catering to the power demand. This ensures the gradual transition from the battery to FC system using the double sigmoid function, as discussed before. It can be observed in Figure 4.24 that the power output from the battery progressively decreases as the SOC reduces and after $50s$ when the SOC has almost reached the lower limit the power output from the batteries are close to zero. This highlights the ability of the primary+secondary scheme in preventing deep discharge in batteries and facilitating a smooth transition from battery to FC system while meeting the power imbalance in grid. In the fig.4.23 at around $80s$ the imbalance current becomes negative. This indicates a surplus power in the microgrid which has to be taken in by the ESS. As can be seen from fig.4.23, and Figure 4.24, as the batteries are almost fully discharged the primary+secondary stage forces the battery to take in the surplus power and not the FC to ensure higher operational efficiency. Therefore the primary+secondary stage makes the power splitting decision considering the operational efficiency and degradation of the ESS.

Another important aspect that can be observed in Figure 4.24 is the charge equalisation achieved in the batteries by primary+secondary stage. As the battery with the higher SOC provides more power output, over the course of time this will lead to charge equalisation if the batteries are of the same capacity. This is shown in fig.4.24b where the initial difference in SOC between battery 1 and 2 gradually reduces over time and almost becomes zero resulting in charge equalisation. This is in accordance with the power splitting equation (4.48) used in the primary+secondary stage for the ESS of same type. In the simulation considered here the value of b in (4.48) was chosen to be 3 so as to ensure a faster equalisation of charge. This charge equalisation ensures that one battery is not over utilised or goes into deep discharge. This also ensures that irrespective of the initial SOC of batteries, after prolonged operation, they achieve charge equalisation and contribute equally to the power demand as long as the batteries are of same capacity. Nevertheless, in the scenario were the batteries are of different capacities the charge equalisation will not be achieved. In this case, the primary+secondary stage will still ensure that batteries with higher SOC cater a larger share of the power demand.

The Figure 4.25 shows the power splitting among the two FC systems considered in the simulation. This figure is a reproduction of the FC current profile from Figure 4.23, provided for better assessment of the waveforms. As discussed in Section 4.3, the primary +secondary stage distributes the power demand among the FCs proportional to the power rating of the individual FC electrolyser systems. In order to observe the

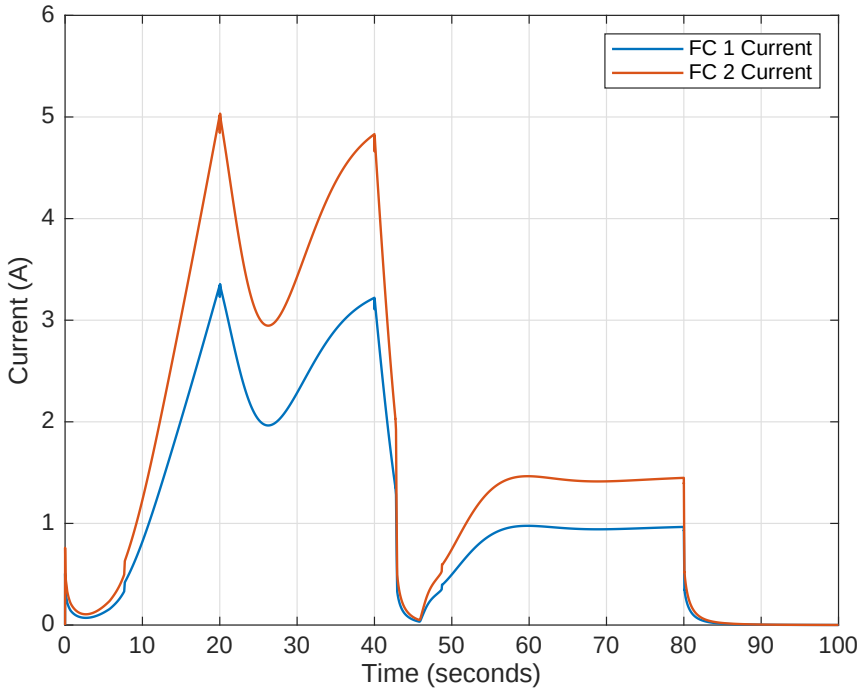

Figure 4.25: Power splitting among the FCs achieved by the primary+secondary stage for the scenario shown in Figure 4.23.

power splitting behaviour in the simulations the FC system 2 was chosen to have higher rating than the FC system 1. As a result it can be observed that the FC system 2 caters to more demand than the FC system 1.

Finally, Figure 4.26 shows the SC charge restoration by the primary+secondary stage. The charge restoration is essential to ensure that the SC is always capable of responding to future power imbalances arising in the grid , thus ensuring stability as well as higher inertia of the grid. Apart from this the model invariance of the inner current loop can only be established if the SC has sufficient energy available at all instances to meet the demands from the grid. Therefore, this SC charge restoration functionality of primary+secondary stage is of great importance. As discussed in Section 4.2.2 the charge restoration is ensured through SC voltage regulation. This is shown in Figure 4.26a where SC voltage is regulated at a nominal value of 35V. This value is chosen based on the SC system used in the test setup shown in Figure 2.4. The 35V corresponds to the voltage value when the SC is at half capacity. This ensures that half the capacity of the SC is always available to supply or absorb the power imbalance in the grid. The Figure 4.26b shows the current profile of the SC system reproduced from Figure

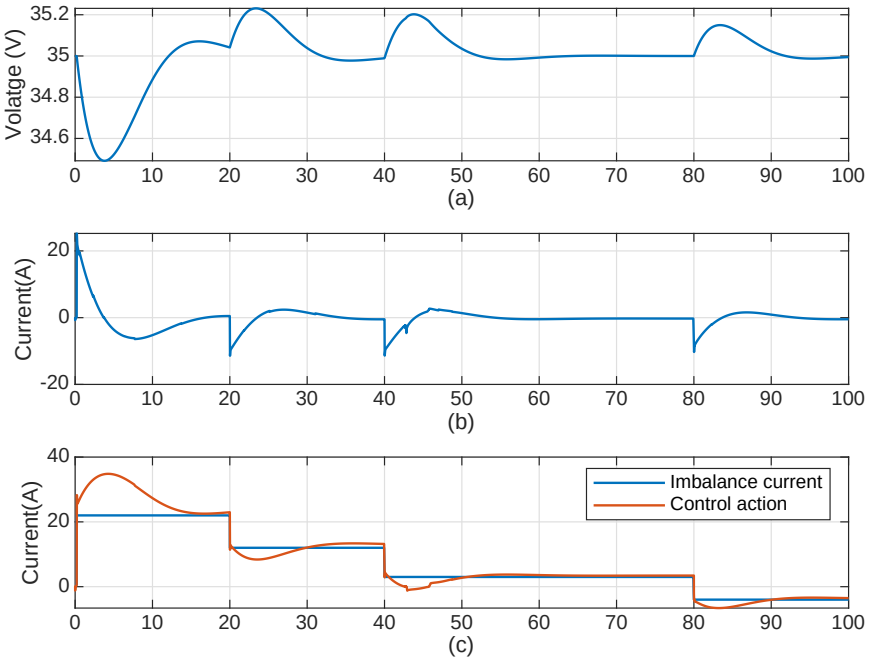

Figure 4.26: SC charge restoration achieved by the primary+secondary stage for the scenario shown in Figure 4.23(a) SC voltage profile (b) SC current profile (c) Imbalance power and the control action (i_{gridr}) from the ADRC scheme.

4.23. The impact of the SC voltage regularization can also be observed in the control action (i_{gridr}), from the outer loop, shown in Figure 4.26c. The large overshoot in the control action after every change in power imbalance set point is the effect of SC voltage regulation carried out by the primary+secondary scheme. As discussed before, this SC charge restoration emulates the secondary response in the conventional grid.

4.5 Concluding remarks

A unified centralised power management framework that ensure stability and voltage regulation in a weak microgrid with renewable generation and hybrid ESS system was developed. The control framework, called the primary+secondary scheme, ensures

- Improved voltage regulation and stability in weak microgrid under power imbalances
- Real time power management among the hybrid ESS emulating inertial, primary

and secondary responses arising in conventional grids

- Real time power management among the hybrid ESS considering operating efficiency of microgrid and degradation mechanisms of different ESS.

In order to ensure improved voltage regulation performance and in-turn disturbance rejection in microgrid, the primary+secondary control proposed in this work utilised an ESO augmented with the conventional dual loop control architecture. This scheme, referred to as ADRC, was capable of robust estimation of the imbalance power (disturbance) arising in the grid without the need for additional sensors and feed forwards it for improved disturbance rejection performance. This work also presented an LMI based method for the gain determination of the ESO, considering the closed-loop system performance. The improvement in the voltage regulation performance was also verified through simulations in this chapter.

The primary+secondary control framework also presented a power splitting strategy among the hybrid ESS considering the ESS characteristic, degradation and the operational efficiency of microgrid. The power splitting between the high power and energy density ESS was achieved using a filter. This resulted in the SC providing the initial response to power imbalance variations in grid, similar to the inertial response in conventional grids. The same was verified through the simulation results. After the SC response the battery or FC system ramp up in power to maintain long term power balance in grid like primary response. The primary+secondary control also proposed a power splitting criteria between battery and FC. The proposed methodology used the output of a double sigmoid function to determine the power split ratio between battery and FC system. This power splitting ensured that deep discharge of battery was prevented and ensured a smooth power transition from battery to FC system. The power splitting strategy also ensured that the operational efficiency of the system is high by ensuring that the FC system is put to use only when the battery cannot be utilised.

Finally the primary +secondary scheme also proposed a power splitting criteria among ESS of same type. The proposed methodology split the power among batteries based on their SOC and among the FC based on their power rating. The SOC based power splitting prevented over utilisation of one battery over another and further prevented deep discharge in battery systems. The design criteria for the different stages of the primary+secondary scheme including the filter, PI controllers and ESO were outlined. The filter design aimed at ensuring model invariance in the equivalent inner

loop dynamic behaviour and discussed the design considerations for the same. Finally the performance of the entire primary+secondary stage was verified through simulation models developed in Matlab- Simulink.

Based on this the novel contributions of this chapter can be summarised as

- Application of ESO for voltage regulation in microgrid and the LMI based methodology applied for gain determination in ESO
- Power management strategy among high energy density ESS like battery and FC using the double sigmoid function
- Design consideration of the power splitting filter, $F(s)$, ensuring invariance in dynamical behaviour of inner loop irrespective of the ESS catering tp the power demand in the grid.

In terms of future line of research the experimental verification of the control strategy should be carried out. Apart from this, the research can be extended to developing decentralised control strategy for microgrid with hybrid ESS system. Finally to conclude publications, based on the work carried out in this chapter is given below:

C1 Nair, Unnikrishnan Raveendran, Ramon Costa-Castelló, and Alfonso Baños. "Grid voltage regulation using a reset PI+ CI controller for energy storage systems." 2018IFAC Conference on Advances in Proportional-Integral-Derivative Control PID, Ghent,Belgium,2018 pp. 226-231.

C2 Nair, Unnikrishnan Raveendran, Ramon Costa-Castelló, and German A. Ramos. "An adaptive disturbance rejection control scheme for voltage regulation in DC micro-grids." 2019 IEEE International Conference on Industrial Technology (ICIT), Melbourne, Australia, 2019, pp. 583-588, doi: 10.1109/ICIT.2019.8755100..

Part III

Energy Management stage

Chapter 5

Forecasting unit for generation and load profiles

This chapter introduces the forecasting unit used in the energy management stage, to aid the decision making of the tertiary controller. The chapter provides an overview of the forecasting techniques that have already been utilised in electrical systems. Based on the conclusions drawn from the survey, a forecasting unit utilising neural network is identified for this work. The formulation of the neural network system for forecasting the generation, load demand and the training process will be discussed. Finally, the chapter presents the results of generation and load forecast from the forecasting unit developed.

The upcoming chapters in this part of the thesis discusses the work done in the development of the energy management stage for the hybrid ESS and the microgrid. The energy management in the microgrid will be carried out by the tertiary control stage. As discussed in Chapter 2 a centralised control system will be considered. The objective of the centralised tertiary level will be to provide an optimal management of the energy among the hybrid ESS, the dispatchable generator (if present) such that there is maximum consumption of energy from RES while also ensuring that they are grid friendly. Apart from this, the energy management stage aims to ensure that the operation of the microgrid is efficient and the rate of degradation of the ESS is minimised.

The decision making, for energy management, in the tertiary control stage can be resolved using heuristic or non-heuristic strategies. In the former, tertiary control uses rule based algorithms [76, 77, 157–159], fuzzy inference schemes [78, 160–163], genetic

algorithm [164–166] or simulated annealing algorithms [167] for its decision making. Among the above mentioned methods the genetic algorithm and simulated annealing can be considered as more of a metaheuristic method. In the non-heuristic methods [168–173] the controller relies on solving various optimisation problems to achieve the optimal decision making in microgrids. The tertiary control schemes relying on heuristic methods for its decision making do not require explicit modelling of the system and are computationally less intensive due to use of simple deterministic rules for its scheduling purposes. The non-heuristic methods, on the other hand, require extensive system modelling, typically uses the forecast of generation/load profiles in its decision making and are computationally more expensive in comparison to heuristics schemes.

However, in terms of system performance non-heuristic methods ensure more optimal operation in comparison to heuristic methods. This is due to their reliance on formal optimisation based techniques in its decision making which guarantees that the decisions made are optimal. In the heuristic methods, as the decision are made depending on some predefined deterministic rules the same cannot be guaranteed. In heuristic schemes, the results always tend to be sub-optimal with the closeness to optimality being heavily reliant on the nature of the rules that are defined. In order to ensure that the appropriate rules are defined, an in-depth prior understanding of the system behaviour is required. Apart from this, the expected optimal system behaviour needs to be explicitly stated through the rules which can be difficult in complex system like electric networks. The same is not the case with the non-heuristic methods, where the expected optimal system behaviour can be defined implicitly through the optimisation problem without need for a deep understanding of the system behaviour.

In tertiary control using non-heuristic methods, the decision making is further aided by the use of forecast of generation/load profiles. The utilisation of the forecast values allow the tertiary control stage to make better energy management decisions accounting for future events, especially in systems having high RES penetration. The use of forecast is not just limited to non-heuristic methods and can also be used in heuristic schemes. However incorporating them in the decision making process can be very tedious, as the rules pertaining to the forecast values have to be defined explicitly accounting for the optimal microgrid operation. In order to enable better decision making, forecast for a longer time period is essential. In this context, the rule formulation accounting for all these forecast values, in the heuristic scheme can become very complex. The advantage with the non-heuristic optimisation based schemes are that they facilitate an easier

incorporation of forecast values through the optimisation problem. Apart from this, as discussed before, the optimal system behaviour incorporating the forecast information can be implicitly defined using the optimisation problem.

Considering these advantages regarding ensuring optimal system behaviour, defining implicitly the required behaviour and easiness in incorporating forecast information in the decision making process, the non-heuristic methods will be considered for decision making at tertiary level. Though the computational complexity is higher the increased availability of cheap computation power, aided by efficient algorithms in solving optimisation problems make these methods more tenable in current scenario.

As discussed above, forecast of the generation and load profile play a significant role in improving the decision making in the tertiary control stage. Nevertheless, it should also be recognized that an inaccurate forecast (high error between predicted and actual value) can deteriorate the system performance considerably than in the case where forecast was not used. For example consider a day where the expected PV generation is high, but due to unexpected weather events the power output is low. If the forecasting system cannot predict this scenario, the tertiary control stage makes decisions accounting for a high PV generation scenario which can lead to poor performance economically and electrically. Therefore, it is imperative to identify an efficient, accurate forecasting unit which can work alongside the tertiary control stage and improve its decision making capabilities. In this context, the chapter discusses the work done in this thesis in identifying an appropriate forecasting unit for the tertiary control. A detailed discussion pertaining to the tertiary control stage will be provided in the next chapter.

5.1 Overview of forecasting units for electrical networks

Forecasting units employed in electrical networks can be classified based on the type of model used for forecasting, the forecasting horizon and the number of steps into future they forecast at any instant [174–176].

5.1.1 Forecasting unit classification based on usage model

One way of classifying forecasting units is based on the nature of the model that has been used in making the forecast. These can be primarily classified into linear and

non-linear model based forecasting units. The difference between the linear, non-linear models is in the nature of the analytical equations used to define these models and theoretical approach undertaken to reach the optimal model parameters. Irrespective of the nature of the model, the underlying principle in the forecasting of time series (generation and load profile) at any instance is the utilisation of previous values of the series for predicting the future values. This process is called regression [174]. An overview of the linear and non-linear models used for forecasting time series is provided next.

Linear model based forecasting unit

The linear models are some of the oldest used models in time series forecasting. The earliest models used in time series predictions, were based on the moving average (MA) [177] and exponential smoothing (ES) [178] techniques. However, the most popular and widely used linear model in time series forecasting have been the *Box and Jenkins model (ARIMA- Auto regressive integrated moving average)* [179] and *ARMA- auto regressive moving average* model [180]. The ARIMA is a more generalised representation of the ARMA model. The ARIMA differs from MA or ES in the sense that ARIMA aims to describe the autocorrelations in the data while the MA or ES try to define the trend/seasonality of data. An ARIMA model is defined using three parameters (p, d, q) where p is the number of regressive terms considered in the model. In other words it defines the number of previous values in the time series considered for forecasting the next value. The p also defines the order of the considered model. The term d defines the degree of differencing that has to be applied to the time series. The differencing is done so as to make the time series stationary and thus eliminate any underlying trends in the data (increasing or decreasing). The stationarity needs to be ensured to facilitate better forecast from ARIMA models. Finally, the term q defines the degree of lagged forecast error used in the model. Therefore, ARIMA takes into account not only the previous values of the time series in its forecasting but also the error in the forecast of the previous values. Considering the same, a discrete-time series, like the generation or load profile, represented as a time-indexed set of values $(v_1, v_2, v_3....v_{k-1})$, where k is the time index can be modelled using ARIMA as [179]

$$\hat{V_k} = \mu + \phi_1 \cdot V_{k-1} + \phi_2 \cdot V_{k-2} + ... + \phi_p \cdot V_{k-p} - \theta_1 \cdot e_{k-1} - \theta_2 \cdot e_{k-2}... - \theta_q \cdot e_{k-q} \tag{5.1}$$

where μ is constant drift term, $e_{t-1} = \hat{V}_{k-1} - V_{k-1}$ and

$$V_{k-1} = \begin{cases} v_{k-1} & \in d = 0 \\ v_{k-1} - v_{k-2} & \in d = 1 \\ (v_{k-1} - v_{k-2}) - (v_{k-2} - v_{k-3}) & \in d = 2 \\ . & \\ (v_{k-1} - v_{k-2}) - (v_{k-2} - v_{k-3})...(v_{k-l} - v_{k-l-1}) & \in d = l. \end{cases} \tag{5.2}$$

The Akaike's Information Criterion (AIC) [181] has been considered as an useful methodology in determination of parameter values (p, d, q) of ARIMA models. Recently various modifications of AIC has been proposed which enable better selection of parameter values under different scenarios [182–184]. In the above when d=0 an ARIMA model becomes equivalent to that of an ARMA model. The MA and ES can also be represented as special case of the ARIMA model [176]. In electrical systems, conventionally, ARIMA and ARMA models has been widely used for load forecasting [185–192].

Non-linear model based forecasting units

The non-linear model based forecasting units, for time series, have achieved widespread research interest and application of lately. Since the 1980s the number of works in this domain has increased significantly. These non-linear model based forecasting units rely mostly on pre-sampled system data driven machine learning based techniques for predicting time series behaviour. Machine learning based non-linear models generally use large amount of sampled data from the actual system to identify the optimal model that defines the system behaviour. This process of identifying the model that best defines the system behaviour from the sampled data is called training. Multiple models like Support vector regressor (SVR) [193], artificial or deep neural networks (ANN,DNN) [194, 195], recurrent neural network (RNN) like Long short term memories (LSTM) [196], Ridge regressor (RR) [197], Lasso regressor (LR) [198], and regression trees utilising gradient boosting [199] or extreme gradient boosting [200] have been proposed for time series forecast. These machine learning based models for time series forecasting can be categorised as supervised or deep-learning models. In supervised learning, the identifying of optimal model that defines the input-output mapping (time series forecasting) is aided using pre-sampled input-output data pairs, referred to as training data. These models

only capture the behavioural aspects that is explicitly presented through the input output pairs. Therefore, to ensure that the model represents all the behavioural patterns of a time series (seasonal, daily patterns, trends) explicit information regarding the same (month, day, time of day etc) should be provided as one of the feature in the input data. Deep learning models still use input-output pairs for model identification in time series forecast. However, they are capable of recognising the behavioural patterns like daily, seasonal cycles, trends etc, on their own without having to provide explicit information, indicating the same, as a feature in the model input. Among the above mentioned models, RNNs like LSTM, SVR are capable of deep learning. The deep learning models are also characterised by the need for high computational power during the training phase, in comparison to the supervised models, due to more complex formulations used in their representation [201]. In electrical systems the above mentioned non-linear models are now being increasingly employed in the prediction of load demand- (electrical [202–204], thermal [205] , PV power generation [206–208], Wind power generation [209, 210] and electrical prices for energy arbitrage [211–213].

Precedent in selecting forecasting models

The linear models, as evident from the above discussion, had been conventionally employed for demand forecast in power system. In traditional power systems, where the generation capacity is dominated by load following, dispatchable power sources based on fossil fuels, there was no requirement for predicting generated power. Apart from this, forecasting in conventional systems mostly focussed on aggregated load demands which tend to exhibit lesser variance in data. In the present scenario this is not the case with increased penetration of RES. This calls for the need to have prediction of generated power to facilitate improved decision making in energy management systems as discussed before. However predicting RES generation presents difficult challenges. They exhibit strong seasonal and yearly behavioural pattern which are not handled well by linear models like ARIMA, resulting in poor forecast. Though a modification of ARIMA called the seasonal ARIMA (SARIMA) have been proposed to handle the seasonal behaviour in time series and provide improved prediction [214], their performance in the RES generation forecast was not highly optimal [215]. Another issue that arises with microgrids, is the need for predicting highly localised load demand which typically exhibits high variance in time series data. Linear models had been found to be inadequate for predicting these type of time series [216]. Considering all the above mentioned scenarios

the non-linear models will be more suited over the classical linear models, in forecasting units, for present day power networks with high RES penetration and incorporation of microgrids. This is justified by the improvement in performance of non-linear models based on neural networks, regression trees over linear models like ARIMA, SARIMA, demonstrated for RES generation [207, 217, 218] and localised load forecast [219, 220]. Though the computational power needed for the non-linear systems, especially in the deep learning scenarios, can be higher than linear models the availability of cheaper computational power nowadays alleviate this issue to some extent.

5.1.2 Forecasting units classification based on prediction horizon

Based on prediction horizon considered the forecasting units can be classified as [174]

- *Very short-term forecasting units*: These units provide forecast for a period ranging from few minutes to hours ahead. These type for forecasting are most suited for real time control purposes (reference tracking, disturbance rejection).

- *Short-term forecasting units*: The units provide forecast in the range from hours to few days ahead. These type of forecasts are best suited for control systems making decisions on optimal energy management and unit commitment in grids. The tertiary control scheme, considered in here, will work with these type of units.

- *Mid and long term forecasting units*: These type of forecasting units provide prediction in range from weeks to years. The results from these units are best utilised for planning the assets that need to be maintained by the electrical utilities to ensure reliable system operation.

5.1.3 Forecasting units classification based on number of forecast steps

The final classification of the forecasting unit is based on the points (steps) forecast in a prediction horizon by the forecasting unit. This can either be a single point (aggregated) or multiple points (distributed) in a horizon. The criteria that determines whether to use a single or multiple step forecasting unit depends on the application for which the predictions from the forecasting unit is used for [174].

5.2 Forecasting unit for the tertiary control stage

In this thesis the tertiary control stage will be developed for the microgrid with localised load and RES generation with PV system. As a result, based on the discussion in Section 5.1.1, non-linear models will be considered in the forecasting unit. The predictions from the forecasting unit will be for the short term and for multiple time steps in a prediction horizon.

The focus of this Ph.D work is primarily on developing optimal control strategies for ESS. The forecasting unit represents an enabler for this optimal decision making. As such in this thesis, developing novel non-linear architectures for forecasting will not be the objective. Based on the literature survey RNN based on LSTM have been found to provide better forecast for PV systems [207,217,218] and localised loads [219,220] among the non-linear models. Feed-forward neural network based ANN have demonstrated almost similar performance compared to the LSTM in forecasting application [205, 221] but with lesser computational demand in training phase. Considering that the objective of this work is on developing control systems for ESS in microgrids and its demonstration, a detailed performance analysis of different forecasting models will be not be carried out and a feed-forward ANN will be used in this work considering lower computational demand.

5.2.1 Time series data for the forecasting unit

The time series data for generation and load profiles will be based on the measurements at a test case microgrid in Lindenberg, Germany [7]. The PV profile will be generated from the irradiation data measurements at Lindenberg. The localised load data represents a 4-person household with annual consumption of 4.5 MWh. One year data will be used in this work for the forecast purposes and for developing the tertiary control stage. The data was measured with a 5 min sampling interval resulting in 288 data points per day and 105120 sampled data points for the whole year. The tertiary energy management stage will be developed considering a 24 hour forecast accounting for the daily periodicity of the load and generation profile. This requires that the forecasting unit provides 288 forecast points in a 24 hour window based on which tertiary control makes the decisions. The time series data used for PV power and load forecasting is shown in Figure 5.1a and Figure 5.1b.

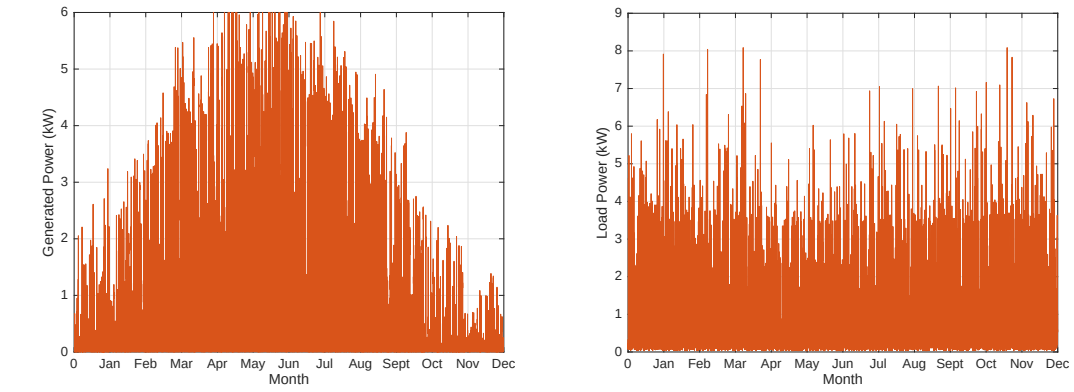

(a) (b)

Figure 5.1: One year's measured data (a) generation and (b) load profile from a test case microgrid in Lindenberg, Germany [7] used in developing forecasting unit.

5.3 Feed-forward artificial neural network forecast model

Neural networks (NN) are a class of machine learning architectures inspired from the biological neurons. NN are constituted by multiple layers and each layer has multiple nodes, analogous to a neuron in a biological system. In the simplest form NN consists of an input, an output and a hidden (intermediary to input and output) layer. However in prediction of complex proposes the basic representation may not be sufficient. In this scenario, multiple additional layers should be used. The same approach is also considered in this work. The additional layers allows for modelling complex behaviours. The ANN, considered here, shown in Figure 5.2a has two hidden layers with N_1 and N_2 nodes respectively and represents a feed forward system. The equivalent representation of each node is given by Figure 5.2b. This represents a fully connected node that receives input from all the nodes in the previous layer through a weighting factor (w_k) along with a biasing factor b as shown in Figure 5.2b. The sum of all this will be provided to an activation function which decides the output from each node [222, 223]. ANNs used in time series forecasting usually employ rectified linear unit (ReLU) as an activation function due to their improved performance [224] A ReLU can be defined as follows

$$f(l) = \begin{cases} l, & \text{for } l \geq 0 \\ 0, & \text{for } l < 0 \end{cases} \tag{5.3}$$

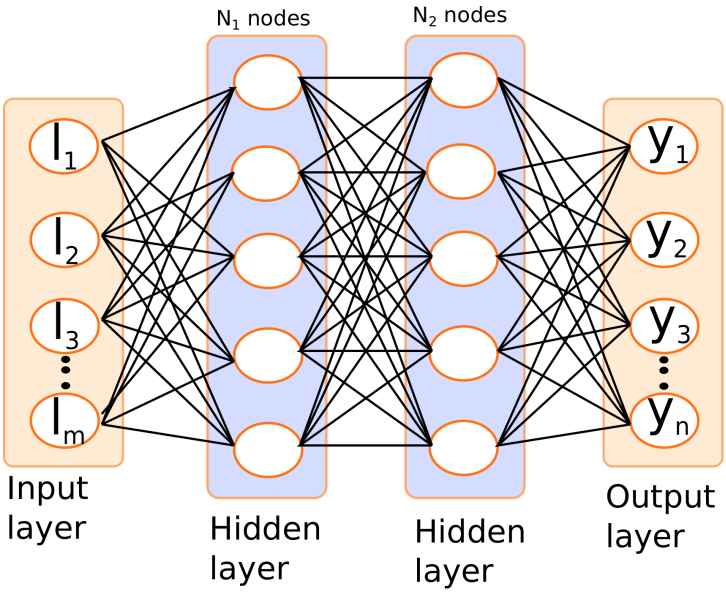

(a)

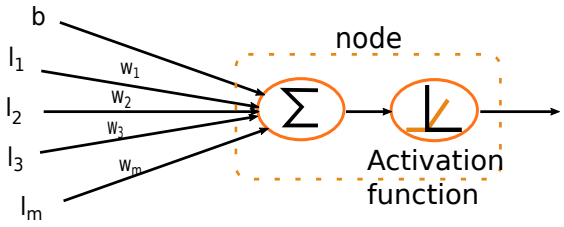

(b)

Figure 5.2: (a) ANN structure used in forecasting unit, (b) Equivalent representation of individual nodes.

5.3.1 Training of the ANN

An overview of the training process of ANN is only provided here and for a detailed exposition of the same, interested readers can refer to [222]. The training of ANN is the process of determining the optimal weights and biasing factor values for each individual node of the network. Once these values are obtained, the trained ANN can be used for forecasting purpose. The training is carried out using already sampled data of the process that needs to be represented by the ANN.

Prior to training, the objective will be to identify the input to the ANN ($l_1, l_2, l_3..l_m$). In the input vector, each element is called a feature and they are selected such that each one of them have significant contribution towards enabling an accurate forecast. In time series forecast, at any instant, a simple method will be to select a certain number of previous values as features, for forecasting at the current time. The process of input

feature selection will be discussed in detail in the upcoming sections.

Once the input features are identified the entire sampled data needs to be split into a training and testing set. These are sets of input-output pairs. The input will be the features that will be required for forecast at any instant. The corresponding output, in the pair, will be the expected output from the ANN. In this way the ANN is informed that, given an input vector the corresponding output pair is the forecast to be provided (supervised learning). The training/testing set split will be usually done in a 70:30 ratio. The training set will be used for training the ANN using its input-output pairs. The testing set will be used to determine the forecasting performance of the ANN. The input from the input-output pair of the test set will be used to generate the forecast. This will be compared with the corresponding output of the input-output pair in the test set to determine the accuracy of forecast.

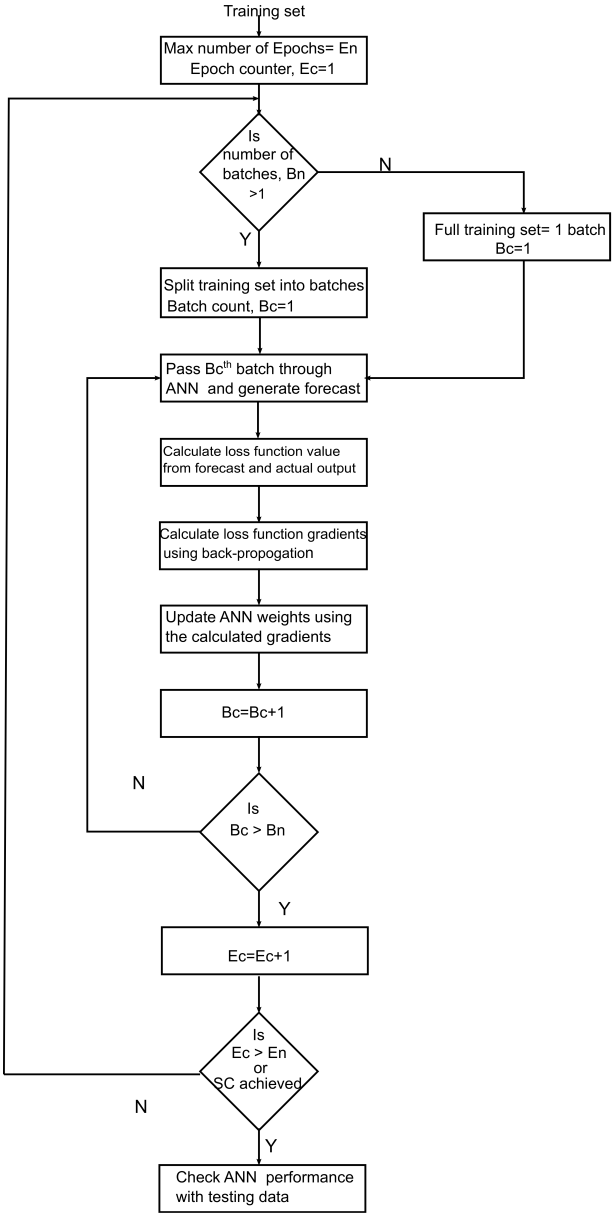

Figure 5.3: Flowchart of ANN training

The training of the ANN is an iterative process. Once the training set has been identified, the first step will be to choose some initial weights and bias value for all the nodes in the ANN. Guidelines for initial weight, bias selection is detailed in [222]. Once the weights have been assigned, the first step will be to pass the entire training set through the ANN to generate outputs. The passing of the entire training set can be done in batches or in one single step, depending on the size of training set data and computation power available. At this juncture a new term needs to be introduced

called the epoch. One pass of the entire training set is defined as one epoch. If the the training set is not divided into batches one epoch is equal to one batch otherwise one epoch is when all the batches have been passed through the NN.

After passing all the inputs, from input-output pair of a batch, the output obtained using the initial values of weights and biases will be compared with actual output from the input-output pair. The accuracy of the forecast, with the present choice of weights, will be quantified using a pre-defined loss function. In time series forecast the most widely used loss function is the mean squared error [225]. The training process will aim at minimising this loss function through updating of the weights and bias. At the end of passing a batch of training data the loss function value and its gradient will be calculated. The gradient calculation will be done with respect to each weights by chain rule starting from outer layer and moving inwards. These gradient values will then be used for updating the respective weights. This process of calculating the gradient is called back propagation algorithm. For detailed analytical analysis on how this back propagation will minimise the loss function and enable optimal weight selection interested reader can refer to the seminal work on the same [226]. Once the weights are updated the same process will be repeated after the next batch. The process of weight updating will continue till a certain number of predefined epochs have reached or when a stopping criteria (SC) is met. The identification of the SC will be discussed in the next section. The entire training process is represented with the flow chart in Figure 5.3

5.3.2 Mitigating over-fitting by ANN

As discussed in the previous section, one of the criteria for stopping the ANN training is when a certain number of pre defined epochs have been reached in the training process. However there is no analytical rule on deciding the optimal number of epochs to be considered in the training stage. An issue with the lack of a well drawn out method for deciding the number of epochs is that it can lead to over-fitting or under-fitting of data by the ANN. Over-fitting occurs when the number of epochs is more than what is needed. This causes the training process of the ANN to accurately map the input-output behaviour in the training set. However this high accuracy in the training set will lead to poor performance in the testing set (unseen data). This is not acceptable as the primary objective of ANN is to give good forecast on the unseen data and the over-fitting on the training set hinder the ANN performance. Under-fitting occurs when the number

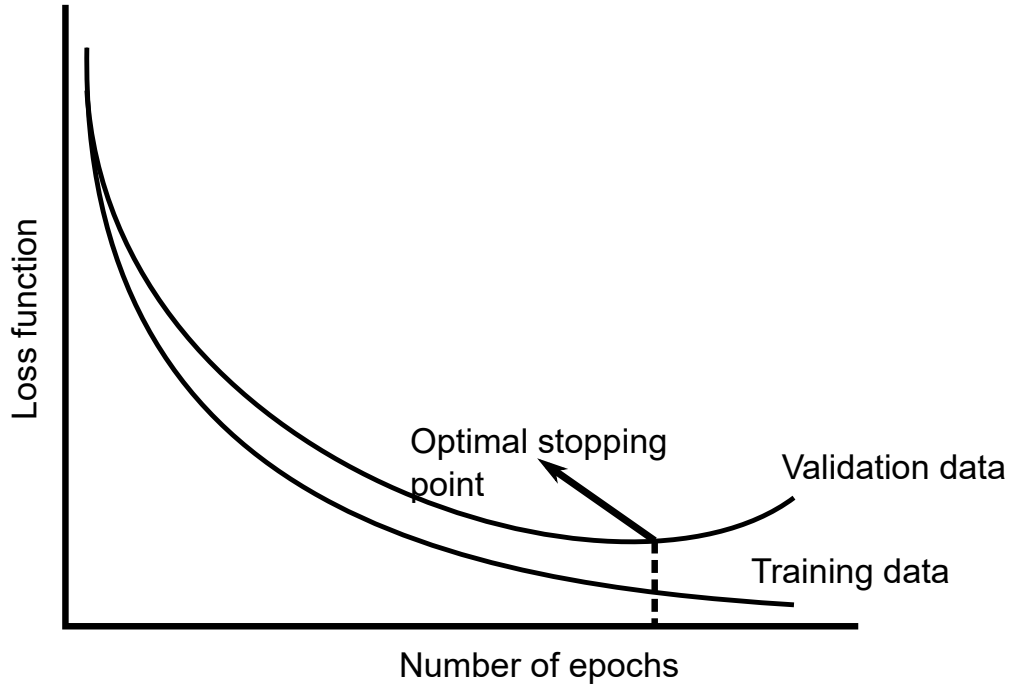

Figure 5.4: Over-fitting elimination with validation dataset. The point where the Loss function value starts increasing for the validation dataset indicates optimal stopping point [8].

of epochs are too low and the weights have not been defined correctly leading to poor forecast.

Under-fitting can be easily avoided by giving a high number of epochs. However, to avoid over-fitting additional stopping criteria (SC) need to be defined that allows early stopping of training process and prevents over-fitting. A widely used and easily implementable method is the use of a validation data set for early stopping of the ANN training [8]. The validation dataset is composed of a small fraction of the original sampled data of the process. Instead of employing 70:30 split of the original data a 70:15:15 split can be used to generate the training, validation and testing data. The validation data set will be used in the training process to avoid the over-fitting. At the end of every epoch, after the weights have been updated, the validation dataset will be used to ascertain the performance of the ANN using the loss function. This allows for an unbiased ascertaining of ANN performance as the validation dataset is an unseen data for the ANN. If the loss function value on the validation dataset is worse than that of the previous epoch it means that on the unseen data the ANN performance is worsening thus indicating over-fitting. This point where the loss function performance degrades on the validation set while improving of training set provides an indication of the optimal

stopping point of the training process. The same is shown through Figure 5.4 [8].

In practical case, the early stopping should not be employed at the first instance when the loss function value deteriorates in the validation set. Instead some more epochs should be executed to ensure that the performance deterioration in validation dataset is sustained. The utilisation of validation data and imposing the early stopping can be easily implemented using the Keras neural network library written in Python [227]. Apart from early stopping other methods that can be employed to minimise over-fitting using L1, L2 regularisation [228] in loss function, using dropout layers [229]. All these aspects can be implemented in the Keras package in Python.

5.4 Results and discussion

The ANN architecture used in the forecasting unit is as shown in Figure 5.2. All the nodes in the ANN are fully connected. As mentioned before the objective of the forecasting unit is to predict the PV generation and load profile for the tertiary control stage. The forecast of the same will be carried out using two different neural networks having the same layer structure but different number of nodes in each layer. The neural network architecture will be realised in Python using the Keras package. The ADAM optimiser [230] will be used in the training of the NN. Validation dataset based early stopping will be implemented for the NN to avoid over-fitting, using the Keras framework. Prior to presenting results, the process of input feature identification (input vector) for the PV and load forecasting NN is outlined.

5.4.1 Input feature selection for the PV forecasting ANN

An analysis of the one year PV profile, based on the data given in [7] will be carried out to identify which information should be given as input to the ANN. The auto correlation plot shown in Figure 5.5 is used for the same. This allows to identify dependency of any value in a time series with that of the previous values. Here the plot shows the dependency with last one week value. Based on Figure 5.5 it can be concluded that the generation data at any instant is highly correlated with the value from the same instant of the previous day. Therefore, for predicting the next 24 hours generation the last 24 hour values should be sufficient. Nevertheless, for better performance last three days

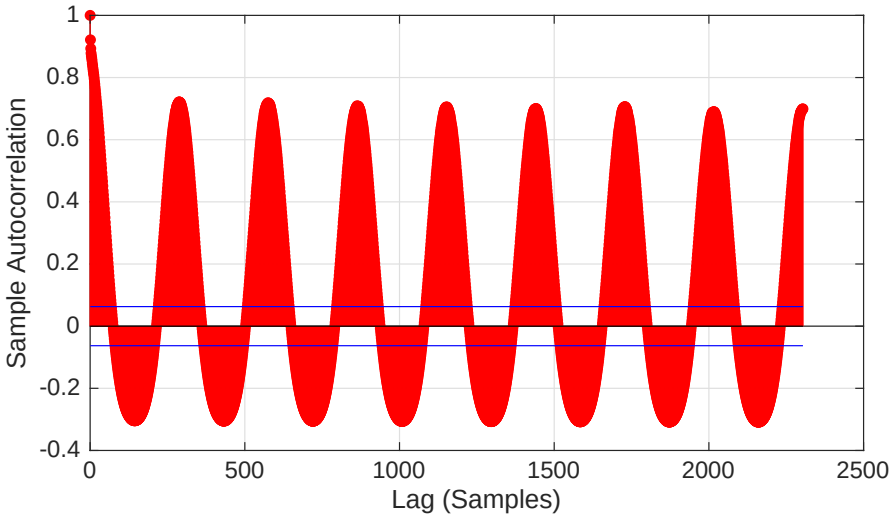

Figure 5.5: Auto correlation plot for PV generation data.

value was used as input for prediction. This resulted in a NN with input layer size of 864 ($288 \cdot 3$). The hidden layer size N_1 and N_2 was chosen as 300 through multiple trials. It should be noted that no information regarding the month or season is given as an input feature. This is because only one year's data was available. The 70:15:15 split for the training, validation and testing data results in the NN not seeing the profile from some of the months in a year during training phase. Therefore it was decided not to use the information of the month as an input for NN.

5.4.2 Input feature selection for the load forecasting ANN

The methodology applied for the PV generation forecast is also followed in the load forecast. The data analysis is done with the auto correlation plot shown in Figure 5.6. Unlike the PV data the load value at any instant has a lower correlation with that of the value from same instant the previous day. However, it can be observed that load value has higher correlation with the value from the same instant of previous week. Therefore, there is a daily and weekly cyclic behaviour for load demand. Hence for the load forecast last one week value is used as the input. This resulted in an input layer size of 2016 ($288 \cdot 7$). The hidden layer size N_1 and N_2 was 300 again achieved through multiple trials with trade off between accuracy and computational requirement.

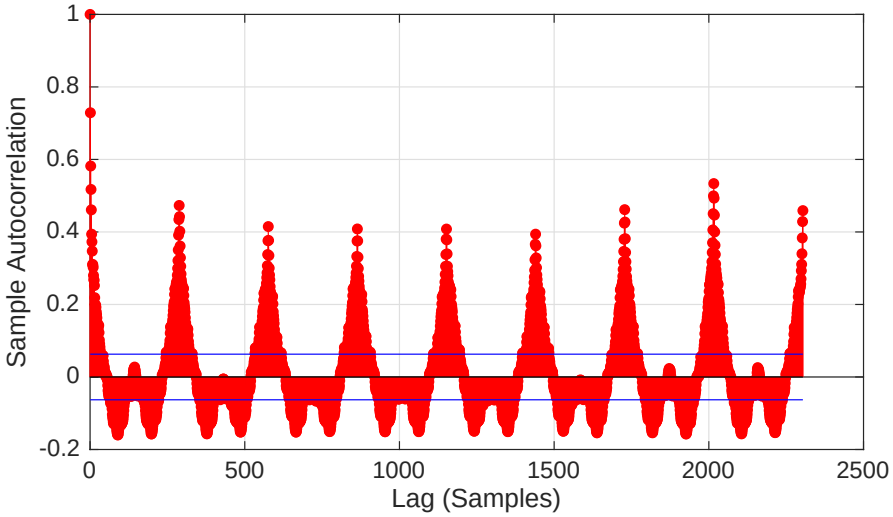

Figure 5.6: Auto correlation plot for the load data.

Hyper-parameter	Value
Input layer size	$288 \cdot 3 = 864$
Output layer size	288
Hidden layer size, N_1, N_2	300
Activation unit	$ReLu$
Loss function	mean squared error
Optimiser	ADAM
Maximum epoch	150
Batch size	2000

Table 5.1: Parameter values used in the ANN formulation and training

5.4.3 Results of PV forecast

The values of hyper-parameters used to define ANN structure for PV forecast and parameters of the training algorithm is summarised in Table.5.1. At any sampling instant the ANN used in PV forecast will provide the predicted generation of PV system for

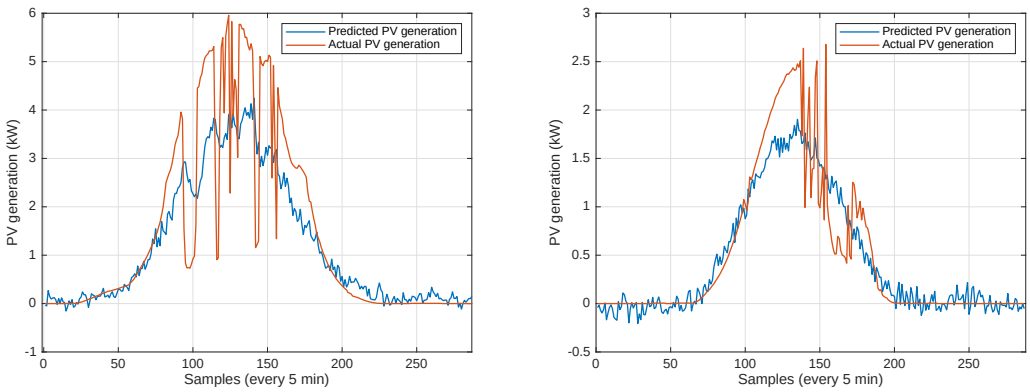

(a) (b)

Figure 5.7: Result of a 24 hour forecast of PV generation using ANN on (a) training and (b) testing data. The results shown for the training set is for the 4 June 2004 while that of testing set is month of 12 October 2004. The result shows the predictions occurring at early morning in a day.

the next 24 hours. The training of ANN was carried out in an Intel i7 2 core, 2.5 GHz machine with 8 GB RAM and NVIDIA quadro 500M GPU. In this case, due to availability of only one years data the training, validation and testing set splitting was not done in the ratio of 70:15:15. Instead, a 70:30 split for training, testing dataset was done and in the training process the testing data was used for validation purpose. The total training time for the ANN was around 10 min and the training process was terminated by the early stopping criteria at 55 epochs. The performance of the trained ANN, defined by the root mean squared error (RMSE), for training, testing set was 0.46 and 0.44 respectively . The effect of the early stopping is clearly observed here with the ANN having very similar performances in both training and unseen test dataset.

The Figure 5.7a and Figure 5.7b shows the forecasting performance of the ANN on the training and testing dataset. These results were generated by providing the data from training and testing set as input to the ANN after the training process was complete. The training set forecast result shown in Figure 5.7a represents prediction for a day in the month of May while the testing set result is that for the month of October. The main observation from both the results are that when there are sudden variations in PV generation (weather induced), as shown Figure 5.7a and Figure 5.7b, the ANN produces a more averaged forecast of the same. The lack of weather data in making the forecast, contributes to the same. In scenarios were there are no such high variation in PV profile, as shown in Figure 5.8 ,the ANN is able to predict the PV generation with

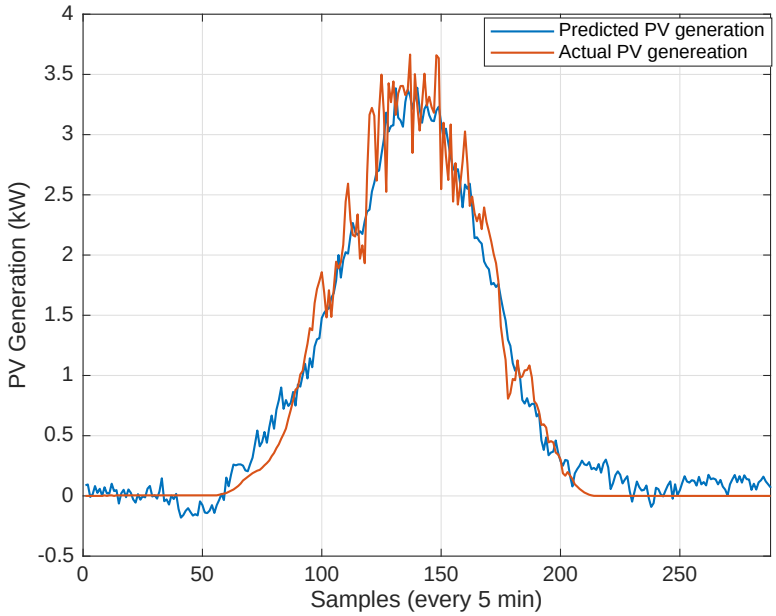

Figure 5.8: Result of PV generation forecast of ANN for a day that do not exhibit high variance in PV generation. The improvement in forecasting performance for the same can be observed. The forecast shown here is for the day, 14 September 2004.

higher accuracy. The results shown in Figure 5.8 is also for the testing dataset from a day in month of September.

5.4.4 Results of load forecast

The hyper-parameters vales used in defining the ANN for load forecast and parameters for the training algorithm is summarised in Table.5.2. Similar to the PV forecast a training, testing data split of 70:30 was used with the testing data also utilised for validation. The total training time for the ANN was around 20 min and the training process was terminated due to early stopping criteria at 35 epochs. The performance of the trained ANN, defined by the root mean squared error (RMSE), for training, testing set was 0.43 and 0.48 respectively. As is the case with PV forecast the performance in training and testing set was very similar, thus ascertaining the absence of over-fitting.

The forecasting results with the load data is provided in Figure 5.9 for the training and testing dataset respectively. The results for training data is from the month of May whereas that of testing data is from month of October. The load forecast is done for a highly localised load and the consequence of the same is that the load data exhibits

Hyper-parameter	Value
Input layer size	$288 \cdot 7 = 2016$
Output layer size	288
Hidden layer size, N_1, N_2	300
Activation unit	$ReLu$
Loss function	mean squared error
Optimiser	ADAM
Maximum epoch	150
Batch size	2000

Table 5.2: Parameter values used in the formulation and training of ANN employed in load forecasting.

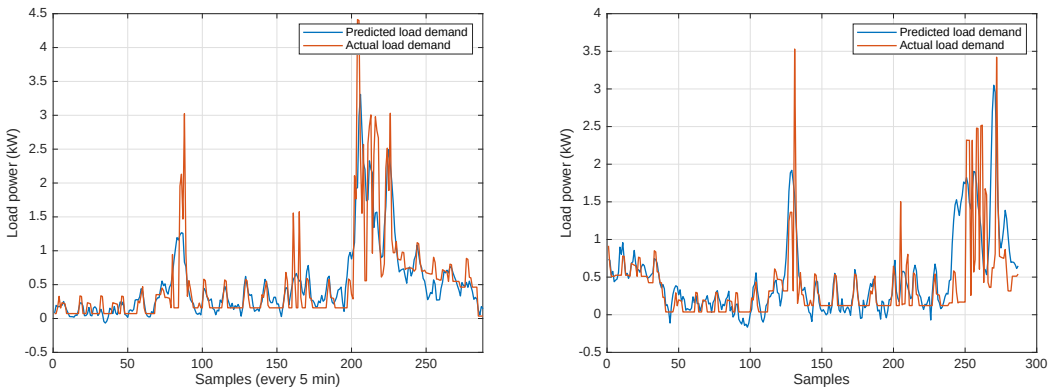

(a) (b)

Figure 5.9: Result of load generation forecast using ANN on (a) training and (b) testing data.

sudden peaks with high variance, as shown above. These high peaks shown in Figure 5.9cannot be accurately predicted by the ANN.

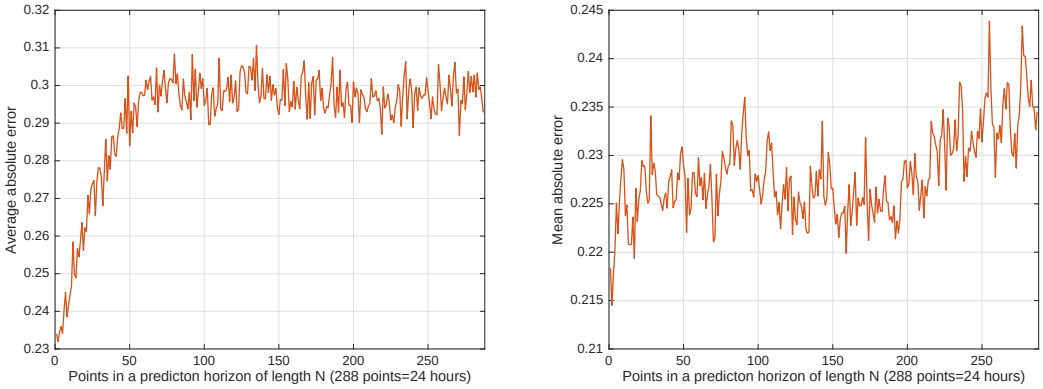

(a) (b)

Figure 5.10: Average absolute error for every point in the prediction window represented for (a) PV generation forecast (b) load demand forecast. The values obtained from analysis of one year forecasting using the ANN.

5.4.5 Quantifying accuracy of PV and load forecast by ANN

As explained before, the ANN provides a moving window forecast where at every 5 minute interval the forecast for the next 24 hours is provided. The loss function values for training and testing data give an indication of point to point accuracy of the forecast in this moving window scenario. The accuracy (error) can be further visualised through Figure 5.10. This shows the mean absolute error for every point in the 24 hour prediction window, based on the results of one year's forecasting. In every prediction window the error at every point was calculated. The mean absolute error of the first point is the average of all the errors at the first point in all the prediction windows for the year. Similarly this was calculated for the $2^{nd}, 3rd...., 288^{th}$ point. These are the values plotted in Figure 5.10. In the case of PV forecast, it can be seen that the mean absolute error is lower at the beginning of the prediction window and increases later in the window. This is in accordance with the correlation plot of Figure 5.5. The high correlation of the PV data with the previous values results in lower error in the beginning of the prediction window. In the case of load forecast it can be seen that there is a slight increase in the absolute error along the prediction window. However, this is not as significant as in the case of PV forecast. This, almost uniform error, can be justified by the low correlation of the load data with the previous values as shown in Figure 5.6. The load data, unlike the PV data, is not highly correlated with the previous values. This arises precisely due to the highly localized nature of the load considered here, as discussed before.

Another perspective for analysing the forecast accuracy can be based on the mean aggregate absolute error in a prediction window. This can be a relevant measure as it provides a less conservative analysis of the ANN accuracy. Along the prediction horizon, the forecast error at every point in the window can vary between positive and negative values. Aggregation of the error and then taking absolute value can help cancel out these point to point variations This can reveal the total error in terms of difference in total energy between predicted and forecast value. For example, in the case of PV forecast, the aggregation of errors will provide an indication of total generated energy difference between real and forecast value, in a prediction window. The same is the case with load forecast. As a result this mean aggregate absolute error is also analysed here. Analysing the actual PV generation data, it was observed that the mean aggregated energy of PV system in a moving 24 hour prediction window was 13.56 kWh. Based on the forecast data the mean absolute aggregate error in the same moving prediction window was 3.28 kWh. This accounted to 23% the average energy value for a prediction window. Similarly for the load, the mean aggregate energy demand of the load in a moving prediction window was 10.81 kWh, whereas the mean aggregate absolute error for the same was 1.015 kWh. This represented an error, that was 9.3% the average energy value. In comparison to load data the aggregated error in PV prediction is higher. This is mainly due to the limited amount of data available for the ANN training (only 1 year data was used) and the lack of weather data as additional input feature.

Analysing the two different methodologies discussed above, it can be seen that the method of using mean aggregate absolute error provides a less conservative error estimate. This can be verified by taking the sum of the mean absolute error for every point in the 24 hour prediction window, given by Figure 5.10. In the case of PV system, given by Figure 5.10a, this equates to 6.99 kWh whereas for the load , given by Figure 5.10b, it is 5.43kWh. These values are higher than the mean aggregate absolute error in a prediction window, calculated for the PV and load forecast data as outlined in the previous paragraph. The lower values are the result of error cancellation through aggregation in the prediction window which will ultimately provide a less conservative accuracy estimation. The error analysis of the forecast using the two methods outlined above describes how different perspectives for assessing the accuracy of a forecast can be developed from the same data.

The tertiary control stage used in the energy management of the microgrid should account for the above discussed errors in forecast and the accuracy of the ANN based

forecasting unit in its decision making. The criteria for selecting the error representation used in the decision making of tertiary control stage, from amongst the two methods outlined above, will be discussed in the next chapter.

5.5 Concluding remarks

This chapter has introduced the role of forecasting unit as a tool towards improved decision making in the tertiary control stage for energy management. Based on the literature survey on the forecasting units employed in electrical networks, the non-linear model based short term multiple step forecasting unit was considered in this work. The proposed unit was required to provide a 24 hour ahead forecast of PV generation and load demand at every sampling instant. The sampling frequency of 5 minutes in accordance with the available data was used and the forecasting unit was required to provide the forecast for every 5 minute interval in the prediction window. The ANN architecture was identified to be used in the forecasting unit. The training process of the ANN and mitigation of over-fitting of data by the ANN using early stopping was outlined. Based on the available data the input feature selection process for ANN was discussed for the PV and load data. The prediction results from the forecasting units were presented. Based on the results, forecasting of the load profile which is not significantly affected by the seasonal behaviour, exhibited better performance over the PV profile forecast. Two major reasons can be attributed to the same. The first being the lack of sufficient data (one year data only used) which prevented the training of NN on a full years data that would have enabled the network to study the yearly behavioural pattern. The second reason was the lack of weather information to be used as input to aid the forecast process. This would have enabled the NN to better predict the weather influenced variations in PV generation. However with increased data logging of generation and load data in electrical systems around the world, large amount of data will be available for the same. This will enable better training of NN or other machine learning based systems to provide more accurate forecast. The work in this chapter highlights the suitability of machine learning based ANN for generation and load forecast.

Another issue observed, was the inability of the forecasting unit in predicting the sudden peaks in the localised loads, evident in the example considered here. This will always be an issue when trying to forecast localised loads, in comparison to aggregated loads that have smoother profiles. Nevertheless, despite the availably of limited data, the

lack of weather information and need to predict localised loads, the performance of ANN based forecast unit was acceptable as evident from the forecast error analysis. It cannot be considered as the best forecasting behaviour but it provides a basis for analysing the performance of forecast based tertiary control stage under prediction uncertainties. The fact that the performance of forecast unit was not the best possible allows for a more worst case scenario analysis of the tertiary control stage performance.

Chapter 6

Tertiary control

This chapter discusses the work done in this thesis pertaining to the tertiary control for energy management in microgrids. The tertiary control forms the highest level in the centralised control architecture of microgrids and provides set points to the power management stage. This chapter tries to identify the control methodology capable of most efficient and optimal energy management of ESS in microgrids. The chapter tries to assess the issues in current power grids due to increased integration of renewable energy sources and how an efficient management scheme can be used to address the same. In this context, energy management of microgrids both in grid connected and islanded mode are discussed.

As outlined in the previous chapter, the objective of the tertiary control is the optimal energy management such that the grid operation is optimised with respect to some criteria. The discussion in the last chapter also provided a categorization of the tertiary control stage based on the decision making process employed for the energy management namely, heuristic and non-heuristic methods. A comparison of the two strategies in terms of their merits and demerits were discussed as well. It was concluded that the non-heuristic methods, even though computationally demanding, ensure more optimal grid operation through energy management. The characteristics of the non-heuristic methods that enable this were the

- Use of optimisation problems in decision making, that guarantee optimal energy management.

- Easiness in defining the required system behaviour implicitly through an optimisation problem and lesser reliance on prior in depth understanding of system behaviour.
- Easiness in incorporating forecast information in the decision making process which facilitates better energy management in microgrids.

Considering the same, the tertiary control stage developed in this work will focus on the utilisation of non-heuristic, optimisation based methods in its decision making for energy management in microgrid.

Nevertheless, an overview of the existing literatures, pertaining to energy management of ESS in microgrids is provided in Table 6.1. The works are classified based on the decision making method employed at the tertiary stage and number of ESS considered in the microgrids. It should be noticed that the literature survey identified works using up to three different ESS in a hybrid storage system. There were very limited relevant literature utilising more than 3 different types of ESS. This also inline with the discussion in Chapter 2, where it was outlined that most of the energy storage demand, arising in the grids, can be realised using not more than three different types of storage elements. In the heuristic methods, the different strategies that have been employed were rule based techniques, fuzzy inferencing, genetic algorithms (GA) or simulated annealing (SA). On the other hand, tertiary control using non-heuristic methods are categorised based on whether the control strategies were implemented offline or online.

The offline methods are employed when the system under consideration is large or distributed [168] or when complex non-linear optimisation problems have to be solved [169,170,231,232]. In either case, the computation times for decision making by tertiary control can be very high which makes an online implementation infeasible. In [75, 233, 234] offline scheduling was used in a system having PV generation with battery storage to define the battery charging and discharging using dynamic programming. In offline scheduling the set points for a certain time period is generated offline aided by a forecast of system behaviour and then applied to the system. In real time operation the actual system behaviour can deviate from the forecast. In this scenario the offline energy management will have to rely on lower level controllers to provide corrective action to compensate for the deviations in forecast. This can lead to the actual system behaviour being further away from the optimal.

	Heuristic			Non heuristic	
Number of ESS	Rules	Fuzzy	GA &SA	Online	Offline
1	[158, 159, 235, 236]	[160–163]	[164, 165, 167]	[172] [237–239]	[168] [169] [75,231,233, 234]
2	[76, 77, 157, 240]	[78, 241]	[166]	[242] [243] [173, 244]	[170] [232]
3				[74, 171]	

Table 6.1: Classification of literatures focussed on developing centralised tertiary control level for energy management.

Online methods, on the other hand, makes the decision for every sampling instance considering the current system state and updated forecast for that instant. This is in contrast to offline methods where the decisions are made for a period. This mode of decision making considering the current nature of the system reduces the reliance on low-level controller for compensation and provides more optimal results. In smaller systems like microgrids, where the number of decision variables are lesser, the computation time for decision making is smaller. This facilitates the use of online non heuristic methods at the tertiary level for energy management in these systems. This low computational demand in microgrids has prompted the use of online non heuristic methods at the tertiary control level, developed in this work for energy management.

A widely used methodology in online scheduling, based on existing literature, is the Model predictive control (MPC) strategy. The MPC is an optimisation based decision making strategy which allows an easy implementation online. The MPC has been increasingly applied in electrical systems to achieve optimal energy scheduling, off lately. In [172], MPC was used in battery management for smoothing the output from a wind power plant. In [239], MPC was used for managing a regenerative FC in a microgrid with PV and wind power to increase the operational efficiency of FC system. In [173], the MPC was used to improve economic benefit from energy arbitrage and operating costs in a microgrid with battery storage. The works in [74, 171, 238, 243] also uses MPC for energy arbitrage. In [74, 171], a microgrid with tri-hybrid storage was considered, while in [238] thermal storage was considered and in [243] FC, battery based storage

system was considered. In [242] MPC was applied to a FC-SC based hybrid drive system with the objective of minimising the deviations in SOC of SC and set points of FC. In [237], MPC was applied to an isolated power grid with battery storage, for reducing operating costs of the grid. Finally, the work in [244] uses MPC to improve demand response capabilities in a microgrid in order to improve the utilisation of generated PV power. More recently, the application of MPC has been extended to large scale systems (distribution networks) using distributed optimisation techniques [245, 246].

Though MPC has shown to be capable of energy management in electrical systems, their application in electric networks has mostly focussed on improving the operational efficiency of grids or achieving a more economic operation through reduction of operating costs or energy arbitrage. However, the application of MPC cannot be just limited to improving the above mentioned criteria in electric grid operation. It can be extended beyond the above mentioned objectives so that the full capability of MPC can be exploited. The MPC allows easy integration of forecast information in its decision making. This additional information can used in better management of ESS so that their degradation can be minimised. The works in [74, 171] address this issue with regards to FC by limiting sudden changes in setpoint so that fuel starvation can be avoided. However, there is no assessment that quantifies by how much ESS degradation or scenarios that stress the ESS has been limited. This demands analysis of long term system behaviour. MPC can be also be used to manage the degradation in the battery using the forecast information. The battery profile can be suitably altered with MPC, so that the stressing scenarios like highly charged states or repeated cycling can be reduced. Quantifying the improvement in battery degradation with MPC again requires an analysis of long term system behaviour.

Another application that the energy management with MPC can be used for, is to address the interaction between renewable sources and main grid. As discussed in Chapter 1, grid congestion is one of the negative outcomes from the increased penetration of renewable generation in power grids. The MPC, with the aid of load and generation forecast, can be utilised to optimally manage the energy injection from the renewable sources into the main grid so that the congestion issues can be overcome. The MPC achieves the same though the optimal scheduling of the different ESS. These represent issues of practical relevance which has not been addressed in previous works.

Finally, in most of the previous works, the focus has been on energy management in microgrid under grid connected scenario, with the exception of few works like [237].

Energy management in islanded microgrids present an interesting and relevant application for MPC based tertiary control system, considering the increasing probability of such operations as discussed in Chapter 1. The management of islanded microgrids is challenging due to the lack of an infinite energy reservoir, in the form of main grid, to handle imbalance power that cannot be catered by the ESS or load. This requires power curtailment capability and dispatchable generators to ensure reliable operation. Islanded microgrids also require hybrid ESS of high energy and power density to sustain the islanded operation. In this context MPC can be utilised in islanded microgrids beyond the domain of economic optimisation. The availability of forecast information can be used for reducing degradation in ESS by altering their charge discharge cycle. The forecast information can also be used for increasing the utilisation of energy from renewable sources by reducing their power curtailment while ensuring uninterrupted operation.

In light of this discussion the work carried out in the tertiary control stage of this work will focus on the use of MPC based energy management for mitigating issues of grid congestion and ESS degradation, increasing renewable energy utilisation while ensuring higher operational efficiency in microgrids. Studies will be carried out to quantify the improvements achieved with MPC and to analyse the computational demand resulting from MPC. Unlike the previous chapters were generic control framework was developed, this chapter focusses on specific issues arising in the grids and the application of MPC to overcome them. Two specific problems, one pertaining to grid connected system with ESS and another regarding an islanded grid with hybrid ESS will be presented through the upcoming sections in this chapter.

6.1 Model predictive control framework for energy management

The MPC belongs to the optimal control framework. One of the earliest controllers studied in the optimal control framework is the Linear quadratic regulator (LQR), which aimed at determining the optimal control action for a system defined by an unconstrained linear time invariant plant [137]. However, in practical problems the system cannot be considered to be unconstrained as there are usually limits on the control action that can be exerted or on the values the system states can take. The MPC was first

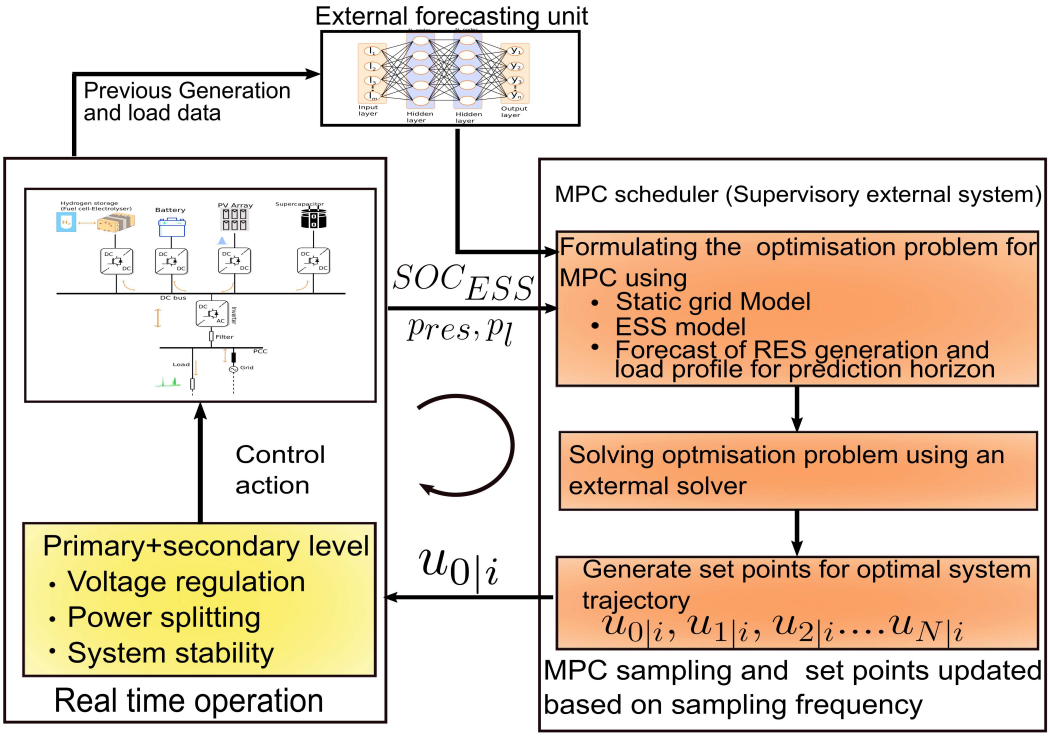

Figure 6.1: Schematic representation of the MPC scheduling process.

introduced in the process industry to address the optimal control problem in systems with constraints [247]. The capability of the MPC to provide optimal control while effectively handling system constraints, non-linearities and model uncertainties has since led to increased application of them in the process industry [248].

Economic MPC is another sub-division of the MPC control framework [249]. In economic MPC instead of optimising the control action on the plant, the economic cost associated with a process is optimised. The economic MPC, neither focusses on ensuring system stability nor reference tracking as an objective. This is because the economic MPC is usually implemented in the upper level of a hierarchical control scheme with the lower control levels ensuring the stability of the system. In the energy management problem of electric grids it is the economic MPC framework that has found increased application. In the electric grids the economic cost of the process mostly implies the operating cost of the grid, energy arbitrage to name a few. In this work whenever the term MPC is used it always refers to economic MPC.

The set points in MPC are generated by solving a constrained optimisation problem. At any sampling instant, i, the controller is provided with the sampled value of the system states and the value of exogenous input to the system at that instant. The

MPC makes the decision on the setpoint such that the future behaviour of the system is optimised based on the cost function in the optimisation problem. In order to achieve this the future behaviour of the system needs to be identified. The MPC uses the system model and the forecast of the exogenous inputs acting on the system for the same. In the electric grids since the exogenous inputs are formed by the renewable generation and load demand the forecasting unit discussed in the previous chapter provides the prediction of the same. At any sampling instant, the forecasting unit provides a forecast to the MPC regarding the generation and load demand for a finite period into the future comprising of N discrete points $(i+1, i+2, ..., i+N)$. The period for which the forecast is provided is the prediction horizon.

Once the inputs to the MPC, which are the sampled states, generation/load demand at sampling instance and their forecast for the prediction window, are available the required optimal behaviour of the system for the prediction horizon will be implicitly defined through the optimisation problem. The output from the optimisation problem will be the manipulated inputs of the system. In the case of the microgrid this will be setpoints of the dispatchable sources like ESS or generators. At any sampling instant the MPC generates a sequence of $N+1$ setpoints given by $u_{0|i}, u_{1|i}, u_{2|i}...u_{N|i}$ where $u_{k|i} = u(k+i)\ \ \forall k = 0, 1, ..., N$. Among the set points the first one, $u_{0|k}$, will be applied to the system. This process will be repeated at every sampling instance using the current system state, current generation/load demand and updated forecast for that instance. This utilisation of current system values and forecast provide a sense of feedback to the controller. As the forecast is updated at every sampling instant, the prediction horizon is receded by one sampling time period. Due to this nature of the prediction horizon the MPC is also called the receding horizon MPC framework [250, 251]. The entire process of MPC scheduling in electric grids, discussed above, is represented by Figure 6.1.

6.2 MPC for grid connected microgrids with PV generation and battery storage

The first application of the MPC at the tertiary level, considered in this work, is for the mitigation of grid congestion arising in grids due to increased penetration of renewable sources. As discussed in Chapter 1 the renewable energy sources integrated to the power grids has not been grid friendly. Multiple issues pertaining to grid congestion, voltage

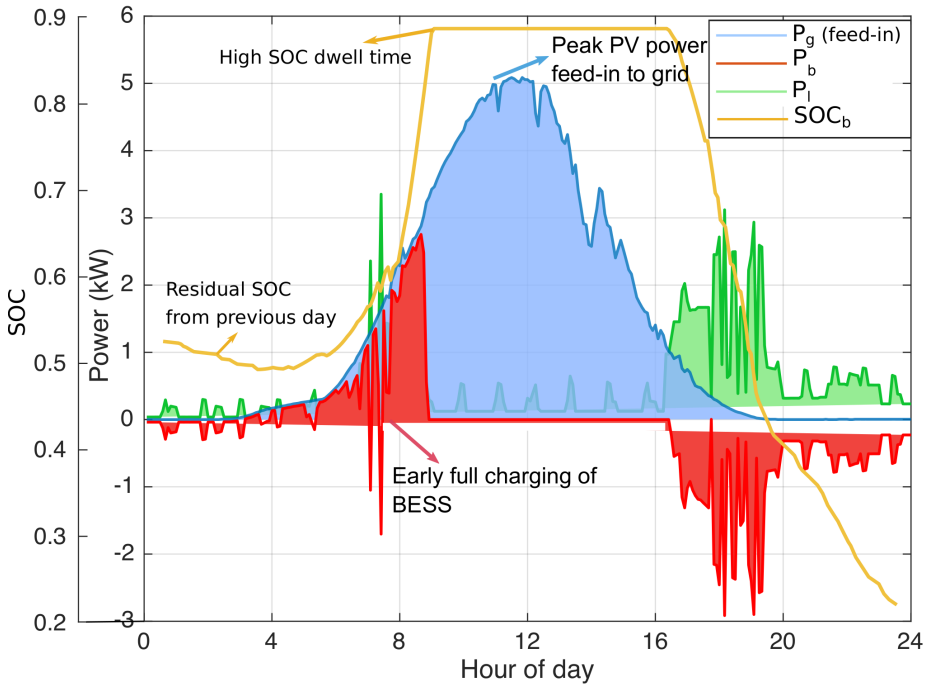

Figure 6.2: Typical BESS, SOC and grid feed-in profile with maximising self-consumption strategy for high PV generation scenario. Early full charging of BESS and ensuing peak PV power feed-in is shown. Profiles are based on data from [7].

regulation and grid stability have been reported due to the load-decoupled, intermittent nature of power generation from renewable sources [12, 13, 15].

As discussed before ESS can be used to overcome these issues. Battery based energy storages are being increasingly adopted in systems with PV generation [236, 252, 253]. However, integration of ESS alone will not solve the issues arising from the addition of renewable sources. An effective energy scheduling strategy for the battery systems is also essential to ensure that PV generation is grid friendly when employed together with battery energy storage system (BESS). In many European countries the extend of PV integration in the grid has resulted in achievement of grid parity where, for a consumer it is cheaper to utilise their own PV generation than buying from the grid [75, 254, 255]. This has resulted in the widely used maximising self-consumption control (MSC) in PV-BESS system [236] to maximize PV power usage by consumer. In the MSC strategy, PV power is stored in BESS as soon as surplus power is available until full charge. This is shown in Figure 6.2 where typical BESS profile under MSC scheme is shown. Though economically beneficial, MSC may lead to grid congestion. The reason being, charging

BESS as soon as surplus power is available forces BESS to reach the fully charged state early in the day, as shown in Figure 3.3. As a result when peak PV generation occurs later in the day BESS capacity cannot be used to cater this peak power which will then be injected into the grid. Such power injection from many PV systems can lead to grid congestion and voltage rise at the point of common coupling, if there is no sufficient load demand in the grid [256].

Another major drawback with the MSC strategy is related to BESS degradation. The major ageing mechanisms in BESS are the calender and cycling ageing. The calender ageing arises from the BESS being kept at high SOC for long duration, whereas cycling ageing arises from repeated deep charging/discharging cycles of BESS [83, 235]. In PV BESS system eliminating charge/discharge cycles are inevitable without compromising on self consumption. However, triggering factors for calender ageing can be reduced. In MSC strategy, the early full charging of BESS results in longer dwell times at high SOC levels, as shown in Figure 6.2, thus accelerating calender ageing. These longer dwell times at high SOC can be eliminated with improved energy management. Therefore, grid congestion and battery degradation are the two major concerns when employing the MSC strategy.

Energy scheduling of PV-BESS system aided by forecast of generation and load profiles can alleviate these drawbacks. The knowledge of future generation and load demand can be used to modify the BESS charging behaviour, such that the storage system capacity can be made available during peak generation. This can reduce the grid congestion by reducing the feed in power to grid. The modification of BESS charging profile can also be utilised to minimise the scenarios that can stress the BESS thus reducing the degradation. These approach of energy scheduling with forecast information has been considered in [75,233,257] where the decision on BESS scheduling was done offline, based on forecast value of generation and load. However, as discussed before the use of offline methods leads to increased reliance on the lower level controllers to compensate for the deviations in system behaviour (generation or load). In this case, online methods like MPC can provide a more optimal performance at the energy management level to avoid the issues of grid congestion and BESS degradation.

This application of MPC for grid congestion mitigation, minimising BESS degradation while maximising self-consumption of PV power through optimal energy management is studied in this work for grid connected PV systems. In order to effectively quantify and demonstrate the improvement with MPC, the scheduling performance for

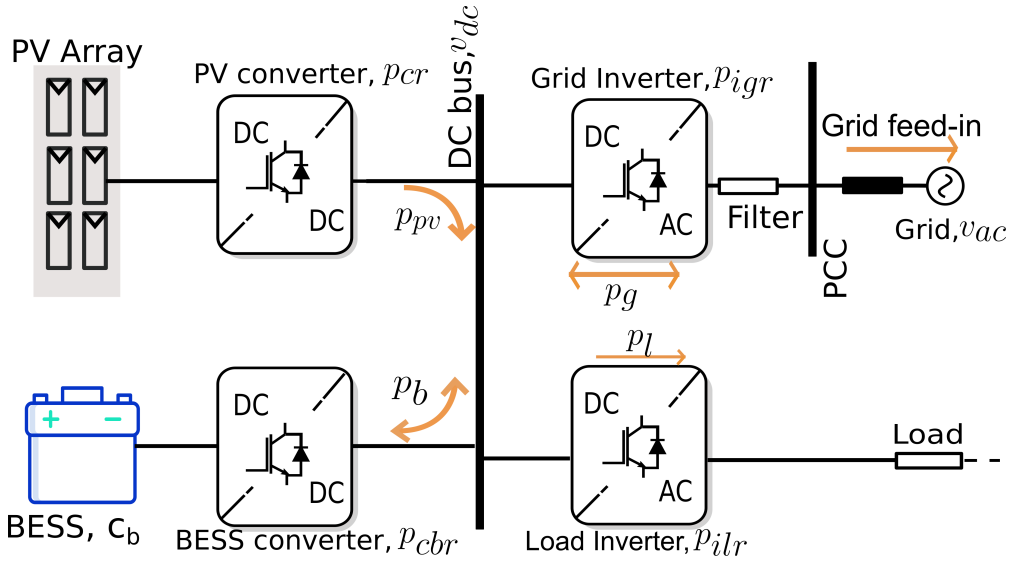

Figure 6.3: Schematic of the test case microgrid [7].

one year will be assessed. As the MPC makes the decision considering the future value of generation and load using their forecast, the performance of the energy management system is reliant on the accuracy of the forecast. In the scenario where the forecast is poor, the performance of MPC based system can be significantly poorer than the conventional MSC scheme. Therefore, in this thesis an analysis will also be carried out regarding the performance deterioration of the MPC based energy management scheme under prediction error. Finally, a corrective methodology will be proposed in the MPC scheme to account for the prediction error and the one year performance of the system in this scenario will also be analysed in comparison to the conventional MSC scheme.

6.2.1 System description

The system considered in this energy scheduling problem is shown in Figure 6.3. It represents a DC coupled configuration where both the PV and BESS are connected to the same DC bus via interfacing DC/DC converters. The PV converter is unidirectional and works in boost mode with power flow to the grid. The BESS converter is capable of bi-directional operation allowing for compensating the imbalance power in the DC bus. The BESS converter will work in buck-boost mode. The main grid is interfaced to the system through a DC/AC converter and filter. The objective of the MPC, in this problem, will be to generate optimal setpoints for the battery and grid converter systems such that the above mentioned objectives can be achieved. The setpoints for

Parameter	Value
Rated power of PV array	6 kW
PV converter rated power, p_{cr}	6
BESS capacity, c_{b}	9.375 kWh
BESS converter rated power, p_{cbr}	3kW
Load inverter rated power, p_{ilr}	3kW
Grid interfacing inverter rated power, p_{igr}	6kW
Nominal DC link voltage	450 V
Nominal AC bus voltage (AC)	230 V

Table 6.2: Parameter values for PV BESS system.

the PV converter will not be generated by the MPC. Rather, it is assumed that the PV system is always generating the maximum power possible at any irradiation level. This is conventionally ensured through the maximum power point tracking (MPPT) [258] strategy, typically employed at the converter control level of the PV system. A detailed discussion of the MPPT methods will not be provided in this thesis as it is beyond the scope of this work. The set points generated by the MPC will be augmented with the control action generated by the lower level power management control. The PV power profile is emulated using the irradiation and ambient temperature data measured at Lindenberg, Germany [7]. The PV power will be calculated from this measured data and will be used as set points for the PV converter. The load data emulates a 4-person household with an annual consumption of 4.5 MWh. The sampling frequency of generation and load data were 5 minutes. The parameter values of the systems used in the PV BESS configuration is given in Table 6.2.

Battery storage for the PV BESS system

The proper sizing of the BESS system also plays an important role in the improvement of self consumption and degradation. As the objective of this work is on proposing an efficient energy management strategy, the problem of optimal sizing of BESS is not considered in detail here. Nevertheless a short discussion is provided on the the rationale

behind the criteria for determination of the BESS capacity, considered here, based on the methodology presented in [75]. If the total energy annually generated by PV system (E_{pv}) is higher than the energy demanded by load (E_{load}) then total BESS capacity, c_b, is determined based on load demand

$$c_\mathrm{b} = 0.5 \cdot E_{load} \tag{6.1}$$

whereas if annual PV power generated (E_{pv}) is less than load demand then

$$c_\mathrm{b} = 0.5 \cdot E_{pv}. \tag{6.2}$$

This sizing criteria ensures that there is a trade-off between operational efficiency and preventing excessive battery degradation according to [75]. The value of the c_b shown in Table 6.2 is obtained based on the data from Lindenberg.

The BESS model utilised here is based on the Coulomb counting approach [259] which demonstrates the evolution of BESS SOC, SOC_b, based on BESS power set points p_b. Considering SOC_b as a system state x, the BESS model is defined as

$$x(k+1) = \begin{cases} x(k) - \frac{T_s \cdot \eta}{c_\mathrm{b}} \cdot p_\mathrm{b}(k) & \text{if } p_\mathrm{b} \leq 0 \\ x(k) - \frac{T_s}{\eta \cdot c_\mathrm{b}} \cdot p_\mathrm{b}(k) & \text{if } p_\mathrm{b} > 0 \end{cases} \tag{6.3}$$

where η is power converter efficiency and T_s is the sampling time. The above model is a hybrid representation of BESS wherein the system behaviour differs based on the nature of p_b. As shown in Table 1.3 the BESS has a very high round cycle efficiency ($> 90\%$). Commercial converters used in PV system also have very high efficiency. For example SMA solar, one of the leading providers of the commercial PV converter systems have the DC-DC converters of efficiency $> 98\%$. In this scenario, due to the high efficiency of BESS energy system (BESS+ converter) the hybrid model shown in (6.3) can be relaxed using the assumption $\eta \approx 1$. The resulting model for the BESS can now be written as

$$x(k+1) = x(k) - \frac{T_s}{c_\mathrm{b}} \cdot p_\mathrm{b}(k) \tag{6.4}$$

It should also be noted that when the sampling time T_s is small, the above model also gives a fairly accurate representation of BESS behaviour.

Grid

As the objective of the MPC is to ensure the optimal energy management and not controlling the dynamic behaviour of the grid, a static model of the grid is only considered at this stage. This is sually represented using the power balance condition given by

$$p_{\mathrm{b}}(k) + p_{\mathrm{g}}(k) + p_{\mathrm{pv}}(k) + p_{\mathrm{l}}(k) = 0 \tag{6.5}$$

where $p_{\mathrm{pv}}, p_{\mathrm{l}}$ are PV and load power respectively. The other relevant parameters of the PV BESS system and converter ratings are given in Table 6.2 based on the system at Lindenberg, Germany.

6.2.2 Formulation of MPC based tertiary control for PV-BESS system

As already mentioned the decision making in MPC is carried out by solving an optimisation problem. The formulation of the multi-objective optimisation problem used in MPC for optimal energy scheduling in PV-BESS system is discussed next. In order to account for the prediction errors some corrective measures will be proposed for the MPC in this thesis. These corrective measures will also be included in the optimisation problem formulation discussed in this section. First the optimisation problem will be formulated without considering correction for the prediction error.

Cost function for optimisation problem

The energy scheduling objective is to minimise grid congestion, BESS degradation while maximising the self consumption. The cost function chosen to ensure the same is

$$J = \sum_{k=i}^{i+N} (J_{\mathrm{g}}(k) + J_{\mathrm{b}}(k)). \tag{6.6}$$

The first term, J_{g} in the above cost function is given by

$$J_{\mathrm{g}}(k) = \lambda_1 \cdot p_{\mathrm{g}}(k)^2 \tag{6.7}$$

where λ_1 is a weighting factor. As it can be seen, J_{g} penalises power exchange with the grid, the effect of which is twofold. Firstly, by penalising grid power the controller tries to reduce the peak power value that is being injected to the grid. This aims to reduce

grid congestion. Secondly, this forces the PV power generated to be utilised, as much as possible, by the consumer thus promoting self-consumption. The second term in (6.6), J_{b} is chosen as

$$J_{\mathrm{b}}(k) = \lambda_2 \cdot SOC_{\mathrm{b}}(k)^2 + \lambda_3 \cdot \Delta SOC_{\mathrm{b}}(k)^2 \tag{6.8}$$

where λ_2, λ_3 are weighting factors. This term minimises the rate of degradation of BESS. As discussed in Section 2.1.2, the BESS degradation arise from the calender and cycling ageing. Penalising SOC_{b} limits longer dwell time of BESS at high SOC levels, thus limiting the calender ageing. The other factor affecting the calender ageing was the temperature of operation. However, controlling the same with tertiary control is not practical. The $\Delta SOC_{\mathrm{b}} = SOC_{\mathrm{b}}(k+1) - SOC_{\mathrm{b}}(k)$ and penalising this minimises the excessive charge/discharge cycles which affect the cycling ageing in BESS. The exact analytical equation that represents BESS degradation [235] is highly non-linear. An explicit utilisation of the same will result in a complex non-linear optimisation problem that can be difficult to solve [260]. Therefore, the quadratic formulation in (6.8) has been maintained. The resulting quadratic problem, though non-linear, has very efficient algorithms for solving them and guarantees a global optimum [261].

Constraints for optimisation problem

The constraints in the optimisation problem ensure that the energy management system accounts for the behaviour of the storage system, power grids while also ensuring that the operating limits of the BESS and power converters are not violated. In order to account for the ESS and grid behaviour in the energy management stage, the models for the same defined in (6.3),(6.5) are introduced as constraints in the optimisation problem.

Physical operating constraints: The physical operating constraints given by

$$x^{lo} \leq x(k) \leq x^{up} \tag{6.9}$$

ensure that the BESS is not over-charged or deep-discharged, which can affect the BESS degradation [83]. The x^{lo}, x^{up} are the permissible lower and upper limits of SOC_{b}. The above represents a hard constraint on the system state which can, in some cases, lead to a infeasible solution in the optimisation problem. Therefore, to ensure that the on-line implementation of MPC is reliable the above hard constraints are replaced with

soft constraints [262]. The soft constraints allow for constraint violation but at a high penalty to the cost function. This ensures that under most of the conditions the SOC operating limits are not violated. The soft constraint implementation of (6.9) is

$$x^{lo} - \epsilon_b(k) \leq x(k) \leq x^{up} + \epsilon_b(k) \tag{6.10}$$

where ϵ_b is the violation of the SOC bounds. In order to ensure that these violations are very limited an additional term is added to the cost function (6.6) given by

$$J_{\text{vio}}(k) = \lambda_4 \cdot \epsilon_b^2(k) \tag{6.11}$$

where λ_4 is weighting the ϵ_b. Choosing a high value for λ_4 will ensure that ϵ_b value is kept minimal (minimising over-charging or deep-discharge) during the energy scheduling while also ensuring the feasibility of optimisation problem.

Electrical operating constraints: The electrical operating constraints ensure that DC/DC converters are operated within their rated values. This is given by

$$-p_{\text{cbr}} \leq p_{\text{b}}(k) \leq p_{\text{cbr}} \tag{6.12}$$

$$-p_{\text{igr}} \leq p_{\text{g}}(k) \leq p_{\text{igr}} \tag{6.13}$$

where $p_{\text{cbr}}, p_{\text{igr}}$ are as shown in Table 6.2.

Combining (6.7),(6.8), (6.11) the resulting cost function $J = \sum_{k=i}^{i+N} (J_{\text{g}}(k) + J_{\text{b}}(k) + J_{\text{vio}}(k))$. and the resulting optimisation problem in MPC is summarised as

$$\min_{p_{\text{b}}, pg} [J(p_{\text{b}}, pg, x)] \tag{6.14}$$

subject to the constraints

$$\begin{aligned}
&x(k+1) = x(k) - \frac{T_s}{c_{\text{b}}} \cdot p_{\text{b}}(k) \\
&p_{\text{b}}(k) + p_{\text{g}}(k) + p_{\text{pv}}(k) + p_{\text{l}}(k) = 0 \\
&x^{lo} - \epsilon_b(k) \leq x(k) \leq x^{up} + \epsilon_b(k) \\
&-p_{\text{cbr}} \leq p_{\text{b}}(k) \leq p_{\text{cbr}} \\
&-p_{\text{igr}} \leq p_{\text{g}}(k) \leq p_{\text{igr}}.
\end{aligned} \tag{6.15}$$

MPC formulation with corrective measure for prediction errors

The above optimisation problem formulation does not account for the prediction error. As shown in Chapter 5 the forecast is never perfect and it is always bound to have some error. A more effective training of the ANN using a larger data set might reduce the error but not mitigate it. Therefore, modifying the optimisation problem in MPC to account for the prediction errors makes practical sense.

Many works have tried to address the problem of uncertainty in forecast. This has resulted in many methods being proposed like the chance constrained MPC formulation [263], scenario based MPC [264] to name a few. Though these methods provide a solution to the decision making problem, under prediction uncertainty, they can be very conservative. Apart from that they require complex analytical formulations (chance constrained) and computational power (scenario based approach). Apart from this, conservative decision making can severely undermine the economic benefit of the consumer.

Therefore, in this work a simple constraint tightening approach [265] will be considered in the MPC to account for prediction error. In the constraint tightening approach the constraints on the manipulated inputs and system states are tightened based on prediction error. An excessive tightening of the constraint can still lead to conservative decision making and avoiding this aspect will be focussed in this work. First, the implementation of constraint tightening in the optimisation problem of MPC is discussed.

Consider that the forecast used in the MPC is not accurate and can vary within a certain bound $d_{i|k}$ defined as

$$d_{k|i} = \begin{cases} 0, & \text{for } k = 0 \\ [+\Delta\theta_k, -\Delta\theta_k]. & \text{for } k = 1, 2..N \end{cases} \tag{6.16}$$

At the sampling instant i since the PV generation and load demand is known, $d_{0|i} = 0$. Defining $p_{\mathrm{pv(k|i)}} + p_{\mathrm{l(k|i)}}$ as $p_{\mathrm{def(k|i)}}$, the predicted imbalance power in the system, (6.5) can be rewritten under prediction uncertainty for the horizon N as

$$p_{\mathrm{b}(k|i)} + p_{\mathrm{g}(k|i)} + u'_{(k|i)} + p_{\mathrm{def}(k|i)} + d_{(k|i)} = 0. \tag{6.17}$$

Where $u'_{(k|i)}$ is the control action to counteract the uncertainty in forecast defined by the bound, $d_{(k|i)}$. The MPC bases its decision on the $p_{\mathrm{def(k|i)}}$ which is the deterministic

part of the imbalance forecast given by the forecasting unit to MPC. Therefore (6.17) is split into deterministic part which is used in MPC given by

$$p_{\mathrm{b}(k|i)} + p_{\mathrm{g}(k|i)} + p_{\mathrm{def}(k|i)} = 0 \tag{6.18}$$

and uncertain part given by

$$u^{'}_{(k|i)} = -d_{(k|i)}. \tag{6.19}$$

The uncertain part of the control action will be handled in real time by the low level power management stage.

The constraints on the manipulated inputs and the system state will be now be tightened using the uncertain part (6.19) of control action. The electrical operation constraints of (6.12) will be modified as

$$\begin{aligned} -p_{\mathrm{cbr}} + u^{'}_{(k|i)} \leq p_{\mathrm{b}(k|i)} \leq p_{\mathrm{cbr}} - u^{'}_{(k|i)} \\ \Rightarrow -p^{'}_{\mathrm{cbr}} \leq p_{\mathrm{b}(k|i)} \leq p^{'}_{\mathrm{cbr}} \end{aligned} \tag{6.20}$$

where $p^{'}_{\mathrm{cbr}} = p_{\mathrm{cbr}} - u^{'}_{(k|i)}$. It should be noted that the constraints on BESS converter is only modified in this case. The constraints on the grid interfacing converter remains unchanged. This ensures that the BESS capacity is always available to cater the energy associated with forecast error and aid self consumption.

In order to tighten the constraints on the system state, the BESS model in (6.4) is represented as

$$x_{k+1|i} = x_{k|i} - \frac{T_s}{c_{\mathrm{b}}} \cdot (p_{\mathrm{b}(k|i)} + u^{'}_{(k|i)}) \tag{6.21}$$

under the assumption that $d_{(k|i)}$ is always catered by BESS until fully charged/discharged. The above equation can be rewritten in terms of sampled value of SOC_b ($x_{0|i}$) at instant k as

$$x_{k+1|i} = x_{0|i} - \frac{T_s}{c_{\mathrm{b}}} \cdot \sum_{k=0}^{N} (p_{\mathrm{b}(k|i)} + u^{'}_{(k|i)}). \tag{6.22}$$

The deterministic part in the above equation is

$$x_{k+1|i} = x_{0|i} - \frac{T_s}{c_\mathrm{b}} \cdot \sum_{k=0}^{N} (p_{\mathrm{b}(k|i)}). \tag{6.23}$$

and $\sum_{k=0}^{N-1} u_{(k|i)} = dx_{k|i}$ forms the non deterministic part. Based on this, constraint tightening of (6.10) is done as follows

$$x^{lo} - \epsilon_b(k) + dx_{k|i} \leq x_{k|i} \leq x^{up} + \epsilon_b(k) - dx_{k|i}. \tag{6.24}$$

The optimisation problem used in MPC incorporating the tightened constraints for prediction error will be given as

$$\min_{p_\mathrm{b}, p_\mathrm{g}} [J(p_\mathrm{b}, pg, x)] \tag{6.25}$$

subject to constraints

$$\begin{aligned}
& x(k+1) = x(k) - \frac{T_s}{c_\mathrm{b}} \cdot p_\mathrm{b}(k) \\
& p_\mathrm{b}(k) + p_\mathrm{g}(k) + p_\mathrm{pv}(k) + p_\mathrm{l}(k) = 0 \\
& x^{lo} - \epsilon_b(k) + dx_{k|i} \leq x_{k|i} \leq x^{up} + \epsilon_b(k) - dx_{k|i} \\
& -p^{'}_{\mathrm{cbr}} \leq p_{\mathrm{b}(k|i)} \leq p^{'}_{\mathrm{cbr}} \\
& -p_{\mathrm{igr}} \leq p_\mathrm{g}(k) \leq p_{\mathrm{igr}}.
\end{aligned} \tag{6.26}$$

The tightening of constraints having been implemented, the next step is to determine how to choose $d_{k|i}$ so that the MPC does not make very conservative decisions. In order to decide this, consider the decision making process in MPC. At any sampling instant there are two critical informations that the MPC need. The first is the total imbalance energy to be handled in a prediction horizon. The knowledge of this allows the MPC to decide how much BESS capacity is to be made available so that maximum PV power generated can be utilised through stored energy in BESS. This enables improved self consumption. The second information is the period at which peak imbalance, typically caused by peak PV generation, occurs. The knowledge of this allows the MPC to decide when to charge the BESS so that peak power injection to grid can be eliminated and BESS degradation can be minimised.

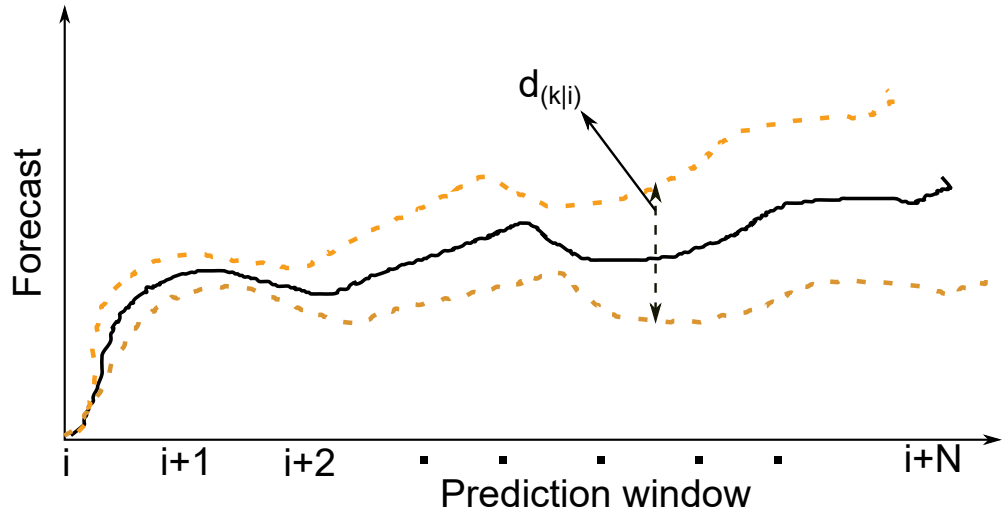

Figure 6.4: Representation of error propagation along prediction horizon

The ANN based forecasting unit, discussed in Chapter 5, had shown that it is capable of giving a good indication as to when the peak PV generation occurs in a day. Therefore, this critical information is available to the MPC. In terms of total imbalance energy that needs to be managed in prediction horizon, the accuracy of the ANN forecast, analysed in Section 5.4.5, should be considered. In this analysis of ANN accuracy, two perspectives were discussed to assess the error in forecast. As mentioned above, one of the critical information that the MPC requires to make its decision is the total amount of imbalance energy in a prediction horizon. Since the aggregate energy in a horizon is required, the mean absolute aggregate error of the ANN can be used as an indication of forecast accuracy. Therefore, the same will be considered is defining $d_{k|i}$. The utilisation of the mean absolute aggregate error also provides a less conservative estimate of ANN accuracy as highlighted in Section 5.4.5. This is essential in the case of the highly localised PV BESS system which exhibit high variability in load behaviour which can be difficult to predict.

As shown in Section 5.4.5 the forecast error is lower at the beginning of the prediction window and increase along the same. Therefore, the $d_{k|i}$ should also exhibit similar behaviour. Since the mean aggregate absolute error, e_a, for the prediction window is used, this needs to be distributed such that the $d_{k|i}$ exhibits this increasing behaviour as shown in Figure 6.4. Though not an exact representation of the error behaviour shown in Section 5.4.5, the Figure 6.4 still provides a good approximation of the error behaviour of the ANN forecast.

6.2.3 Results of MPC based energy management in PV BESS system

The optimisation problems in MPC were solved using Gurobi (version 8) [266] with YALMIP as the parser in the MATLAB environment. All the algorithms were run in an Intel i7 2 core machine having, 2.5 GHz processor and 8 GB RAM.

In order to assess the performance of the MPC at the tertiary control level four cases of energy management in the PV BESS system are identified for a comparative study. These cases are:

- *Case 1:* Energy management in a PV BESS system using the MSC scheme
- *Case 2:* Energy management in a PV BESS system using the MPC scheme but with perfect forecast. The MPC will use the optimisation problem defined in (6.14),(6.15). In order emulate the perfect forecast the actual generation and load value will be given as the forecast value in every prediction window. Henceforth, this case will be referred to as *Ideal MPC*
- *Case 3:* Energy management in a PV BESS system using the MPC scheme but without taking into account the forecast error. In this case, the forecast will be provided by the ANN based forecasting unit of Chapter 5. However no corrective measure will considered in the MPC decision making. As a result MPC will use the optimisation problem defined in (6.14),(6.15). The analysis of this energy management case will give an indication of the degree of performance deterioration in MPC if forecast error is not considered in decision making. Henceforth this case will be referred to as *MPC without correction.*
- *Case 4:* Energy management in a PV BESS system using the MPC scheme but accounting for forecast error. In this case forecast will be provided by the ANN based forecasting unit of Chapter 5. As the correction for forecast error is considered the optimisation problem of (6.25), (6.26) will be used in MPC. Henceforth this case will be referred to as *MPC with correction.*

Performance indices

Prior to presenting the results some performance indices considered in this thesis to quantify the performance of the energy management system is introduced. The self

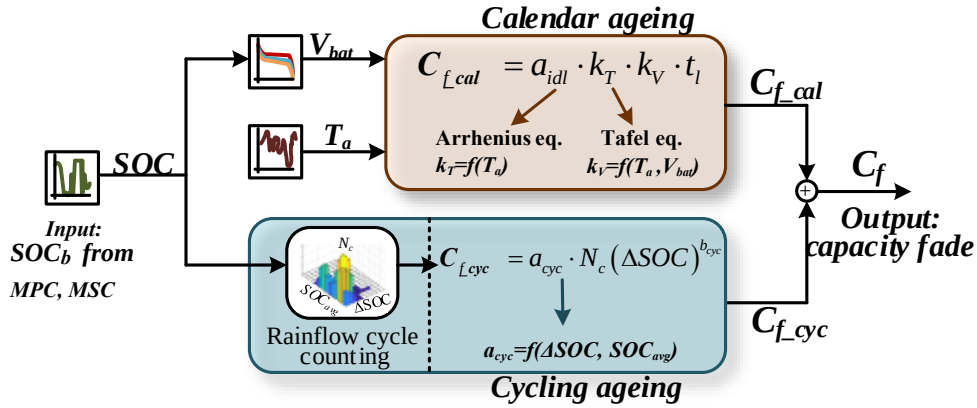

Figure 6.5: Flow chart for capacity fade, C_f, mapping from SOC_b with overview of calender and cycling ageing calculation.

consumption is quantified using the annual self-consumption ratio (ASCR) defined as the following

$$ASCR = \frac{pv_{cons}}{pv_{gen}} \cdot 100(\%) \tag{6.27}$$

where pv_{cons} is the amount of annual PV energy generated that has been utilised by the consumer through the load demand and BESS storage, while pv_{gen} is the total annual PV energy generated. In order to ensure maximum economic benefit for the consumer, this value should be as high as possible

The BESS end-of-life is defined when the capacity has faded to 80% of the nominal rated value (C_b). Under this scenario, the effect of energy scheduling on BESS degradation is quantified by assessing the capacity loss in the battery after one year's scheduling. The degradation model of Li-ion battery provided in [235] will be used. The BESS SOC profile from the different scheduling methods will be used to calculate annual capacity fade (C_f) of BESS due to its utilisation. The entire process in the calculation of C_f from BESS SOC profile (SOC_b) is represented using the flow chart shown in Figure 6.5. The T_a is ambient temperature, also available in the Lindenberg data.

Finally, the electrical performance associated with grid congestion will be assessed through the peak power injected into the grid using the index, annual average peak power reduction (APPR). This index is defined as

$$APPR = \frac{1}{D} \sum_{n=1}^{D} \left(\frac{p_{\mathrm{pvp(n)}} - p_{\mathrm{gp(n)}}}{p_{\mathrm{pvp(n)}}} \right) \cdot 100(\%) \tag{6.28}$$

where D is the total of days in a year, $p_{\mathrm{pvp}}(n)$ is the peak PV power injected to grid for

Parameter	***value***
Sampling time (T_s)	5 min
N	288
x^{lo}	0.1
x^{up}	0.9
$\lambda_1, \lambda_2, \lambda_3$	500,400,3
λ_4	1000
ρ	100
D	365

Table 6.3: Parameter values used in MPC.

the n^{th} day without BESS integration, and $p_{\mathrm{gp(n)}}$ the peak grid power on the n^{th} day with BESS integration under a scheduling strategy (MSC or MPC). This index gives the percentage reduction in peak power injection to grid achieved with a scheduling method in comparison to the case where the BESS integration was not available.

Analysis of annual energy scheduling results in PV BESS system

The values of the parameters used in the optimisation problem of MPC is given in Table 6.3. The prediction horizon value, N, was chosen to be 24 hours considering the daily periodicity of the PV and load profiles. The scheduling of the PV BESS system was carried out for one year for the four cases mentioned above. The results for the same is shown in Figure 6.6 for the 4 different cases mentioned above.

In order to better conceive the improvement in energy scheduling achieved with MPC consider Figure 6.7, which shows the BESS profile for a typical day with the different energy management cases. The major difference between all the MPC schemes and MSC is that the MPC with its knowledge of future generation and load profile shifts the BESS charging to the period of peak generation as shown in Figure 6.7. This allows MPC to minimise the cost function of (6.6) and achieve the desired performance criteria. This shifting to peak generation period in all MPC schemes ensured that the BESS capacity is available to meet the peak PV generation. This allows for significant reduction in the

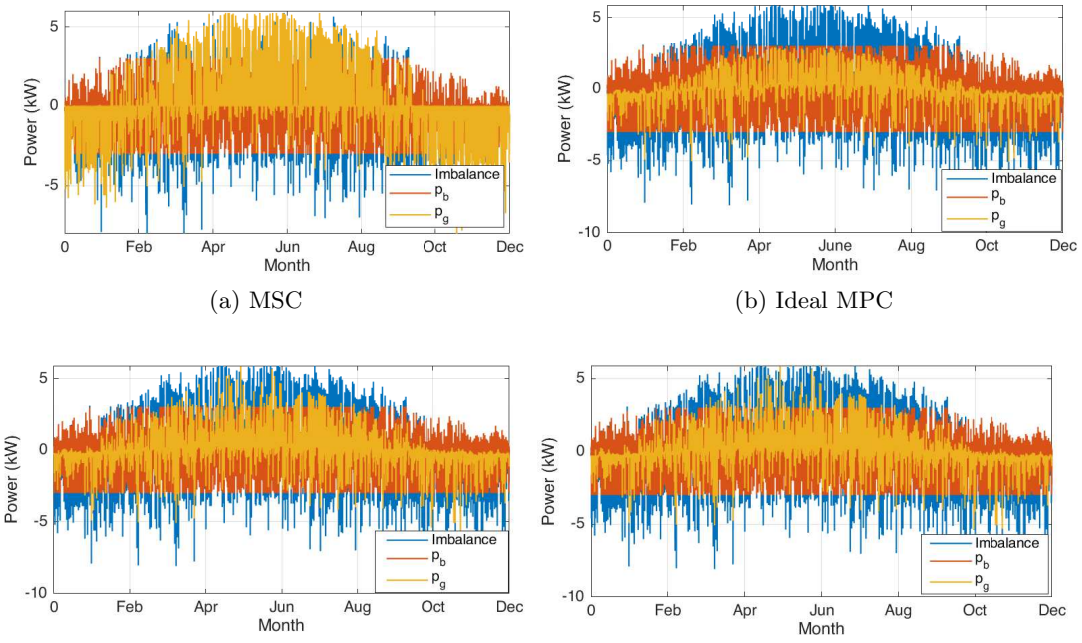

(a) MSC

(b) Ideal MPC

(c) MPC without correction

(d) MPC with correction

Figure 6.6: One year energy scheduling in PV BESS system under the 4 cases of energy management considered.

peak PV power being injected into the grid with the MPC schemes thus promoting grid congestion mitigation. Another effect of this shifting is that in all the MPC schemes the BESS gets fully charged later in the day. This reduces the dwell time of BESS at high SOC levels unlike MSC scheme where dwell times are higher due to early BESS charging. Among the MPC schemes, as can be seen in Figure 6.7, the *ideal MPC* with the perfect forecast shifts the BESS charging exactly to the period of actual peak PV generation. As shown in Figure 6.7, the PV generation forecast from ANN for the particular day is lower than actual forecast. This resulted in both the MPC *with* and *without correction* to charge the BESS slightly earlier than the ideal MPC case but still close to peak of the PV generation.

The reduction in the peak power feed-in to grid due to the shifting of BESS charging with MPC schemes can be observed in Figure 6.8. The figure shows the daily power feed-in to the grid with the 4 energy management schemes for the whole year. The peak PV power feed-in to grid with the MSC scheme due to early BESS charging can be clearly observed here. It should also be noted that the power feed-in to grid with the MSC scheme is concentrated over a shorter time period in day (peak generation). In comparison, the *ideal MPC* scheme has completely eliminated the peaks and exhibits a

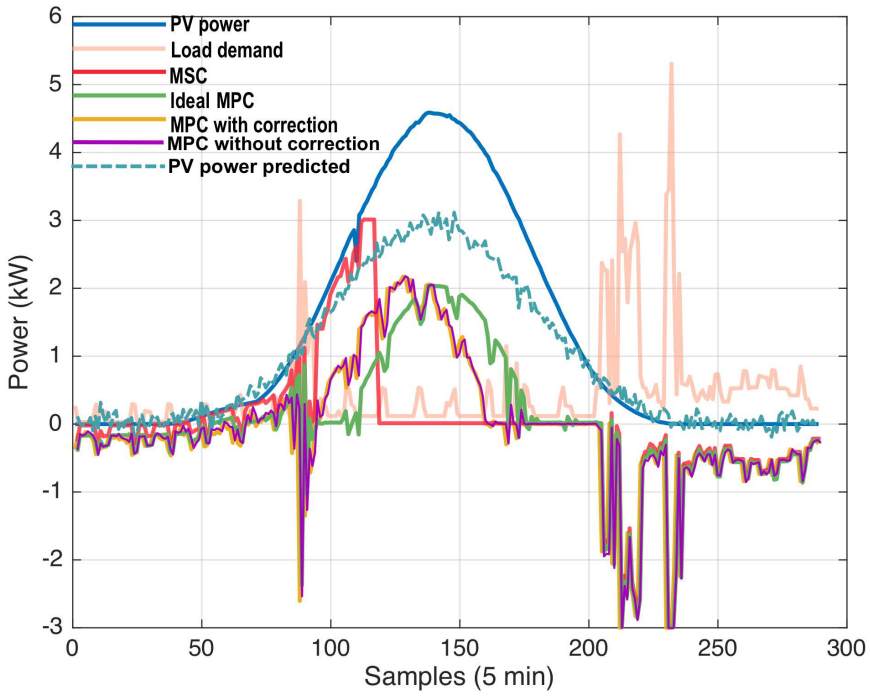

Figure 6.7: Typical daily battery power profiles achieved with the four cases of the energy management strategies mentioned. This shows a case where forecast is less than the actual generation.

smooth, uniform power injection, distributed over a larger time window. However, the performance of the MPC *with* and *without correction* does not completely eliminate the peak power injection. The performance of the two schemes is still better than the MSC scheme. Nevertheless, as shown in Figure 6.7 the error in forecast results in a slightly earlier charging of the BESS in comparison to the *ideal MPC*. This results in some peak PV power being injected into the grid.

The amount of peak power feed-in to grid in the MPC scheme with and without corrections can be more clearly understood using the Figure 6.9. The figure shows a bar plot highlighting the dwell times at various power levels of p_g during the annual scheduling with the 4 cases. It can be seen that with *ideal MPC* the power injection to the grid is always less than 3 kW which is half the rated power of the PV array (Table 6.2). In the case of MPC scheme with and without correction there is power injection to the grid above $3k$W. However, in comparison to the MSC scheme the dwell times at power levels $> 3kW$ is significantly lower for MPC schemes with and without correction. It should also be noted that the MSC scheme has significant peak power

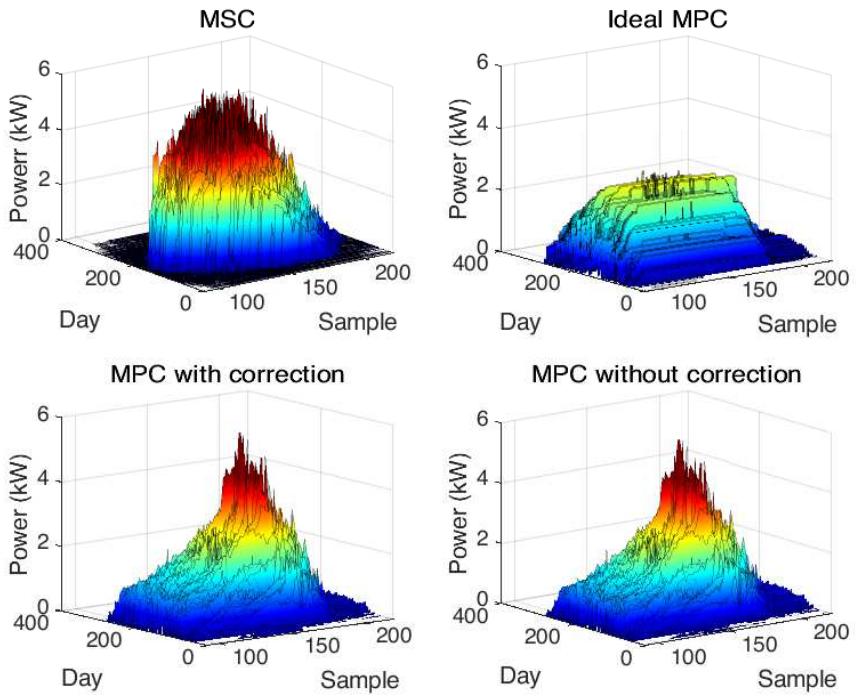

Figure 6.8: Annual daily grid feed-in power with (a) MSC, (b) Ideal MPC, (c) MPC with correction (d) MPC without correction

drawn in from grid ((-6)- (-4) kW) in comparison to all the MPC schemes due to lack of forecast information. This highlights the improvement in the grid feed-in performance in a PV BESS system achieved with MPC due to the knowledge of future generation and load demand.

Finally, the improvement in the grid feed-in performance with the MPC schemes is quantified using the APPR given in Table 6.4. Comparing to a system having PV generation without BESS the *ideal MPC* has reduced the peak power injection by 80% whereas MSC was able to reduce only 49.72%. The MPC scheme *with* and *without correction* has an APPR of 74.28 and 72.96 respectively. Despite having higher power injection to the grid than the ideal MPC scheme the APPR of MPC schemes with and without correction was almost 1.5 times than MSC. This highlights the role of an effective control strategy for grid congestion mitigation in a PV BESS system. It should be noted that the MPC scheme with correction exhibited a a slightly improved grid feed-in performance over the scheme without correction according to the APPR values.

In terms of BESS degradation, the annual capacity fade, C_f, arising from the 4 energy management cases is given in Table 6.4. As expected with the shifting of the

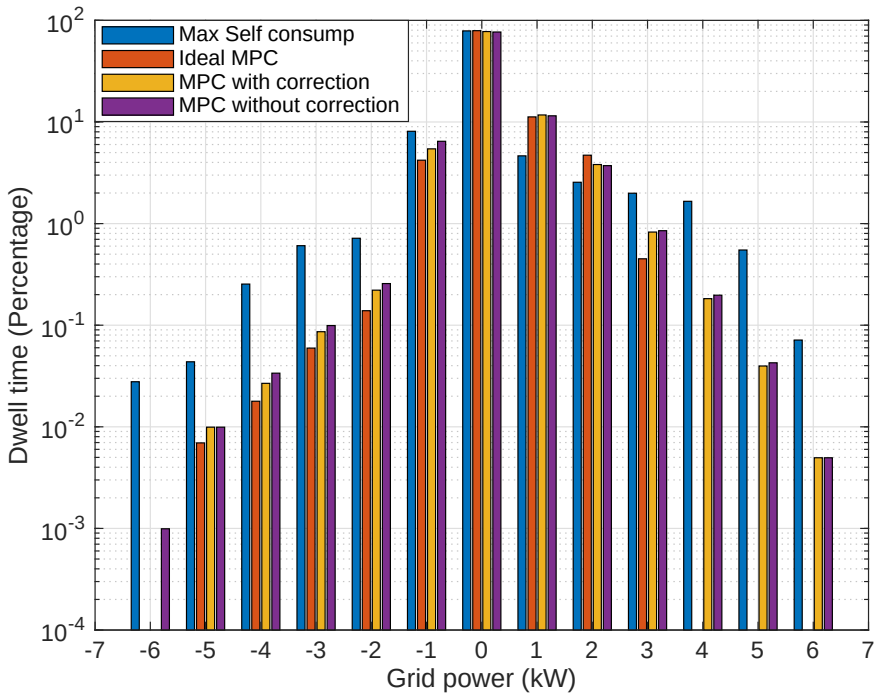

Figure 6.9: Bar-plot comparing the dwell times at different power levels of the p_g in all the 4 energy management schemes.

Method	**ASCR** (%) :	**Annual** C_f (%):	**APPR** (%):
MSC	54.60	3.94	49.72
Ideal MPC	54.32	3.71	80.38
MPC with correction	52.71	3.73	74.28
MPC without correction	52.73	3.65	72.96

Table 6.4: Comparison of performance indices values for different scheduling schemes

BESS charging to peak generation period and subsequent elimination of high SOC dwell times has resulted in a lesser capacity fade with the MPC schemes. The C_f with *ideal MPC* is 3.71 which is almost a 6% reduction in C_f from the MSC (3.94). The MPC scheme *with correction* has a very similar C_f to the *ideal MPC* scheme while the *MPC without correction* exhibited a lower annual capacity fade. The reduction in BESS dwell time at high SOC levels that has led to lower C_f values with MPC scheme can be better visualised through the Figure 6.10. The figure shows the dwell times at various SOC levels by the BESS for the four energy management cases. The increased dwell

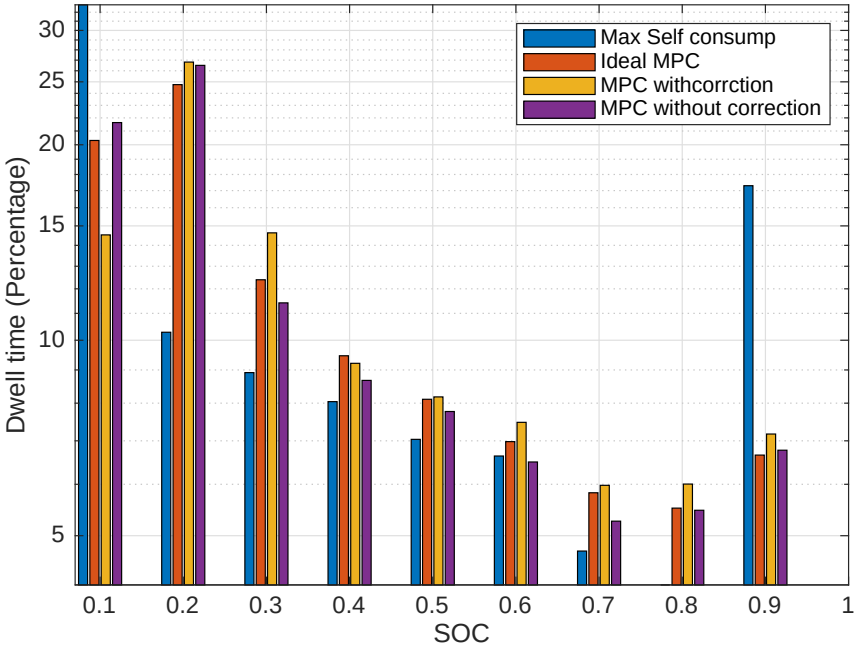

Figure 6.10: Bar plot comparing dwell times at various SOC levels by BESS with the 4 energy management cases.

time at high SOC level(0.9) with MSC scheme is clearly observed here in comparison to MPC schemes. This further justifies the lesser annual capacity fades achieved with MPC schemes.

It should be noted that in the process of eliminating the high SOC dwell times the MPC scheme tend to undergo higher BESS cycling. This can increase the cycling ageing with MPC scheme. Nevertheless, the impact of the reduction of dwell times at higher SOC levels with MPC schemes is still higher and as a result leads to lower overall capacity fade with MPC scheme. The higher cycling of BESS with the MPC schemes can be observed in Figure 6.11. The plots for Figure 6.11 was generated using the BESS SOC profile obtained from the different energy management cases. These profiles where then used in the rainflow counting algorithm [267] to generate the information on BESS cycling. The x-axis of Figure 6.11 indicate half of the cycle magnitude whereas the y-axis indicates the mean SOC value of a cycle. For example, if BESS undergoes a cycling from 10-90% of SOC the x-axis value will be 45 and y-axis will be 45 as well. The tall bars in the plots shown in Figure 6.11, indicates the number full cycles (0.1-0.9) undergone by the BESS. In the case of MPC this ids higher than that of the MSC scheme.

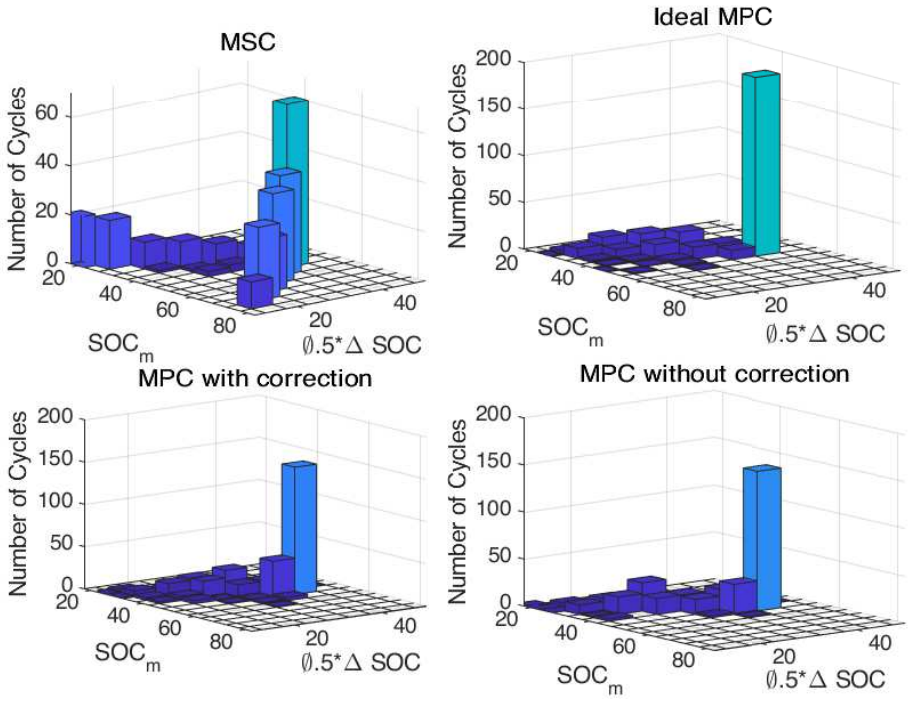

Figure 6.11: BESS cycling undergone with different energy management schemes.

Finally, the economic performance is assessed through the self-consumption given by the annual ASCR in Table 6.4. It can be seen that for the MPC schemes, the ASCR is lower than that of the MSC based energy management. The ASCR value for $idealMPC$ at 54.32% is 99.5% of MSC scheme's ASCR. This slight drop arises due to the multi-objective optimisation considered in MPC. The ASCR and C_f exhibits complementary behaviour resulting in deterioration of one performance with the improvement in another. This can better demonstrated through Figure 6.12 showing the variation of ASCR and C_f, in *ideal MPC*, with different weighting set $(\lambda_1, \lambda_2, \lambda_3, \lambda_4)$ values. The values of the weighting coefficients where chosen such that ASCR exhibits a variation from low to higher values as shown in Figure 6.12. It can be seen that when the ASCR is high, C_f tends to be higher indicating an increase in degradation of BESS and vice versa. The ASCR and C_f values for the weighting set, $\lambda_1, \lambda_2, \lambda_3, \lambda_4$, given in Table 6.3 is highlighted in Figure 6.12 as the red point. It represents an optimal trade-off between ASCR and C_f as seen from results. This also explains the rationale behind the selection of the $\lambda_1, \lambda_2, \lambda_3, \lambda_4$ values shown in Table 6.3 for the optimisation problem in MPC.

The self consumption in the case of MPC *with* and *without correction*, however, is further lesser than ideal MPC. The SCR values of 52.71% and 52.73% for MPC scheme

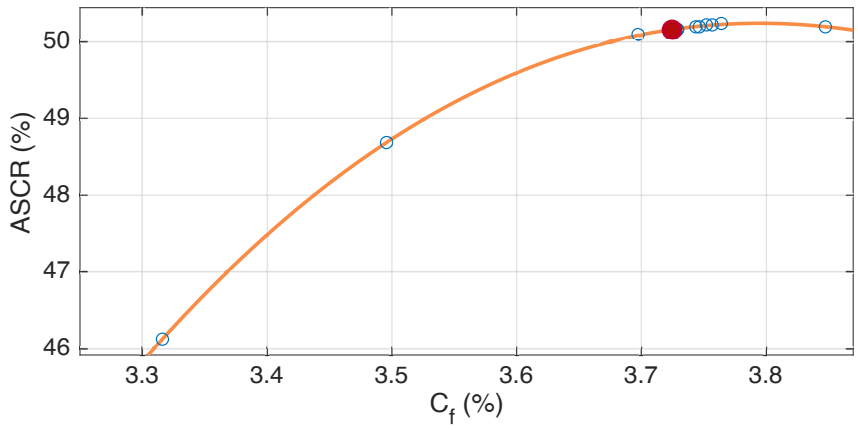

Figure 6.12: Variation of annual self-consumption rate with C_f for different weighting sets of $(\lambda_1, \lambda_2, \lambda_3, \lambda_4)$ in ideal MPC. The highlighted point (red) corresponds to the value shown in Table 6.3.

with and *without correction* is almost 96.5% of that of the MSC scheme. This is a drawback of the forecast based scheduling strategies wherein, the error in forecast affects the system's economic performance. The error in forecast leads to the MPC scheme sending more energy to grid than being used at the consumer premises. Nevertheless, it should be noted that the reduction in SCR due to forecast error is not significantly high and is only 3.5%. This was achieved even when the PV forecast was done without using any weather data, which contributes to the higher forecast error as shown in Section5.4.5. The availability of weather data will only improve the prediction accuracy and as such will bring the SCR value closer to the *ideal MPC* scheme. It should also be noted that despite a 3.5 % reduction in SCR value, the MPC schemes *with* and *without correction* exhibited a significantly better performance in grid feed-in reduction and BESS degradation compared to MSC scheme.

The average computational time by the MPC schemes at any sampling instant was $0.17s$. This was significantly lower than the sampling time of 5 minutes thus highlighting their suitability for online implementation.

Comments on MPC scheme with and without correction

In the analysis presented in the previous section the performance of the MPC scheme with and without correction resulted in very similar behaviour. This is due to the conscious efforts to ensure that the decision making was not conservative when corrections

are introduced for the forecast error. Nevertheless, some impact of the correction to prediction error was observable. Consider the SCR performance of the two schemes. The SCR for MPC *with* and *without correction* was 52.71 and 52.73 respectively. Despite the lower value of SCR the C_f for MPC scheme with correction was very similar to the ideal MPC at 3.73. As the energy handled by the BESS (due to lower SCR) is lesser the C_f was expected to be lower. This anomaly occurred because MPC, in order to account for prediction errors always tend to store more energy in BESS than necessary when corrective measures were employed. This can also be seen in Figure 6.10 where the dwell time at different SOC levels was higher for MPC scheme *with correction* in comparison to MPC scheme *without correction*. This was responsible for the higher capacity fade in MPC scheme *with correction*.

This highlights the impact of introducing corrective measures for forecast errors. In this work since the mean aggregate absolute error for the prediction window was used to define the $d_{i|k}$ a less conservative decision making was achieved while accounting for forecast error. This was highlighted by the similar performance of MPC scheme *with* and *without correction*. However, if a more conservative decision making was made by considering a larger bound on prediction errors the performance of MPC in terms of SCR or C_f can further deteriorate which can lead to difficulty in justifying use of MPC in PV BESS system.

6.2.4 Concluding remarks on MPC scheduling in PV BESS system

The MPC based energy scheduling developed for the PV BESS system presented an improved performance in multiple objectives like grid feed-in and capacity fade minimisation of BESS. This was achieved as MPC, due to additional information available from forecast, caused shifting of BESS charging to peak generation period thus reducing the dwell times at charged levels and power injection to grid. However, this was achieved at the cost of economic performance in terms of self consumption in PV BESS system. The MPC schemes were not able to achieve the same SCR as that of the MSC scheme. Nevertheless, even with error in forecast the maximum drop in self consumption was only 3.5% in one year while there was significant improvement in APPR and C_f. This was expected as the MPC is a method that utilises forecast in its decision making and the error in forecast will affect its performance. The most important aspect to be ensured is that the deterioration in performance is not high enough that the utilisation of MPC

cannot be justified. In this context, the work carried in this thesis is able to justify the use of MPC in PV BESS system due to the improvement in multiple objective that it provides.

It should also be considered that the performance of the MPC achieved here is by using PV forecast made without using any weather data. The availability of weather data can significantly improve the ability of forecasting unit to provide better predictions of PV generation. As the uncertainty in forecast affected the ability of self consumption the most, this economic performance of MPC can be improved with better prediction of PV generation.

6.3 MPC for energy scheduling in islanded grids with hybrid ESS

This section discusses the application of MPC for energy management in a microgrid during the scenario of islanded operation. Islanded microgrids require both high energy and power density ESS to sustain the islanded operation. As a result, in this case, the hybrid ESS system described in Chapter 2 comprising of very high energy density ESS in FC-electrolyser system, batteries and high power density ESS in SC is considered. As discussed in Section 2.1 the use of two higher energy density ESS in FC and BESS system is essential in islanded operation. The FC system, despite the poor efficiency has very low storage costs due to energy being stored in an external fuel [37]. The BESS on other hand has high storage cost as the energy is stored internally. In order to store all the imbalance power arising in islanded operation using a BESS alone will require a battery with high storage capacity. This will drive up the cost of storage systems. In order to avoid this, as a trade-off between operational efficiency and cost of storage, both the FC and BESS is used in the islanded microgrid [1,37]. This utilisation of tri-hybrid storage system helps to outline the the energy management strategy when using ESS of different types. The islanded operation presents a relevant scenario in future electric networks as discussed in Chapter 1 and as a result the energy management in islanded operation presents practical significance.

The main challenge in islanded operation is the lack of an infinite reservoir in the form of main grid which can absorb the power imbalance that arises with greater resilience. In islanded operation the microgrids tend to operate with low inertia and the

power imbalance that occurs should be avoided with RES power curtailment or using dispatchable generation . Therefore, the MPC at the energy management level should be capable of making the decision regarding the amount of power to be curtailed and energy to be used from dispatchable generator. The MPC can facilitate a better management of hybrid ESS so as to ensure that this curtailment of RES generation is minimised and in-turn the the dependency on dispatchable sources. The information of future generation and load demand enables the MPC to achieve the same which will be highlighted in the upcoming sections. Apart from increasing the utilisation of RES generation MPC can be used, as highlighted in the PV BESS system, to minimise the degradation in the ESS. Finally, the last aspect which the MPC will try to address through the energy management in islanded microgrid will be to ensuring a high operational efficiency of the system.

In order to highlight the improvement that can be achieved with MPC based energy management, a comparative analysis with an energy management system using fuzzy inference for decision making will be carried out. This analysis also tries to highlight the advantage of online MPC based scheduling over heuristic schemes. Therefore, the main objective of this section can be summarised as follows: Develop an energy management scheme with MPC for an islanded microgrid with tri-hybrid ESS that ensure

- Uninterrupted autonomous operation of islanded microgrid
- Maximisation of RES generation utilisation, minimisation of ESS degradation and maximisation of microgrid operational efficiency
- Decision making for power curtailment and dispatchable generator utilisation
- Improved operation over a heuristic fuzzy inference based energy management scheme.

The energy management of hybrid ESS developed here can be easily extended to the grid connected scenario of the microgrid as well. As discussed before the MPC only ensures the energy management and the stability will be maintained by the fast acting, real time primary+secondary stage. In islanded operation considering the weaker inertia of system this is very essential. As such an analysis of MPC with correction to forecast error will not be carried out as in the previous section. Instead a discussion on ideal MPC performance and MPC scheme without correction will only be presented.

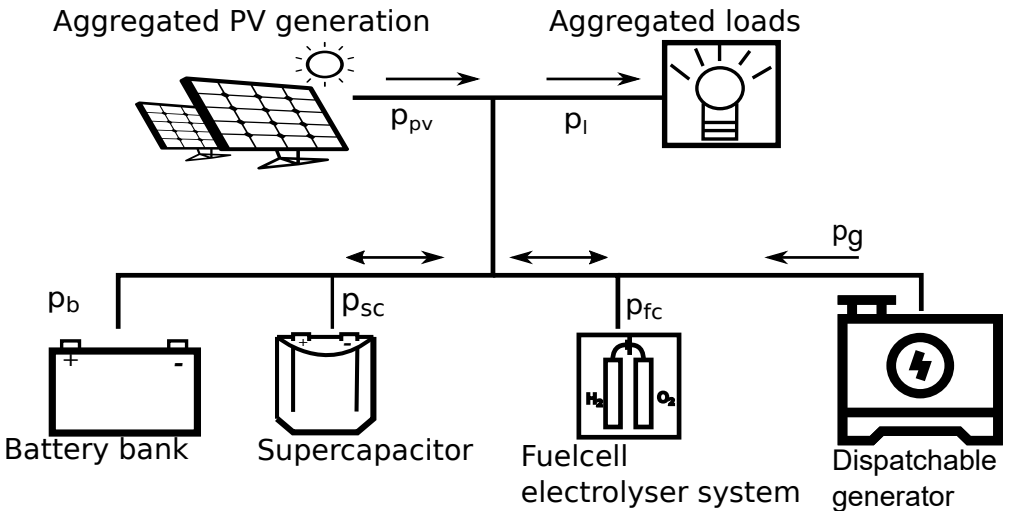

Figure 6.13: Schematic of the generic microgrid of Figure 2.1 in islanded mode.

6.3.1 System description

The system under consideration for energy management will be the generic microgrid scheme presented in Figure 2.1 but for the islanded microgrid operation. This requires that dispatchable generators be also considered to ensure the stable operation of the system. Considering the same, the generic microgrid scheme is reproduced in Figure 6.13 to represent the grid composition in the islanded scenario. The schematic represents an aggregated system. The setpoints from MPC will be augmented with the set points generated at the primary+secondary stage. The decision making by MPC for the aggregated representation is also suited in the case where the ESS capacity is distributed, like multiple batteries or FC. The primary+secondary stage has the power splitting strategy implemented for ESS of same type and aggregated set point from the MPC level will be split at the primary+secondary stage. This reduces the number of decision variable for the MPC optimisation problem thus reducing the computation burden. The PV generation and load demand of the microgrid will be emulated using the same data from Lindenberg, Germany.

Dispatchable generators

The dispatchable generating sources were considered in the islanded microgrid to provide power balance at times when both the RES and ESS cannot cater the load demand. This facilitates energy security in the islanded grid. In order to ensure the same, load following

reserves capable of fast responses and very little start up time like, diesel or gas engine power plants were considered as generating units [268]. The very little starting time of these generators ensure that they can be brought into operation quickly with minimum delay and also have no restrictions in being turned off quickly. These type of generating sources can also deliver to sudden changes in set points and do not have limitations in terms of ramp rate of power output. As such, in the optimisation problem of MPC, extensive models of these sources are not included. They are considered as a decision variable with limits on power output. The power imbalances created by the small delay in deployment will be compensated by the SC unit under the control action generated by the primary+secondary stage.

ESS for islanded microgrid

The ESS in the hybrid system are modelled in a similar way as that of the PV BESS case. The state evolution in the ESS is given by

$$x_\alpha(k+1) = \begin{cases} x_\alpha(k) - \frac{T_s \cdot \eta_\alpha}{C_\alpha} \cdot p_\alpha(k) & \text{if } p_\alpha \leq 0 \\ x_\alpha(k) - \frac{T_s}{\eta_\alpha \cdot C_\alpha} \cdot p_\alpha(k) & \text{if } p_\alpha > 0 \end{cases} \tag{6.29}$$

$\forall x = \{SOC, LOH\}, \forall \alpha = \{bat, SC, FC\}$, T_s is the sampling time, $p_\alpha(i)$ is the power set point and c_α is the capacity of respective ESS. In the hybrid ESS the FC electrolyser system has poor round cycle efficiency ($< 60\%$) and as such the linear approximation employed for the storage system model, in the PV BESS case, cannot be employed. In this case it has also been decided to retain the hybrid model for the BESS and SC system despite them having high round cycle efficiency. Retaining the hybrid model will require that the optimisation problem in the MPC to be formulated as a mixed integer quadratic programming (MIQP) problem. Mixed integer problems tend to be computationally more demanding than the QP problem. Therefore, retaining the hybrid formulation for all ESS enable a more worse case scenario analysis of MPC in terms of computational complexity and provide a more accurate representation of ESS behaviour.

PV system

As is the case with the PV BESS system, the PV array in this case is also considered to be operating at the maximum power output for the irradiation level, using the MPPT

algorithm. However, in islanded mode the ability to curtail the PV power generation in case the ESS and load cannot cater it should be ensured, for energy security. This curtailment can be implemented using the modified MPPT strategy with constant power generation (CPG) [269] capability. In this method, the PV array generates maximum power (p_{pvm}) in normal condition. However, if the PV power generated cannot be met by the load or ESS the array output is curtailed to a constant power value based on grid conditions. The PV array output (p_{pv}) in the MPPT with CPG scheme is given by

$$p_{\text{pv}} = \begin{cases} p_{\text{pvm}} & \text{No curtailement} \\ p_{\text{pvm}} - p_{\text{curr}} & \text{Under power curtailemt} \end{cases} \tag{6.30}$$

where p_{curr} is the PV power to be curtailed. The value for p_{curr} will be decided by the tertiary level. A detailed discussion on the MPPT or MPPT with CPG are not provided in this work as they represent a domain, already, widely researched and beyond the scope of this work. Interested readers are directed to [269] and references therein.

Grid

The grid is modelled as a static system using the power balance equation given by

$$p_{\text{sc}}(k) + p_{\text{b}}(k) + p_{\text{fc}}(k) + p_{\text{pvm}}(k) + p_{\text{gen}}(k) - p_{\text{l}}(k) - p_{\text{curr}}(k) = 0 \tag{6.31}$$

where $p_{\text{b}}, p_{\text{sc}}, p_{\text{fc}}$ are the power set points for the BESS, SC and FC systems while $p_{\text{l}}, p_{\text{gen}}$ are load demand and power from the dispatchable generation unit respectively.

6.3.2 Optimisation problem in MPC for islanded microgrid system

Cost function

The MPC for energy management in islanded microgrid is tasked with maximising operating efficiency, renewable energy utilisation and minimising ESS degradation. In this context the multi objective cost function considered in MPC is chosen as

$$J = \sum_{k=i}^{i+N} [J_{\text{b}}(k) + J_{\text{fc}}(k) + J_{\text{sc}}(k) + J_{\text{bal}}(k)] \tag{6.32}$$

where $J_{\mathrm{b}}, J_{\mathrm{fc}}, J_{\mathrm{sc}}$ are the cost terms pertaining to BESS, FC-electrolyser system, SC while J_{bal} pertains to cost of using dispatchable generation and imposing power curtailment in the microgrid.

The battery cost term J_{b} is chosen as

$$J_{\mathrm{b}}(k) = \lambda_{\mathrm{soc}} \cdot SOC_{\mathrm{b}}(k)^2 + \lambda_{\mathrm{dbat}} \cdot \Delta SOC_{\mathrm{b}}(k)^2 \tag{6.33}$$

where $\lambda_{\mathrm{soc}}, \lambda_{\mathrm{dbat}}$ are weighting factors for each term in J_{b}. The cost function for the BESS is the same as that for the PV BESS system with the objective of minimising battery degradation. It should also be noted that J_{b} does not explicitly penalise the battery power, p_{b}. As there is no explicit penalisation, the surplus power from PV system will be readily stored in the BESS for later use. This facilitates increased utilisation of PV power. The lack of penalisation also ensure that the BESS is used first whenever imbalance power is available, just like in the primary+secondary stage to ensure higher operational efficiency of microgrid. This establishes a correlation in the decision making between the power and energy management stages.

The fuel cell cost term J_{fc} is given by

$$J_{\mathrm{fc}}(k) = \lambda_{\mathrm{fc}} \cdot \frac{p_{\mathrm{fc}}(k)}{p_{\mathrm{fc}}^{max}}^2 + \lambda_{\mathrm{rate}} \cdot (p_{\mathrm{fc}}(k+1) - p_{\mathrm{fc}}(k))^2 \tag{6.34}$$

where $\lambda_{\mathrm{fc}}, \lambda_{\mathrm{rate}}$ are the weighting factors and p_{fc}^{max} is the maximum power that can be delivered by FC system. The FC-electrolyser system is characterised by poor round cycle efficiency and in order to maintain high operational efficiency of microgrid, the FC system should be utilised only if the BESS cannot cater the imbalance power. This is achieved by penalising the FC power as shown in (6.34). This ensures that the FC utilisation happens only after the battery is either fully charged or discharged thereby increasing the operating efficiency. The second term in (6.34) penalises the set point change in FC system. This helps in limiting the degradation in FC system due to fuel starvation induced by sudden set point change. The availability of forecast again provides the MPC with the knowledge of future generation and load which allows it to modify the FC profile such that these sudden changes in set points can be minimised.

In the case of SC, the objective of the energy management stage is to ensure that sufficient reserves is maintained in the SC at all instances. This allows the SC to meet the sudden imbalances arising in the grid and maintain system stability by emulating

inertial response. To this extent the J_{sc} penalises the deviation of SOC_{sc} from a nominal value (SOC_{nom}) . The J_{sc} is chosen as

$$J_{sc}(k) = \lambda_{\text{sc}}(SOC_{\text{sc}}(k) - SOC_{\text{nom}})^2 \tag{6.35}$$

where λ_{sc} is the weighting factor. The SOC_{nom} is chosen as 0.5 so that there is always half the SC capacity available to cater the imbalance. This mode of energy management in SC is similar to the charge restoration function in the primary+secondary stage. This further enforces that the SC has sufficient reserves at all instances, necessary for ensuring the model invariance and equivalence of inner loop dynamics to SC current loop dynamics.

As discussed in Section 6.3.1, the energy scheduling stage determines the optimal value of p_{curr}. The higher curtailment of PV power leads to reduced operation of the PV array in the MPPT mode, thus reducing the PV power utilisation. Therefore, the objective of the MPC will be to minimise the p_{curr} as much as possible for increasing PV power utilisation. The same is applied to p_{gen}. The higher value of p_{gen}, the more the load demand is catered by the dispatchable generator unit and lesser the utilisation of PV power. Nevertheless, these two variable are also essential to ensure the reliable grid operation according to (6.31). Minimising the value of $p_{\text{curr}}, p_{\text{gen}}$ can be achieved using the cost function

$$J_{\text{bal}}(k) = \lambda_{\text{gen}} \cdot \frac{p_{\text{gen}}(k)}{p_{\text{gen}}^{max}}^2 + \lambda_{\text{curr}} \cdot \frac{p_{\text{curr}}(k)}{p_{\text{pv}}^{max}}^2 \tag{6.36}$$

where $\lambda_{\text{curr}}, \lambda_{\text{gen}}$ are the weighting factors, p_{gen}^{max} is the maximum power rating of the generator and p_{pv}^{max} is the maximum power rating of the PV array. In order to ensure maximum utilisation of renewable generation the weighting factors $\lambda_{\text{curr}}, \lambda_{\text{gen}}$ are chosen to be greater than that of BESS and FC cost function.

The use of forecast in the decision making of MPC allows better utilisation of PV power with minimal curtailment and reliance on dispatchable generation. The forecast information enables the MPC to manipulate the ESS profile such that their capacity will be available as much as possible to cater the PV power.

Constraints

Physical constraints: The physical limits of ESS are imposed by soft constraints

$$x_\alpha^{lo} - \epsilon_\alpha \leq x_\alpha(k) \leq x_\alpha^{up} + \epsilon_\alpha|_{\alpha=\{bat,sc,FC\}} \tag{6.37}$$

to ensure feasibility of optimisation problem, similar to PV BESS system. The x_α^{lo}, x_α^{up} are the upper, lower bounds of ESS storage capacity and $\epsilon_\alpha \in \mathbb{R}^3$ is the slack variable. In order to minimise constraint violation an additional term is added to (6.32) given by

$$J_{\text{slack}} = \rho^T \cdot \epsilon_\alpha \tag{6.38}$$

where $\rho \in \mathbb{R}^3$ represents the penalising factor for the slack variables.

Electrical constraints: Constraints on the power handling capability of interfacing power converters and dispatchable generator are introduced through

$$\begin{aligned} p_\alpha^{min} \leq p_\alpha(k) \leq p_\alpha^{max}|_{\alpha=\{bat,sc,fc\}} \\ 0 \leq p_{\text{gen}}(k) \leq p_{\text{gen}}^{max} \end{aligned} \tag{6.39}$$

where p_α^{min}, p_α^{max} are the minimum, maximum power ratings of interfacing converters respectively. These are maintained as hard constraints as violation of the same can result in irreversible damage to power electronic and generator systems.

MLD constraints: The hybrid ESS model of (6.29) cannot be directly utilised in the optimisation problem. They need to be transformed into a mixed logical dynamic (MLD) model, that provides a linear equality representation of (6.29). The guidelines in [270] is used in this transformation to MLD. In (6.29) the value of p_α defines the ESS behaviour. A boolean variable δ_α is now introduced to define the nature of p_α such that when $[\delta_\alpha(k) = 1] \leftrightarrow [p_\alpha(k) \geq 0]$. This MLD representation of this condition is given by

$$\begin{aligned} -p_\alpha^{min} \cdot \delta_\alpha(k) \leq p_\alpha(k) - p_\alpha^{min} \\ -p_\alpha^{max} \cdot \delta_\alpha(k) \leq -p_\alpha(k). \end{aligned} \tag{6.40}$$

This introduction of boolean variable allows (6.29) to be represented as

$$x_\alpha(k+1) = x_\alpha(k) + \frac{T_s}{c_\alpha} \cdot \delta_\alpha(ik) \cdot p_\alpha(k) \cdot (\eta_\alpha - \frac{1}{\eta_\alpha}) - \frac{T_s \cdot \eta_\alpha}{c_\alpha} \cdot p_\alpha(k). \tag{6.41}$$

The multiplicative term above is eliminated using an auxiliary variable $z_\alpha(k) = \delta_\alpha(k) \cdot p_\alpha(k)$ to maintain a linear formulation of (6.41). This is enforced using

$$\begin{aligned} &z_\alpha(k) \leq p_\alpha^{max} \cdot \delta_\alpha(k) \\ &z_\alpha(k) \geq p_\alpha^{min} \cdot \delta_\alpha(k) \\ &z_\alpha(k) \leq p_\alpha(k) + p_\alpha^{max} \cdot (1 - \delta_\alpha(k)) \\ &z_\alpha(k) \geq p_\alpha(k) + p_\alpha^{min} \cdot (1 - \delta_\alpha(k)) \end{aligned} \tag{6.42}$$

resulting in (6.29) represented as

$$x_\alpha(k+1) = x_\alpha(k) + \frac{T_s}{c_\alpha} \cdot z_\alpha(k) \cdot (\eta_\alpha - \frac{1}{\eta_\alpha}) - \frac{T_s \cdot \eta}{c_\alpha} \cdot p_\alpha(k) \tag{6.43}$$

The use of MLD constraints in an optimisation problem with quadratic cost results in a Mixed integer quadratic programming (MIQP) problem. Solvers like Gurobi [266] has algorithms like branch and bound (BB) methods [271] to solve problems. Representing the manipulated inputs ($\left[p_\alpha, p_{\text{gen}}, p_{\text{curr}}, \epsilon_\alpha\right]$) to the microgrid as u, the cost function as $J(u, x_\alpha) = \sum_{k=i}^{i+N} [J_{\text{b}}(k) + J_{\text{fc}}(k) + J_{\text{sc}}(k) + J_{\text{bal}}(k) + J_{slack}]$ the optimisation problem considered in MPC is summarised as

$$\min_u \left[J(u, x_\alpha) \right] \tag{6.44}$$

subject to

$$\begin{aligned} &x_\alpha(k+1) = x_\alpha(k) + \frac{T_s}{c_\alpha} \cdot \delta_\alpha(ik) \cdot p_\alpha(k) \cdot (\eta_\alpha - \frac{1}{\eta_\alpha}) - \frac{T_s \cdot \eta_\alpha}{c_\alpha} \cdot p_\alpha(k) \\ &p_{\text{sc}}(k) + p_{\text{b}}(k) + p_{\text{fc}}(k) + p_{\text{pv}}(k) + p_{\text{g}}(k) - p_{\text{l}}(k) - p_{\text{curr}}(k) = 0 \\ &x_\alpha^{lo} - \epsilon_\alpha \leq x_\alpha(k) \leq x_\alpha^{up} + \epsilon_\alpha|_{\alpha=\{bat,sc,FC\}} \\ &0 \leq p_{\text{g}}(k) \leq p_{\text{g}}^{max} \\ &-p_\alpha^{min} \cdot \delta_\alpha(k) \leq p_\alpha(k) - p_\alpha^{min} \,|_{\alpha=\{bat,sc,fc\}} \\ &-p_\alpha^{max} \cdot \delta_\alpha(k) \leq -p_\alpha(k) \,|_{\alpha=\{bat,sc,fc\}} \\ &z_\alpha(k) \leq p_\alpha^{max} \cdot \delta_\alpha(k) \,|_{\alpha=\{bat,sc,fc\}} \\ &z_\alpha(k) \geq p_\alpha^{min} \cdot \delta_\alpha(k) \,|_{\alpha=\{bat,sc,fc\}} \\ &z_\alpha(k) \leq p_\alpha(k) + p_\alpha^{max} \cdot (1 - \delta_\alpha(k)) \,|_{\alpha=\{bat,sc,fc\}} \\ &z_\alpha(k) \geq p_\alpha(k) + p_\alpha^{min} \cdot (1 - \delta_\alpha(k)) \,|_{\alpha=\{bat,sc,fc\}}. \end{aligned} \tag{6.45}$$

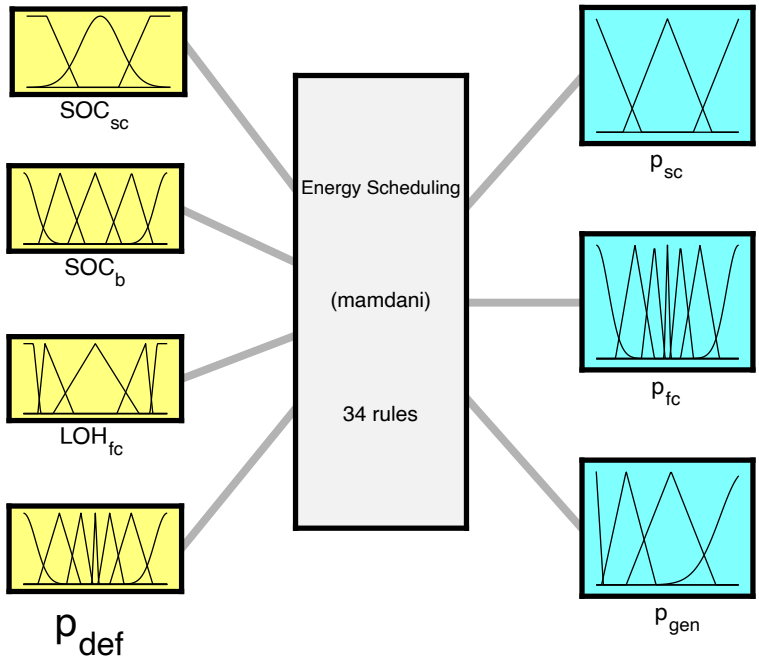

Figure 6.14: Fuzzy inference scheme for the energy management in islanded microgrid system.

6.3.3 The Fuzzy inference based energy management scheme for islanded microgrids

In order to highlight the improvement in energy management performance of the MPC, it will be compared with the energy scheduling performance achieved with Fuzzy inference based scheduler. Fuzzy inference is a method of mapping input variables to output decision variables using a defined procedure that is heuristic in nature. In fuzzy inferencing the space of each input is divided into fuzzy sets [272]. Each fuzzy set will be associated with a membership function which can take a value between 0 to 1 and defines the degree of membership of an input variable to each set. In the first step of the inferencing process fuzzification of the inputs are carried out. This is the process of identifying the degree of membership of each input, based on its value, to a fuzzy set using the membership function. The next step involves fuzzy implication where fuzzy rules are used to map the fuzzified inputs to an output. Simple *if-then* rules which are defined based on the designers prior knowledge of the system are considered for the

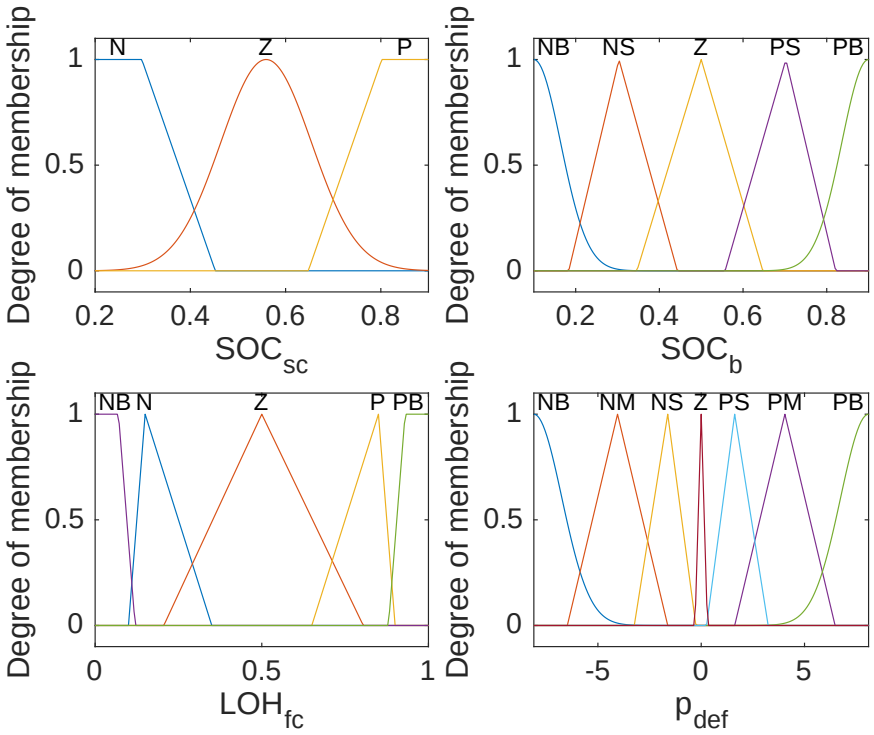

Figure 6.15: Fuzzy sets for the input variables and their membership functions.

same. The *if* part of the rule is the antecedent which are combined through *AND/ OR* logical operators for the different inputs. The consequent is the *then* part of the rule which defines to which fuzzy set of the output variable the antecedent is mapped. The implication process also defines the degree of membership of the output variable to an output fuzzy set. The final step is aggregation and defuzzification. At any instant for a given input value, multiple rules can be active resulting in multiple outputs with varying degree of membership to output fuzzy sets. In the aggregation process they are aggregated and using defuzzification methods like centroid or bisector or middle of maximum they are converted to a crisp output value. For a detailed exposition on fuzzy systems and inferencing process interested readers are directed to [273, 274]. Through proper selection of fuzzy sets and membership functions fuzzy inferencing have been proved to provide a reasonable approximation of an optimal input-output mapping in the decision making problem [275] and hence considered in this work to represent heuristic decision making process. It should be noted that despite the capability of fuzzy inference system to ensure an approximation of the optimal input-output mapping, a prior understanding of system behaviour and resulting rule formulation from the designer is necessary for the same. Defining such optimal rules can be difficult in systems like electrical networks.

The input-output mapping in the Fuzzy inference based energy scheduler for the islanded microgrid is shown in Figure 6.14. The inputs are the ESS states and imbalance power, $p_{\text{def}} = p_{\text{pvm}} - p_{\text{l}}$, in the grid. The outputs are set points for $p_{\text{sc}}, p_{\text{fc}}$ and p_{gen}. Mamdani fuzzy inference [276] is employed here with 34 rules for input-output mapping.

The fuzzy sets for the input, output variables and the associated membership functions are shown in Figure 6.15. The range of fuzzy sets and the membership function shapes were decided using an iterative procedure to obtain the best results. The underlying objective in defining the rules for fuzzy based energy scheduling was to ensure maximum operational efficiency and utilisation of renewable source. In this contex,t the rules were defined such that any imbalance power in the grid will be catered by the BESS first. The FC electrolyser system will cater to the imbalance only after the BESS is fully charged or discharged. In this way the energy management follows the same strategy as in the primary+secondary stage. The SC rules where formulated such that any deviation from its nominal SOC value (0.5) will result in charging or discharging just like in MPC. The Figure 6.16 shows resulting outputs and their dependency on relevant inputs as a surface plot. In comparison to MPC it is difficult to address the degradation issues with fuzzy inference. This requires incorporating future generation and load values to calculate the evolution of SOC_{b} and ΔSOC_{b}. Even if this can be achieved, incorporating them as inputs and defining explicit rules so that battery degradation is minimised based on ΔSOC_{b} or SOC_{b} is complex. The need for explicitly stating the rules is the major drawback with heuristic schemes in comparison to MPC where it is only necessary to implicitly define the desired system behaviour.

In the fuzzy system it can be noticed that p_{b} is not considered as one of the output variables. This has been left as a free variable and the value was decided outside the fuzzy system to ensure the power balance in the grid. It is difficult to incorporate the power balance constraint inside the fuzzy system. The decision process for p_{b} is explained with Figure 6.17. The decisions on p_{curr} and modification of p_{gen}, to ensure power balance, is also made outside the fuzzy system as shown in Figure 6.17.

6.3.4 Sizing of hybrid ESS

Prior to presenting the results, a short discussion to explain the rationale behind sizing ESS in islanded microgrid is provided . As discussed in Chapter 1, the islanded operation in current grid is mostly enforced during exigencies, like faults. Unless in the

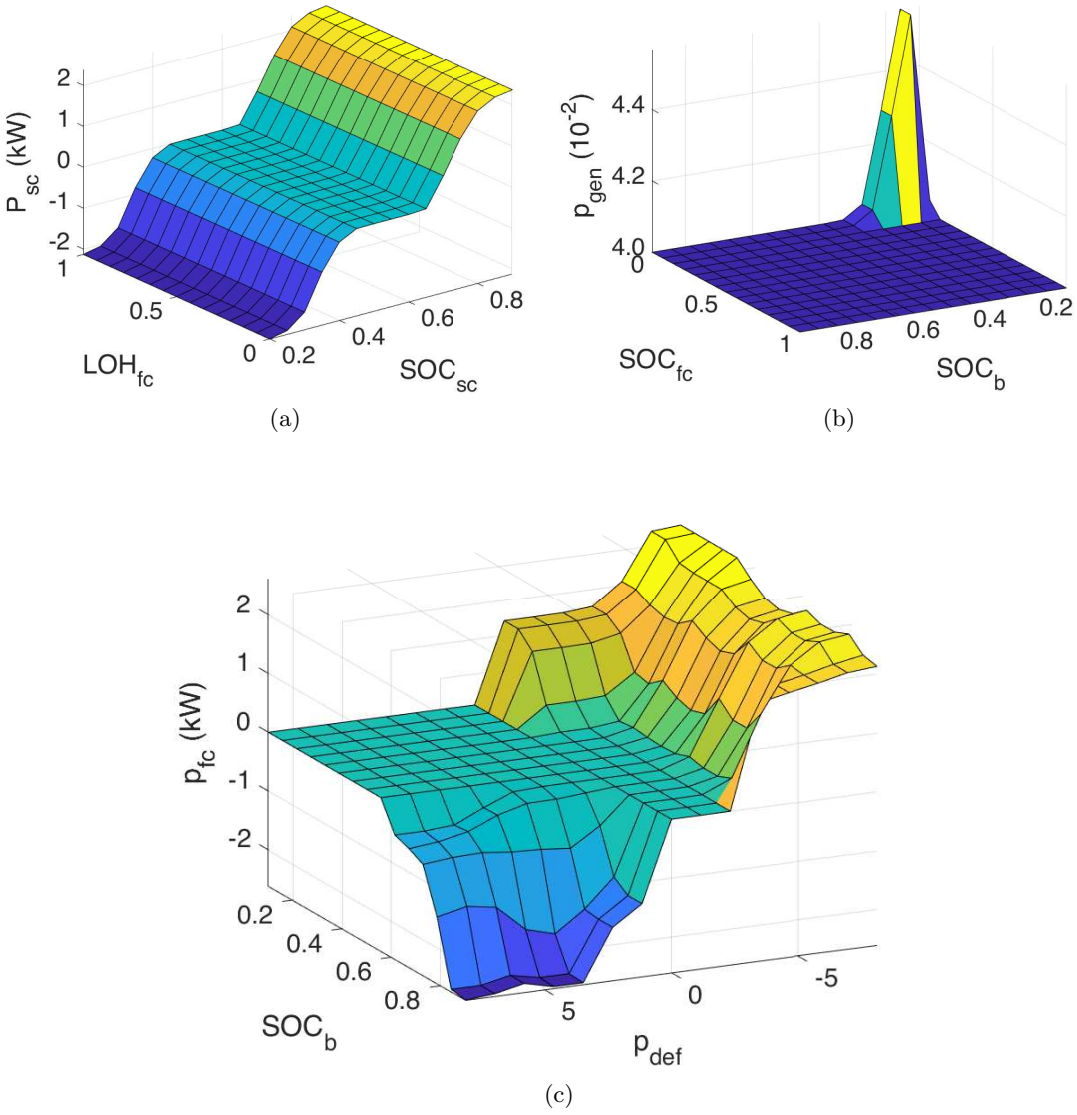

Figure 6.16: The different output surfaces from fuzzy inference scheme showing the correlation between (a) p_{sc} with LOH_{fc} and SOC_{sc}, (b) p_{g} with LOH_{fc} and SOC_{b} and (c) p_{fc} with SOC_{b} and p_{def}, based on the rules defined.

scenario where due to physical constraints the microgrid is operated in islanded mode, the operational time in intentional islanded mode will not be long. The islanded operation can typically extend from days to week [60]. Considering this, the energy scheduling in the islanded mode will be carried out for one week in this work, unlike the year long scheduling carried out in PV BESS system. The ESS will also be sized accordingly.

The sizing of the BESS will done using the same criteria as that presented in PV BESS case to ensure a trade-off between battery degradation and economic cost of BESS

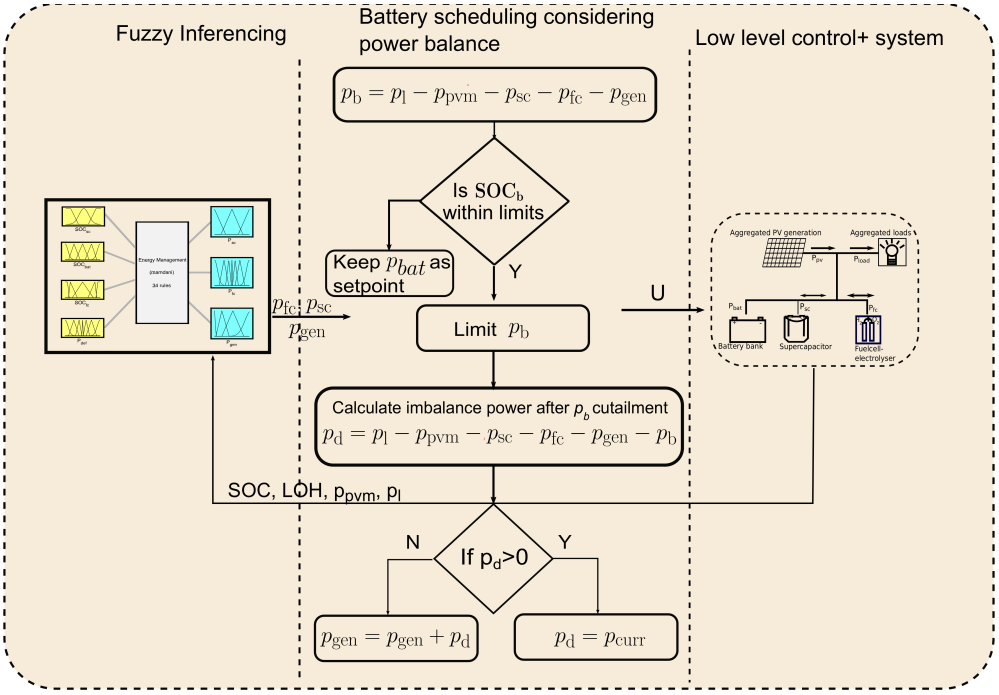

Figure 6.17: Flow chart of decision making process with fuzzy inference based energy management for the islanded microgrid.

storage. The regenerative FC's hydrogen storage capacity was chosen such that it can cater to at least one week operation. This ensures energy sufficiency for a week under islanded operation. The SC capacity was chosen such that it can take in the peak power of the PV array for the sampling period considered. It should be noted that this selection of ESS capacity is not claimed as the optimal. It just provides a starting point to test the energy management scheme. The optimal sizing of the ESS, as discussed before, is an entire research problem on its own, which demands a comprehensive economic and lifetime analysis of storage systems. This analysis is beyond the scope of this work.

6.3.5 Results for energy management in islanded microgrid

The capacity of hybrid ESS, dispatchable generating unit, the parameters and the penalisation weights values used in the MPC are listed in Table 6.5. The optimisation problems in MPC were solved using Gurobi (version 8) [266] with YALMIP as the parser in the MATLAB environment. The fuzzy inference scheme was realised using the Fuzzy Logic Designer tool box from Matlab. All the algorithms were run in a machine having Intel i7 2 core, 2.5 GHz processor and 8 GB RAM. The capacity of the ESS was chosen based on the data from Lindenberg.

Parameter	**Value**
PV array rated output	6kWh
c_{sc}	0.5 kWh
c_b	9.375 kwh
c_{fc}	32 kWh
Prediction horizon length, N	24 hours
Sampling time (T_s)	5 min
p_b^{min}, p_{bat}^{max}	3 kW
$p_{sc}^{min}, p_{sc}^{max}$	32 kW
$p_{fc}^{max}, p_{fc}^{min}$	3kW
p_{gen}^{max}	5kW
$SOC_b^l, SOC_{sc}^l, LOH_{fc}^l$	0.1
$SOC_b^u, SOC_{sc}^u, LOH_{fc}^u$	0.9
SOC_{nom}	0.5
$\lambda_{SOC}, \lambda_{\text{dbat}}$	1, 10
$\lambda_{fc}, \lambda_{rate}$	10,10
$\lambda_{gen}, \lambda_{curr}$	25,25
λ_{sc}	10
ρ	100

Table 6.5: Islanded Microgrid and MPC parameter values used in the energy scheduling

The weighting factors in the optimisation problem of the MPC was chosen through multiple trials, such that the utilisation of p_{pv} is maximised. In this context, it was always ensured that $\lambda_{\text{gen}}, \lambda_{\text{curr}}$ was kept higher that the penalising weights of ESS. Another important criteria in the weight selection was to keep λ_{soc} of the BESS low. A high value for the same will result in battery SOC being kept at a low value during the operation which will inadvertently lead to underutilisation of the BESS and increased utilisation of FC system.

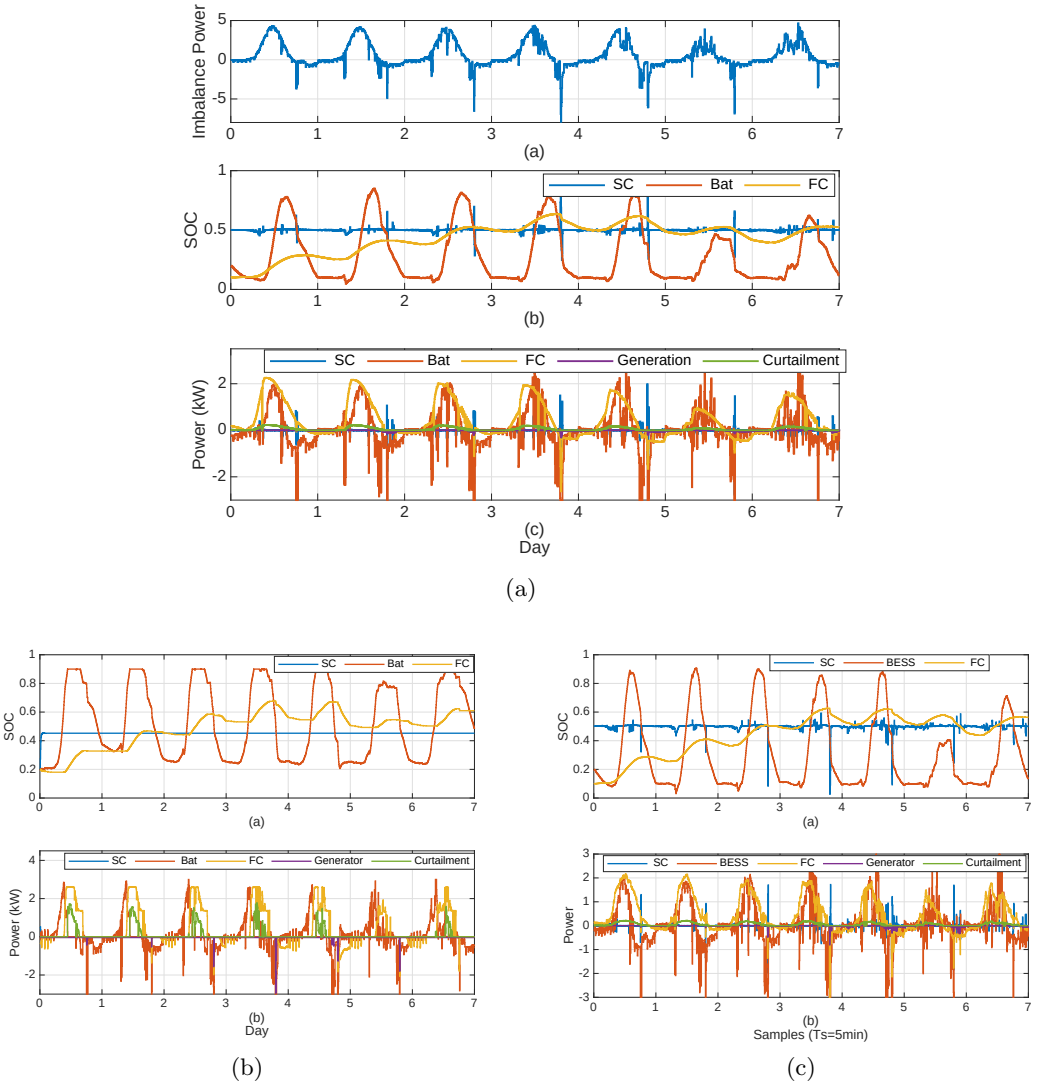

Figure 6.18: One week energy management performance in the islanded microgrid with (a) Ideal MPC (b) Fuzzy inference scheme (c) MPC without correction.

The simulation of MPC and fuzzy based energy management in the islanded microgrid was carried for one week. The results presented here is for the second week of April. Three energy management cases where simulated and the results will be compared. These cases include the ideal MPC and MPC without correction similar to that considered in the PV BESS case. The third one will be the energy management case with fuzzy inference scheme. The Figure 6.18 shows the one week's energy management performance in the microgrid using the three energy managment cases. The MPC schemes with its knowledge of forecast information is always capable of better decision making.

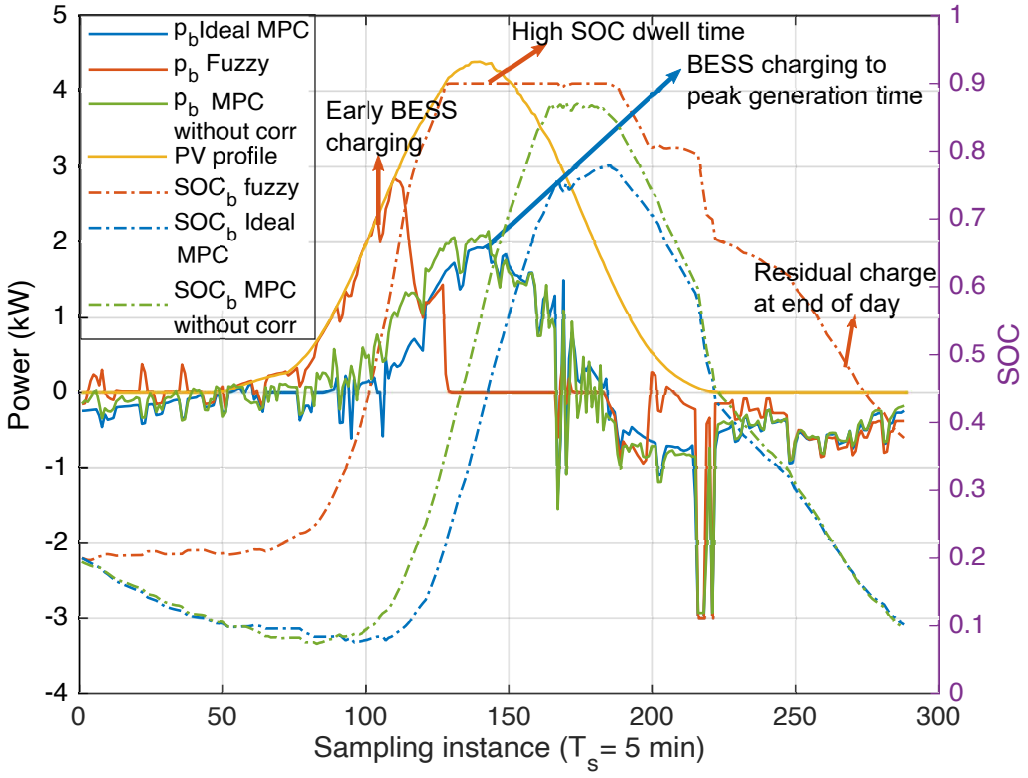

Figure 6.19: Comparison of BESS power and SOC profile with ideal MPC, MPC without correction and fuzzy based energy management in a day.

In order to comprehend the same consider Figure 6.19. The figure shows the BESS power and SOC profiles for a day using three energy management cases. The particular day shown in the figure corresponds to the first day of the week shown in Figure 6.18. The major difference between the MPC schemes and fuzzy based scheduler is in temporal behaviour of the battery charging profile. As discussed before the fuzzy scheduler rules are defined to improve operational efficiency. As there is no information regarding the predicted generation or load, this results in BESS being charged earlier in the day whenever surplus power is available, as shown in Figure 6.19. The charging of the FC electrolyser system will happen only after the BESS is fully charged, as shown in Figure 6.18. This limits the use of FC system and improves operational efficiency. The charging of the BESS, whenever there is surplus power in the grid leads to BESS being fully charged earlier in the day as shown in Figure 6.19. This leads to larger dwell times of BESS at high SOC levels with fuzzy scheme. This increased dwell time at high SOC is detrimental to battery as it leads to calender ageing, as discussed before.

In comparison, the MPC schemes have BESS charging shifted to the period of peak PV generation as shown in Figure 6.19. The availability of forecast and the multi-objective optimisation problem used in MPC forces this shift in BESS charging. The charging of BESS during peak period of PV generation results in the BESS being fully charged later in the day. This reduces the dwell time at high SOC levels in the BESS which can reduce calender ageing. Another important aspect is that since the forecast is available, the MPC knows in advance the load demand for the day and the battery will be charged considering the same. This ensures that later in the day when the battery caters the load demand (under no PV generation), the stored charge is completely utilised and the BESS will have no residual charge, as shown Figure 6.19. The same is not the case with fuzzy scheduler which will always have some residual charge in BESS at the end of the day. This further increases the time BESS spent in a charged state which can affect calender ageing.

Among the MPC schemes, the ideal MPC with perfect forecast ensures that BESS is charged exactly during peak generation period and the amount of energy stored in BESS is equivalent to that demanded by the load later in the day. In contrast, the MPC without correction has to make decisions based on forecast with prediction errors. This results in BESS being charged slightly earlier than the ideal MPC scheme as shown in Figure 6.19. The more significant impact resulting from the prediction error is that the BESS will tend to store more energy than what will be demanded by the load later in the day. This arises from the load forecast being higher than actual values. As a result, it can seen from Figure 6.19 that the SOC of BESS, in the MPC scheme without correction, lies between the ideal MPC and fuzzy scheme. However, it should also be noticed the time spent by the BESS in the highly charged state is lower in the MPC scheme without correction compared to fuzzy scheduler.

The impact of MPC and Fuzzy based energy scheduling, on the BESS, can be better conceived through Figure 6.20. The figure shows the percentage dwell time at various SOC levels by the BESS under the different energy management cases. As expected, the dwell time at high SOC levels (> 0.7) is greater for the fuzzy scheme compared to MPC schemes. Among the MPC schemes, the MPC without correction has longer dwell time at high SOC (0.9) compared to the ideal MPC. As discussed above, the earlier charging and higher energy storage in BESS due to prediction errors is responsible for the same. Nevertheless, even with forecast error the MPC without correction performs better than Fuzzy scheduling in terms of BESS management.

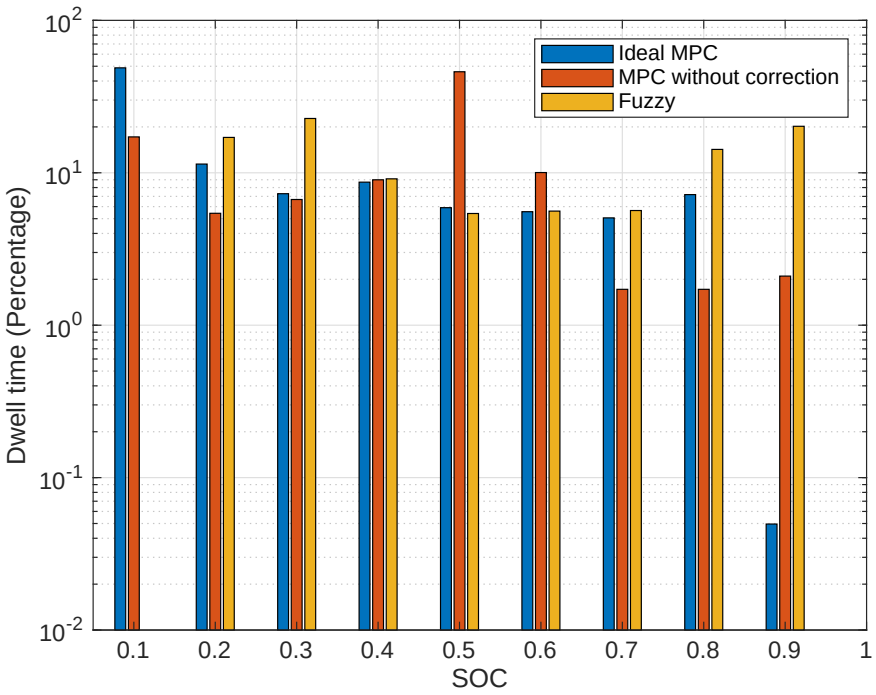

Figure 6.20: Comparison of the dwell times at different SOC levels in the battery for MPC and Fuzzy based scheme.

Scheduling method	**Curtailment**(kWh)	**Generation** (kWh)
Ideal MPC	9.27	1.70
MPC without correction	10.58	3.37
Fuzzy scheduler	19.51	8.28

Table 6.6: Curtailed and generated energy with different scheduling methods.

In the case of FC electrolyser system, MPC scheduling schemes (both ideal and MPC without) ensures a very smooth set point (p_{fc}) variation unlike the Fuzzy scheme as shown in Figure 6.18 The degradation in the FC system is mainly caused by fuel starvation at the electrode membranes caused by sudden changes in the FC set points, as discussed before. Preventing these sudden set point changes can be easily handled with MPC schemes through the cost function formulation as in (6.34). Incorporating the same in the Fuzzy scheduler makes the decision making process complicated as the control system designer will have to state explicitly what the optimal set point change should be in the FC. As a result, incorporating this constraint on the FC set point

change is difficult in fuzzy scheduling. However the issue of sudden set point variation can be effectively addressed in the low-level controllers using rate limiting techniques which can protect the FC by providing a gradual set point variation.

In terms of energy curtailment and utilisation of dispatchable generation, the performance of both MPC schemes and fuzzy based scheduler is given in Table.6.6. The MPC schemes are capable of sustaining the islanded operation with lesser PV power curtailment and dependence on the dispatchable generation, compared to the fuzzy scheme. The ability to reduce PV power curtailment is a direct consequence of the shifting of BESS charging to peak generation period in MPC. As shown in Table.6.3, there is an upper limit on the power that can be handled by the ESS, imposed by the power rating of interfacing converters. The shifting of BESS charging by MPC ensure that during peak PV generation both the capacities of BESS and FC is available to handle the generated power. As a result the power limits of the individual ESS are not reached and there is less need for PV power curtailment. In the fuzzy scheduling, due to BESS being fully charged early in the day the FC capacity is only available during peak generation. Based on the PV array rating shown in Table 6.5 this peak PV power exceeds the power rating of FC converters. Therefore, to ensure power balance the PV power has to be curtailed in fuzzy scheduling. This justifies the higher PV power curtailment values for fuzzy scheme given in Table 6.6. As the power curtailment is more, so does the dependency on dispatchable generator in fuzzy scheme.

Comparing the performance of ideal MPC and MPC without correction, the forecast error has resulted in higher curtailment of PV power in MPC without correction compared to ideal MPC. Nevertheless, the increase in PV power curtailment in MPC scheme without correction is only 14.13% of that of ideal MPC compared to the fuzzy scheme where the increase is almost 110.46%. The small increase in PV power curtailment in the MPC scheme without correction is also due to the fact that in the week pertaining to the results Figure 6.18, the forecast of PV and load demand had only small errors.

Finally, in terms of operational efficiency both the MPC schemes and the fuzzy scheduling demonstrated similar performance. The FC electrolyser system was used only when the BESS could not cater the imbalance power in all the schemes.

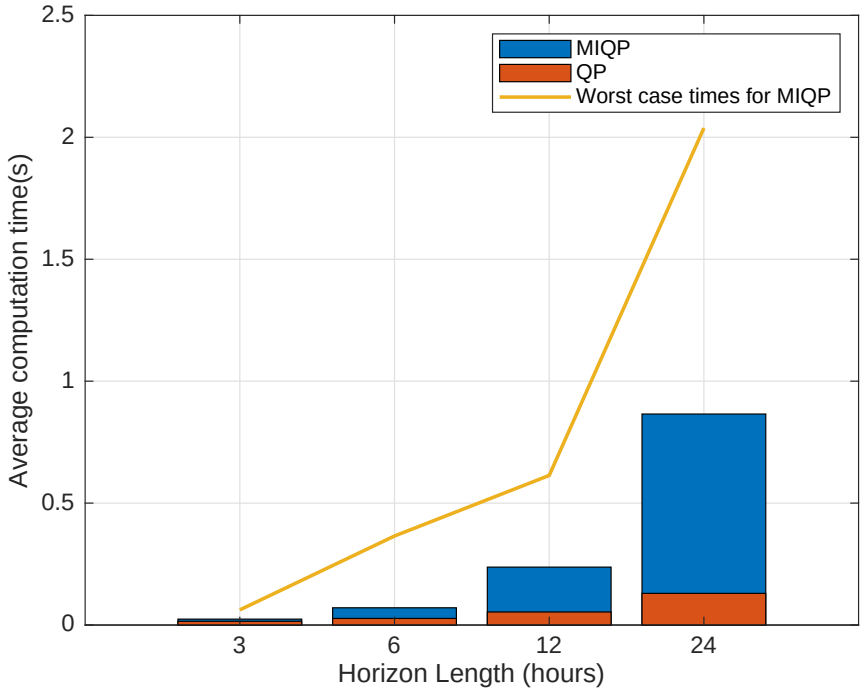

Figure 6.21: Bar plot showing average computation times for MIQP and QP optimisation problems in MPC, at any sampling instant, for various control horizon lengths. The worst case time in the MIQP for different horizon lengths is also presented.

6.3.6 Impact of prediction horizon on MPC performance

The performance of MPC based scheduling is influenced by the choice of the prediction horizon, which affects the computational resources required and the performance of the microgrid. Irrespective of the prediction horizon used the increased need for computational resources with MPC is a major drawback over fuzzy scheme. The impact of the increased computational complexity with MPC is analysed here.

Computational complexity analysis

As longer prediction horizons are considered the number of decision variables in the optimisation problem of MPC increases. This results in an increase in computational time for solving the optimisation problem. Besides, the nature of the optimisation problem also affect the computational complexity. In this work the optimisation problem is of MIQP type, as MLD formulations were used for incorporating the hybrid ESS models. However, it has been well established that MIQPs are NP-complete [277].

They are usually solved with algorithms like Branch and Bound techniques [271]. The computational complexity of these algorithms in the worst case scenario is a function of the entire search space [278]. In this problem, expressing the models of the three ESS using MLD formulation resulted in three binary variables. The computational complexity in this case is therefore, $\mathcal{O}(2^{3 \cdot N})$. However, solvers like Gurobi employs significantly efficient implementation of Branch and Bound algorithm which reduces the computation time complexity significantly. Despite this, as the length of the prediction horizon increases the algorithm tend to show a rapid increase in computation time. This is highlighted in Figure 6.21, where the average computation time for the MPC, at any sampling instant, is compared for a MIQP and QP problem for varying lengths of prediction horizon. The QP problem was realised without considering the hybrid model of the ESS. Though the QP problem cannot capture the hybrid behaviour of ESS this comparison allows to highlight the exponential increase in computational time encountered with MIQP. The QP problems are solved in polynomial time [261].

The significant increase in computational times for MPC (having MIQP) with longer prediction horizon highlights some scalability issues. In a small system, as considered here, this does not pose a major problem as the average computation time and the worst case times for solving MIQP in all the cases (horizon length) is still less than sampling interval of 5 min. However, in larger systems where more ESS are needed to be represented with hybrid models, the computation time with MIQP in MPC can reach very high values. This can lead to computation times exceeding the inter-sampling interval, at least in some worst case scenarios. This can make the implementation of online scheduling with MPC utilising hybrid models in their optimisation impractical.

In comparison the heuristic fuzzy inference based system had an average computation time of $1ms$.

Analysis of microgrid performance with prediction horizon

The 24 hour prediction horizon was considered in the MPC due to the daily periodicity of generation and load profiles. This ensures that at any instant the MPC makes it decision considering entire load demand and generation for the day. However, if scalability is an issue ,as discussed in the previous section, it will be beneficial to analyse the system performance when MPC is utilising shorter prediction horizons.

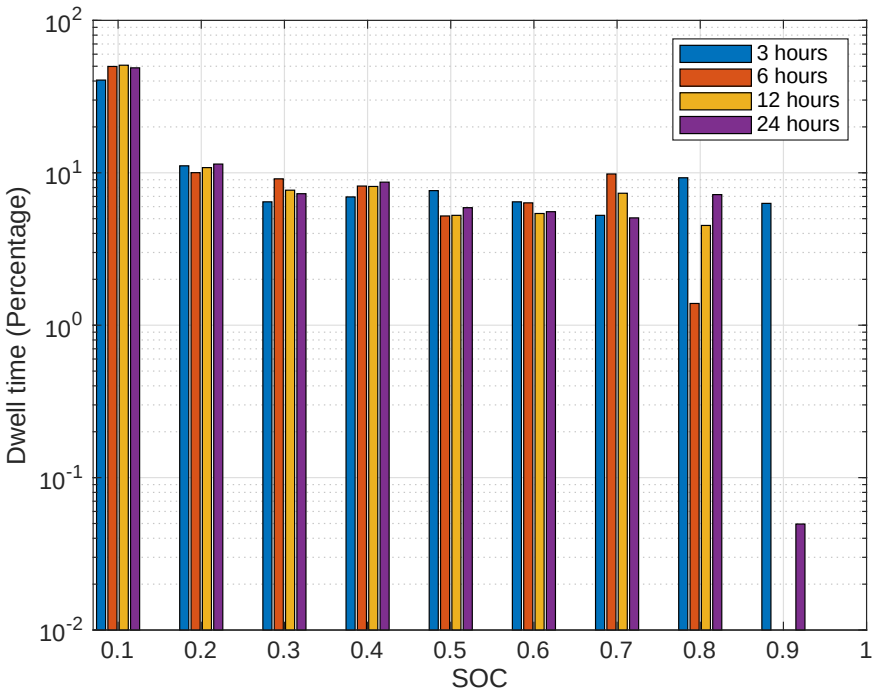

Figure 6.22: Comparison of dwell times at various SOC levels of BESS for different length of prediction horizon with MPC.

The Figure 6.22 and Figure 6.23 shows the performance of the MPC for shorter lengths of prediction horizon (3,6,12 hours) in comparison to 24 hour length discussed before. The performance is assessed based on the BESS behaviour, PV power curtailment and utilisation of the dispatchable generator unit for the same one week period discussed before. As the prediction horizon is shortened the MPC will have to make the scheduling decisions without having the full information of the generation profile. This can lead to early battery charging and increased dwell times at high SOC levels as in Fuzzy scheduling. This is ascertained through Figure 6.22 where the BESS dwell times at various SOC levels are compared when using MPC with different prediction horizons. In the case of 3 hour prediction horizon, the the dwell time of the BESS at high SOC levels (> 0.8) is comparable to the fuzzy scheme as shown in Figure 6.9.

In the case of 6 and 12 hour prediction horizon the MPC has more information regarding the generation profile. This shifts the BESS charging more towards the peak generation period leading to lower dwell times at high SOC levels as shown in Figure 6.22. It should be noted that, with the 24 hour prediction horizon the battery is kept at a highly charged state (0.9) for more time than in the case of 6 and 12 hours. This

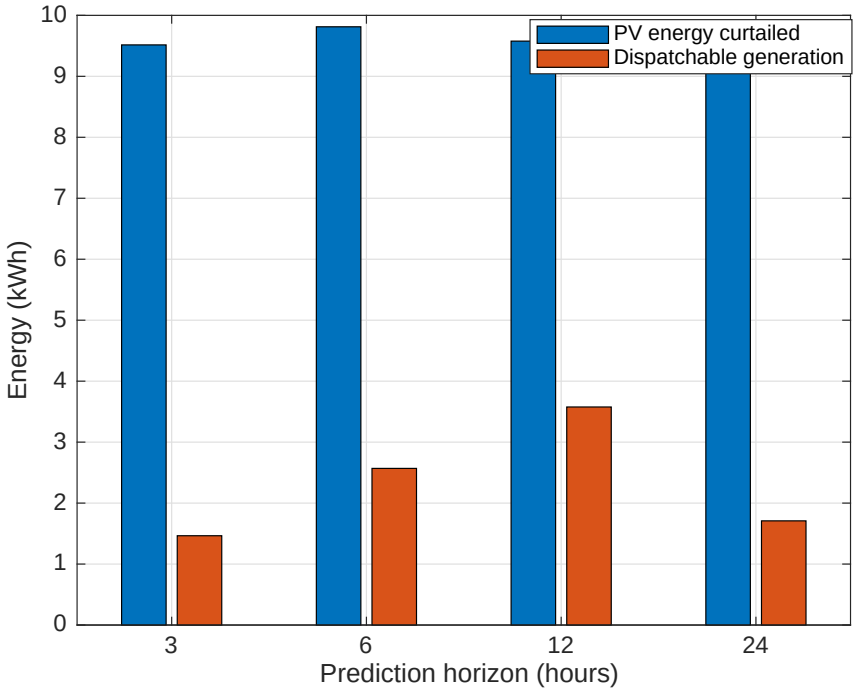

Figure 6.23: Comparison of PV power curtailment and energy utilisation from dispatchable generating units for different lengths of prediction horizon with MPC.

is because with the shorter prediction horizon when the charging decisions are made in the day, the load information in the night maybe not be completely available to the MPC scheduler. As a result the charging is not done taking the entire load demand into account. In some cases this can lead to BESS not storing sufficient charge for meeting entire load demand. In the 24 hour prediction window this is not the case. The entire load demand information is available and the BESS will store higher charge to cater them leading to increased dwell times at higher SOC levels. This is also clear from Figure 6.23, where the 6 and 12 hour prediction window cases has to rely more on the dispatchable generating unit to cater the load demand in comparison to the 24 hour case.

In terms of PV power curtailment and utilisation of dispatchable generator, the performance with shorter prediction horizon was similar to that of the 24 hour case. In all the cases (3, 6, 12 hours) the PV curtailment with MPC was lesser than that of the fuzzy scheduler system.

This concludes that with shorter prediction horizon in MPC (6, 12 hours), the microgrid performance does not undergo significant deterioration, At the same time the

number of decision variables in the optimisation problem for shorter horizon are lesser thus reducing computational complexity. Apart from this, in comparison to the fuzzy scheme the MPC performance with shorter horizons are still better.

It should also be noted the problem with feasibility of online implementation in larger system can be addressed using an aggregated representation of the system in the energy management stage. For example, by representing ESS of same type as one aggregated ESS . In this process, the number of decision variable at the energy management level can be reduced thus reducing the computational demand. The aggregated control action for the ESS can then be send to the primary+secondary stage, where the individual set point can be generated using the power splitting strategy incorporated. In this way the computational burden can be removed from the tertiary control stage.

6.3.7 Concluding remarks on MPC scheduling in islanded microgrid

The MPC based energy management system was developed for autonomous operation of islanded microgrid with PV array, dispatchable generator and tri-hybrid ESS . The MPC based tertiary control system exhibited an improved performance over a fuzzy based heuristic scheme as it made decisions based on forecast of generation and load. The improvements with MPC can be summarised as

- Significant reduction in dwell time at high SOC levels of battery (> 0.7), with MPC, by shifting battery charging to peak generation period.
- Smoother set-point variation in regenerative FC with MPC over fuzzy system.
- Almost 50% and 70% reduction in PV power curtailment and dispatchable generator use respectively with MPC. This highlights increased utilisation of PV power.

In terms of computational requirement, MPC was more demanding in comparison to the fuzzy scheme. Nevertheless for the islanded microgrid considered in this work, the worst case computational time encountered with the 24 hour prediction window was significantly lower than the 5 minute sampling interval used. This confirms the suitability of MPC for online energy scheduling in the islanded microgrid considered here.

Finally, comparing the two schemes MPC without correction performed slightly below par to the ideal MPC. This was expected due to the forecast error from the prediction. Nevertheless, the drop in performance in different objectives were not significant. Compared with the fuzzy based heuristic schemes, even with forecast error, the performance of MPC was better.

6.4 Concluding remarks on tertiary control stage

The tertiary control or energy management stage for a microgrid with RES generation and ESS was discussed in this chapter. Online strategies using non-heuristic decision making, accounting for forecast information of generation and load demand was identified as the better choice for the tertiary control. These methods mostly rely on solving an optimisation problem for generating the control action. Generating set points by solving optimisation problems guarantee optimality of solution, easiness in incorporating forecast information and easiness in defining the desired optimal behaviour of microgrid implicitly. The MPC was therefore identified to be used at tertiary control stage.

The chapter tried to address different scenarios of energy management namely: grid connected scenario, islanded grids, hybrid storage, single storage and Mixed integer programming in optimisation problems. The objective was to develop a comprehensive analysis of MPC in energy management stage of electric grids. In the grid connected scenario, the energy management problem of the PV BESS system was addressed using MPC based tertiary control. The objective was to maximise self consumption of PV power while also mitigating grid congestion and minimising BESS degradation. In this way, the MPC could overcome the drawbacks of the conventional maximising self consumption control used in PV BESS system. The discussion in this chapter tried to quantify the improvement with MPC by analysing one year operation. The MPC, even with forecast error in the predicted data, was able to achieve improved performance in grid congestion mitigation and BESS degradation over MSC scheme while encountering a slight loss of self consumption. The study also highlighted the importance of avoiding conservative decision making with MPC when addressing prediction errors, as it can significantly undermine the economic performance of microgrid. Finally, a major take away from the analysis of PV BESS system was highlighting the role of an efficient control strategy in mitigating the issues arising from RES generation integration in power grids. The study effectively demonstrated that integrating ESS alone will not solve the issues

from RES generation integration but they should also be backed up with an efficient control strategy as well.

In the case of islanded scenario, the MPC was employed in the energy management of an islanded microgrid with tri-hybrid ESS and PV generation. This problem addressed the issue of sustaining islanded operation through RES power curtailment and utilisation of dispatchable generation. Another objective of the energy management system was defining how to manage the energy among the hybrid ESS to ensure maximum operational efficiency and minimum ESS degradation. In this problem, also, the MPC based scheme, even with forecast error, performed better than a heuristic energy management system based on fuzzy inference. The improvement were in terms of minimising PV power curtailment, reducing the dwell time of BESS at high SOC levels while maintaining good operational efficiency. In this case an analysis on the computational demand with MPC, especially when using MIQP problem in optimisation was assessed. Compared to fuzzy based energy scheduling, MPC with MIQP problem for optimisation exhibited significant increase in computational demand. In larger systems this can lead to infeasibility for online implementation when using longer prediction horizon like 24 hours. Nevertheless, an analysis with different lengths of prediction horizon highlighted that comparable performance can be achieved with shorter horizons as well. Another method to avoid the computation burden, can be using the aggregated system representation at energy management stage and using the power splitting strategy at the power management level to generate the control action for individual systems in the microgrid.

Assessing the behaviour of MPC based energy management system it was obvious that MPC can ensure better all round energy management performance in grids compared to heuristic methods. Even with uncertainty in forecast information used in MPC, the performance was found to be better than heuristic schemes, considering all round system behaviour. This could be ensured as long as the forecasting unit can predict with reasonable accuracy the total imbalance power in a prediction horizon and the time period at which peak generation occurs. Though the MPC is computationally demanding, the same is not a major issue nowadays due to availability of cheap computation power. Considering all these aspects, this work concludes that MPC based tertiary control presents an effective solution for energy management in electric grids.

Finally, the work here addressed only centralised energy management strategy. Considering the small size of the microgrid system this represents an effective solution. However, to address the generic problem of energy management in large scale transmission

and distribution networks these centralised schemes may not be suitable. In this scenario, distributed energy management strategies should be explored in the future work. Apart from this, it should be observed that the constraint tightening approach for addressing the forecast uncertainty may not be the most optimal, despite their easiness in implementation. Future works, can focus on developing more efficient strategies to address prediction error while also eliminating conservative decision making. In order to conclude the publications (under based on the work carried out in this chapter is given below:

J1 Nair, Unnikrishnan Raveendran, and Ramon Costa-Castelló, "A model predictive control based energy management scheme for hybrid storage system in islanded microgrids," in IEEE Access, doi: 10.1109/ACCESS.2020.2996434.

C1 Nair, Unnikrishnan Raveendran, and Ramon Costa-Castelló. "An analysis of energy storage system interaction in a multi objective model predictive control based energy management in DC microgrid." In 2019 24th IEEE International Conference on Emerging Technologies and Factory Automation (ETFA), pp. 739-746. IEEE, 2019.

Part IV

Concluding Remarks

Chapter 7

Concluding Remarks

This chapter provides a summary of the work carried out in the Ph.D study- "Control and management of energy storage systems in microgrids" along with the main results and outcomes. The main contributions of this work are discussed and perspectives for future research are highlighted.

7.1 Summary

In this Ph.D thesis, the main research focus has been on developing an efficient control strategy for the ESS in microgrids that ensures grid stability, real time power management among ESS and energy management. A hierarchical control scheme was identified for the same. Several issues at the different levels of control architecture were identified and solutions were proposed to address the same. The thesis work also aimed at highlighting the concern that integrating ESS in future grids, alone will not solve the issues arising from renewable energy integration in future grids. The ESS integration should be backed up with an efficient and optimal control strategy to exploit the full capabilities that ESS can offer. In the following, a brief summary of the work done in this thesis to ensure the same is provided.

In *Chapter* 1 the issues pertaining to increased integration of renewable generation and the evolution of modern grids, due to the same, was discussed. The intermittent, non-dispatchable nature of power generation from renewable sources have resulted in multiple issues pertaining to grid congestion and stability in power networks. The chapter discussed how in future grids, energy storage systems can play a pivotal role in

avoiding and overcoming these issues. A comprehensive study on the functionalities that ESS can provide in future grids, the classification of ESS based on physical capabilities and operational efficiencies was carried out. This study helped to establish the need for hybrid ESS in future grids to solve the various issues. However, as discussed in *Chapter 1* the issues in modern electrical systems, due to the renewable generation integration, will not be solved just by integrating ESS. The ESS should be controlled and managed efficiently/optimally so that the problems in modern grids are effectively dealt with. This calls for developing an effective control system for the hybrid ESS in modern grids, which is the focus of this thesis work. A hierarchical control architecture with a lower level power management stage and higher level energy management stage was identified for the same. The power management stage was responsible for maintaining the stability of the grid and the real time optimal power distribution among the ESS in a hybrid system framework. The energy management stage manages the energy of the ESS in an optimal manner such that the problems arising from the renewable generation integration is effectively dealt with and the operation of the grid is optimised. The distributed nature of the renewable generation have given rise to the concept of microgrids which is becoming increasingly prominent in future electrical networks. As such, in this thesis work control and management of the ESS in a DC microgrid is the focus. The *Chapter* 2 introduces the microgrid and the hybrid ESS system considered in this work. A detailed discussion on the different ESS (supercapacitor, battery and FC electrolyser system) considered for the hybrid ESS framework, in this thesis, was provided in this chapter.

The second part of the thesis in *Chapter* 3, 4 pertains to the power management stage. The power management stage comprises of two levels, converter control and primary+secondary control. The *Chapter 3* deals with the control of the power converter systems interfacing the ESS to power grids and presents the contributions of this PhD work towards the converter control level. The chapter focussed on the aspect of improving the dynamic performance of the converter controller during reference tracking. In this context, the chapter introduced the reset PI+CI controller for the converter system. The proposed reset controller replaces the conventional PI control, used for reference tracking. The chapter highlighted the ability of the PI+CI controller in achieving a flat response to step changes in reference input thus improving the dynamic performance over the PI controller. The design criteria, stability and robustness analysis of the proposed controller was presented in this chapter. The improvement achieved with the PI+CI controller was verified through simulation and experimental validations.

The Chapter 4 discussed the real time control of the microgrid having multiple ESS. The work presented in this chapter focussed on developing a unified, centralised control framework, called the primary+secondary stage, that ensures grid stability, voltage regulation and power splitting among the ESS in real time. The primary+secondary stage emulated the inertial, primary and secondary responses of the conventional grid through the control of ESS in microgrids. The chapter proposed an adaptive disturbance rejection control scheme for improved voltage regulation and grid stability under power variations (generation or load) in the microgrid. The scheme proposed the augmentation of an extended state observer to the conventional nested loop control structure to improve the dynamics of voltage regulation control. The ESO achieved this by providing the feed forward of the estimated disturbance in the grid. The chapter also outlined an LMI based design procedure for the observer gains, which ensured a bound on the H_∞ norm of closed loop system transfer function. Another contribution in the chapter is the proposal of a power splitting strategy among the hybrid ESS using a filter based approach. This ensured that the first response to disturbance is from the fast acting ESS like SC, while the ESS with slower response capability like battery or FC electrolyser system ramps up in power. The power splitting strategy also addressed the criteria for power splitting among multiple high energy density ESS, like battery and FC, based on the SOC of battery. This ensured higher operational efficiency of grid by limiting utilisation of FC system which had poor efficiency. The design criteria of the filter which ensures model invariance of inner loop and its equivalence to SC current loop transfer function was proposed. Finally, the chapter also presented the power splitting criteria among the ESS of same type. The proposed control architecture and the designs were verified though simulation models developed using Matlab-Simulink.

The final part of the thesis comprising of *Chapter* 5 ,6 discussed the energy management stage of the control architecture. Developing the tertiary control level for the energy management was the main focus in this part. In order ensure an optimal performance of the microgrid, through the energy management of ESS, non heuristic methods were identified to be used in the tertiary control for set point generation. The non-heuristic methods enabled an easier integration of forecast information, which allowed better decision making. The *Chapter* 5 discussed the work done in this Ph.D work pertaining to forecasting the renewable generation and load demand, to be used in the tertiary control level. The different techniques in forecasting time series were identified and analysed. Based on the study conducted, a feed forward deep neural network was identified to be used in the forecasting unit for the tertiary control level. The chapter

discussed the input feature selection and training process of the neural network used in the forecast of generation and load demand. The discussion in the chapter also addressed the quantification of the forecast accuracy along with the results from the forecasting unit developed.

Finally the *Chapter*6 presented the tertiary control level used for the centralised energy management in the microgrid. The online MPC based control was used in this stage to make decisions on energy management of the microgrid aided by the information from the forecasting unit. The chapter discussed how efficient energy management of battery storage with MPC can be used to mitigate the grid congestion arising from peak power feed-in from PV system while maintaining maximum self consumption of the generated PV power. The ability of the MPC based energy scheduling in limiting scenarios that can stress the ESS , thus reducing their degradation during operation was also demonstrated. The chapter also presented the work done in developing an MPC based energy management system for islanded grids with tri-hybrid ESS. This application of MPC in islanded grids demonstrated MPC's ability to achieve increased utilisation of PV power by limiting the power curtailment while maximising the operational efficiency and minimising the stressing scenarios of the ESS. The analysis carried out in the chapter demonstrated that even with deterioration in MPC performance, arising from prediction errors, the overall performance of the microgrid was better than with the heuristics decision making methods employed in tertiary control. Finally, the study on computational demand by MPC ascertained the suitability of the same for online implementation.

7.2 Main contributions of this work

Based on the work presented in the previous chapters the main contribution of this thesis can be summed up as "*The development of a unified , hierarchical control system comprising of power and energy management stages for governing the ESS in microgrid with renewable energy integration. The Ph.D work contributed by proposing a scalable and flexible power management stage which ensures improved voltage regulation and power distribution among ESS accounting for operational efficiency and ESS degradation. In the energy management stage, the work proposed the application of an optimal energy management system using MPC, to efficiently manage the ESS such that the full capability of ESS is exploited in mitigating the issues arising from renewable generation*

integration.". The specific technical contributions at each control level can be summed up as:

- **Converter control stage:** Proposal of PI+CI reset controller to replace the conventional PI controller in the reference tracking current control loop of DC-DC converters for improved dynamic performance . The work in this thesis defined a design criteria of PI +CI controller and frequency domain based techniques to analyse stability and robustness of control systems. The performance of the proposed controllers where verified experimentally.
- **Primary+secondary control** Proposal of a unified, scalable, centralised power management scheme for microgrid with hybrid ESS that ensures stability of microgrid and power splitting among ESS. In this power management scheme the specific contributions are
  - Proposal of ADRC scheme using ESO for improved voltage regulation performance in microgrids. The work also contributed by identifying an LMI based procedure for optimal gain determination in ESO, considering the closed loop system behaviour. The proposed design ensure that the H_∞ norm of the closed loop transfer function is bounded thus preserving the system stability while integrating the ESO.
  - Proposal of power splitting strategy among the high energy density ESS like the battery and FC-electrolyser system that ensures a high operational efficiency of microgrid. The proposed strategy utilises a double sigmoid function, using the SOC of the battery as input, to decide the power splitting among the ESS. The proposed method ensures a smooth power transition from the battery to FC system while also ensuring that the battery is not deep discharged which can lead to degradation.
  - Defining the criteria for deciding the cut-off frequency of filter in the power splitting stage, to ensure model invariance of the inner loop. This ensures that irrespective of the ESS compensating the imbalance in the grid the dynamics of inner loop can be defined by a time invariant model. This facilitates easiness in system stability/robustness analysis and design of outer loop controller parameters

  The performance of the proposed, unified primary+secondary control scheme was verified through simulations.

- **Tertiary control stage**: Proposal of MPC based tertiary controller for energy management of ESS coupled with RES in microgrid, to ensure that renewable generation is more reliable and grid friendly. In order to achieve the same, the proposed tertiary control strategies (using MPC) focussed on mitigating grid congestion arising from renewable generation integration, minimising ESS degradation by modifying their charge/discharge cycle and maximising the self consumption of generated renewable energy. The performance of the tertiary control , with the above objectives, was assessed for grid connected and islanded grid operation mode.

7.3 Future research perspectives

Although this Ph.D work had tried to mitigate some of the issues arising from renewable energy integration in microgrids through the development of an optimal control strategy for the ESS, there is still scope for more research in this domain of ESS control so that the large scale incorporation of renewable sources expected in future grids is feasible. In this context the some of the perspective for future research can be summed up as follows.

- The research focus in this thesis had been on developing centralised control schemes for ESS in microgrid. The large scale integration of renewable sources expected in future grids will lead to large scale distributed integration of ESS. This will also lead to more microgrids incorporated into main grid. In this scenario, the control system should be extended above the tertiary control to include the *grid control unit* discussed in Chapter 1. Considering the distributed nature of nature of RES and ESS integration, centralised control schemes may not be practically feasible due to the large communication requirements and for the ensuring the reliability of grid operation. In this scenario distributed control schemes can be considered as an interesting domain of research. Multi agent based control where each microgrid can form an agent can be looked upon. Approaches like distributed MPC, game theory can be used for the energy management among the multiple agents.
- In the event of distributed RES and ESS integration the centralised primary+secondary scheme, discussed in this thesis, should be extended to a decentralised scheme. In this context research focus can be on droop based decentralised

schemes [117] with the objective of improving their dynamic performance through the incorporation of ESO in the decentralised architecture. The research focus should also be on integrating power splitting strategies among multiple different high energy density ESS when they are integrated in a distributed manner.

- Another important perspective of research is from the domain of MPC. As demonstrated in this work the decision making with MPC when accounting for forecast error can lead to conservative decisions. This can make the justification of use MPC in grid connected applications difficult especially when the conservative decisions affect economic aspects of grid operations. In this context future research should focus on developing more efficient decision making strategies in MPC while accounting for forecast uncertainties.

- Finally, a very interesting domain for future research is the application of machine learning techniques in the energy management of microgrids. Recently, there has been an increased focus on the use of reinforcement learning approaches for energy management of stand alone BESS systems in microgrids. Reinforcement learning techniques like Q iterative learning are being employed for the same. These techniques can be expanded to the address the problem of energy management in microgrids with hybrid storage. Investigations should be done comparing the reinforcement learning techniques with the MPC strategies to quantify how their performances compare with each other.

Part V

Appendices

Appendix A

Norms for signals and systems

An important requirement in control system design and analysis is the ability to define the size of a signal (input or output) or that of LTI systems is a quantitative manner. This is facilitated by the norms of signals and systems which allows for quantifying the size of the same. The norm for signal is referred to as **L** norm and that of an LTI system is called **H** norm. For a signal $z(t)$, the norm defined by $\|z\|$ have the following properties

- $\|z\| \geq 0$
- $\|z\| = 0 \Leftrightarrow z(t) = 0 \quad \forall t$
- $\|az\| = \|a\|\|z\|$
- $\|y + z\| = \|y\| + \|z\|$

Three major norms typical defined for the signals, namely the $\mathbf{L}_1, \mathbf{L}_2, \mathbf{L}_\infty$ norms. The $\mathbf{L}_1$ norm is defined as the integral of absolute value of a signal given by

$$\|z\|_1 = \int_{-\infty}^{\infty} |z(t)| dt \tag{A.1}$$

The $\mathbf{L}_2$ norm is defined as

$$\|z\|_2 = \left(\int_{-\infty}^{\infty} z(t)^2 dt \right)^{\frac{1}{2}} \tag{A.2}$$

The $\mathbf{L}_2$ norm of a signal is indicative of the energy associated with a signal.

	$\|z\|_2$	$\|z\|_\infty$
$\|y\|_2$	$\|G\|_\infty$	∞
$\|y\|_\infty$	$\|G\|_2$	$\|G\|_1$

Table A.1: Relation between **L** norm of input-output signals based on **H** norm of their transfer function.

Finally, the $\mathbf{L}_\infty$ norm is given by

$$\|z\|_\infty = \sup_t |z(t)| \tag{A.3}$$

The norms are usually associated with vector spaces. In this context $\mathbf{L}_1$, $\mathbf{L}_2, \mathbf{L}_\infty$ spaces represents a set of signals having finite $\mathbf{L}_1$ $\mathbf{L}_2$, $\mathbf{L}_\infty$ norms values respectively.

The norms typically defined for the systems are the $\mathbf{H}_2$ and $\mathbf{H}_\infty$ norms. For a system with transfer function G(s) the $\mathbf{H}_2$ norm is given by

$$\|G\|_2 = \frac{1}{2\pi}\left(\int_{-\infty}^{\infty} G(j\omega)^2 d\omega\right)^{\frac{1}{2}} \tag{A.4}$$

and the $\mathbf{H}_\infty$ norm is given by

$$\|G\|_\infty = \sup_\omega |G(j\omega)|. \tag{A.5}$$

The $\mathbf{H}_\infty$ norm is observed as the peak value occurring the bode plot of $G(s)$.

Consider an LTI system $G(s)$ with input signal $z(t)$. The knowledge of the **L** and **H** norms of the input and system can be used to develop an understanding of the size of output signal $y(t)$ using the relation [140] in TableA.1. This highlights how the output signals are bounded if **L** and **H** norms of the input and system is known. For example, consider that $\|z\|_2$ is norm for an input signal, like a disturbance to plant, and $\|G\|_\infty$ represents the infinity norm of the disturbance to output transfer function. Then it can be said that $\|y\|_2$, the plant response to the disturbance input, is bounded by $\|G\|_\infty$ according to TableA.1 . This is relevant, since exogenous inputs to plant, like disturbance, are typically not known a priori. In this case if the $\|G\|_\infty$ norm of the disturbance rejection transfer function is known then an understanding of the plant response under an unknown disturbance can be developed.

Bibliography

[1] H. Chen, T. N. Cong, W. Yang, C. Tan, Y. Li, and Y. Ding, "Progress in electrical energy storage system: A critical review," *Progress in natural science*, vol. 19, no. 3, pp. 291–312, 2009.

[2] S. O. Amrouche, D. Rekioua, T. Rekioua, and S. Bacha, "Overview of energy storage in renewable energy systems," *International Journal of Hydrogen Energy*, vol. 41, no. 45, pp. 20914–20927, 2016.

[3] D. Gibb, H. Murdock, F. Appavou, A. Brown, B. Epp, B. Kondev, A. McCrone, L. Renalder, E. Musolino, J. Sawin, K. Seyboth, J. Skeen, and F. Sverrisson, "Renewables 2019 global status report," *Paris: REN21 Secretariat*, 2019.

[4] M. G. Molina, "Energy storage and power electronics technologies: A strong combination to empower the transformation to the smart grid," *Proceedings of the IEEE*, vol. 105, no. 11, pp. 2191–2219, 2017.

[5] "Opportunities and barriers to pumped-hydro energy storage in the United tates, author=Yang, Chi-Jen and Jackson, Robert B, journal=Renewable and Sustainable Energy Reviews, volume=15, number=1, pages=839–844, year=2011, publisher=Elsevier,"

[6] J. Larminie, A. Dicks, and M. S. McDonald, "Fuel cell systems explained," vol. 2, 2003.

[7] K. Behrens, "Basic measurements of radiation at station Lindenberg (2004-12)," 2011.

[8] L. Prechelt, "Early stopping-but when?," in *Neural Networks: Tricks of the trade*, pp. 55–69, Springer, 1998.

[9] M. e. a. Allen, "Special report: Global warming of 1.5 degree celcius(Geneva: Intergovernmental Panel on Climate Change (IPCC), 2018),"

[10] "Renewables 2018,market analysis and forecast from 2018 to 2023,"

[11] A. Hirsch, Y. Parag, and J. Guerrero, "Microgrids: A review of technologies, key drivers, and outstanding issues," *Renewable and sustainable Energy reviews*, vol. 90, pp. 402–411, 2018.

[12] H. Schermeyer, M. Studer, M. Ruppert, and W. Fichtner, "Understanding distribution grid congestion caused by electricity generation from renewables," in *Smart Energy Research. At the Crossroads of Engineering, Economics, and Computer Science*, pp. 78–89, Springer, 2017.

[13] B. Bayer, P. Matschoss, H. Thomas, and A. Marian, "The German experience with integrating photovoltaic systems into the low-voltage grids," *Renewable energy*, vol. 119, pp. 129–141, 2018.

[14] S. Papathanassiou, N. Hatziargyriou, P. Anagnostopoulos, L. Aleixo, B. Buchholz, C. Carter-Brown, N. Drossos, B. Enayati, M. Fan, V. Gabrion, *et al.*, "Capacity of distribution feeders for hosting der," *CIGRÉ Working Group C6*, vol. 24, 2014.

[15] D. Maxwell, "Parts of Northern Ireland's electricity grid overloaded."

[16] L. Hobday, "Electricity distributors warn excess solar power in network could cause blackouts, damage infrastructure."

[17] "Ministry of energy, agriculture, the environment and rural areas schleswig-holstein (melur)abregelung von strom aus erneuerbaren energien und daraus resultierende entschadigungsanspruche in den jahren 2010 bis 2014," 2015.

[18] M. H. Bollen, "Understanding power quality problems," in *Voltage sags and Interruptions*, IEEE press, 2000.

[19] A. Bracale, P. Caramia, G. Carpinelli, A. Russo, and P. Verde, "Site and system indices for power-quality characterization of distribution networks with distributed generation," *IEEE Transactions on Power Delivery*, vol. 26, no. 3, pp. 1304–1316, 2011.

[20] B. Renders, L. Vandevelde, L. Degroote, K. Stockman, and M. Bollen, "Distributed generation and the voltage profile on distribution feeders during voltage dips," *Electric power systems research*, vol. 80, no. 12, pp. 1452–1458, 2010.

[21] G. Pepermans, J. Driesen, D. Haeseldonckx, R. Belmans, and W. D haeseleer, "Distributed generation: definition, benefits and issues," *Energy policy*, vol. 33, no. 6, pp. 787–798, 2005.

[22] P. Tielens and D. Van Hertem, "The relevance of inertia in power systems," *Renewable and Sustainable Energy Reviews*, vol. 55, pp. 999–1009, 2016.

[23] E. Iii, "Black system 456," no. SEPTEMBER 2016, pp. 589–591, 2017.

[24] T. Stetz, F. Marten, and M. Braun, "Improved low voltage grid-integration of photovoltaic systems in germany," *IEEE Transactions on sustainable energy*, vol. 4, no. 2, pp. 534–542, 2012.

[25] O. Ma and K. Cheung, "Demand response and energy storage integration study," tech. rep., Office of Energy Efficiency and Renewable Energy, Office of Electricity , 2016.

[26] R. A. Verzijlbergh, L. J. De Vries, and Z. Lukszo, "Renewable energy sources and responsive demand. do we need congestion management in the distribution grid?," *IEEE Transactions on Power Systems*, vol. 29, no. 5, pp. 2119–2128, 2014.

[27] B. Dunn, H. Kamath, and J.-M. Tarascon, "Electrical energy storage for the grid: a battery of choices," *Science*, vol. 334, no. 6058, pp. 928–935, 2011.

[28] A. Poullikkas, "A comparative overview of large-scale battery systems for electricity storage," *Renewable and Sustainable energy reviews*, vol. 27, pp. 778–788, 2013.

[29] P. Punys, R. Baublys, E. Kasiulis, A. Vaisvila, B. Pelikan, and J. Steller, "Assessment of renewable electricity generation by pumped storage power plants in eu member states," *Renewable and Sustainable Energy Reviews*, vol. 26, pp. 190–200, 2013.

[30] S. Karellas and N. Tzouganatos, "Comparison of the performance of compressed-air and hydrogen energy storage systems: Karpathos island case study," *Renewable and Sustainable Energy Reviews*, vol. 29, pp. 865–882, 2014.

[31] G. Gahleitner, "Hydrogen from renewable electricity: An international review of power-to-gas pilot plants for stationary applications," *international Journal of hydrogen energy*, vol. 38, no. 5, pp. 2039–2061, 2013.

[32] J. Noriega, O. Iyore, C. Budime, B. Gnade, and J. Vasselli, "Characterization system for research on energy storage capacitors," *Review of Scientific Instruments*, vol. 84, no. 5, p. 055109, 2013.

[33] J. Baker and A. Collinson, "Electrical energy storage at the turn of the millennium," *Power Engineering Journal*, vol. 13, no. 3, pp. 107–112, 1999.

[34] P. Denholm, E. Ela, B. Kirby, and M. Milligan, "Role of energy storage with renewable electricity generation," tech. rep., National Renewable Energy Lab.(NREL), Golden, CO (United States), 2010.

[35] P. Agrawal, A. Nourai, L. Markel, R. Fioravanti, P. Gordon, N. Tong, and G. Huff, "Characterization and assessment of novel bulk storage technologies," *Sandia National Laboratories, Albuquerque*, 2011.

[36] M. S. Whittingham, "History, evolution, and future status of energy storage," *Proceedings of the IEEE*, vol. 100, no. Special Centennial Issue, pp. 1518–1534, 2012.

[37] B. Zakeri and S. Syri, "Electrical energy storage systems: A comparative life cycle cost analysis," *Renewable and sustainable energy reviews*, vol. 42, pp. 569–596, 2015.

[38] J. Eyer and G. Corey, "Energy storage for the electricity grid: Benefits and market potential assessment guide," *Sandia National Laboratories*, vol. 20, no. 10, p. 5, 2010.

[39] S. Vazquez, S. M. Lukic, E. Galvan, L. G. Franquelo, and J. M. Carrasco, "Energy storage systems for transport and grid applications," *IEEE Transactions on Industrial Electronics*, vol. 57, no. 12, pp. 3881–3895, 2010.

[40] T. W. Patterson and R. M. Darling, "Damage to the cathode catalyst of a pem fuel cell caused by localized fuel starvation," *Electrochemical and Solid-State Letters*, vol. 9, no. 4, pp. A183–A185, 2006.

[41] T. Dai, Y. Tang, J. Shi, F. Jiao, and L. Wang, "Design of a 10 mj hts superconducting magnetic energy storage magnet," *IEEE Transactions on Applied Superconductivity*, vol. 20, no. 3, pp. 1356–1359, 2010.

[42] A. Burke, "Ultracapacitors: why, how, and where is the technology," *Journal of power sources*, vol. 91, no. 1, pp. 37–50, 2000.

[43] E. Schaltz, A. Khaligh, and P. O. Rasmussen, "Influence of battery/ultracapacitor energy-storage sizing on battery lifetime in a fuel cell hybrid electric vehicle," *IEEE Transactions on Vehicular Technology*, vol. 58, no. 8, pp. 3882–3891, 2009.

[44] J. Cao and A. Emadi, "A new battery/ultracapacitor hybrid energy storage system for electric, hybrid, and plug-in hybrid electric vehicles," *IEEE Transactions on power electronics*, vol. 27, no. 1, pp. 122–132, 2011.

[45] B. Steffen, "Prospects for pumped-hydro storage in Germany," *Energy Policy*, vol. 45, pp. 420–429, 2012.

[46] M. Mesbahi, "Top 35 Solar Project in Australia."

[47] D. Weston, "Equinor installs Batwind battery."

[48] A. Colthorpe, "50MWh battery completed in Germany, claims Europes largest crown."

[49] L. Stoker, "EDF's completed 49MW battery system brings nearly all EFR projects over the line."

[50] J. Spector, "Pg&e's Record Breaking Battery Proposal Wins Approval From Regulators."

[51] M. Maisch, "South Australia's Tesla big battery saves $40 million in grid stabilization costs."

[52] T. Wilberforce, A. Alaswad, A. Palumbo, M. Dassisti, and A.-G. Olabi, "Advances in stationary and portable fuel cell applications," *International journal of hydrogen energy*, vol. 41, no. 37, pp. 16509–16522, 2016.

[53] E. Taibi, R. Miranda, W. Vanhoudt, T. Winkel, J.-C. Lanoix, and F. Barth, "Hydrogen from renewable power Technology outlook for the energy transition," *International Renewable Energy Agency report*, 2018.

[54] T. Hornyak, "How Toyota is helping Japan with its multibillion-dollar push to create a hydrogen-fueled society."

[55] Y. Sun, "China to support hydrogen and fuel cell vehicles to go green."

[56] T. Ackermann, G. Andersson, and L. Söder, "Distributed generation: a definition," *Electric power systems research*, vol. 57, no. 3, pp. 195–204, 2001.

[57] J. J. Iannucci, L. Cibulka, J. Eyer, and R. Pupp, "Der benefits analysis studies: Final report," *Nat. Renewable Energy Lab., Golden, CO, USA, Rep. NREL/SR-620-34636*, 2003.

[58] E. Z. Gumerman, R. R. Bharvirkar, K. H. LaCommare, and C. Marnay, "Evaluation framework and tools for distributed energy resources," tech. rep., Lawrence Berkeley National Lab.(LBNL), Berkeley, CA (United States), 2003.

[59] D. T. Ton and M. A. Smith, "The us department of energy's microgrid initiative," *The Electricity Journal*, vol. 25, no. 8, pp. 84–94, 2012.

[60] J. P. Lopes, C. Moreira, and A. Madureira, "Defining control strategies for microgrids islanded operation," *IEEE Transactions on power systems*, vol. 21, no. 2, pp. 916–924, 2006.

[61] T. Basso, "Ieee 1547 and 2030 standards for distributed energy resources interconnection and interoperability with the electricity grid," tech. rep., National Renewable Energy Lab.(NREL), Golden, CO (United States), 2014.

[62] I. Hadjipaschalis, A. Poullikkas, and V. Efthimiou, "Overview of current and future energy storage technologies for electric power applications," *Renewable and sustainable energy reviews*, vol. 13, no. 6-7, pp. 1513–1522, 2009.

[63] C. Zhang, Y.-L. Wei, P.-F. Cao, and M.-C. Lin, "Energy storage system: Current studies on batteries and power condition system," *Renewable and Sustainable Energy Reviews*, vol. 82, pp. 3091–3106, 2018.

[64] J. M. Guerrero, J. C. Vasquez, J. Matas, L. G. De Vicuña, and M. Castilla, "Hierarchical control of droop controlled ac and dc microgrids a general approach toward standardization," *IEEE Transactions on industrial electronics*, vol. 58, no. 1, pp. 158–172, 2010.

[65] S. Hamilton, E. Gunther, R. Drummond, and S. E. Widergren, "Interoperability: A key element for the grid and der of the future," *Proceedings of IEEE PES transmission and distribution*, pp. 927–931, 2006.

[66] "Ieee draft standard for the specification of microgrid controllers," *IEEE P2030.7/D11, August 2017*, pp. 1–42, Jan 2017.

[67] R. W. Erickson and D. Maksimovic, *Fundamentals of power electronics*. Springer Science & Business Media, 2007.

[68] R. Venkataramanan, *Sliding mode control of power converters*. PhD thesis, California Institute of Technology, 1986.

[69] P. Thounthong, P. Tricoli, and B. Davat, "Performance investigation of linear and nonlinear controls for a fuel cell/supercapacitor hybrid power plant," *International Journal of Electrical Power & Energy Systems*, vol. 54, pp. 454–464, 2014.

[70] Y. Gu, W. Li, and X. He, "Frequency-coordinating virtual impedance for autonomous power management of dc microgrid," *IEEE Transactions on Power Electronics*, vol. 30, no. 4, pp. 2328–2337, 2014.

[71] X. Lu, K. Sun, J. M. Guerrero, J. C. Vasquez, and L. Huang, "State-of-charge balance using adaptive droop control for distributed energy storage systems in dc microgrid applications," *IEEE Transactions on Industrial electronics*, vol. 61, no. 6, pp. 2804–2815, 2013.

[72] G. Ferrari-Trecate, E. Gallestey, P. Letizia, M. Spedicato, M. Morari, and M. Antoine, "Modeling and control of co-generation power plants: A hybrid system approach," *IEEE Transactions on Control Systems Technology*, vol. 12, no. 5, pp. 694–705, 2004.

[73] A. Parisio, E. Rikos, and L. Glielmo, "A model predictive control approach to microgrid operation optimization," *IEEE Transactions on Control Systems Technology*, vol. 22, no. 5, pp. 1813–1827, 2014.

[74] F. Garcia-Torres and C. Bordons, "Optimal economical schedule of hydrogen-based microgrids with hybrid storage using model predictive control," *IEEE Transactions on Industrial Electronics*, vol. 62, no. 8, pp. 5195–5207, 2015.

[75] J. Moshövel, K.-P. Kairies, D. Magnor, M. Leuthold, M. Bost, S. Gährs, E. Szczechowicz, M. Cramer, and D. U. Sauer, "Analysis of the maximal possible grid relief from pv-peak-power impacts by using storage systems for increased self-consumption," *Applied Energy*, vol. 137, pp. 567–575, 2015.

[76] H. Kanchev, D. Lu, F. Colas, V. Lazarov, and B. Francois, "Energy management and operational planning of a microgrid with a pv-based active generator for smart grid applications," *IEEE transactions on industrial electronics*, vol. 58, no. 10, pp. 4583–4592, 2011.

[77] A. Aktas, K. Erhan, S. Ozdemir, and E. Ozdemir, "Experimental investigation of a new smart energy management algorithm for a hybrid energy storage system in smart grid applications," *Electric Power Systems Research*, vol. 144, pp. 185–196, 2017.

[78] A. Mohamed, V. Salehi, and O. Mohammed, "Real-time energy management algorithm for mitigation of pulse loads in hybrid microgrids," *IEEE Transactions on Smart Grid*, vol. 3, no. 4, pp. 1911–1922, 2012.

[79] H. I. Becker, "Inventor :," pp. 2–4, 1957.

[80] R. Kötz and M. Carlen, "Principles and applications of electrochemical capacitors," *Electrochimica acta*, vol. 45, no. 15-16, pp. 2483–2498, 2000.

[81] A. Pandolfo and A. Hollenkamp, "Carbon properties and their role in supercapacitors," *Journal of power sources*, vol. 157, no. 1, pp. 11–27, 2006.

[82] J. Goodenough, H. Abruna, and M. Buchanan, "Basic research needs for electrical energy storage. report of the basic energy sciences workshop on electrical energy storage, april 2-4, 2007," tech. rep., DOESC (USDOE Office of Science (SC)), 2007.

[83] A. Barré, B. Deguilhem, S. Grolleau, M. Gérard, F. Suard, and D. Riu, "A review on lithium-ion battery ageing mechanisms and estimations for automotive applications," *Journal of Power Sources*, vol. 241, pp. 680–689, 2013.

[84] O. Erdinc, B. Vural, and M. Uzunoglu, "A dynamic lithium-ion battery model considering the effects of temperature and capacity fading," in *2009 International Conference on Clean Electrical Power*, pp. 383–386, IEEE, 2009.

[85] S. B. Peterson, J. Apt, and J. Whitacre, "Lithium-ion battery cell degradation resulting from realistic vehicle and vehicle-to-grid utilization," *Journal of Power Sources*, vol. 195, no. 8, pp. 2385–2392, 2010.

[86] E. Lockhart, X. Li, S. S. Booth, D. R. Olis, J. A. Salasovich, J. Elsworth, and L. Lisell, "Comparative study of techno-economics of lithium-ion and lead-acid batteries in microgrids in sub-saharan africa," tech. rep., National Renewable Energy Lab.(NREL), Golden, CO (United States), 2019.

[87] A. Heinzel and V. Barragan, "A review of the state-of-the-art of the methanol crossover in direct methanol fuel cells," *Journal of Power Sources*, vol. 84, no. 1, pp. 70–74, 1999.

[88] W. Vielstich, A. Lamm, and H. A. Gasteiger, *Handbook of fuel cells: fundamentals technology and applications*, vol. 2. Wiley New York, 2003.

[89] A. Taniguchi, T. Akita, K. Yasuda, and Y. Miyazaki, "Analysis of electrocatalyst degradation in pemfc caused by cell reversal during fuel starvation," *Journal of Power Sources*, vol. 130, no. 1-2, pp. 42–49, 2004.

[90] Z. Ma, J. Eichman, and J. Kurtz, "Fuel cell backup power system for grid service and microgrid in telecommunication applications," *Journal of Energy Resources Technology*, vol. 141, no. 6, p. 062002, 2019.

[91] J. Eichman, K. Harrison, and M. Peters, "Novel electrolyzer applications: providing more than just hydrogen," tech. rep., National Renewable Energy Lab.(NREL), Golden, CO (United States), 2014.

[92] N. Mohan, T. M. Undeland, and W. P. Robbins, *Power electronics: converters, applications, and design*. John wiley & sons, 2003.

[93] R. S. Ashok and Y. B. Shtessel, "Sliding mode control of electric power system comprised of fuel cell and multiple-modular dc-dc boost converters," in *2014 13th International Workshop on Variable Structure Systems (VSS)*, pp. 1–7, IEEE, 2014.

[94] R. S. Ashok, Y. B. Shtessel, and J. E. Smith, "Sliding mode control of electric power system comprised of fuel cells, dc-dc boost converters and ultracapacitors," in *2013 American Control Conference*, pp. 5766–5771, IEEE, 2013.

[95] J. Clegg, "A nonlinear integrator for servomechanisms," *Transactions of the American Institute of Electrical Engineers, Part II: Applications and Industry*, vol. 77, no. 1, pp. 41–42, 1958.

[96] K. R. Krishnan and I. M. Horowitz, "Synthesis of a non-linear feedback system with significant plant-ignorance for prescribed system tolerances," *International Journal of Control*, vol. 19, pp. 689–706, apr 1974.

[97] I. Horowitz and P. Rosenbaum, "Non-linear design for cost of feedback reduction in systems with large parameter uncertainty," *International Journal of Control*, vol. 21, no. 6, pp. 977–1001, 1975.

[98] L. Zaccarian, D. Nešić, and A. R. Teel, "Analytical and numerical lyapunov functions for siso linear control systems with first-order reset elements," *International Journal of Robust and Nonlinear Control*, vol. 21, no. 10, pp. 1134–1158, 2011.

[99] L. Zaccarian, D. Nesic, and A. R. Teel, "First order reset elements and the clegg integrator revisited," in *Proceedings of the 2005, American Control Conference, 2005.*, pp. 563–568 vol. 1, June 2005.

[100] D. Nesic, A. R. Teel, and L. Zaccarian, "Stability and performance of siso control systems with first-order reset elements," *IEEE Transactions on Automatic Control*, vol. 56, pp. 2567–2582, Nov 2011.

[101] O. Beker, C. Hollot, Y. Chait, and H. Han, "Fundamental properties of reset control systems," *Automatica*, vol. 40, no. 6, pp. 905 – 915, 2004.

[102] A. Baños and A. Barreiro, *Reset control systems*. Springer Science & Business Media, 2012.

[103] A. Baños and A. Barreiro, "Delay-independent stability of reset systems," *IEEE Transactions on Automatic Control*, vol. 54, no. 2, pp. 341–346, 2009.

[104] A. Baños and A. Vidal, "Design of Reset Control Systems: The PI+CI Compensator," *Journal of Dynamic Systems, Measurement, and Control*, vol. 134, no. 5, p. 051003, 2012.

[105] A. Baños and M. Davó, "Tuning of reset proportional integral compensators with a variable reset ratio and reset band," *IET Control Theory and Applications*, vol. 8, no. 17, pp. 1949–1962, 2014.

[106] O. Beker, C. V. Hollot, and Y. Chait, "Plant with integrator: an example of reset control overcoming limitations of linear feedback," *IEEE Transactions on Automatic Control*, vol. 46, pp. 1797–1799, Nov 2001.

[107] A. Baños, J. I. Mulero, A. Barreiro, and M. A. Davo, "An impulsive dynamical systems framework for reset control systems," *International Journal of Control*, vol. 89, no. 10, pp. 1985–2007, 2016.

[108] J. Carrasco, A. Baños, and A. van der Schaft, "A passivity-based approach to reset control systems stability," *Systems & Control Letters*, vol. 59, no. 1, pp. 18–24, 2010.

[109] A. F. Villaverde, A. B. Blas, J. Carrasco, and A. B. Torrico, "Reset control for passive bilateral teleoperation," *IEEE Transactions on Industrial Electronics*, vol. 58, pp. 3037–3045, July 2011.

[110] A. Vidal, A. Baños, J. C. Moreno, and M. Berenguel, "PI+CI compensation with variable reset: Application on solar collector fields," in *2008 34th Annual Conference of IEEE Industrial Electronics*, pp. 321–326, Nov 2008.

[111] M. F. Heertjes, K. G. J. Gruntjens, S. J. L. M. van Loon, N. van de Wouw, and W. P. M. H. Heemels, "Experimental Evaluation of Reset Control for Improved Stage Performance," *IFAC-PapersOnLine*, no. 13, pp. 93–98, 2016.

[112] A. Vidal and A. Baños, "Reset compensation for temperature control: Experimental application on heat exchangers," *Chemical Engineering Journal*, vol. 159, no. 1-3, pp. 170–181, 2010.

[113] R. Goebel, R. G. Sanfelice, and A. R. Teel, *Hybrid Dynamical Systems: modeling, stability, and robustness*. Princeton University Press, 2012.

[114] S. van Loon, K. Gruntjens, M. Heertjes, N. van de Wouw, and W. Heemels, "Frequency-domain tools for stability analysis of reset control systems," *Automatica*, vol. 82, pp. 101–108, 2016.

[115] J. Rocabert, A. Luna, F. Blaabjerg, and P. Rodriguez, "Control of power converters in ac microgrids," *IEEE transactions on power electronics*, vol. 27, no. 11, pp. 4734–4749, 2012.

[116] A. Engler, "Control of inverters in isolated and in grid tied operation with regard to expandability," in *Tutorial: Power Electronics for Regenerative Energy at IEEE Power Electronics Specialists Conference (PESC04) Conference, Aachen*, 2004.

[117] K. De Brabandere, B. Bolsens, J. Van den Keybus, A. Woyte, J. Driesen, and R. Belmans, "A voltage and frequency droop control method for parallel inverters," *IEEE Transactions on power electronics*, vol. 22, no. 4, pp. 1107–1115, 2007.

[118] F. Guinjoan, J. Calvente, A. Poveda, and L. Martinez, "Large-signal modeling and simulation of switching dc-dc converters," *IEEE Transactions on Power Electronics*, vol. 12, no. 3, pp. 485–494, 1997.

[119] P. Chrin and C. Bunlaksananusorn, "Large-signal average modeling and simulation of dc-dc converters with simulink," in *2007 Power Conversion Conference-Nagoya*, pp. 27–32, IEEE, 2007.

[120] T. Hägglund and K. J. Åström, "Revisiting the ziegler-nichols tuning rules for pi control," *Asian Journal of Control*, vol. 4, no. 4, pp. 364–380, 2002.

[121] A. Bergen and R. Franks, "Justification of the describing function method," *SIAM Journal on Control*, vol. 9, no. 4, pp. 568–589, 1971.

[122] A. Mees and A. Bergen, "Describing functions revisited," *IEEE Transactions on Automatic Control*, vol. 20, pp. 473–478, August 1975.

[123] S. R. Sanders, "On limit cycles and the describing function method in periodically switched circuits," *IEEE Transactions on Circuits and Systems I: Fundamental Theory and Applications*, vol. 40, pp. 564–572, Sept 1993.

[124] K. J. Aström and R. M. Murray, *Feedback systems: An introduction for scientists and engineers*. Princeton university press, 2010.

[125] F. Blaabjerg, R. Teodorescu, M. Liserre, and A. V. Timbus, "Overview of control and grid synchronization for distributed power generation systems," *IEEE Transactions on industrial electronics*, vol. 53, no. 5, pp. 1398–1409, 2006.

[126] A. Timbus, M. Liserre, R. Teodorescu, P. Rodriguez, and F. Blaabjerg, "Evaluation of current controllers for distributed power generation systems," *IEEE Transactions on power electronics*, vol. 24, no. 3, pp. 654–664, 2009.

[127] S. A. Khajehoddin, M. Karimi-Ghartemani, P. K. Jain, and A. Bakhshai, "Dc-bus design and control for a single-phase grid-connected renewable converter with a small energy storage component," *IEEE Transactions on Power Electronics*, vol. 28, no. 7, pp. 3245–3254, 2012.

[128] M. Hagiwara and H. Akagi, "An approach to regulating the dc-link voltage of a voltage-source btb system during power line faults," in *38th IAS Annual Meeting on Conference Record of the Industry Applications Conference, 2003.*, vol. 3, pp. 1504–1510, IEEE, 2003.

[129] B. Parkhideh and S. Bhattacharya, "Vector-controlled voltage-source-converter-based transmission under grid disturbances," *IEEE transactions on power electronics*, vol. 28, no. 2, pp. 661–672, 2012.

[130] F. Bakhshande and D. Söffker, "Proportional-integral-observer: A brief survey with special attention to the actual methods using acc benchmark," *IFAC-PapersOnLine*, vol. 48, no. 1, pp. 532–537, 2015.

[131] E. Davison, "The output control of linear time-invariant multivariable systems with unmeasurable arbitrary disturbances," *IEEE Transactions on Automatic Control*, vol. 17, no. 5, pp. 621–630, 1972.

[132] C. Johnson, "Theory of distrubance-accommodating controllers," in *Control and Dynamic Systems*, vol. 12, pp. 387–489, Elsevier, 1976.

[133] J. Liu, S. Vazquez, L. Wu, A. Marquez, H. Gao, and L. G. Franquelo, "Extended state observer-based sliding-mode control for three-phase power converters," *IEEE Transactions on Industrial Electronics*, vol. 64, no. 1, pp. 22–31, 2017.

[134] C. Wang, X. Li, L. Guo, and Y. W. Li, "A nonlinear-disturbance-observer-based dc-bus voltage control for a hybrid ac/dc microgrid," *IEEE Transactions on Power Electronics*, vol. 29, no. 11, pp. 6162–6177, 2014.

[135] J. You, M. Vilathgamuwa, and N. Ghasemi, "Dc bus voltage stability improvement using disturbance observer feedforward control," *Control Engineering Practice*, vol. 75, pp. 118–125, 2018.

[136] D. G. Luenberger, "Observing the state of a linear system," *IEEE transactions on military electronics*, vol. 8, no. 2, pp. 74–80, 1964.

[137] K. Ogata and Y. Yang, *Modern control engineering*, vol. 5. Prentice hall Upper Saddle River, NJ, 2010.

[138] S. Endo, H. Kobayashi, C. Kempf, S. Kobayashi, M. Tomizuka, and Y. Hori, "Robust digital tracking controller design for high-speed positioning systems," *Control Engineering Practice*, vol. 4, no. 4, pp. 527–536, 1996.

[139] Y. Choi, K. Yang, W. K. Chung, H. R. Kim, and I. H. Suh, "On the robustness and performance of disturbance observers for second-order systems," *IEEE Transactions on Automatic Control*, vol. 48, no. 2, pp. 315–320, 2003.

[140] J. C. Doyle, B. A. Francis, and A. R. Tannenbaum, *Feedback control theory*. Courier Corporation, 2013.

[141] P. Gahinet and P. Apkarian, "A linear matrix inequality approach to h control," *International journal of robust and nonlinear control*, vol. 4, no. 4, pp. 421–448, 1994.

[142] L. El Ghaoui and P. Gahinet, "Rank minimization under lmi constraints: A framework for output feedback problems," 1993.

[143] L. El Ghaoui, F. Oustry, and M. AitRami, "A cone complementarity linearization algorithm for static output-feedback and related problems," *IEEE transactions on automatic control*, vol. 42, no. 8, pp. 1171–1176, 1997.

[144] R. de Castro, C. Pinto, R. E. Araújo, P. Melo, and D. Freitas, "Optimal sizing and energy management of hybrid storage systems," in *2012 IEEE Vehicle Power and Propulsion Conference*, pp. 321–326, IEEE, 2012.

[145] J. P. F. Trovão, M.-A. Roux, É. Ménard, and M. R. Dubois, "Energy-and power-split management of dual energy storage system for a three-wheel electric vehicle," *IEEE Transactions on Vehicular Technology*, vol. 66, no. 7, pp. 5540–5550, 2016.

[146] J. Snoussi, S. Ben Elghali, M. Benbouzid, and M. Mimouni, "Auto-adaptive filtering-based energy management strategy for fuel cell hybrid electric vehicles," *Energies*, vol. 11, no. 8, p. 2118, 2018.

[147] N. R. Tummuru, M. K. Mishra, and S. Srinivas, "Dynamic energy management of renewable grid integrated hybrid energy storage system," *IEEE Transactions on Industrial Electronics*, vol. 62, no. 12, pp. 7728–7737, 2015.

[148] S. Dusmez and A. Khaligh, "A supervisory power-splitting approach for a new ultracapacitor–battery vehicle deploying two propulsion machines," *IEEE Transactions on Industrial Informatics*, vol. 10, no. 3, pp. 1960–1971, 2014.

[149] S. Dusmez and A. Khaligh, "Wavelet-transform based energy and power decoupling strategy for a novel ultracapacitor-battery hybrid power-split gear powertrain," in *2013 IEEE Transportation Electrification Conference and Expo (ITEC)*, pp. 1–7, IEEE, 2013.

[150] O. Erdinc, B. Vural, and M. Uzunoglu, "A wavelet-fuzzy logic based energy management strategy for a fuel cell/battery/ultra-capacitor hybrid vehicular power system," *Journal of Power sources*, vol. 194, no. 1, pp. 369–380, 2009.

[151] M. Tommiska, "Efficient digital implementation of the sigmoid function for reprogrammable logic," *IEE Proceedings-Computers and Digital Techniques*, vol. 150, no. 6, pp. 403–411, 2003.

[152] F. YANG, L. Lu, Y. Yang, and Y. He, "Characterization, analysis and modeling of an ultracapacitor," *World Electric Vehicle Journal*, vol. 4, no. 2, pp. 358–369, 2010.

[153] X. Lu, K. Sun, J. M. Guerrero, J. C. Vasquez, L. Huang, and R. Teodorescu, "Soc-based droop method for distributed energy storage in dc microgrid applications," in *2012 IEEE International Symposium on Industrial Electronics*, pp. 1640–1645, IEEE, 2012.

[154] X. Lu, K. Sun, J. M. Guerrero, J. C. Vasquez, and L. Huang, "Double-quadrant state-of-charge-based droop control method for distributed energy storage systems in autonomous dc microgrids," *IEEE Transactions on Smart Grid*, vol. 6, no. 1, pp. 147–157, 2014.

[155] N. L. Diaz, T. Dragičević, J. C. Vasquez, and J. M. Guerrero, "Fuzzy-logic-based gain-scheduling control for state-of-charge balance of distributed energy storage systems for dc microgrids," in *2014 IEEE Applied Power Electronics Conference and Exposition-APEC 2014*, pp. 2171–2176, IEEE, 2014.

[156] N. L. Diaz, T. Dragičević, J. C. Vasquez, and J. M. Guerrero, "Intelligent distributed generation and storage units for dc microgridsa new concept on cooperative control without communications beyond droop control," *IEEE Transactions on Smart Grid*, vol. 5, no. 5, pp. 2476–2485, 2014.

[157] J. Torreglosa, P. García, L. Fernández, and F. Jurado, "Hierarchical energy management system for stand-alone hybrid system based on generation costs and cascade control," *Energy Conversion and Management*, vol. 77, pp. 514–526, 2014.

[158] S. Teleke, M. E. Baran, S. Bhattacharya, and A. Q. Huang, "Rule-based control of battery energy storage for dispatching intermittent renewable sources," *IEEE Transactions on Sustainable Energy*, vol. 1, no. 3, pp. 117–124, 2010.

[159] Y. Zhang, A. Lundblad, P. E. Campana, F. Benavente, and J. Yan, "Battery sizing and rule-based operation of grid-connected photovoltaic-battery system: A case study in sweden," *Energy conversion and management*, vol. 133, pp. 249–263, 2017.

[160] I. B. Ali, M. Turki, J. Belhadj, and X. Roboam, "Optimized fuzzy rule-based energy management for a battery-less pv/wind-bwro desalination system," *Energy*, vol. 159, pp. 216–228, 2018.

[161] S. Berrazouane and K. Mohammedi, "Parameter optimization via cuckoo optimization algorithm of fuzzy controller for energy management of a hybrid power system," *Energy conversion and management*, vol. 78, pp. 652–660, 2014.

[162] D. Arcos-Aviles, J. Pascual, L. Marroyo, P. Sanchis, and F. Guinjoan, "Fuzzy logic-based energy management system design for residential grid-connected microgrids," *IEEE Transactions on Smart Grid*, vol. 9, no. 2, pp. 530–543, 2016.

[163] D. Oliveira, A. Z. de Souza, M. Santos, A. Almeida, B. Lopes, and O. Saavedra, "A fuzzy-based approach for microgrids islanded operation," *Electric Power Systems Research*, vol. 149, pp. 178–189, 2017.

[164] A. Askarzadeh, "A memory-based genetic algorithm for optimization of power generation in a microgrid," *IEEE transactions on sustainable energy*, vol. 9, no. 3, pp. 1081–1089, 2017.

[165] H. Liang and H. Gooi, "Unit commitment in microgrids by improved genetic algorithm," in *2010 Conference Proceedings IPEC*, pp. 842–847, IEEE, 2010.

[166] J. P. Fossati, A. Galarza, A. Martín-Villate, J. M. Echeverría, and L. Fontán, "Optimal scheduling of a microgrid with a fuzzy logic controlled storage system," *International Journal of Electrical Power & Energy Systems*, vol. 68, pp. 61–70, 2015.

[167] C.-L. Chen, "Simulated annealing-based optimal wind-thermal coordination scheduling," *IET Generation, Transmission & Distribution*, vol. 1, no. 3, pp. 447–455, 2007.

[168] D. Gayme and U. Topcu, "Optimal power flow with large-scale storage integration," *IEEE Transactions on Power Systems*, vol. 28, no. 2, pp. 709–717, 2013.

[169] T. A. Nguyen and M. Crow, "Stochastic optimization of renewable-based microgrid operation incorporating battery operating cost," *IEEE Transactions on Power Systems*, vol. 31, no. 3, pp. 2289–2296, 2016.

[170] R. Dufo-Lopez, J. L. Bernal-Agustín, and J. Contreras, "Optimization of control strategies for stand-alone renewable energy systems with hydrogen storage," *Renewable energy*, vol. 32, no. 7, pp. 1102–1126, 2007.

[171] F. Garcia-Torres, L. Valverde, and C. Bordons, "Optimal load sharing of hydrogen-based microgrids with hybrid storage using model-predictive control," *IEEE Transactions on Industrial Electronics*, vol. 63, no. 8, pp. 4919–4928, 2016.

[172] M. Khalid and A. Savkin, "A model predictive control approach to the problem of wind power smoothing with controlled battery storage," *Renewable Energy*, vol. 35, no. 7, pp. 1520–1526, 2010.

[173] A. Parisio, E. Rikos, and L. Glielmo, "A model predictive control approach to microgrid operation optimization," *IEEE Transactions on Control Systems Technology*, vol. 22, pp. 1813–1827, Sep. 2014.

[174] L. Hernandez, C. Baladron, J. M. Aguiar, B. Carro, A. J. Sanchez-Esguevillas, J. Lloret, and J. Massana, "A survey on electric power demand forecasting: future trends in smart grids, microgrids and smart buildings," *IEEE Communications Surveys & Tutorials*, vol. 16, no. 3, pp. 1460–1495, 2014.

[175] D. L. Marino, K. Amarasinghe, and M. Manic, "Building energy load forecasting using deep neural networks," in *IECON 2016-42nd Annual Conference of the IEEE Industrial Electronics Society*, pp. 7046–7051, IEEE, 2016.

[176] J. G. De Gooijer and R. J. Hyndman, "25 years of time series forecasting," *International journal of forecasting*, vol. 22, no. 3, pp. 443–473, 2006.

[177] G. U. Yule, "Vii. on a method of investigating periodicities disturbed series, with special reference to wolfer's sunspot numbers," *Philosophical Transactions of the Royal Society of London. Series A, Containing Papers of a Mathematical or Physical Character*, vol. 226, no. 636-646, pp. 267–298, 1927.

[178] R. G. Brown, *Statistical forecasting for inventory control*. McGraw/Hill, 1959.

[179] G. E. Box, G. M. Jenkins, G. C. Reinsel, and G. M. Ljung, *Time series analysis: forecasting and control*. John Wiley & Sons, 2015.

[180] G. E. Box and D. A. Pierce, "Distribution of residual autocorrelations in autoregressive-integrated moving average time series models," *Journal of the American statistical Association*, vol. 65, no. 332, pp. 1509–1526, 1970.

[181] H. Bozdogan, "Model selection and akaike's information criterion (aic): The general theory and its analytical extensions," *Psychometrika*, vol. 52, no. 3, pp. 345–370, 1987.

[182] T. Nijman and F. Palm, "Parameter identification in arma processes in the presence of regular but incomplete sampling," *Journal of Time Series Analysis*, vol. 11, no. 3, pp. 239–248, 1990.

[183] M. S. Voss and X. Feng, "Arma model selection using particle swarm optimization and aic criteria," *IFAC Proceedings Volumes*, vol. 35, no. 1, pp. 349–354, 2002.

[184] F. De Ridder, R. Pintelon, J. Schoukens, and D. P. Gillikin, "Modified aic and mdl model selection criteria for short data records," *IEEE Transactions on Instrumentation and Measurement*, vol. 54, no. 1, pp. 144–150, 2005.

[185] A. M. Schneider, T. Takenawa, D. A. Schiffman, and D. Bunn, *24-hour electric utility load forecasting*. Wiley, 1985.

[186] K. Poysti, "Box-jenkins method in short-term forecasting of grid load in finland," in *Proc. 8th Power Systems Computation Conf.*, pp. 357–368, 1984.

[187] M. T. Hagan and S. M. Behr, "The time series approach to short term load forecasting," *IEEE transactions on power systems*, vol. 2, no. 3, pp. 785–791, 1987.

[188] S. Vemuri, B. Hoveida, and S. Mohebbi, "Short term load forecasting based on weather load models," in *Power Systems and Power Plant Control*, pp. 315–320, Elsevier, 1987.

[189] G. Gross and F. D. Galiana, "Short-term load forecasting," *Proceedings of the IEEE*, vol. 75, no. 12, pp. 1558–1573, 1987.

[190] L. Ljung and T. Söderström, *Theory and practice of recursive identification*. MIT press, 1983.

[191] R. Campo and P. Ruiz, "Adaptive weather-sensitive short term load forecast," *IEEE Transactions on Power Systems*, vol. 2, no. 3, pp. 592–598, 1987.

[192] J. Fan and J. McDonald, "A real-time implementation of short-term load forecasting for distribution power systems," *IEEE Transactions on Power Systems*, vol. 9, no. 2, pp. 988–994, 1994.

[193] A. J. Smola and B. Schölkopf, "A tutorial on support vector regression," *Statistics and computing*, vol. 14, no. 3, pp. 199–222, 2004.

[194] A. Mellit and A. M. Pavan, "A 24-h forecast of solar irradiance using artificial neural network: Application for performance prediction of a grid-connected pv plant at trieste, italy," *Solar Energy*, vol. 84, no. 5, pp. 807–821, 2010.

[195] W. Liu, Z. Wang, X. Liu, N. Zeng, Y. Liu, and F. E. Alsaadi, "A survey of deep neural network architectures and their applications," *Neurocomputing*, vol. 234, pp. 11–26, 2017.

[196] F. A. Gers, J. Schmidhuber, and F. Cummins, "Learning to forget: Continual prediction with lstm," 1999.

[197] A. E. Hoerl and R. W. Kennard, "Ridge regression: applications to nonorthogonal problems," *Technometrics*, vol. 12, no. 1, pp. 69–82, 1970.

[198] R. Tibshirani, "Regression shrinkage and selection via the lasso," *Journal of the Royal Statistical Society: Series B (Methodological)*, vol. 58, no. 1, pp. 267–288, 1996.

[199] J. H. Friedman, "Stochastic gradient boosting," *Computational statistics & data analysis*, vol. 38, no. 4, pp. 367–378, 2002.

[200] T. Chen and C. Guestrin, "Xgboost: A scalable tree boosting system," in *Proceedings of the 22nd acm sigkdd international conference on knowledge discovery and data mining*, pp. 785–794, 2016.

[201] E. Alpaydin, *Introduction to machine learning*. MIT press, 2014.

[202] A. Ahmad, M. Hassan, M. Abdullah, H. Rahman, F. Hussin, H. Abdullah, and R. Saidur, "A review on applications of ann and svm for building electrical energy consumption forecasting," *Renewable and Sustainable Energy Reviews*, vol. 33, pp. 102–109, 2014.

[203] W. Kong, Z. Y. Dong, Y. Jia, D. J. Hill, Y. Xu, and Y. Zhang, "Short-term residential load forecasting based on lstm recurrent neural network," *IEEE Transactions on Smart Grid*, vol. 10, no. 1, pp. 841–851, 2017.

[204] F. Ziel, "Modelling and forecasting electricity load using lasso methods," in *2015 Modern Electric Power Systems (MEPS)*, pp. 1–6, IEEE, 2015.

[205] G. Suryanarayana, J. Lago, D. Geysen, P. Aleksiejuk, and C. Johansson, "Thermal load forecasting in district heating networks using deep learning and advanced feature selection methods," *Energy*, vol. 157, pp. 141–149, 2018.

[206] H.-T. Yang, C.-M. Huang, Y.-C. Huang, and Y.-S. Pai, "A weather-based hybrid method for 1-day ahead hourly forecasting of pv power output," *IEEE transactions on sustainable energy*, vol. 5, no. 3, pp. 917–926, 2014.

[207] M. Abdel-Nasser and K. Mahmoud, "Accurate photovoltaic power forecasting models using deep lstm-rnn," *Neural Computing and Applications*, vol. 31, no. 7, pp. 2727–2740, 2019.

[208] S. Tiwari, R. Sabzehgar, and M. Rasouli, "Short term solar irradiance forecast using numerical weather prediction (nwp) with gradient boost regression," in *2018 9th IEEE International Symposium on Power Electronics for Distributed Generation Systems (PEDG)*, pp. 1–8, IEEE, 2018.

[209] A. Torres-Barrán, Á. Alonso, and J. R. Dorronsoro, "Regression tree ensembles for wind energy and solar radiation prediction," *Neurocomputing*, vol. 326, pp. 151–160, 2019.

[210] R. Yu, J. Gao, M. Yu, W. Lu, T. Xu, M. Zhao, J. Zhang, R. Zhang, and Z. Zhang, "Lstm-efg for wind power forecasting based on sequential correlation features," *Future Generation Computer Systems*, vol. 93, pp. 33–42, 2019.

[211] C. González, J. Mira-McWilliams, and I. Juárez, "Important variable assessment and electricity price forecasting based on regression tree models: classification and regression trees, bagging and random forests," *IET Generation, Transmission & Distribution*, vol. 9, no. 11, pp. 1120–1128, 2015.

[212] D. Singhal and K. Swarup, "Electricity price forecasting using artificial neural networks," *International Journal of Electrical Power & Energy Systems*, vol. 33, no. 3, pp. 550–555, 2011.

[213] M. Zahid, F. Ahmed, N. Javaid, R. A. Abbasi, Z. Kazmi, H. Syeda, A. Javaid, M. Bilal, M. Akbar, and M. Ilahi, "Electricity price and load forecasting using enhanced convolutional neural network and enhanced support vector regression in smart grids," *Electronics*, vol. 8, no. 2, p. 122, 2019.

[214] B. M. Williams and L. A. Hoel, "Modeling and forecasting vehicular traffic flow as a seasonal arima process: Theoretical basis and empirical results," *Journal of transportation engineering*, vol. 129, no. 6, pp. 664–672, 2003.

[215] E. G. Kardakos, M. C. Alexiadis, S. I. Vagropoulos, C. K. Simoglou, P. N. Biskas, and A. G. Bakirtzis, "Application of time series and artificial neural network models in short-term forecasting of pv power generation," in *2013 48th International Universities' Power Engineering Conference (UPEC)*, pp. 1–6, IEEE, 2013.

[216] A. Fadhilah, S. Suriawati, H. Amir, Z. Izham, and S. Mahendran, "Malaysian day-type load forecasting," in *2009 3rd International Conference on Energy and Environment (ICEE)*, pp. 408–411, IEEE, 2009.

[217] A. Gensler, J. Henze, B. Sick, and N. Raabe, "Deep learning for solar power forecasting-an approach using autoencoder and lstm neural networks," in *2016 IEEE international conference on systems, man, and cybernetics (SMC)*, pp. 002858–002865, IEEE, 2016.

[218] S. Sobri, S. Koohi-Kamali, and N. A. Rahim, "Solar photovoltaic generation forecasting methods: A review," *Energy Conversion and Management*, vol. 156, pp. 459–497, 2018.

[219] H. Shi, M. Xu, and R. Li, "Deep learning for household load forecastinga novel pooling deep rnn," *IEEE Transactions on Smart Grid*, vol. 9, no. 5, pp. 5271–5280, 2017.

[220] J. Zheng, C. Xu, Z. Zhang, and X. Li, "Electric load forecasting in smart grids using long-short-term-memory based recurrent neural network," in *2017 51st Annual Conference on Information Sciences and Systems (CISS)*, pp. 1–6, IEEE, 2017.

[221] S. Srivastava and S. Lessmann, "A comparative study of lstm neural networks in forecasting day-ahead global horizontal irradiance with satellite data," *Solar Energy*, vol. 162, pp. 232–247, 2018.

[222] S. Haykin, *Neural networks: a comprehensive foundation*. Prentice Hall PTR, 1994.

[223] M. H. Hassoun *et al.*, *Fundamentals of artificial neural networks*. MIT press, 1995.

[224] V. Nair and G. E. Hinton, "Rectified linear units improve restricted boltzmann machines," in *Proceedings of the 27th international conference on machine learning (ICML-10)*, pp. 807–814, 2010.

[225] D. F. Specht *et al.*, "A general regression neural network," *IEEE transactions on neural networks*, vol. 2, no. 6, pp. 568–576, 1991.

[226] D. E. Rumelhart, G. E. Hinton, and R. J. Williams, "Learning internal representations by error propagation," tech. rep., California Univ San Diego La Jolla Inst for Cognitive Science, 1985.

[227] F. Chollet *et al.*, "Keras." `https://keras.io`, 2015.

[228] A. Y. Ng, "Feature selection, l 1 vs. l 2 regularization, and rotational invariance," in *Proceedings of the twenty-first international conference on Machine learning*, p. 78, 2004.

[229] N. Srivastava, G. Hinton, A. Krizhevsky, I. Sutskever, and R. Salakhutdinov, "Dropout: a simple way to prevent neural networks from overfitting," *The journal of machine learning research*, vol. 15, no. 1, pp. 1929–1958, 2014.

[230] D. P. Kingma and J. Ba, "Adam: A method for stochastic optimization," *arXiv preprint arXiv:1412.6980*, 2014.

[231] A. C. Luna, N. L. Diaz, M. Graells, J. C. Vasquez, and J. M. Guerrero, "Mixed-integer-linear-programming-based energy management system for hybrid pv-wind-battery microgrids: Modeling, design, and experimental verification," *IEEE Transactions on Power Electronics*, vol. 32, no. 4, pp. 2769–2783, 2016.

[232] J. Shen and A. Khaligh, "A supervisory energy management control strategy in a battery/ultracapacitor hybrid energy storage system," *IEEE Transactions on Transportation Electrification*, vol. 1, no. 3, pp. 223–231, 2015.

[233] J. Li and M. A. Danzer, "Optimal charge control strategies for stationary photovoltaic battery systems," *Journal of Power Sources*, vol. 258, pp. 365–373, 2014.

[234] A. Zeh and R. Witzmann, "Operational strategies for battery storage systems in low-voltage distribution grids to limit the feed-in power of roof-mounted solar power systems," in *8th International Renewable Energy Storage Conference (IRES 2013)*, 2013.

[235] G. Angenendt, S. Zurmühlen, H. Axelsen, and D. U. Sauer, "Comparison of different operation strategies for pv battery home storage systems including forecast-based operation strategies," *Applied energy*, vol. 229, pp. 884–899, 2018.

[236] V. Bertsch, J. Geldermann, and T. Lühn, "What drives the profitability of household pv investments, self-consumption and self-sufficiency?," *Applied Energy*, vol. 204, pp. 1–15, 2017.

[237] E. Mayhorn, K. Kalsi, M. Elizondo, W. Zhang, S. Lu, N. Samaan, and K. Butler-Purry, "Optimal control of distributed energy resources using model predictive control," in *2012 IEEE power and energy society general meeting*, pp. 1–8, IEEE, 2012.

[238] J. Ramos-Teodoro, F. Rodríguez, M. Berenguel, and J. L. Torres, "Heterogeneous resource management in energy hubs with self-consumption: Contributions and application example," *Applied energy*, vol. 229, pp. 537–550, 2018.

[239] M. Trifkovic, M. Sheikhzadeh, K. Nigim, and P. Daoutidis, "Modeling and control of a renewable hybrid energy system with hydrogen storage," *IEEE Transactions on Control Systems Technology*, vol. 22, no. 1, pp. 169–179, 2013.

[240] P. Garcia, L. M. Fernandez, C. A. Garcia, and F. Jurado, "Energy management system of fuel-cell-battery hybrid tramway," *IEEE Transactions on Industrial Electronics*, vol. 57, no. 12, pp. 4013–4023, 2009.

[241] M. Kisacikoglu, M. Uzunoglu, and M. Alam, "Load sharing using fuzzy logic control in a fuel cell/ultracapacitor hybrid vehicle," *International journal of hydrogen energy*, vol. 34, no. 3, pp. 1497–1507, 2009.

[242] W. Greenwell and A. Vahidi, "Predictive control of voltage and current in a fuel cell–ultracapacitor hybrid," *IEEE Transactions on Industrial Electronics*, vol. 57, no. 6, pp. 1954–1963, 2009.

[243] F. Garcia and C. Bordons, "Optimal economic dispatch for renewable energy microgrids with hybrid storage using model predictive control," in *IECON 2013-39th Annual Conference of the IEEE Industrial Electronics Society*, pp. 7932–7937, IEEE, 2013.

[244] A. Cecilia, J. Carroquino, V. Roda, R. Costa-Castelló, and F. Barreras, "Optimal energy management in a standalone microgrid, with photovoltaic generation, short-term storage, and hydrogen production," *Energies*, vol. 13, no. 6, p. 1454, 2020.

[245] Y. Du, J. Wu, S. Li, C. Long, and S. Onori, "Coordinated energy dispatch of autonomous microgrids with distributed mpc optimization," *IEEE Transactions on Industrial Informatics*, vol. 15, no. 9, pp. 5289–5298, 2019.

[246] X. Xing, L. Xie, and H. Meng, "Cooperative energy management optimization based on distributed mpc in grid-connected microgrids community," *International Journal of Electrical Power & Energy Systems*, vol. 107, pp. 186–199, 2019.

[247] J. Richalet, A. Rault, J. Testud, and J. Papon, "Model predictive heuristic control," *Automatica (Journal of IFAC)*, vol. 14, no. 5, pp. 413–428, 1978.

[248] S. J. Qin and T. A. Badgwell, "An overview of industrial model predictive control technology," in *AIche symposium series*, vol. 93, pp. 232–256, New York, NY: American Institute of Chemical Engineers, 1971-c2002., 1997.

[249] J. B. Rawlings, D. Angeli, and C. N. Bates, "Fundamentals of economic model predictive control," in *2012 IEEE 51st IEEE conference on decision and control (CDC)*, pp. 3851–3861, IEEE, 2012.

[250] S. V. Raković, "Model predictive control: classical, robust, and stochastic [bookshelf]," *IEEE Control Systems Magazine*, vol. 36, no. 6, pp. 102–105, 2016.

[251] J. M. Maciejowski, *Predictive control: with constraints*. Pearson education, 2002.

[252] Y. Li, W. Gao, and Y. Ruan, "Performance investigation of grid-connected residential pv-battery system focusing on enhancing self-consumption and peak shaving in Kyushu, Japan," *Renewable energy*, vol. 127, pp. 514–523, 2018.

[253] G. d. O. e Silva and P. Hendrick, "Photovoltaic self-sufficiency of Belgian households using lithium-ion batteries, and its impact on the grid," *Applied Energy*, vol. 195, pp. 786–799, 2017.

[254] H. Wirth and K. Schneider, "Aktuelle fakten zur photovoltaik in deutschland,"

[255] C. Breyer and A. Gerlach, "Global overview on grid-parity," *Progress in photovoltaics: Research and Applications*, vol. 21, no. 1, pp. 121–136, 2013.

[256] M. Resch, B. Ramadhani, J. Bühler, and A. Sumper, "Comparison of control strategies of residential pv storage systems," in *Proc 9th International Renewable Energy Storage Conference and Exhibition (IRES 2015), Messe Düsseldorf, 9-11 March 2015*, pp. 1–18, 2015.

[257] A. Zeh and R. Witzmann, "Operational strategies for battery storage systems in low-voltage distribution grids to limit the feed-in power of roof-mounted solar power systems," *Energy Procedia*, vol. 46, pp. 114–123, 2014.

[258] T. Esram and P. L. Chapman, "Comparison of photovoltaic array maximum power point tracking techniques," *IEEE Transactions on energy conversion*, vol. 22, no. 2, pp. 439–449, 2007.

[259] K. S. Ng, C.-S. Moo, Y.-P. Chen, and Y.-C. Hsieh, "Enhanced coulomb counting method for estimating state-of-charge and state-of-health of lithium-ion batteries," *Applied energy*, vol. 86, no. 9, pp. 1506–1511, 2009.

[260] J. W. Chinneck, "Practical optimization: a gentle introduction," *Systems and Computer Engineering), Carleton University, Ottawa. http://www. sce. carleton. ca/faculty/chinneck/po. html*, 2006.

[261] S. Boyd and L. Vandenberghe, *Convex optimization*. Cambridge University Press, 2004.

[262] E. C. Kerrigan and J. M. Maciejowski, "Soft constraints and exact penalty functions in model predictive control," in *Proc. UKACC International Conference (Control*, 2000.

[263] J. Grosso, C. Ocampo-Martínez, V. Puig, and B. Joseph, "Chance-constrained model predictive control for drinking water networks," *Journal of process control*, vol. 24, no. 5, pp. 504–516, 2014.

[264] J. M. Grosso, P. Velarde, C. Ocampo-Martinez, J. M. Maestre, and V. Puig, "Stochastic model predictive control approaches applied to drinking water networks," *Optimal Control Applications and Methods*, vol. 38, no. 4, pp. 541–558, 2017.

[265] A. Richards and J. How, "Robust stable model predictive control with constraint tightening," in *2006 American Control Conference*, pp. 6–pp, IEEE, 2006.

[266] G. Optimization, "Inc.,gurobi optimizer reference manual, 2015," 2014.

[267] I. Rychlik, "A new definition of the rainflow cycle counting method," *International journal of fatigue*, vol. 9, no. 2, pp. 119–121, 1987.

[268] E. Ela, M. Milligan, and B. Kirby, "Operating reserves and variable generation," tech. rep., National Renewable Energy Lab.(NREL), Golden, CO (United States), 2011.

[269] Y. Yang, F. Blaabjerg, and H. Wang, "Constant power generation of photovoltaic systems considering the distributed grid capacity," in *2014 IEEE Applied Power Electronics Conference and Exposition-APEC 2014*, pp. 379–385, IEEE, 2014.

[270] A. Bemporad and M. Morari, "Control of systems integrating logic, dynamics, and constraints," *Automatica*, vol. 35, no. 3, pp. 407–427, 1999.

[271] P. M. Narendra and K. Fukunaga, "A branch and bound algorithm for feature subset selection," *IEEE Transactions on computers*, no. 9, pp. 917–922, 1977.

[272] A. Rosenfeld, "Fuzzy groups," *Journal of mathematical analysis and applications*, vol. 35, no. 3, pp. 512–517, 1971.

[273] C.-C. Lee, "Fuzzy logic in control systems: fuzzy logic controller. ii," *IEEE Transactions on systems, man, and cybernetics*, vol. 20, no. 2, pp. 419–435, 1990.

[274] F. Logic, "Fuzzy logic and neural network handbook," 1996.

[275] B. Kosko, "Fuzzy systems as universal approximators," *IEEE transactions on computers*, vol. 43, no. 11, pp. 1329–1333, 1994.

[276] E. H. Mamdani and S. Assilian, "An experiment in linguistic synthesis with a fuzzy logic controller," *International journal of man-machine studies*, vol. 7, no. 1, pp. 1–13, 1975.

[277] A. Del Pia, S. S. Dey, and M. Molinaro, "Mixed-integer quadratic programming is in np," *Mathematical Programming*, vol. 162, no. 1-2, pp. 225–240, 2017.

[278] W. Zhang, "Branch-and-bound search algorithms and their computational complexity.," tech. rep., UNIVERSITY OF SOUTHERN CALIFORNIA MARINA DEL REY INFORMATION SCIENCES INST, 1996.